COMPETING ELECTRON TRANSFER PATHWAYS IN MOLECULAR SOLAR CELLS

IVAN MONTANARI

Submitted to the University of London in partial fulfillment for the degree of Doctor in Philosophy

2003

Centre for Electronic Materials and Devices

Department of Chemistry

Imperial College, London

To Marinella Appolonia

and my parents

Lino Montanari

and Silvia De Angelis

ACKNOWLEDGEMENTS

I would like to thank my supervisor Dr. James R. Durrant for his help and encouragement over these years and for speedy critical reading of early versions of this thesis. Dr. Alan G. Taylor has been a particularly friendly and down to earth tutor to talk to. Dr. Jenny Nelson for trying to make her theoretical models comprehensible to me. It has been a pleasure to collaborate with Dr. Ana Flavia Nogueira, a lively brazilian spirit under the grey skies of London. Also, for her invaluable help in elucidating the nature of transient species observed in MDMO-PPV:PCBM blends (chapter 5). Thanks go to Dr. Emilio Palomares, the catalan "chemistry junkie" for re-awakenenig my passion for science and supplying me with cheap fags on the home straight and John Clifford for help with data collection. Dr. Chris Barnett for teaching me more practical electronics I ever thought I could learn. Dr. Yasuhiro Tachibana for teaching me a still unrivalled version of the miso soup. Richard Monkhouse for writing a software interface for data collection that suddenly made possible in a couple of hours a previously day long experiment. Dr. Saif Haque for setting up the i-V rig. I'm very grateful to Yeni Astuti for kindly lending me her laptop at a crucial time. People in Linz (Austria) for providing their precious samples and illuminating discussions, in particular with Dr. Christoph Brabec (now at Siemens Forschung) and Prof. N. Serdar Sariciftci. Je Wen Liou for discussions on international politics from a chinese point of view. Finally, I would like to thank Prof. David Phillips, head of the department of Chemistry at Imperial College for his support.

A number of people that made my stay at Imperial College more pleasant: Chris Soberg, Jason Palmer, Byung Cho, Laura Barter, Alex Green and Thierry Lutz among others.

Special thanks to Wolfgang Amadeus Mozart for having composed Die Zauberflöte, the best piece of music ever conceived by a human being and to Richard Wagner for the ouvertures of Rienzi and Tannhauser.

Last but not least, I would like to thank the University of Bologna for some initial funding and the European Union for partly funding my Ph.D. with a Marie Curie Fellowship therefore making this thesis possible.

Abstract

Competition between charge separation and charge recombination processes is a key issue in molecular photovoltaic devices. In this thesis these issues are addressed in nanocrystalline titanium dioxide dye-sensitised (DSSC) and PPV-fullerene derivatives based solar cells.

In dye-sensitised devices photoinduced charge separation is initiated by electron injection from a molecular sensitiser dye to the semiconductor conduction band yielding the dye cation. This charge separation is subsequently stabilised by regeneration of the dye molecule by electron transfer from donor species, iodide ions of the iodide / triiodide redox couple in the electrolyte. Efficient device function requires the dye cation regeneration reaction by the iodide to be faster than dye regeneration by photo-injected electrons (charge recombination).

This thesis focuses on the competition between these two electron transfer pathways. Transient optical absorption spectroscopy was employed to investigate this kinetic competition. Kinetics of dye-sensitised electrodes in a three-electrode electrochemical cell were measured as a function of an externally applied electrical bias and other parameters such as sensitiser employed and electrolyte composition.

The kinetic competition was successfully modelled by extending a continuous time random walk model for the recombination reaction to include a reaction pathway with the iodide anions. The implications of these findings are discussed in relation to the functioning of liquid electrolyte based cells. These studies were extended to complete solar cells where photoinjected electrons can also react with tri-iodide in the electrolyte.

Further studies assessed the function of solar cells fabricated with PPV and fullerene derivatives, blended on a nanometer scale. In these cells the transport of photogenerated carriers to the electrodes is in competition with charge recombination.Trapping of photogenerated positive polarons MDMO-PPV^{+} is found to play an important role in these films and a "mobility edge" is found.

Contents

Title 1

Acknowledgements 3

Abstract 4

Contents 5

List of tables 12

List of figures 13

Abbreviations 21

Chapter 1 23

1. Introduction 24

1.1 Solar energy conversion 24

1.1.1 Inorganic solar cells 25

1.1.2 Dye sensitised solar cells (DSSCs) 25

1.1.3 Plastic (conjugated polymers) solar cells 26

1.2 Different types of solar cells and their principles of operation 27

1.2.1 Crystalline silicon (c-Si) solar cells 27

1.2.2 Dye sensitised solar cells 29

1.2.3 Plastic solar cells 33

1.2.3.1 Conducting polymers and the 2000 Nobel Prize in Chemistry 33

1.2.3.2 Photophysics of conducting polymers 34

1.2.3.3 Donor/Acceptor architectures and plastic solar cells 35

1.3 Similarities and differences 39

1.4 Key issues adressed in this thesis 40

1.4.1 Importance of charge recombination dynamics in DSSCs and PSCs 40

1.4.2 This thesis 41

Chapter 2 42

2. Experimental Techniques 43

2.1 Introduction 43

2.2 Sample preparation 43

2.2.1 Preparation of nanocrystalline titanium dioxide films 43

2.2.1.1 Preparation of titanium dioxide colloidal paste 43

2.2.1.2 Deposition of titanium dioxide on glass substrates 44

2.2.1.3 Film sintering 45

2.2.2 Dye sensitisation 46

2.2.2.1 Sensitising dyes employed 46

2.2.2.2 Preparation of dye solutions and sensitisation procedure 47

2.3 Experiments in a three electrode electrochemical cell 47

2.3.1 Description of the three-electrode cell 48

2.3.2 The application of an external potential 49

2.3.3 Choice of electrolytes 49

2.3.3.1 Electrolytes for dye sensitised electrodes experiments 49

2.3.3.2 Electrolytes for solar cells 49

2.4 Dye sensitised solar cells 49

2.5 Plastic solar cells and reference samples 51

2.5.1 Devices 51

2.5.2 Reference samples 52

2.6 Transient absorption spectroscopy 52

2.6.1 Theory 53

2.6.2 Origin of the transient signals 54

2.6.3 Calculating changes in optical density 55

2.7 Transient absorption apparatus 56

2.7.1 Pump light source 56

2.7.2 The microsecond transient absorption (MTA) spectrometer 56

2.7.3 The nanosecond transient absorption (NTA) spectrometer 57

2.8 Transient absorption experiments 59

2.8.1 Basic transient absorption experiments 59

2.8.2 Experiments as a function of electrical bias 59

2.8.3 Experiments under white light 59

2.9 Other experimental techniques 60

2.9.1 Steady state UV/visible absorption spectroscopy 60

2.9.2 Photocurrent measurements of solar cells 60

2.10 Conclusions 61

Chapter 3 62

3. Kinetic competition in dye sensitised electrodes 63

3.1 Introduction 63

3.1.1 Competing reactions in dye sensitized electrodes 63

3.1.2 Charge recombination k_{CR1} 64

3.1.3 The I^-/I_3^- redox couple and the mechanism of the regeneration reaction 69

3.1.4 Aims of the chapter 74

3.2 Materials and methods 75

3.3 Results 77

3.3.1 Charge recombination in propylene carbonate 77

3.3.2 Dye cation regeneration kinetics 79

3.3.2.1 Results 79

3.3.3 Sensitiser dye dependence **82**

3.3.3.1 Results **83**

3.3.4 Kinetics in presence of iodine **86**

3.3.4.1 Results **86**

3.3.5 Kinetic competition in presence of an externally applied bias **87**

3.3.5.1 Materials and methods **87**

3.3.5.2 Results **87**

3.3.6 Summary of results **89**

3.3.7 Numerical modeling **91**

3.3.7.1 CTRW modeling of the charge recombination reaction **91**

3.3.7.2 Extending the CTRW model to the kinetic competition **94**

3.4 Discussion **98**

3.4.1 Charge recombination (k_{CR1}) **99**

3.4.2 Dye regeneration reaction (k_{RG}) **99**

3.4.3 Iodide concentration dependence of k_{RG} **100**

3.4.4 The dye cation kinetics are not monoexponential when k_{RG} dominates **101**

3.4.5 Comparison with other studies **102**

3.4.6 Nature and decay of regeneration reaction products **102**

3.4.7 Implications for solar cell function **104**

Chapter 4 **106**

4. Kinetic competitions in dye sensitised solar cells **107**

4.1 Introduction **107**

4.1.1 Recombination losses in dye sensitised cells **108**

4.1.2 General i-V characteristics of solar cells **109**

4.1.3 Relationship between i-V characteristics and recombination losses **112**

4.1.4 Frequency domain studies **113**

4.1.5 Aims and methodology **115**

4.2 Materials and methods **116**

4.3 Results and discussion **118**

4.3.1 Transient kinetics in the dark **118**

4.3.2 Transient kinetics under illumination: k_{CR1} in propylene carbonate **120**

4.3.3 Transient absorption studies under white light: acetonitrile cells **122**

4.3.4 Transient absorption studies under white light: PC cells **124**

4.3.5 i-V characteristics **126**

4.4 Conclusions **128**

Chapter 5 **130**

5. Charge recombination in PPV / C_{60} blends **131**

5.1 Introduction **131**

5.1.1 Conducting polymers / fullerene solar cells **131**

5.1.2 Time and frequency domain transient absorption **134**

5.1.3 The bulk heterojunction picture **136**

5.1.4 Charge recombination vs. charge transport **138**

5.1.5 Aims of this chapter **139**

5.2 Materials and methods **140**

5.2.1 Samples studied **140**

5.2.2 Transient absorption measurements **141**

5.3 Results **142**

5.3.1 i-V characteristics of the complete cells **142**

5.3.2 Transient absorption kinetics 143

5.3.3 Absorption spectrum of the observed transient species 144

5.3.4 Excitation power dependence 146

5.3.5 Spin casting solvent dependence 150

5.3.6 Experiments under white light illumination 151

5.4 Discussion 152

5.4.1 Assignment of transient spectrum: polarons 152

5.4.2 Power law kinetics and excitation power dependence 153

5.4.3 Model: Shklovskii vs. CTRW 157

5.4.4 Blend morphology and localised polaron density 159

5.4.5 Implications for cell function 159

5.5 Conclusions 162

Chapter 6 163

6. Conclusions and further work 164

Appendix: Standard solar cells efficiencies 166

List of publications 167

Bibliography 168

The difference in approach between the British and Continental science is illustrated by another story of James's. In 1931 he went as a Rockfeller Fellow to Leipzig, which counted among its reigning luminaries both Heisenberg and Debÿe. What struck James was the impressive learning in theoretical physics and mathematics not only of the leaders, as might have been expected, but also of all the junior workers. As Cambridge undergraduates in physics they had hardly been exposed to any formal teaching in mathematics, and James had learned it only as it was needed in various parts of physics.

The lack of rigorous training among their English contemporaries had not gone unnoticed by their German counterparts. "Tell me", said one of James's colleagues, emboldened after several months acquaintance, "How does Bragg discover things? He doesn't know anything."

Sir Aaron Klug, FRS, OM

List of Tables

Table 1.1: *Comparison of best efficiencies under standard conditions obtained with various types of solar cells (Green et al. 2002). * 11.0 ± 0.5 % for a 0.25 cm^2 cell, ** not certified, research results (Shaheen et al. 2001; Brabec et al. 2002) under 80 mW/cm^2 AM 1.5 illumination (AM 1.5 spectral mismatch 0.753 in the 2.5% case).* 25

Table 1.2: *Comparison of some of the characteristics of crystalline silicon, dye-sensitised and conjugated polymer - fullerene solar cells.* 39

Table 2.1: *Sensitising solutions for the dyes employed.* 47

Table 3.1: *Summary of the most relevant literature results on the iodide reaction at dye sensitised colloids, films and solar cells as of early 2002.* 72

Table 3.2: *Excitation and probe wavelength for transient absorption measurements with TiO_2 films sensitised with $Ru(dcbpy)_2(NCS)_2$, $Os(dcbpy)_2(CN)_2$ and ZnTCPP dyes.* 76

Table 4.1: *Electrolytes employed in dye sensitised solar cells studied in this chapter.* 117

List of Figures

***Figure 1.1**: A schematic representation of the junction formed at the interface between lightly p- and n- doped monocrystalline silicon (from Markvart 2000).* 27

***Figure 1.2**: Structure of the most popular dye employed in dye sensitised solar cells:* cis-*bis (thiocyanato) bis (2,2'-bypiridine-4,4'-dicarboxylato) ruthenium(II) di-(tetrabutylammonium), often referred to as $Ru(dcbpy)_2(NCS)_2$ or N719.* 29

***Figure 1.3:** Diagram illustrating a liquid dye sensitised nanocrystalline solar cell. The cell consists of the dye sensitised TiO_2 film, the platinum counter electrode and the redox active electrolyte. Absorption of incident light by adsorbed dye molecules is enhanced by the high surface area of the film resulting from sintered semiconductor particle size (average diameter ~ 15 nm).* 30

***Figure 1.4:** Energy diagram for the kinetic steps in a dye-sensitised solar cell. Shown are the electron injection step (k_{inj}), dye excited state radiative decay (dotted line), the charge recombination reactions between electrons in the semiconductor and dye cations (k_{CR1}) and triiodide (k_{CR2}) and the dye regeneration reaction by iodide (k_{RG}). The origin of the open-circuit voltage V_{OC} given by the difference of the Fermi level in the semiconductor and the redox potential of the iodide/triiodide couple is also shown.* 31

***Figure 1.5**: Donor-Acceptor architectures employed in organic solar cells. A blend, double layer and laminated device approaches are shown (from Petrisch 2000).* 36

***Figure 1.6**: Comparison of transmission spectra and external quantum efficiency (IPCE) for MDMO-PPV: PCBM (1:4 w/w) devices spin cast from toluene or chlorobenzene. In the latter case the internal quantum efficiency is close to 100 % (Shaheen et al. 2001).* 37

***Figure 1.7:** Schematic diagram of a MDMO-PPV : PCBM solar cell (Brabec, Sariciftci, and Hummelen 2001) Light absorption results in $\pi \rightarrow \pi^*$ photoexcitation of the conjugated polymer and ultrafast electron transfer to the fullerene acceptor unit resulting in delocalised cations on the PPV backbone (positive polarons) and fullerene anions. Charges are collected at the Al (electrons) and ITO (holes) electrodes, respectively.* 38

***Figure 2.1:** The doctor blade technique. The conducting glass slide was fixed to the working surface with Scotch® tape that also determines the thickness of the final film. A drop of colloidal paste was spread between the spacer tapes with a glass rod.* 44

***Figure 2.2:** Scanning Electron Micrograph of a TiO_2 nano-crystalline film. The highly porous nature of the films is clear.* 45

Figure 2.3: *Structure of dyes employed. $Ru(dcbpy)_2(NCS)_2$, Zn-tetra-carboxy-phenyl-porphyrin (ZnTCPP) and $Os(dcbpy)_2(CN)_2$.* 46

Figure 2.4: *The three-electrode cell. The bottom of the cell is especially designed for optical experiments. The middle electrode is the working electrode made of a platinum wire supported by a glass rod. The conducting glass with the dye sensitised TiO_2 film is inserted in a PTFE pocket where the connection between the wire and the conducting glass is achieved and acts as the working electrode (WE). The left-hand side electrode is the counter electrode (CE) consisting of a platinum wire. The right hand side electrode is the Ag/AgCl reference electrode connected to the main cell by a salt bridge.* 48

Figure 2.5: *Schematic of a DSSC assembled at Imperial College (courtesy of Richard Monkhouse). The active area is approximately 1 cm^2. The working and counter electrodes are sealed with a Surlyn® square gasket. The electrolyte is introduced in the air pocket through holes sand-blasted in the counter electrode and sealed with Surlyn®.* 51

Figure 2.6*: Schematic of a conducting polymer solar cell. The active layer is a 100 nm thick blend of MDMO-PPV and PCBM (a soluble derivative of fullerene). It is sandwiched between the negative (20 nm thick aluminium with a 0.6 nm LiF layer in contact with the blend) and positive (ITO glass covered with PSS:PEDOT) electrodes.* 52

Figure 2.7: *Schematics of the Microsecond Transient Absorption spectrometer. The nitrogen laser pumped dye laser provides the excitation source. A stabilised tungsten lamp provides the probe beam. The first monochromator is used to choose the probe wavelength while the second monochromator helps to reduce the amount of scattered light and sample emission reaching the detector photodiode.* 57

Figure 2.8: *Nanosecond transient absorption (NTA) spectrophotometer shown in both transmission and reflection mode. The excitation source is a nitrogen laser pumped dye laser while the probe beam is provided by a laser diode (830 nm).* 58

Figure 2.9: *Simplified schematics of the apparatus employed to measure the i-V characteristics of solar cells. A xenon lamp provides the light source and its spectral composition is adjusted with an AM 1.5 solar filter. The potentiostat is controlled by a PC and the i-V curves are recorded with software developed by Richard Monkhouse.* 60

Figure 2.10: *Comparison between the spectral composition of AM 1.5 and a tungsten lamp (black body @ 3200K) and the sun black body radiation.* 61

Figure 3.1: *Schematic diagram showing the main interfacial electron transfer steps involved in a dye-sensitised cell. D is the $Ru(dcbpy)_2(NCS)_2$ dye. Highlighted are the recombination of electrons with dye cations k_{CR1} and the dye cations regeneration by iodide k_{RG}. The competition between these two reaction pathways is the subject of the experiments presented in this chapter.* 64

Figure 3.2*: Dependence of the charge recombination reaction dynamics as a function of the electrical potential applied to a $Ru(dcbpy)_2(NCS)_2$ electrode. All potentials vs. Ag/AgCl (From Haque et al. 2000).* 66

Figure 3.3: *Schematic illustration of the Continuous Time Random Walk (CTRW) performed by the electrons in the TiO_2 film. Electron transport is diffusion-limited with the trapped electrons de-trapping after, on average, the time required for thermal activation from the trap currently occupied. The shape of the density of trap states is chosen to be exponential. The model predicts stretched exponential dye cation kinetics (Nelson 1999).* 67

Figure 3.4: *Double logarithmic plot of the initial number of electrons per nanoparticle after excitation by laser pulse against the $t_{50\%}$ of the charge recombination kinetics for a $Ru(dcbpy)_2(NCS)_2$ sensitised TiO_2 electrode in 0.1 M tetra-butyl ammonium triflate in ethanol. The straight line is the best fit to the data. n was determined by spectroelectrochemical measurements (Nelson et al. 2001).* 68

Figure 3.5: *Transient absorption spectra measured 4 μs after excitation for a $Ru(dcbpy)_2(NCS)_2$ sensitised film covered in 0.1M $LiClO_4$ in propylene carbonate.* 77

Figure 3.6: *Kinetic decays for a $Ru(dcbpy)_2(NCS)_2$ sensitised TiO_2 film in a three electrode cell measured as a function of externally applied bias. The electrolyte was 0.1 M $LiClO_4$ in propylene carbonate. All voltages vs. Ag/AgCl. The excitation wavelength was 620 nm and the signal was probed at 800 nm where the dye cation absorbs.* 78

Figure 3.7: *Kinetic decays for a $Ru(dcbpy)_2(NCS)_2$ sensitised film measured as a function of iodide concentration. The electrolytes consisted of $LiClO_4$ and LiI in propylene carbonate, with the lithium perclorate concentration adjusted to maintain a constant Li^+ concentration (0.1 M) and iodide concentrations as indicated in the figure. Also shown is an expansion of data collected at early times for the 0 and 100 mM I^- concentrations, respectively.* 79

Figure 3.8: *Comparison of the transient absorption spectra measured for a $Ru(dcbpy)_2(NCS)_2$ sensitised film immersed in 0.1 M LiI in propylene carbonate. Spectra are shown at A) 10 μs and B) 1 ms after excitation at 620 nm. Also shown (smooth line) is the spectrum of I_2^- determined previously by UV flash photolysis (Devonshire and Weiss 1968; Hug 1981).* 81

Figure 3.9: *Transient absorption decays observed for $Ru(dcbpy)_2(NCS)_2$ (black) and ZnTCPP (grey) sensitised TiO_2 films immersed in 0.1 M LiI in propylene carbonate. In*

the former case the excitation and probe wavelengths were 620 and 800 nm respectively while in the latter these were 560 and 740 nm. 84

***Figure 3.10**: Comparison of the transient absorption spectra measured for a ZnTCPP sensitised film immersed in 0.1 M LiI in propylene carbonate. Spectra are shown at 10 μs (black) and 1 ms (grey) after excitation at 560 nm. The long lived product has a spectra similar to the products at 1 ms observed with $Ru(dcbpy)_2(NCS)_2$ sensitised films.* 84

***Figure 3.11:** Kinetic decays for a $Os(dcbpy)_2(CN)_2$ sensitised film measured in a redox inactive electrolyte (EC:PC 1:1, black) and in the presence of 0.1 M lithium iodide in propylene carbonate (grey). The excitation and probe wavelengths were 530 and 430 nm respectively. The experiment monitors the recovery of the dye ground state bleach. In the presence of iodide the signal becomes positive at approximately 800 μs as products of the dye regeneration reaction are formed.* 85

***Figure 3.12:** Transient kinetic decays recorded for a $Ru(dcbpy)_2(NCS)_2$ sensitised film in 0.1 M LiI in propylene carbonate (black) and with the addition of 0.01 M I_2 to the electrolyte (grey). The dye regeneration kinetics is unaffected while the decay of the products accelerates slightly.* 86

***Figure 3.13:** Transient absorption decays observed at 800 nm for $Ru(dcbpy)_2(NCS)_2$ sensitised films as a function of externally applied bias in a three electrode cell in 0.1 M LiI propylene carbonate. The kinetics are not effected by the applied bias up to -0.5 V vs. Ag/AgCl where a small decrease in I_2^-/e_{TIO2} yield is just noticeable (grey line).* 88

***Figure 3.14:** Transient absorption decays at 800 nm for $Ru(dcbpy)_2(NCS)_2$ sensitised films as a function of externally applied bias in a three electrode cell in 0.03 M LiI and 0.07 M $LiClO_4$ propylene carbonate. The bias applied ranged from 0 to -0.5 V vs. Ag/AgCl. The dye regeneration reaction k_{RG} prevails at potentials > -0.2 V while at potentials ≤ -0.2 V kinetic competition with the charge recombination reaction k_{CR1} is observed, resulting in a reduction of products yield.* 89

***Figure 3.15:** Comparison of the theoretical prediction of the charge recombination rate k_{CR1} as a function of the number of electrons per particle (in turn, the applied electrical bias) for: A) CTRW, B) hopping C) diffusion of the electrons through the semiconductor (from Nelson et al. 2001).* 93

***Figure 3.16:** Bias dependent charge recombination kinetics for a $Ru(dcbpy)_2(NCS)_2$ sensitised TiO_2 film in 0.1 M $LiClO_4$ in propylene carbonate (data from figure 3.5) All voltages vs. Ag/AgCl. Superimposed are fittings of the data (continuous line) in terms of a Continuous Time Random Walk performed by the electrons through an exponential distribution of trap states. (modelling by Dr. Jenny Nelson in the Physics Department).* 94

***Figure 3.17:** Comparison of experimental transient absorption data at 800 nm (+) with CTRW model calculations (smooth lines) (a) as a function of iodide concentration in the absence of applied bias and (b) as function of applied bias with a iodide concentration*

of 0.03 M. Data for (a) and (b) taken from figures 3.6 and 3.14 respectively. (a) data and model calculations for iodide concentrations of 0, 1, 30 and 100 mM, (b) data and model calculations for applied bias of -0.3, -0.4 and -0.5 V vs. Ag/AgCl in 0.03 M LiI. 97

Figure 4.1: *Recombination loss mechanisms in dye sensitised solar cells in the dark under applied bias (V_{ext}, left) and under illumination (right). In the dark, electrons reduce I_3^- to I^- in the solution. Under illumination they can also react with dye cations in competition with I^-. The latter recombination route is often neglected, but may be significant at voltages approaching open circuit conditions.* 108

Figure 4.2: *Generic i-V curves of a solar cell in the dark (grey) and under illumination (black). The open circuit voltage V_{OC} and short-circuit current i_{SC} correspond to the intersection with the x (V) and y (A) axis respectively. The inner rectangle corresponds to the maximum power point (i_{max}, V_{max}) and defines the fill-factor FF.* 109

Figure 4.3*: Equivalent circuit diagram employed to simulate a solar cell. All components are ideal. A current source i_L represents the light-generated current and the diode D account for the non-linear voltage dependence. R_s and R_{sh} are the series and shunt resistance of the device. R_L represents an external load. The cell output voltage is V_{ext} while the junction voltage is $V_j = V_{ext} + iR_s$.* 110

Figure 4.4: *Transient absorption kinetics in the dark for a standard acetonitrile cell (A1, black) and two cells employing propylene carbonate electrolytes (standard B_1, grey and 0.1 M iodide B_2, light grey).* 118

Figure 4.5: *Plot of log $t_{50\%}$ vs applied potential to the dye sensitized TiO_2 electrode in a three electrode electrochemical cell, employing different electrolytes in propylene carbonate: (triangles) 0.1 M $LiClO_4$;(circles) 0.1 M $NaClO_4$;(squares) 0.1 M $NaClO_4$ with additional 0.5 M tert-butyl-pyridine.* 119

Figure 4.6*: Charge recombination kinetics probed at 800 nm in the dark (black) and under white light illumination from the tungsten lamp (grey). The incident power in the latter case is approximately ¼ of a Sun.* 121

Figure 4.7: *Transient absorption spectroscopy of a standard acetonitrile solar cell in the dark (black) and under white light (¼ Sun) at open circuit (grey, 675 mV) and in short circuit conditions (light grey, i= 2.67 mA). The cation decay kinetics and the I_2^- /e_{TiO2} formation yield are unaffected by the applied voltage. The products lifetime is strongly reduced by the background illumination and slightly reduced at short circuit.* 123

Figure 4.8: *Transient absorption spectroscopy of a propylene carbonate solar cell (electrolyte B_1) in the dark (black) and under white light (¼ Sun) both at open circuit (dark grey, 676 mV) and at short circuit (light grey, i=2.3 mA). The cation decay*

kinetics are faster under white light and become even faster at open circuit voltage conditions. The product yield is affected by both the white light and the voltage. The products' lifetime is strongly reduced by the background illumination and increases at open circuit voltage. 124

Figure 4.9: *Transient absorption spectroscopy of a propylene carbonate solar cell (electrolyte B2) in the dark (black) and under white light (¼ Sun) both at open circuit (dark grey, 635 mV) and at short circuit (light grey, 1.8 mA). The cation decay kinetics are faster at open circuit. The I_2^- / e_{TiO2} formation yield is affected by both the white light and the voltage. The lifetime is strongly reduced by the background illumination and increases at open circuit voltage.* 125

Figure 4.10: *i-V characteristics of a standard acetonitrile (electrolyte A1) DSSC in the dark (black) and under white light (grey) from the probe beam of the MTA. The incident white light was approximately ¼ of a Sun in intensity.* 126

Figure 5.1: *Chemical structure of MEH-PPV, MDMO-PPV, C_{60} and PCBM.* 132

Figure 5.2: *Schematic illustration of a MDMO-PPV: PCBM solar cell (courtesy of Dr. Christoph Brabec).* 133

Figure 5.3: *Polaron-exciton, positive polaron, negative polaron, positive bipolaron, negative bipolaron (from J. J. Dittmer Ph.D. thesis adapted from N. C. Greenham and R. H. Friend in Solid State Physics – Advances in Research and Applications, edited by H. Ehrenreich and F. Spaepen (Academic Press, New York, 1995) vol. 49 p.1* 135

Figure 5.4: *The Bulk Heterojunction concept. The simplified diagram shows the energy levels of a MEH-PPV/C_{60} bulk heterojunction system taken as example under flat band conditions (higher half) and under short circuit conditions (lower half) and does not take into account possible interfacial barriers at the metal/semiconductor interface (from Brabec et al. 2001).* 136

Figure 5.5: *AFM images showing the morphology of MDMO-PPV:PCBM (1:4 in weight) spin cast from toluene (left) and chlorobenzene (right); (from Shaheen et al. 2001).* 137

Figure 5.6*: Absorption spectrum of a MDMO-PPV: PCBM 1:4 w/w blend deposited from chlorobenzene.* 140

Figure 5.7*: i-V characteristics of a 7 mm^2 MDMO-PPV : PCBM 1:4 w/w solar cell under 1sun illumination (black) and in the dark (grey). The open circuit voltage is approximately 0.84 V and the short circuit current density of the order of 3 mA / cm^2.* 142

***Figure 5.8**: Microsecond decay kinetics from a MDMO-PPV : PCBM 1:4 w/w device. (transmission mode - complete cell) The excitation wavelength was 500 nm and the signal was probed at 950 nm The decay is long-lived and extends from the instrument response (several hundreds of nanoseconds) to the millisecond time- domain (data by Dr. Sven Södergren)* 143

***Figure 5.9**: Nanosecond transient absorption measured on a MDMO-PPV : PCBM 1:4 w/w blend. A fast (instrument response limited) and a longer lived component (almost constant on this timescale) can clearly be distinguished. The excitation intensity was 80 $\mu J\ cm^{-2}$ per pulse.* 144

***Figure 5.10:** (a) Transient absorption spectra of a MDMO-PPV/PCBM blend obtained 125 μs after excitation at 500 nm (80 $\mu J.cm^{-2}$ per pulse), T = 300 K; (b&c) Frequency domain photoinduced absorption spectra of (b) pristine MDMO-PPV and (c) of a MDMO-PPV/PCBM blend employing excitation at 488 nm with 40 mW and 132 Hz modulation, T = 100 K (courtesy of Dr. Gerald Zerza).* 145

***Figure 5.11**: Nanosecond flash photolysis excitation power dependence. The signal is affected by electronic noise from the amplifiers. It is nevertheless obvious that the fast spike has a strong power dependence while the amplitude of the slower phase is hardly affected by the excitation power.* 147

***Figure 5.12:** Laser excitation power dependence of kinetics observed pumping MDMO-PPV : PCBM 1:4 w/w from chlorobenzene at 500 nm and probing at 940 nm. The microsecond timescale is reported here. The excitation power ranged between about 80 and 2 $\mu J/pulse\ x\ cm^2$. The range is further extended in the inset where 2, 0.22 and 0.03 $\mu J/pulse\ x\ cm^2$ are compared.* 148

***Figure 5.13:** Relative amplitude of the transient absorption signal for a MDMO-PPV/PCBM blend as a function of laser excitation power: (--●--) amplitude of instrument response (~ 20 ns) limited decay; (--▲--) transient signal at 50-100 ns; (--■--) transient signal at 100-400 μs.* 149

***Figure 5.14:** Micro-millisecond decay kinetics at the threshold excitation energy E_{th}.(2 $\mu J\ cm^{-2}$ per pulse) The decay follows a power law with $\alpha = 0.4 \pm 0.02$.* 149

***Figure 5.15:** MDMO-PPV polaron dynamics of MDMO-PPV / PCBM heterojunctions cast from chlorobenzene (black) and toluene (grey) solutions. The charge recombination dynamics is indistinguishable in the two samples.* 150

***Figure 5.16**: Comparison between kinetics observed exciting a MDMO-PPV: PCBM 1:4 blend cast from chlorobenzene in the dark (A) and under approximately ¼ of a sun ($I \sim 25\ mW\ cm^{-2}$) power (B, tungsten lamp spectral composition, see chapter 2).* 151

***Figure 5.17:** Schematic representation of the energy levels available to photogenerated polarons in MDMO-PPV / PCBM blends. A certain amount of localised states*

(inhomogeneous broadening) lie at the lowest energy extending into the bandgap of MDMO-PPV, while at higher energy a thicker manifold of states are present. 154

Figure 5.18: *Photoinduced population of the energy level available to MDMO-PPV polarons (as of figure 5.17) under different excitation density levels. Excitation density levels smaller (a), comparable (b) and exceeding (c) an excitation energy threshold E_{th} characteristic of the material.* 155

Figure 5.19: *Pictorial representation of photoinduced polaron dynamics in a blend under steady-state white light background illumination picoseconds and milliseconds after pulsed excitation. A steady state of polarons occupying the lower localised states is present at all times and the tail of states available to polarons produced by the laser pulse is effectively cut off resulting in faster recombination of the polarons whose energy is closer to the continuum of states.* 160

Abbreviations

AM 1.5	Air Mass 1.5
CE	Counter Electrode
c-Si	monocrystalline silicon
CW	Continuous Wave
DC	Direct Current
DSSC	Dye-Sensitised Solar Cell
ΔOD	change in Optical Density
ECD	Equivalent Circuit Diagram
EPFL	Ecole Polytechnique Federal Lausanne, Switzerland
FT-IR	Fourier Transform - InfraRed
IPCE	Incident Photons to Current Efficiency
ITO	Indium Tin Oxide
LED	Light Emitting Diode
MEH-PPV	poly(2-methoxy, 5-(2'-ethyl-hexyloxy)-p-phenylene-vinylene]
MDMO-PPV	poly(2-methoxy-5-(3,7-dimethyloctyloxy)-1,4-phenylene vinylene))
MTA	Microsecond transient absorption
N3	*cis*-bis (thiocyanato) bis (2,2'-bypiridine-4,4'-dicarboxylic acid) ruthenium(II)
N719	*cis*-bis (thiocyanato) bis (2,2'-bypiridine-4,4'-dicarboxylato) ruthenium(II) di-(tetrabutylammonium)
NTA	Nanosecond transient absorption
OD	Optical Density
OLED	Organic Light Emitting Diode
PCBM	(1-(3-methoxycarbonyl)-propyl-1-1-phenyl-(6,6)C_{61})
PEDOT	[poly(poly(3,4-ethylenedioxythiophene)]
PIA	PhotoInduced Absorption
PPV	poly-*p*-phenylenevinylene
PSC	plastic solar cell
PSS	poly(styrenesulfonate)
PTFE	poly-tetra-fluoro-ethylene
SCE	standard calomel electrode

SEM	scanning electron microscopy
TA	transient absorption
TAS	transient absorption spectroscopy
WE	Working Electrode
Wp	Watt-peak
ZnTCPP	Zn-tetra-p-carboxy-phenyl-porphyrin

CHAPTER 1

INTRODUCTION

1 INTRODUCTION

1.1 Solar energy conversion

The simplest definition of a solar cell is that of a device employing solar radiation (photons) to produce electricity (electrons). The power rating of solar cell modules is expressed in Watt-peak (Wp), the power generated at the height of the day in optimal illumination conditions. Nine tenth of the world's yearly shipping of solar cells modules are based on silicon and their total power stands currently at approximately 200 MWp per year - about a fifth of a single nuclear reactor (on a summer sunny day!) - though this figure is increasing by about 20% a year.

Silicon solar cell production is however energy-intensive and the cost of solar cell modules presently stands at about 5 ε / Wp to the end user, still too expensive for photovoltaics to be widely adopted without government subsidies. A key issue is therefore the reduction in the cost of photovoltaic cells. Both the EU and Japan are aiming to bring the cost of solar cell modules down to approximately 1 ε / Wp by the year 2010 and have set ambitious targets of 3 and 5 GWp installed photovoltaics by that year, respectively (XIV European Photovoltaics Conference, Glasgow 2000).

Mono- and poly- crystalline silicon devices have an approximately equal share of 90% of the photovoltaics market. Alternative approaches to all-inorganic solar cells have been pursued in order to produce solar cells from cheaper materials by less energy-intensive approaches. Among those that have received a considerable amount of attention during the last decade are dye-sensitised and, more recently, conjugated polymers solar cells.

The most widely adopted standard for solar cells efficiencies is the electrical power output under the AM 1.5 spectral composition under 1000 W/m^2 irradiation at 25 °C (see Appendix, also for institutions that provide certified efficiencies). The best certified efficiencies achieved by different types of solar cells to date are briefly summarised in table 1.1. The first four entries are all inorganic solar cells while the last two are recent molecular approaches to solar light conversion. This thesis addresses charge recombination processes in these cells.

Cell Type	*Best certified efficiency to date (%)*
monocrystalline Si	24.7 ± 0.5
multicrystalline Si	19.8 ± 0.5
gallium arsenide	25.1 ± 0.8
amorphous Si	12.7 ± 0.4
DSSC	**6.5 ±0.3***
plastic solar cells	**2.5 - 3.3****

Table 1.1: *Comparison of best efficiencies under standard conditions obtained with various types of solar cells (Green et al. 2002). * 11.0 ± 0.5 % for a 0.25 cm^2 cell, ** not certified, research results (Shaheen et al. 2001; Brabec et al. 2002) under 80 mW/cm^2 AM 1.5 illumination (AM 1.5 spectral mismatch 0.753 in the 2.5% case).*

1.1.1 Inorganic solar cells

Commercial silicon solar cells have standard efficiencies in the range of 5 to 15%. Mono-crystalline (c-Si) solar cells require high-grade silicon that is at present mainly provided as a by-product by the electronics industry, a dependency that limits the amount of silicon solar cells that can be produced. Despite unlimited availability of silicon oxide (sand), the purification into c-Si is a highly energy-intensive process and therefore paradoxically linked to the cost of oil. The main factor determining the high cost of silicon solar cells is the high purity requirement for the silicon employed.

The most efficient single junction solar cells reported to date employ gallium arsenide and have reached an efficiency of 25.1% under standard conditions (Green et al. 2002). They are however very expensive and only employed in applications were device costs are not an issue, such as solar panels for satellites. Gallium arsenide is closely followed by crystalline silicon solar cells with a verified maximum efficiency of 24.7% (Green et al. 2002). Amorphous silicon is cheaper but results in lower efficiency solar cells. Alternative materials such cadmium telluride and copper indium selenide are employed in thin film solar cells but involve potential pollution if a module is not disposed of properly.

1.1.2 Dye sensitised solar cells (DSSCs)

The idea of employing dye sensitised titanium dioxide to achieve solar energy conversion was patented in the late seventies (Skotheim 1978). However, the efficiency

of cells was low, primarily limited by the small amount of light that could be absorbed by a dye monolayer on the flat semiconductor surface. The breakthrough was the preparation of what have become known as nanocrystalline films (O' Regan and Grätzel 1991). It is now 11 years since an efficient cell employing this design was first reported. A 11% efficient cell has been certified by the Fraunhofer Institute (although with an area of only 0.25 cm^2) and larger devices with an efficiency of approximately 5% can be routinely assembled. At least one attempt to commercialise dye-sensitised solar cells has failed so far (STA in Australia, last year) though there is still hope for improvement and eventual commercialisation of DSSCs.

1.1.3 Plastic (conjugated polymers) solar cells

The 2000 Nobel Prize for Chemistry was awarded for the discovery of conducting polymers with huge potential in plastic electronics applications. Organic light-emitting diodes have been demonstrated (Burroughes et al. 1990) and photovoltaic devices have been obtained mixing conjugated polymers with suitable electron acceptors (Sariciftci et al. 1992; Granström et al. 1998). The efficiency of these "plastic" solar cells has now reached 2.5-3.3% under 80 mW/cm^2 (Shaheen et al. 2001; Brabec et al. 2002) and attempts to commercialise them are presently in progress (e.g LIOS - Linz Organic Solar cells).

In the next sections the fundamentals of device function for crystalline silicon, nanocrystalline dye-sensitised and conjugated polymer solar cells will be briefly reviewed and compared.

1.2 Different types of solar cells and their principles of operation

1.2.1 Crystalline silicon (c-Si) solar cells

A brief summary of the principles of operation of a mono-crystalline silicon solar cell is given here. Monographs on the subject abound (see for example, Van Overstraeten and Mertens 1986; Markvart 2000). At their heart is a p-n junction between boron (p) and phosphorus (n) -doped silicon. Its formation is illustrated schematically in figure 1.1.

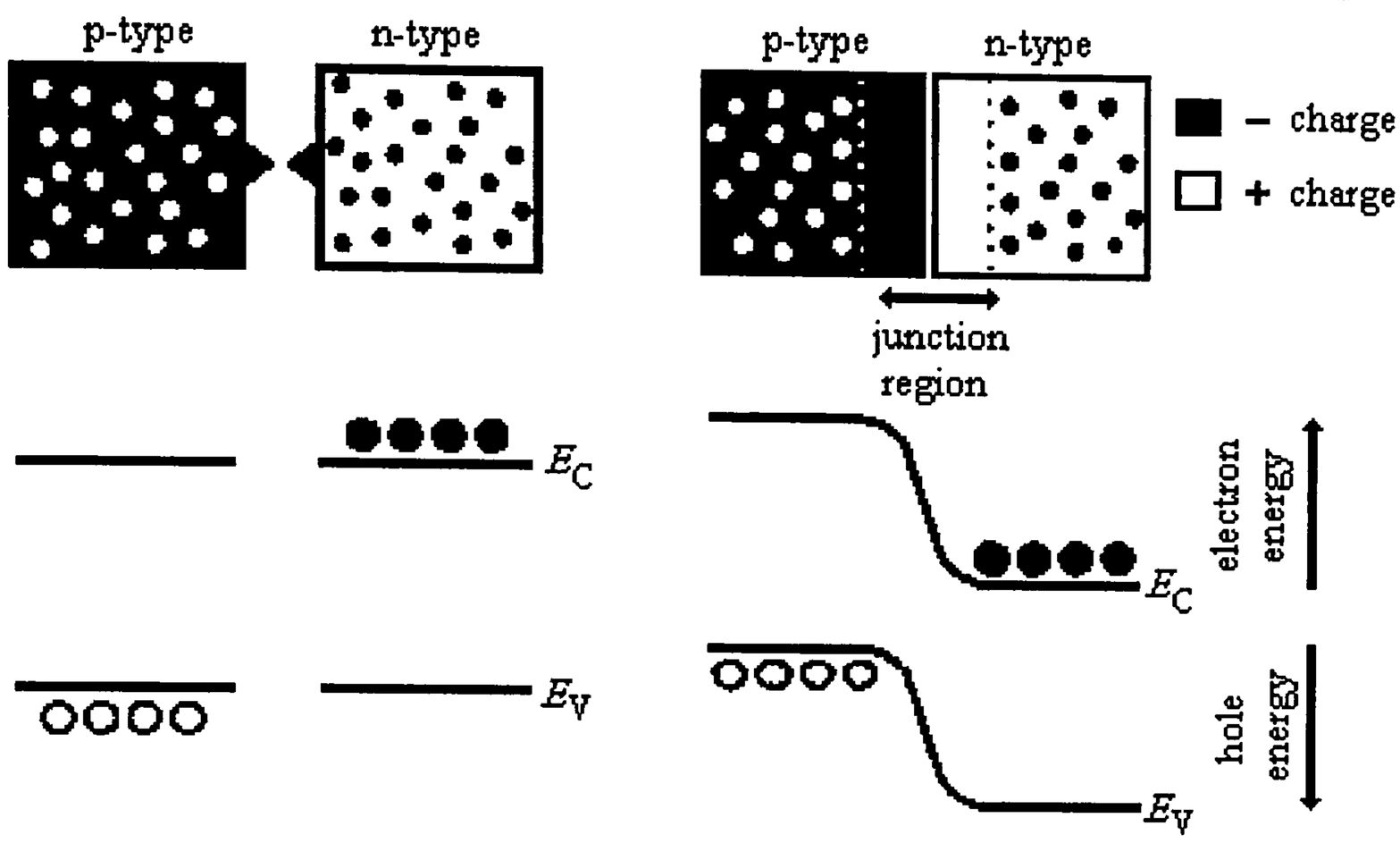

***Figure 1.1**: A schematic representation of the junction formed at the interface between lightly p- and n- doped monocrystalline silicon (from Markvart 2000).*

The contact between p- and n- doped silicon results in some majority carriers (e.g. holes in the p-region, electrons in the n-region) recombining across the junction. The resulting charge imbalance gives rise to an in-built electric field. This area is called the space-charge region. Charge separation takes place when a photogenerated minority carrier reaches the space charge region and is swept across it by the in-built electric field.

A typical c-Si solar cell, starting from the surface exposed to the light, consists of a thin (~ 0.5 μm) layer of phosphorus (n) doped layer followed by the p-n junction extending for another 0.5 μm and a much thicker layer (~ 300 μm) of lightly boron (p) doped silicon. Mono-crystalline silicon is an indirect semiconductor, therefore electronic transitions are only partially allowed resulting in a low extinction coefficient. As a consequence, visible light penetrates in crystalline silicon for hundreds of microns and most of the light is absorbed by the thick p-layer, away from the junction. Photon absorption results in free carrier generation (Fahrenbruch and Bube 1983). The hole

diffuses to the contact and the electron (minority carrier) diffuses to the p-n junction. Low impurity levels (< 1 in 10^7 atoms) are required in order for photogenerated electrons (minority carriers) to diffuse to the p-n junction with minimal charge recombination losses and contribute to the photocurrent. Once the hole and electron are separated by the electric field at the junction, charge recombination is prevented.

The above description introduces the role of diffusive and drift currents in solar cells as summarised in the fundamental equation of electron current density J (Shockley 1949):

$$J_n = qD_n \nabla n + qn\mu_n E \qquad (1.1)$$

The first term is *diffusive* and depends on the electron diffusion coefficient D and electron gradient while the second is the *drift* component dependent on the electric field E and the electron mobility μ. n is the electron concentration and q the elementary charge. The first term of the equation dominates in the thick p-doped layer where charge diffusion to the p-n junction takes place. The second term becomes important at the junction where the electric field separates the charges.

1.2.2 Dye sensitised solar cells

One possible approach to cheaper solar cells consists of using a design that avoids the low impurity requirements of minority carrier diffusion and can therefore be achieved with cheaper materials. Dye sensitised solar cells satisfy these requirements since carrier generation is confined to the semiconductor / electrolyte interface and results in direct injection of electrons and holes into two different phases (semiconductor and electrolyte, respectively), avoiding any requirement for minority carrier transport.

Dye sensitised solar cells employ an approximately 10 μm thick film of sintered titanium dioxide (TiO_2) nanocrystals. TiO_2 is a wide band gap semiconductor and only absorbs in the ultraviolet. Sintered films have a microscopic surface area up to 1000 times larger than their macroscopic one. Monolayer dye coverage is achieved over the large folded surface, resulting in high optical densities (OD >2) in the absorption range of the sensitiser dye. The most popular dye employed is a derivative of tris-bypiridyl complexes of ruthenium, *cis*-bis (thiocyanato) bis (2,2'-bypiridine-4,4'-dicarboxylato) ruthenium(II) di-(tetrabutylammonium) from here on referred to as $Ru(dcbpy)_2(NCS)_2$ (figure 1.2). The nano-structured nature of the electrode gives rise to a huge contact area between the semiconductor and the redox electrolyte in contact with the sensitised film. Light absorption by the dye molecules is confined to this interface.

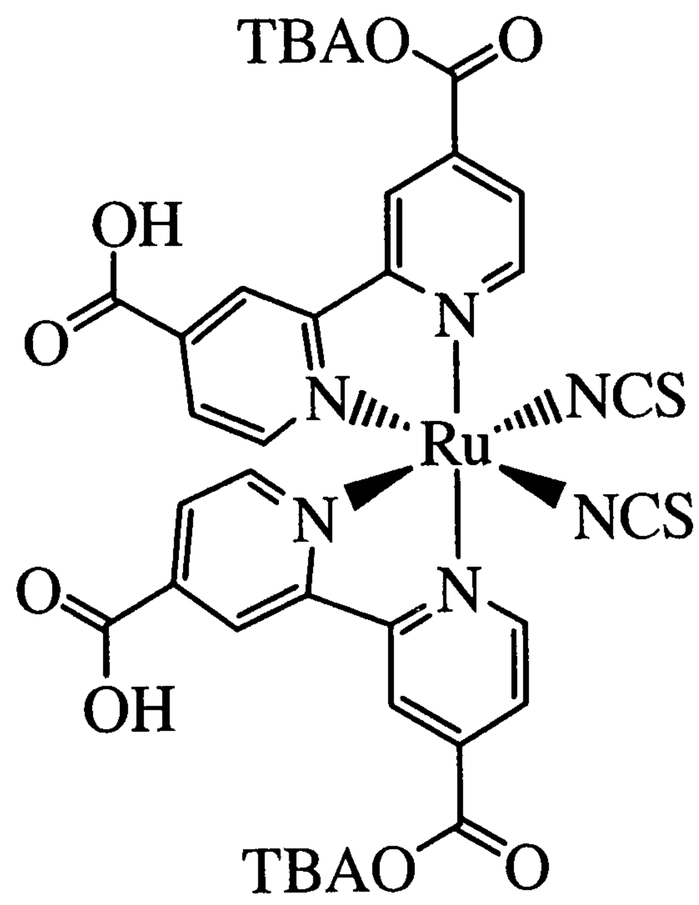

***Figure 1.2**: Structure of the most popular dye employed in dye sensitised solar cells:* cis-*bis (thiocyanato) bis (2,2'-bypiridine-4,4'-dicarboxylato) ruthenium(II) di-(tetrabutylammonium), often referred to as $Ru(dcbpy)_2(NCS)_2$ or N719.*

Figure 1.3 shows schematically a dye sensitised solar cell (DSSC). The dye-sensitised TiO_2 nanocrystalline film is deposited on transparent fluorine doped tin oxide conducting glass (F-SnO_2 glass) to form the working electrode. The counter electrode is an F-SnO_2 glass plate coated with catalytic platinum. The liquid electrolyte contains the iodide-triiodide couple responsible for shuttling electrons between the electrodes. Finding solid state alternatives to the liquid electrolyte is an active area of research at present (Bach et al. 1998; Nogueira, De Paoli, and Durrant 2001).

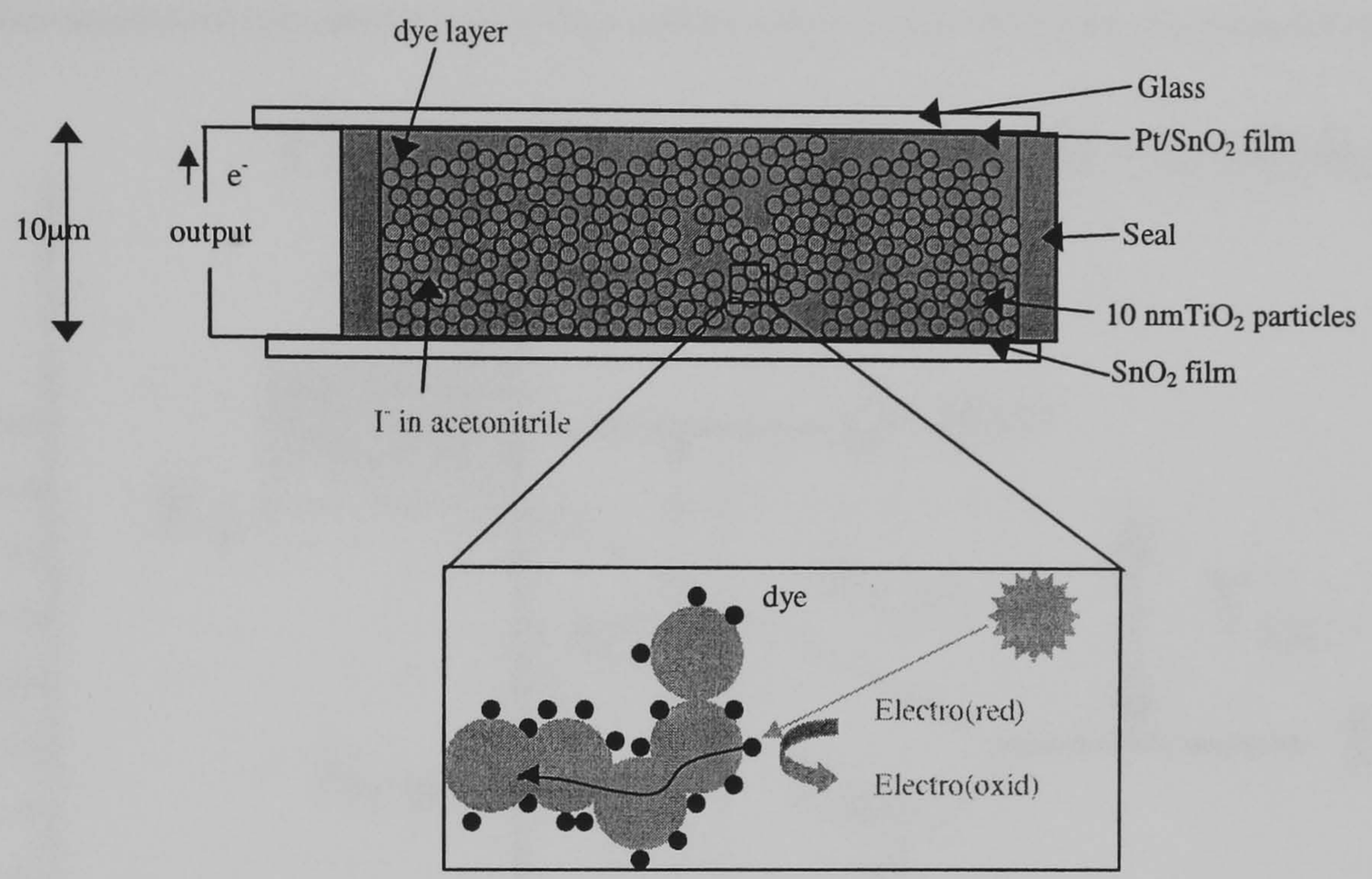

Figure 1.3: *Diagram illustrating a liquid dye sensitised nanocrystalline solar cell. The cell consists of the dye sensitised TiO_2 film, the platinum counter electrode and the redox active electrolyte. Absorption of incident light by adsorbed dye molecules is enhanced by the high surface area of the film resulting from sintered semiconductor particle size (average diameter ~ 15 nm).*

Absorption of visible light by the ruthenium sensitiser leads to photoinduced electron transfer from a molecular excited state to the TiO_2 film. The driving force for charge separation is provided by the difference between the excited state energy and the semiconductor conduction band. Electron transport takes place within the network of inter-connected semiconductor particles to the conducting glass substrate and the external circuit. The size of the particles is thought to be too small to sustain electric fields and charge transport in the semiconductor occurs by diffusion rather than by field induced drift (O' Regan et al. 1990; Cao et al. 1996; Solbrand et al. 1997; Zaban, Meier, and Gregg 1997). In a standard cell the dye is regenerated by the oxidation of I^- to I_3^-. Triiodide needs to diffuse to the counter-electrode where its re-reduction to iodide by electrons from the external circuit is catalysed by the sputtered platinum.

The function of the device is primarily *controlled by the kinetics of interfacial electron transfer reactions* (see for example, Hagfeldt and Grätzel 1995; Grätzel 2001; Gregg, Zaban, and Ferrere 1999). These reactions, and their energetics are summarised in figure 1.4. The open circuit voltage V_{OC} is also shown. The electron injection process (k_{inj}) is in competition with the dye excited state decay to the ground state (dotted line). The regeneration of the dye by iodide (k_{RG}) is in competition with recombination of the injected electrons with the dye cations (k_{CR1}).

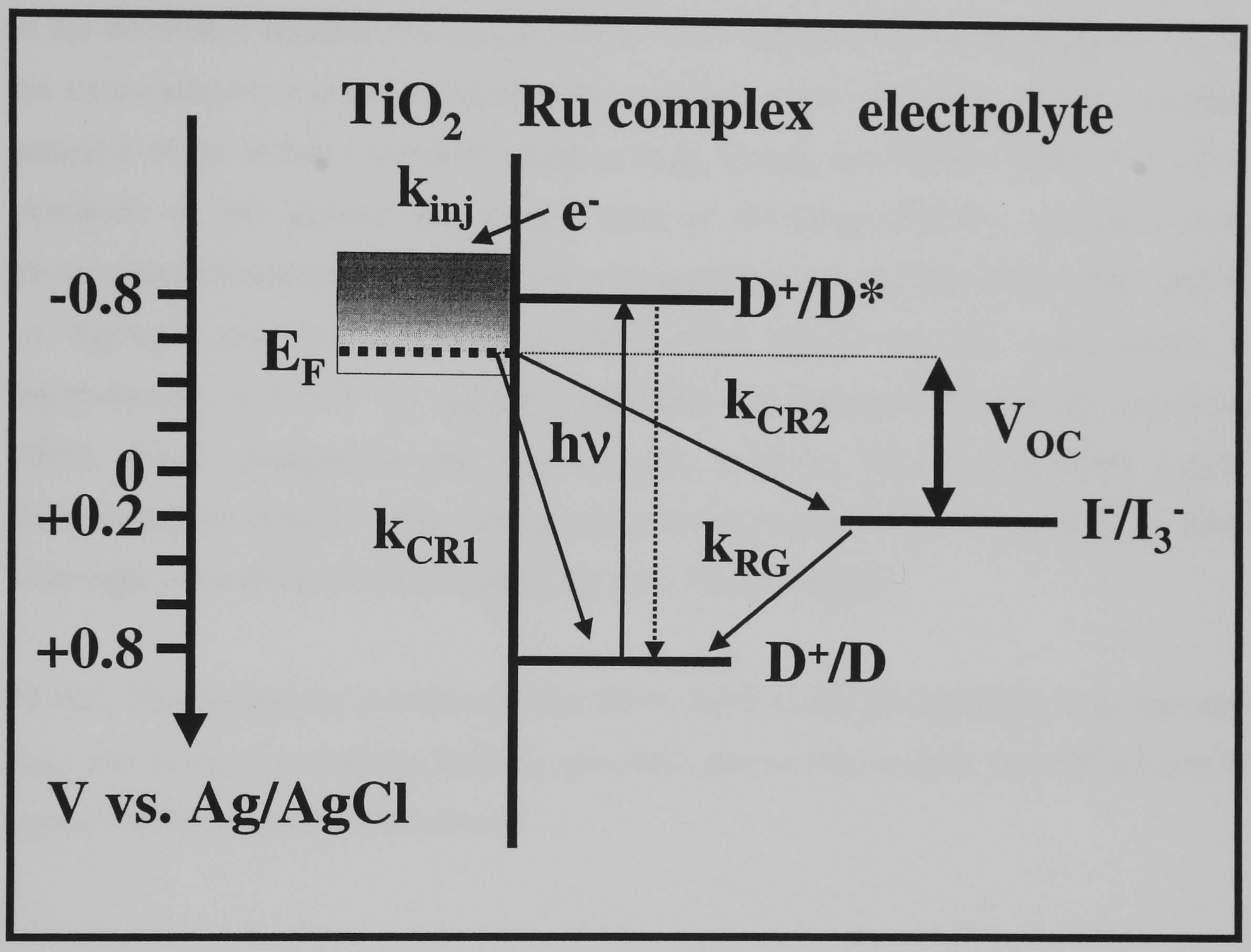

Figure 1.4: Energy diagram for the kinetic steps in a dye-sensitised solar cell. Shown are the electron injection step (kinj), dye excited state radiative decay (dotted line), the charge recombination reactions between electrons in the semiconductor and dye cations (k_{CR1}) and triiodide (k_{CR2}) and the dye regeneration reaction by iodide (k_{RG}). The origin of the open-circuit voltage V_{OC} given by the difference of the Fermi level in the semiconductor and the redox potential of the iodide/triiodide couple is also shown.

Electron transport within the semiconductor particles network competes with charge recombination reactions with dye cations (k_{CR1}) and with the tri-iodide in the electrolyte (k_{CR2}). Both recombination reactions take place at the huge semiconductor / electrolyte interface. Minimising these reactions is therefore central to the functioning of devices.

The high ionic concentration of electrolytes used in most dye sensitised solar cells ensures that no electric field exceeding a range of about 1 nm exist in solution (Gregg, Zaban, and Ferrere 1999). It is generally assumed that the only place where substantial electric fields occur in DSSCs is at the semiconductor / electrolyte interface (across the electrochemical double layer).

The open circuit voltage of a cell (V_{OC} in figure 1.4) is generally thought to correspond to the difference between the (quasi-) Fermi level (represented by E_F in figure 1.4) in the semiconductor and the electrochemical potential of the electrolyte, that is, the redox potential of the iodide / triiodide couple (Gregg, Zaban, and Ferrere 1999). The redox potentials of the ground and excited state of $Ru(dcbpy)_2(NCS)_2$, estimated from electrochemical and photophysical data are reported to be +0.75~0.8 and –0.85~-0.8 V vs. Ag/Agcl, respectively (Tachibana 2000) while that of the I^-/I_3^- redox couple is approximately + 0.15 V vs. Ag/AgCl (Hagfeldt and Grätzel 1995; Myung and Licht 1995). Upon illumination the (quasi)-Fermi level of the semiconductor raises, determining the output voltage. The acceleration of recombination losses as E_F is raised is thought to be the key factor limiting the open circuit voltage.

NOTE: Throughout the reminder of this thesis, for the sake of simplicity, k_{CR1}, k_{RG} and k_{CR2} will be used to indicate both the processes themselves or their rate. Which one is meant will be clear from the context.

1.2.3 Plastic solar cells

1.2.3.1 Conducting polymers and the 2000 Nobel Prize in Chemistry

The birth of semiconducting polymer research can be traced to an attempt by one of Hideki Shirakawa's Ph.D. students to polymerise acetylene in the early 70s. He mistakenly added a thousand times the amount of catalyst required by the published procedure and obtained a shiny aluminium-like film (Ito, Shirakawa, and Ikeda 1974). The product attracted the attention of Alan G. MacDiarmid who was thinking of ways of producing "synthetic metals" - non-metallic substances that could conduct electricity. In 1977 Shirakawa joined MacDarmid and Alan J. Heeger at the University of Pennsylvania to investigate this form of polyacetylene. When they doped it with iodine the conductivity increased by about 7 orders of magnitude opening the way to organic semiconductors research (Shirakawa et al. 1977).

Beside polyacetylene, several other polymers have been found to have semiconducting properties when doped. Among them are polypyrroles, polythiophenes and polyanilines. The long-term goal of this research is the prospect of "conductive plastic" and therefore the possibility of organic electronics, a prospect that has also attracted military research world-wide. Garnier et al. (Garnier et al. 1994) have made a thin-film field-effect transistor with polymerised sexithiophene that can be twisted, rolled and bent without compromising the electrical characteristics of the device. Conducting polymers can also be used in the optoelectronics industry. In 1987 Tang, working at Eastman Kodak, demonstrated that 8-hydroxyquinoline aluminium (Alq_3) can be used as active layer in organic light-emitting-diodes (OLEDs). In 1990 the first LED employing a polymer - poly-*p*-phenylenevinylene (PPV) was reported (Burroughes et al. 1990). Furthermore, it was shown that by blending organic materials of suitable electron affinities and ionisation potentials (a donor D and acceptor A couple) a high quantum efficiency of photoinduced charge separation can be achieved leading to photovoltaic device function (Sariciftci et al. 1992; Granström et al. 1998). The appeal of polymer photovoltaics is mainly related with the possibility of cheap material processing and the prospect of producing flexible solar cells. The Nobel Prize for Chemistry 2000 was awarded to Heeger, MacDiarmid and Shirakawa for their pioneering work on doped polyacetylene.

1.2.3.2 Photophysics of conducting polymers

There has been controversy in the literature on whether a semiconductor band model or one based on excitons (first used to describe electronic properties in molecular organic crystals) is best suited to account for the experimental observations for conducting polymers (Sariciftci 1997). The field is highly multidisciplinary with chemists, physicists and material scientists working side by side. Chemists treating these systems as molecular materials and physicists coming from bulk semiconductors employ different terminologies. This thesis covers both molecular materials and semiconductors and it is therefore useful to define some terms here (see also figure 5.3, page 135):

exciton: a bound electron-hole pair in physicists' jargon. Excitons differ in terms of the amount of correlation between the electron and hole. Spatially confined ones are referred as Frenkel excitons and in many respects correspond to molecular excited states. When the electron is delocalised over many molecular units (crystal lattice elementary cells when a solid is considered) this species is called a Mott-Wannier exciton. Excitons are thought to be associated with a diffusion length that in the case of PPV is of the order of 10 nm (Stübinger and Brütting 2001). A photochemist would probably be satisfied by describing the same process in terms of resonant energy transfer.

polaron: this is a term originating from polar crystal theory to describe the totality of the distortions created in a lattice by the electrostatic imbalance due to the removal or addition of an elementary charge. The term is also employed to describe charged species in semiconducting polymers due to the large distortion of the polymer structure caused by an electronic charge. A PPV cation produced by photoinduced electron transfer to fullerene will have its positive charge delocalised over the π backbone (even of adjacent molecules) and is often referred to as a positive polaron.

Early transient photocurrent measurements in conducting polymers (Lee, Yu et al. 1994) were interpreted in terms of a semiconductor band model while in recent years the excitonic picture has become more widely accepted. In the latter case the photoexcitation process is described in terms of bound electron – hole pairs formation (excitons, normally of the Frenkel type (Peierls 1932; Frenkel 1931)) followed by exciton diffusion and dissociation at oxygen traps or donor / acceptor interfaces

(Petrisch 2000). The latter step is assumed to be associated with an exciton binding energy, which should affect the rate of charge separation, that has been fiercely debated over the last decade. Some research groups believe its value to be of the order of 0.4 eV (Marks et al. 1994; d. Costa and Conwell 1993; Barth and Bässler 1997) while other groups estimated it to be anywhere between 0 (Lee, Janssen et al. 1994) and approximately 1 eV (Chandross et al. 1994). Recently a value of 60 meV for the exciton binding energy in PPV has been reported (Moses et al. 2001).

The value of the exciton binding energy is linked to the semiconductor vs. exciton controversy as no exciton binding energy corresponds to a band description. In the excitonic picture the photoinduced charge separation is thought to lead to the formation of positive and negative polarons (in the case of PPV-C_{60} devices, the former delocalised on the PPV backbone). Charge collection at the electrodes leads to photovoltaic function.

As mentioned above, the term polaron is inherited from polar crystals theory. The systems described in this thesis differ markedly from polar crystals, being amorphous and disordered. However, given the fact that the use of the term polaron for charged intermediates ın these systems is widespread, charged products of photoinduced electron transfer will also be referred to as polarons here. In molecular photochemistry terms an exciton correspond to an excited state and a polaron to a radical ion. Clearly the use of the term "singlet polaron exciton" (Harrison et al. 1996) does not help reducing the confusion in the literature so that some prefer not to take side and use terms such as "primary photoexcitations" (Sariciftci 1997) in conducting polymers. In conclusion it will be many years before a coherent picture of the photophysics of these widely differing and highly disordered materials emerge.

1.2.3.3 Donor / Acceptor architectures and plastic solar cells

A thin-film photovoltaic cell fabricated depositing two layers of copper phthalocyanine and a perylene tetracarboxylic derivative was reported by Tang in a seminal paper in 1986 (Tang 1986). The device function was described in terms of excitons formed in both layers and dissociating at the interface. Though not explicitly mentioned, the phthalocyanine acted as a electron donor (and hole transporting material) and the

perylene as an acceptor. An asymmetry in the energy levels of donor and acceptor molecules is required for efficient charge separation though the ΔG of the charge separation reaction remains poorly understood. Several donor/acceptor (D/A) architectures for organic solar cells have been tested (Petrisch 2000) including depositing separate D and A layers, blending them and laminated devices that can be seen as a hybrid between the two (see figure 1.5). The photoactive layer(s) are usually sandwiched between an electron- (Al) and hole- (ITO) collecting electrodes.

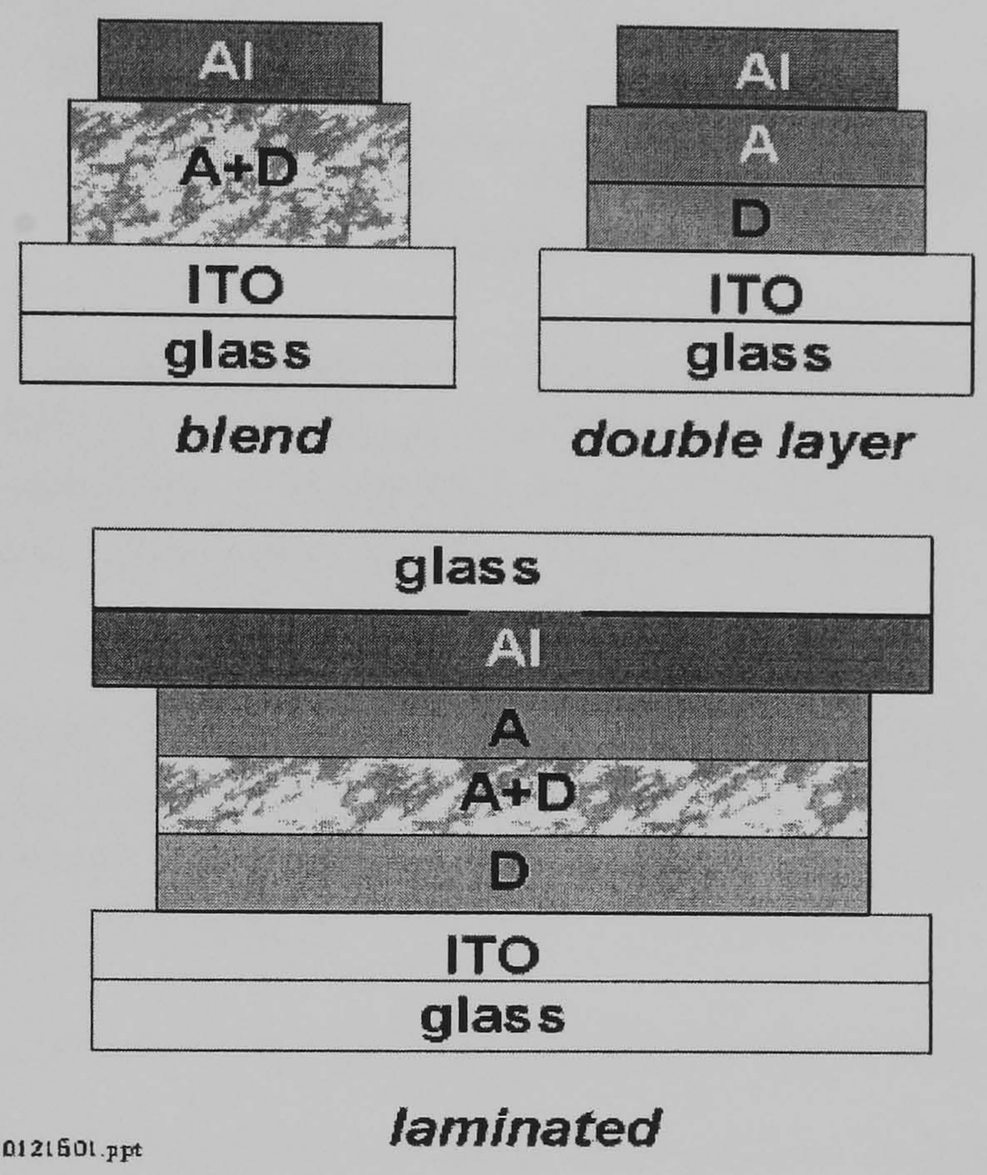

***Figure 1.5**: Donor-Acceptor architectures employed in organic solar cells. A blend, double layer and laminated device approaches are shown (from Petrisch 2000).*

The most efficient conjugated polymer solar cells to date employ a soluble PPV derivative as electron donor and a soluble fullerene derivative as acceptor. The two components are blended in solution and spin-coated on a conducting substrate to yield photoactive films of approximately 100 nm thickness (Brabec, Sariciftci, and Hummelen 2001). The donor and acceptor molecules are in close contact on a nanometer scale and the blending leads to the majority of photogenerated excitons (or excited states in molecular terms) to be within their diffusion length from an electron-accepting fullerene unit, resulting in virtually unity charge separation efficiency. This is illustrated in figure 1.6 where the external quantum efficiency (see Appendix) and absorption characteristics of devices are compared.

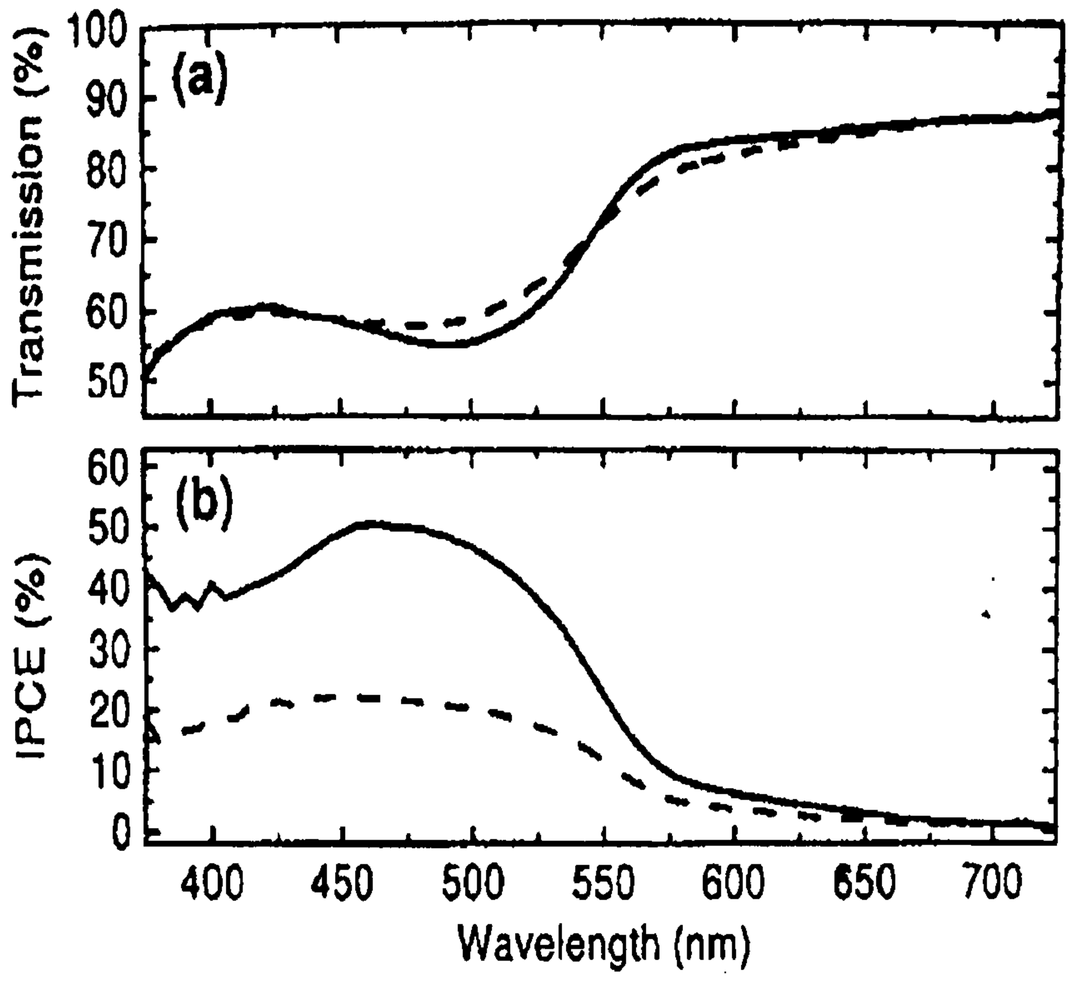

FIG. 3. (a) Optical transmission spectra of 100-nm-thick MDMO-PPV:PCBM (1:4 by wt.) films spin coated onto glass substrates from either toluene (dashed line) or chlorobenzene (solid line) solutions. (b) IPCE spectra for photovoltaic devices using these films as the active layer.

***Figure 1.6**: Comparison of transmission spectra and external quantum efficiency (IPCE) for MDMO-PPV: PCBM (1:4 w/w) devices spin cast from toluene or chlorobenzene. In the latter case the internal quantum efficiency has been reported as close to 100 % (Shaheen et al. 2001).*

After $\pi \rightarrow \pi^*$ photoexcitation of the conjugated polymer (and possibly exciton diffusion), an electron is transferred to the fullerene molecule, leaving a positive delocalised charge (polaron) on the polymer. Charge carriers are collected at the ITO and Al electrodes with a remarkable efficiency (close to unity in 100 nm thick devices (Brabec, Sariciftci, and Hummelen 2001)) though the charge transport mechanism is not well understood.

Lower efficiencies are normally obtained with bi-layer structures but encouraging (Peumans and Forrest 2001) although controversial (Peumans and Forrest 2002) results have recently been reported for a bi-layer of phtalocyanines and fullerenes. The high efficiency observed was attributed to longer exciton diffusion length in phthalocyanines (~40 nm).

In a plastic solar cell the electric field is expected to be constant across the device (as a first order approximation) as the potential drops between the workfunctions of the aluminium electrode on one side to that of the ITO electrode on the other, facilitating

charge collection at the electodes. However, negative (electron collecting) electrodes with work functions varying over 2 eV have been found to be less important in determining the photovoltage of devices than, say, the energy levels of the acceptor fullerene derivative (Brabec, Cravino, Meissner et al. 2001), a fact best reconciled with a (supra)-molecular treatment of the blends.

Although the close proximity of donor and acceptor molecules throughout the blended film facilitates charge separation, it could also favour charge recombination losses. Blending also potentially leads to structurally metastable films.

In polymer cells the materials perform both light absorption and charge transport functions. One of the main limitations on device efficiency is the scarcity of polymers combining good transport properties with high extinction coefficients in the red region of the solar spectrum.

A typical cell is shown in figure 1.7. The term plastic solar cells (PSCs) is often used when referring to these devices (Brabec, Sariciftci, and Hummelen 2001).

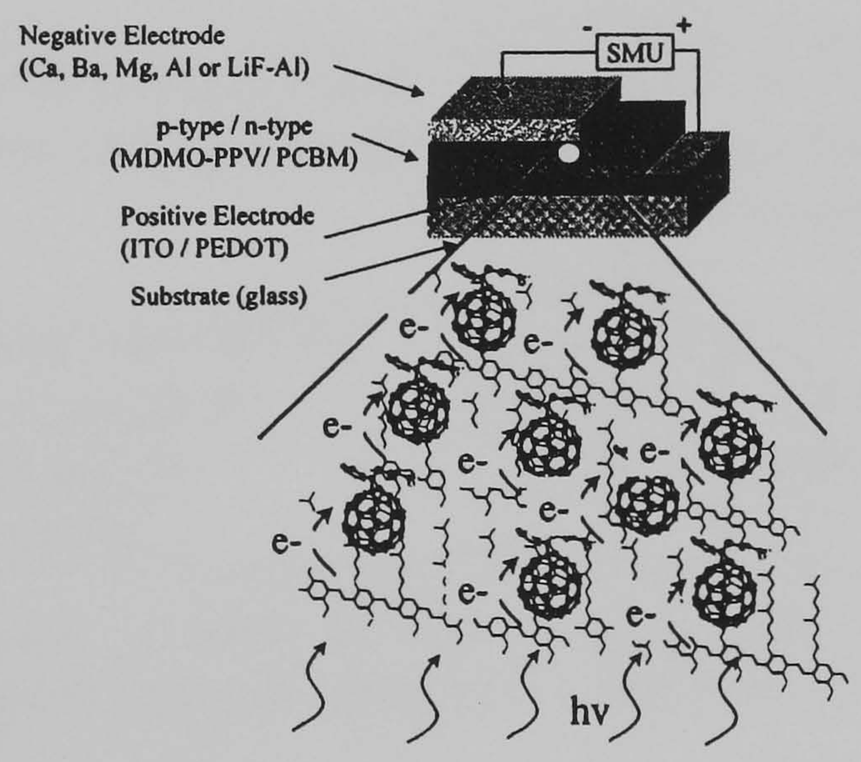

Figure 1.7: *Schematic diagram of a MDMO-PPV : PCBM solar cell (Brabec, Sariciftci, and Hummelen 2001). Light absorption results in $\pi \rightarrow \pi^*$ photoexcitation of the conjugated polymer and ultrafast electron transfer to the fullerene acceptor unit resulting in delocalised cations on the PPV backbone (positive polarons) and fullerene anions. Charges are collected at the Al (electrons) and ITO (holes) electrodes, respectively.*

1.3 Similarities and differences

The main characteristics of the three approaches to solar energy conversion described in the previous sections are summarised in table 1.2.

	Crystalline silicon	Dye sensitised photoelectrochemical cells	Conjugated polymer / fullerene solar cells
Component function	light absorption and charge transport mainly in the p-doped bulk	light absorption and charge transport separated	conjugated polymers must both absorb light and transport charge
Cell thickness	>300 μm	10 μm	0.1 μm
Components	high grade crystalline lightly doped silicon	mixed inorganic/ molecular. May contain liquid	all molecular, solid state. "Plastic solar cell"
Electric fields	electric fields confined to the thin (~0.5 μm) p-n junction	electric fields confined to semi-conductor / electrolyte interface	macroscopic electric fields ?
Charge transport	diffusion in the bulk drift at the interface	diffusion in both semiconductor and electrolyte	diffusion or drift?
Stability	commercially proven	sealing / chemical stability of dye and electrolyte	oxygen sensitive thermal stress affects morphology
Nature of recombination reactions	bulk electron – hole pairs recombination	interfacial process between electrons and dye cations or triiodide	interfacial process at the huge donor / acceptor interface
Efficiency	best ever 24.7 % commercially attainable 5-15 %	6.4 % liquid (11.0%, A = ¼ cm^2) 1-2 % solid state	2.5-3.3 %

Table 1.2: *Comparison of some of the characteristics of crystalline silicon, dye-sensitised and conjugated polymer - fullerene solar cells.*

1.4 Key issues addressed in this thesis

1.4.1 Importance of charge recombination dynamics in DSSCs and PSCs

Charge recombination in silicon solar cells is a bulk process occurring between free charge carriers mainly in the p-doped layer. It is minimised employing high purity materials. Once photogenerated minority carriers reach the p-n junction, charge recombination is inhibited by the spatial separation of the two carrier types.

In dye-sensitised solar cells, bulk recombination is avoided as the charge separation takes place at the semiconductor / electrolyte interface. However, poor spatial separation of photogenerated carriers leads to interfacial charge recombination dynamics playing a crucial role in limiting the efficiency of devices. These reactions and the parameters affecting them remain however poorly understood. Transport of charges to the electrodes must take place before they are wasted in recombination losses.

In the case of dye-sensitised cells, two different mechanisms for charge recombination are present. Photoinduced electron injection into TiO_2 is followed by kinetic competition between charge recombination of electrons in the semiconductor with dye cations (k_{CR1} in figure 1.4) and the dye regeneration reaction (k_{RG} in figure 1.4). This electron – dye cation recombination reaction k_{CR1} is only present under illumination and it has been suggested to limit the cell performance in the proximity of the open circuit voltage (Franco et al. 1999; Nelson 2001). To contribute to the photocurrent, the average photoinjected electron must diffuse through hundreds of nanocrystalline particles while being never more than ~10 nm from the oxidised redox species in solution. The close proximity of electrons and triiodide throughout the nanoporous film and the lack of a substantial potential barrier at the interface between them ensure that interfacial charge recombination (k_{CR2} in figure 1.4) after initial charge separation can be a major energy loss mechanism in these cells. This reaction is responsible for the dark current of devices. In plastic solar cells the majority of recombination losses can be attributed to reverse electron transfer between photogenerated MDMO-PPV positive polarons and fullerene anions.

1.4.2 This thesis

Having reviewed the background to this work the aims of this thesis are:

- study the dye cation regeneration reaction in dye sensitised electrodes as a function of reaction conditions employing time-resolved spectroscopy. The possible formation of reaction intermediates will be evaluated and compared with reaction mechanisms proposed in the literature.
- assess the competition between the above mentioned reaction and recombination of injected electrons with dye cations on the electrode surface and thereby test the importance of the kinetic competition for device function.
- to compare these experimental data against an extended version of the CTRW model including both the recombination and regeneration reactions
- to extend these experimental studies to complete photovoltaic devices working under illumination. Evalutation of the importance of the kinetic competition between recombination and regeneration reactions in complete cells and correlation with device current-voltage characteristics.
- extension of these experimental techniques to address recombination dynamics of photogenerated charges in PPV/C_{60} blends.
- determination of the timescale of charge recombination in such blends at room temperature. Assignment of transients observed and preliminary assessment of the parameters affecting the reaction.

2.2.1.3 Film sintering

Once dried in air the films were sintered in hot air (~ 450°C) for 20 minutes using a paint-stripper as a hot gun. Care was taken not to exceed 500 °C as over that temperature the crystal structure of the films is thought to revert to the thermodynamically more stable rutile form. After 20 minutes the hot gun was switched off and the films were allowed to cool to room temperature. During the heating procedure the films turn black temporarily as the Carbowax burns off leaving a highly porous film of electrically connected titanium dioxide particles. The films were stored in the dark under anhydrous conditions.

The thickness of the films obtained is approximately 4n μm where n is the number of Scotch® tape layers employed and the roughness factor - defined as the ratio between the microscopic and macroscopic surface area- is thickness dependent but of the order of 1000 (as it can be seen in fig. 2.2 obtained with scanning electron microscopy).

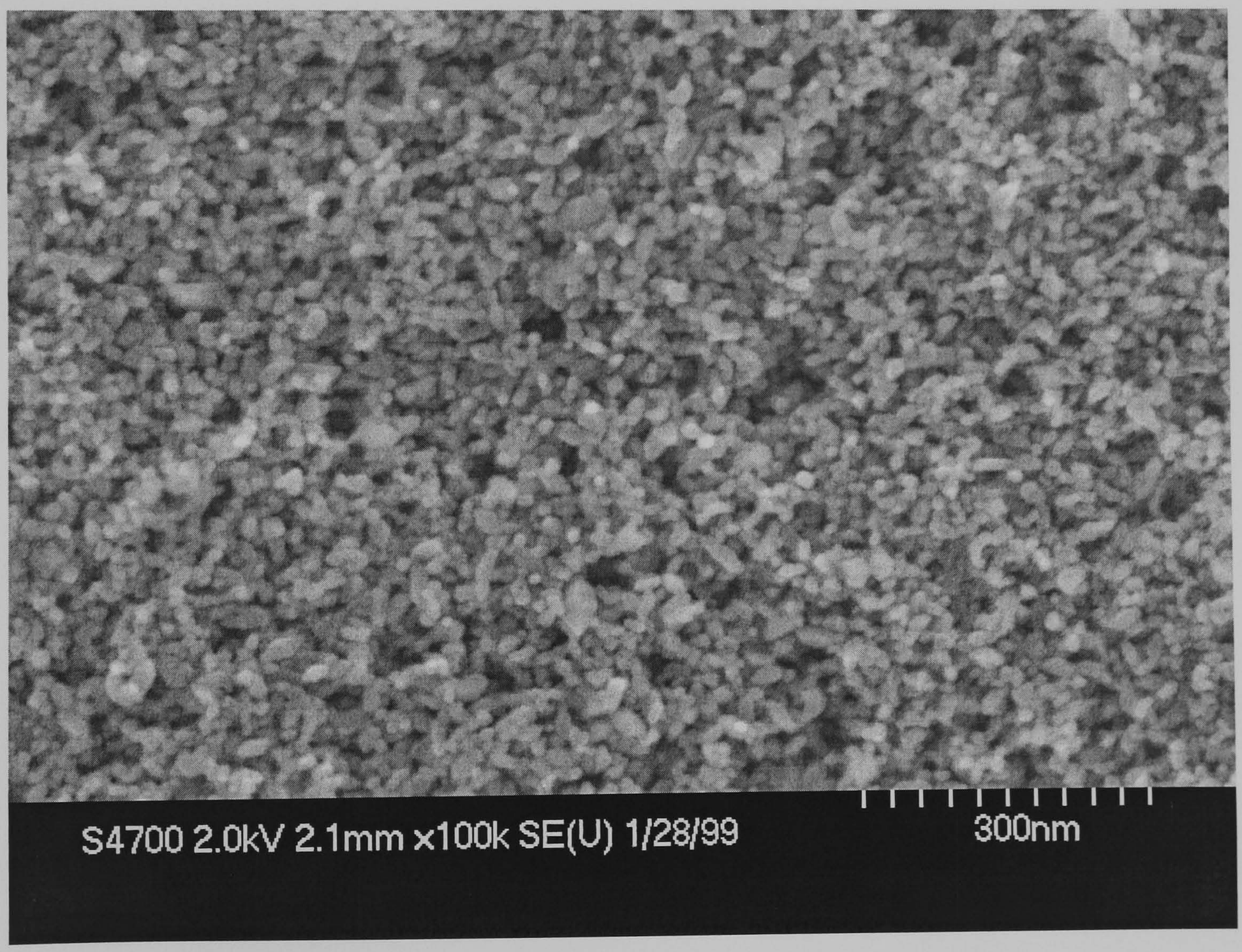

Figure 2.2: *Scanning Electron Micrograph of a TiO_2 nano-crystalline film. The highly porous nature of the films is clear.*

CHAPTER 2

EXPERIMENTAL TECHNIQUES

2. EXPERIMENTAL TECHNIQUES

2.1 Introduction

In this chapter the preparation of nanocrystalline TiO_2 electrodes and their sensitisation with Ru and Os complexes or porphyrins is presented. A three electrode electrochemical cell employed in optical experiments as a function of electrical bias is detailed. Next the procedure employed to assemble photoelectrochemical devices is explained. This section goes on to describe how MDMO-PPV : PCBM blends and devices were produced at the University of Linz, Austria.

The rest of the chapter focuses on the main experimental technique employed in this thesis work: transient absorption spectroscopy. The apparatus for both microsecond and nanosecond experiments is described, along with the most common types of experiments performed, including those as a function of applied electrical bias and white light illumination. To conclude, an experimental set-up employed to assess the i-V characteristics of solar cells is briefly reviewed.

2.2 Sample preparation

At the heart of a dye-sensitised solar cell is what has become known as a nanocrystalline TiO_2 semiconductor film made of approximately 10^{14} colloidal particles per cm^2 sintered together (for an 8 μm thick film). The semiconductor particles average approximately 15 nm in diameter. The films are sensitised to visible light with molecular dyes. The following sections describe how these electrodes are prepared and sensitised.

2.2.1 Preparation of nanocrystalline titanium dioxide films

2.2.1.1 Preparation of titanium dioxide colloidal paste

Sol-gel chemistry is employed to produce an aqueous colloidal solution of anatase titanium dioxide particles (Nazeeruddin et al. 1993). This is autoclaved at 230 °C to obtain a distribution of particle sizes centred at about 15 nm and then concentrated in a rotovapor in order to obtain a thick white "paste" which is about 12.5% in weight of anatase titanium dioxide. The paste employed in this thesis was either prepared by Dr. Pascal Compte [(Nazeeruddin et al. 1993), method B] at EPFL, Lausanne, Switzerland or by Dr. Thierry Lutz and Richard Willis at Imperial College. Once concentrated the paste can be stored at 1-4 °C for months.

2.2.1.2 Deposition of titanium dioxide on glass substrates

In order to prepare semiconductor films a portion of the paste was mixed with Carbowax (polyethyleneglycol MW 20000) in the amount of 50% in weight of titanium dioxide. The mixture was stirred slowly (~ 1 Hz) at room temperature for several hours in order to achieve thorough mixing. Carbowax was added in order to obtain highly porous films. Fluorine doped tin oxide coated glass slides with a resistivity of 15 Ω / □ (LOF TEC 15 glass), 3" by 1" in size and 3 mm thick were thoroughly washed in ethanol before deposition. The glass was provided by Hartford Glass Co. Ltd. The Carbowax / colloidal paste mixture is deposited on the conducting side of the glass slides. One or two layers of Scotch® tape (one layer resulting in a final thickness of 4 μm) were then applied on each side of the slide in order to fix it to the working surface and to form a central area 1 cm wide as can be seen in Fig.2.1. A drop of paste was deposited at one end of the slide between the two Scotch® tapes and a clean Pasteur pipette or other glass rod was used to spread the paste swiftly and evenly over the conducting glass. This technique is normally referred to as "doctor - blading". After about 10 minutes (once the films dry partially up and become semitransparent) the tapes are removed and the film is let to dry further in a dust-free environment.

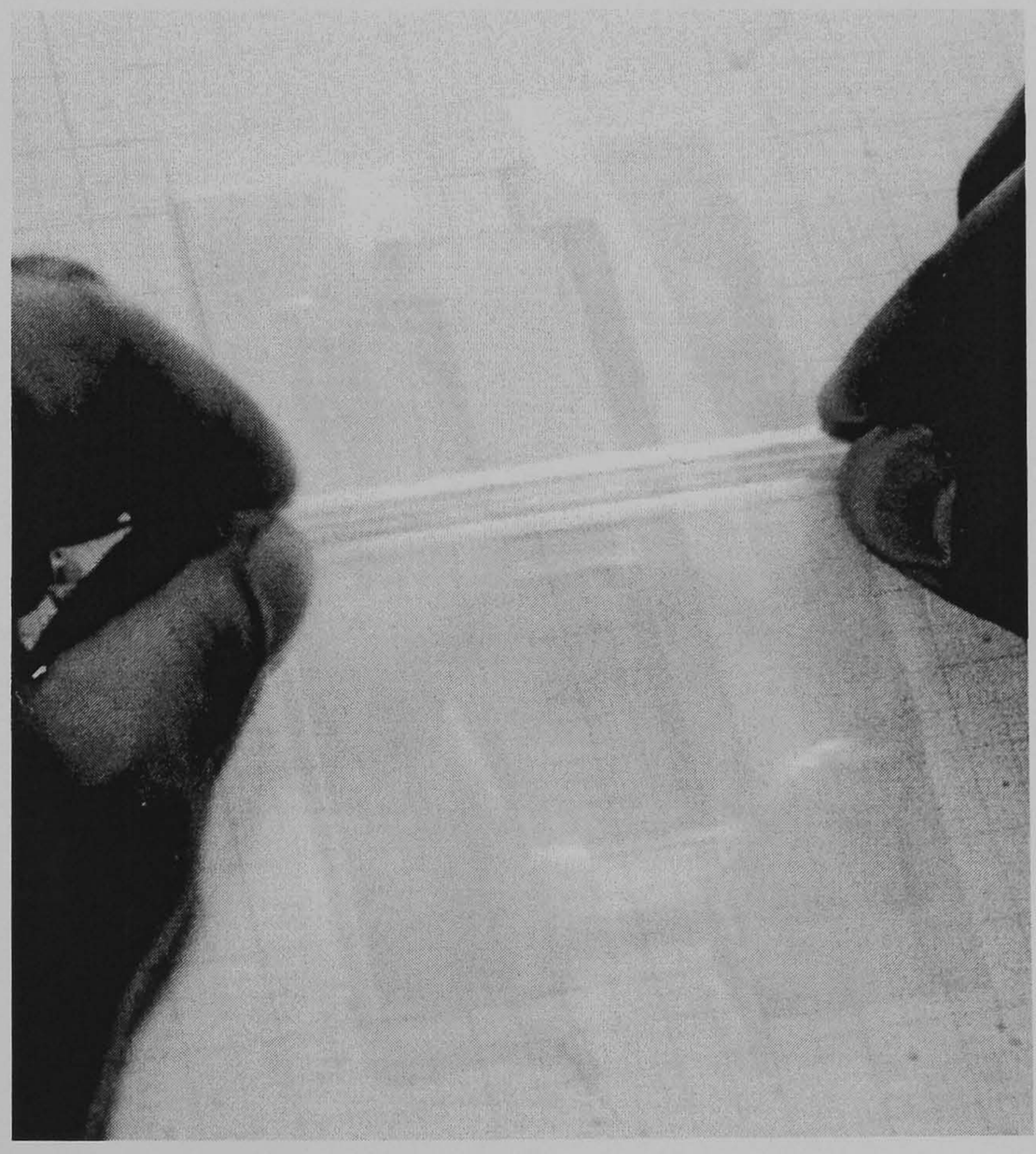

Figure 2.1: *The doctor blade technique. The conducting glass slide was fixed to the working surface with Scotch® tape that also determines the thickness of the final film. A drop of colloidal paste was spread between the spacer tapes with a glass rod.*

2.2.1.3 Film sintering

Once dried in air the films were sintered in hot air (~ 450°C) for 20 minutes using a paint-stripper as a hot gun. Care was taken not to exceed 500 °C as over that temperature the crystal structure of the films is thought to revert to the thermodynamically more stable rutile form. After 20 minutes the hot gun was switched off and the films were allowed to cool to room temperature. During the heating procedure the films turn black temporarily as the Carbowax burns off leaving a highly porous film of electrically connected titanium dioxide particles. The films were stored in the dark under anhydrous conditions.

The thickness of the films obtained is approximately 4n μm where n is the number of Scotch® tape layers employed and the roughness factor - defined as the ratio between the microscopic and macroscopic surface area- is thickness dependent but of the order of 1000 (as it can be seen in fig. 2.2 obtained with scanning electron microscopy).

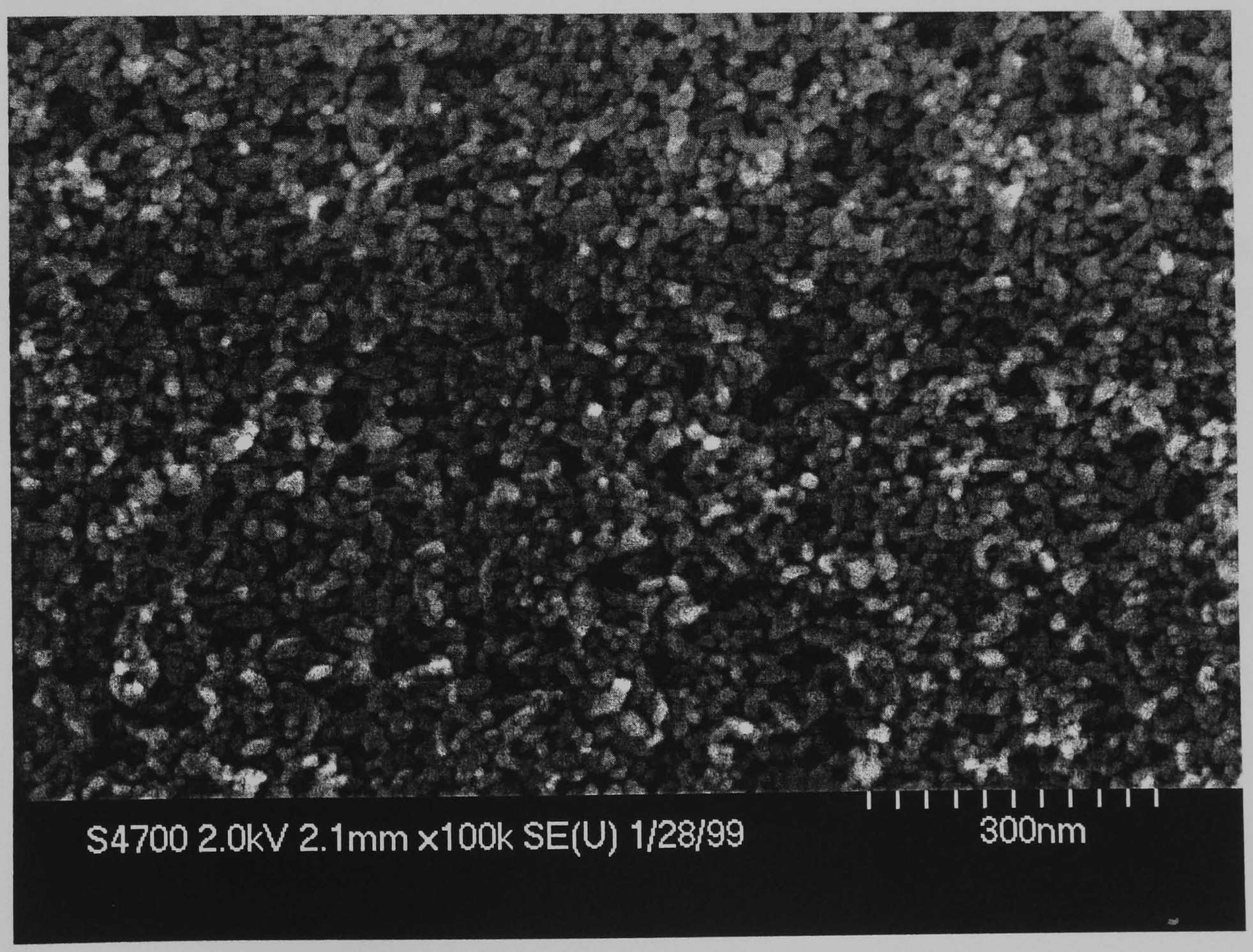

Figure 2.2: *Scanning Electron Micrograph of a TiO_2 nano-crystalline film. The highly porous nature of the films is clear.*

2.2.2 Dye sensitisation

Dye sensitisation is achieved by immersion of the TiO_2 films in dilute dye solutions. The details of the dyes employed and the sensitisation procedure are described below.

2.2.2.1 Sensitising dyes employed

The films used in the experiments reported in this thesis are mainly sensitised using cis-Ru (2,2'- bipyridyl-4-4'-dicarboxylic acid)$_2$(NCS)$_2$ often referred to as N3 from the personal naming scheme of the person that synthesised it first (Dr. Nazeeruddin from EPFL., Lausanne, Switzerland) or a variation of it referred to as N719. The latter is the same compound with two carboxyl groups deprotonated and crystallised with two ter-butyl ammonium counterions. These two ruthenium dyes were provided either by EPFL, Lausanne, Switzerland or by Johnson Matthey Ltd. Other sensitising dyes employed in some experiments are Os(dcbpy)$_2$(CN)$_2$ provided by Dr. Nazeeruddin at EPFL Lausanne and Zn-tetra-p-carboxy-phenyl-porphyrin (ZnTCPP) which was bought from Porphyrin Products Ltd. (Logan, Utah, USA). Fig. 2.3 shows the chemical structure of the dyes employed.

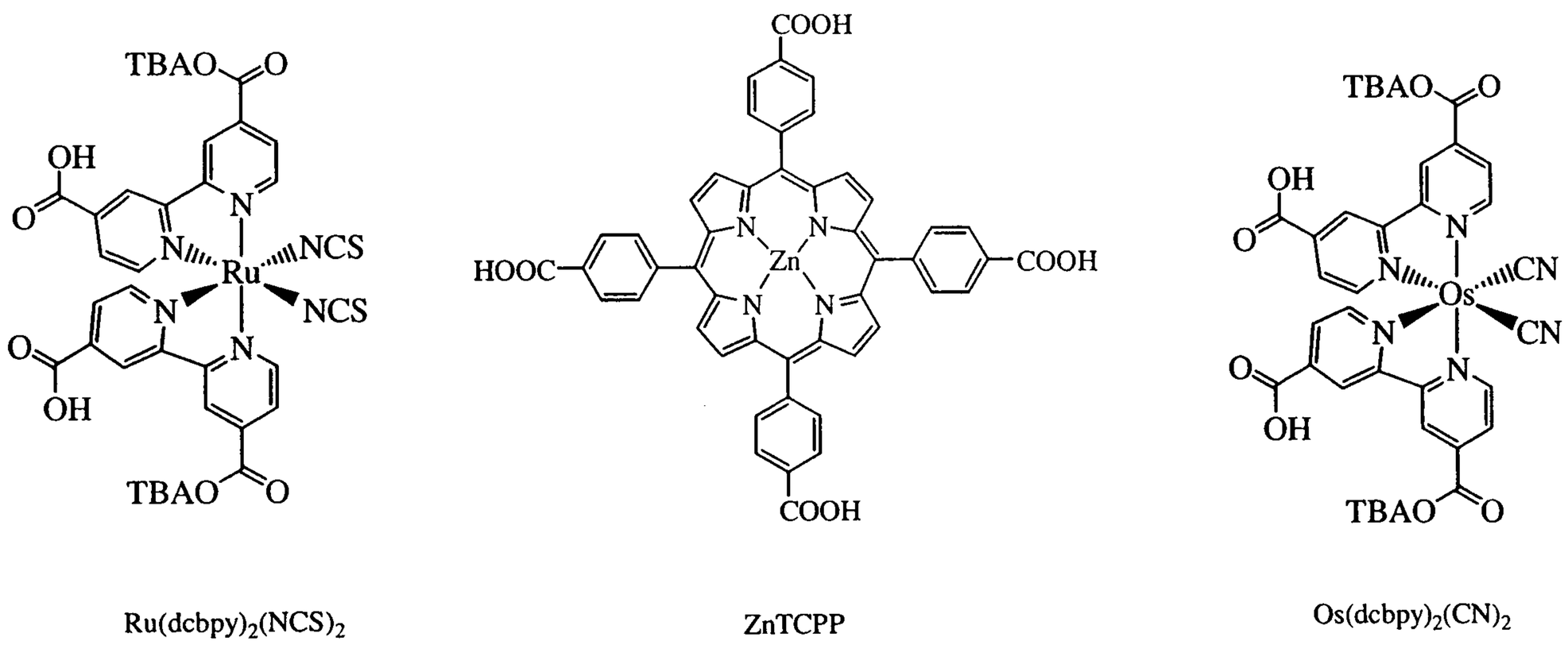

Figure 2.3: *Structure of dyes employed. Ru(dcbpy)$_2$(NCS)$_2$, Zn-tetra-carboxy-phenyl-porphyrin (ZnTCPP) and Os(dcbpy)$_2$(CN)$_2$.*

2.2.2.2 *Preparation of dye solutions and sensitisation procedure*

A small amount of concentrated HCl (37% w/w) was added to ethanol (Aldrich 99.7%) so as to obtain a proton concentration of 10^{-3} M. The acidified ethanol was used to prepare 1.2 mM solutions of N3 that were employed - either directly or after dilution - to sensitise films. The TiO_2 films stored in the dark and in dry conditions were cut in about 1 cm wide pieces with a glass cutter and then re-fired at 450°C for about 15 minutes in order to remove adsorbed water from the surface. The hot gun was then switched off and once the films cooled down to below 100 °C the films where dropped in 10 ml vials containing about 5 ml of sensitising solution. The vials were capped and wrapped in aluminium foil to protect the samples from stray light. The sensitisation procedure for N719 films was equivalent apart from the solvent employed that consisted of a 1:1 mixture of t-butanol and acetonitrile. A 0.2mM $Os(dcbpy)_2(CN)_2$ solution was prepared in ethanol with the addition of 30 mM taurodeoxycholic acid sodium salt (Fluka). The addition of this acid was found to result in better films and it is thought to reduce the aggregation of dye molecules. In the case of ZnTCPP the solution was 1mM in ethanol. The sensitisation time determined the degree of dye coverage and was chosen according to the goal of the experiments. Table 2.1 summarises the solvent system and the sensitisation time employed for different dyes and applications.

Dye	**Sensitising solution**	**Sensitisation time**
N3	ethanol 1mM in $[H^+]$	2 hours
N719	acetonitrile : iso-propanol 1:1	overnight
$Os(dcbpy)_2(CN)_2$	30 mM taurodeoxycholic acid sodium salt in ethanol	overnight
ZnTCPP	ethanol	overnight

***Table 2.1**: Sensitising conditions for the dyes employed.*

2.3 Experiments in a three electrode electrochemical cell

A series of experiments were carried out applying an electrical bias to the sensitised electrodes. This was achieved employing a three-electrode electrochemical cell with the sensitised films as working electrode (WE). In the following such a cell and the apparatus employed to control the electrical bias applied to the sensitised electrodes is described.

2.3.1 Description of the three-electrode cell

The three-electrode cell can be seen in figure 2.4. The bottom part of the cell is made of a 5 * 2 * 1 cm quartz cuvette that allows optical experiments in the visible region of the spectrum to be performed. The dye sensitised film is clipped to a PTFE rod in turn fixed to the end of a glass rod. A Pt wire runs inside the glass and PTFE rods and is in contact with the conducting face of the dye-sensitised electrode. This ensures electrical connection and the dye sensitised film therefore becomes the working electrode (WE) of the cell. The cell is completed by a counter electrode (CE) consisting of a Pt wire cap-screwed to one side of the cell and an Ag/AgCl reference electrode mounted on a frit cap-screwed to the other side of the cell. A home built potentiostat allows the application of electrical bias in the range -1.6 to +1.6 Volts. The reference electrode determines the potential of the working electrode while currents flow in the cell through the counter electrode.

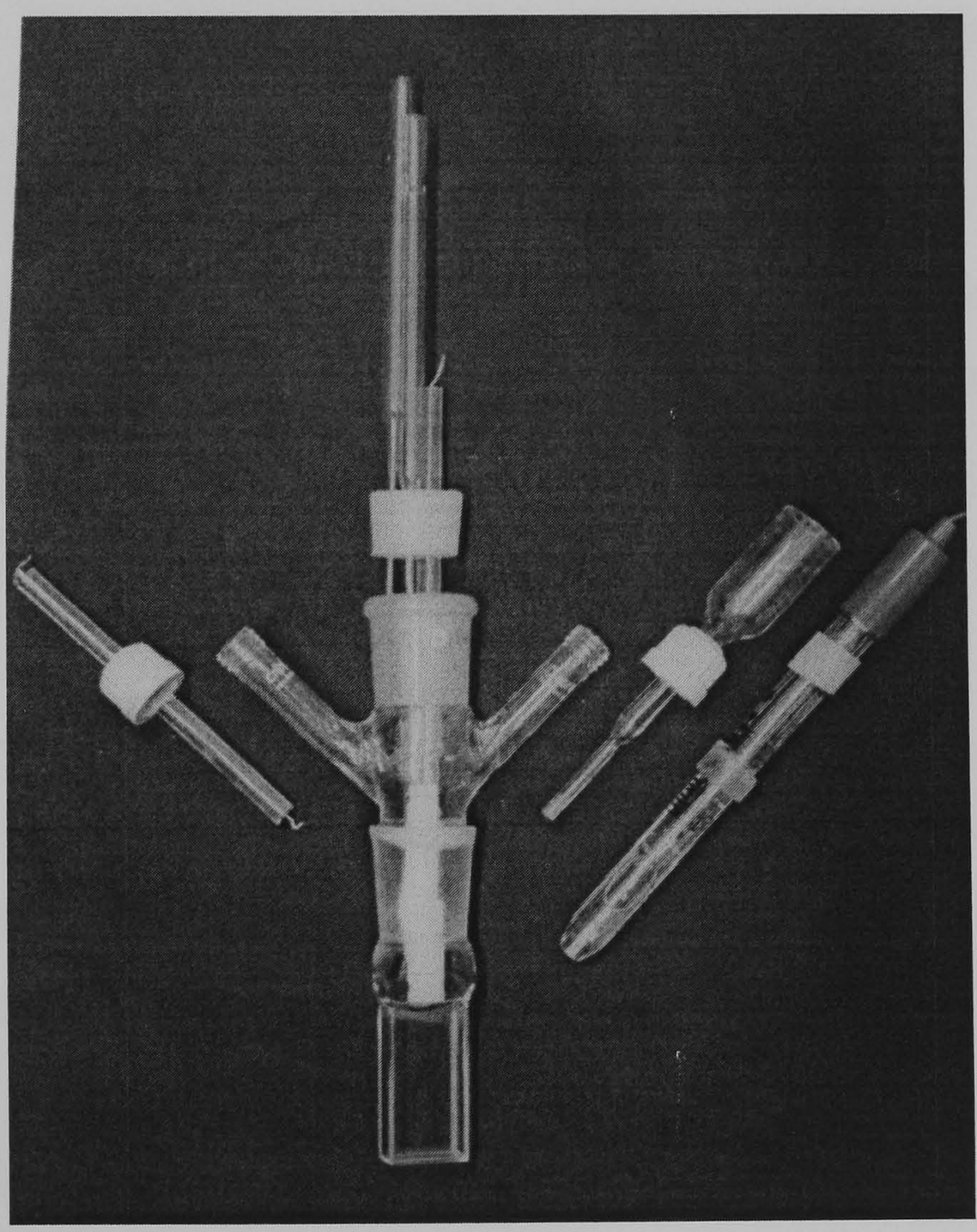

Figure 2.4: *The three-electrode cell. The bottom of the cell is specially designed for optical experiments. The middle electrode is the working electrode made of a platinum wire supported by a glass rod. The conducting glass with the dye sensitised TiO_2 film is inserted in a PTFE pocket where the connection between the wire and the conducting glass is achieved and acts as the working electrode (WE). The left-hand side electrode is the counter electrode (CE) consisting of a platinum wire. The right hand side electrode is the Ag/AgCl reference electrode connected to the main cell by a salt bridge.*

2.3.2 The application of an external potential

Once the three electrode cell is assembled with a suitable dye sensitised electrode as WE and filled with electrolyte a bias potential can be applied to the WE using an home-built potentiostat. Applying a potential to the working electrode relative to the reference electrode has the effect of raising or lowering the Fermi level of the electrons in the semiconductor depending on the sign of the applied potential and in turn controls the electron occupancy of the semiconductor film. All electrolytes contained at least 0.1 M of solutes in order to minimise ohmic potential drops between the working and reference electrode.

2.3.3 Choice of electrolytes

Various types of electrolytes were employed in the experiments. A brief description is given below while the experimental details are reported in the relevant chapters on experiments with dye sensitised electrodes (Chapter 3) and complete solar cells (Chapter 4).

2.3.3.1 Electrolytes for dye sensitised electrodes experiments.

In the case of iodide kinetics experiments with sensitised films the solvent was anhydrous ($ppm_{H_2O} < 100$) propylene carbonate (Aldrich). Solution of different concentration of LiI were prepared. The experimental details of these experiments are given in Chapter 3, section 3.3.2

2.3.3.2 Electrolytes for solar cells

When assembling working solar cells (devices) two different solvents were employed either propylene carbonate or acetonitrile. The electrolytes contained LiI, I_2, and 4-t-butyl-pyridine. $LiClO_4$ was also added to some electrolytes in order to maintain the Li^+ concentration equal to 0.1 M. The experimental details of the electrolytes employed are reported in Chapter 4, section 4.2.

2.4 Dye sensitised solar cells

Conducting glass covered with 8 μm thick and 1 cm wide titanium dioxide stripes were cut in rectangular shapes about 25 mm wide (the width of the conducting glass slide) and about 15 mm long. This yielded a sample with a 15 by 10 mm semiconductor film area. The samples were sensitised in high strength (1.2 mM) N719 dye solutions in acetonitrile : isopropanol 1:1 to obtain maximum dye coverage corresponding to an

optical density in excess of 2 at the ruthenium complex absorption maximum of about 540 nm. These are the working electrodes of complete cells.

A few tens of microliters of a 0.5 M solution of hexachloroplatinic acid (H_2PtCl_6, Aldrich grade) in isopropanol was "doctor-bladed" on conducting glass slides and let to dry in air. The slides were subsequently fired in an air-flow at approximately 380°C for 10 minutes and cut in rectangles of circa 15 by 25 mm in size. They were employed as counter-electrodes. A sand blaster was employed to produce two holes on the non-conducting side of the counter-electrodes at the two opposite vertices of an imaginary 10 mm by 10 mm square at the centre of the counter-electrodes. The shape of the holes was conical with an aperture of approximately 1 mm in diameter on the platinised side of the counter-electrodes. At this stage a scalpel was employed to scrape off the excess of the dye-sensitised titanium dioxide on the working electrodes so as to leave a 10 by 10 mm portion centred on the film. Surlyn® 1702 (Du Pont) gaskets of a square shape (internal dimensions 10 by 10 mm, external approximately 12 by 12 mm) were obtained from large sheets of the polymer with a press system designed by Mr. Richard Monkhouse.

The Surlyn® gaskets were sandwiched carefully between the working and counter electrodes with their conductive sides facing each other. This semi-assembled cell was taken through a mild (110 °C for 10 seconds; applied to the counter electrode side to minimise possible thermal damage to the working electrodes) heat cycle to allow the melting of the Surlyn® polymer and ensure sealing of an air pocket between the two glass electrodes. The appropriate electrolyte for the experiment at hand was introduces between the two electrodes through one of the holes produced on the CE with the sand blaster while the other hole allowed air to exit the compartment. The two holes were then sealed with circular (5 mm diameter) microscope cover slides held in position thanks to some more Surlyn® which was melted with a soldering iron. The whole process was optimised for speed as to minimise the chances of any of the components to degrade in air. Last but not least, the exposed electrodes were painted with RS silver conducting paint to minimise the resistivity of the contacts in subsequent experiments involving the application of an electrical bias to the cells. Figure 2.5, courtesy of Richard Monkhouse, is a representation of a complete device.

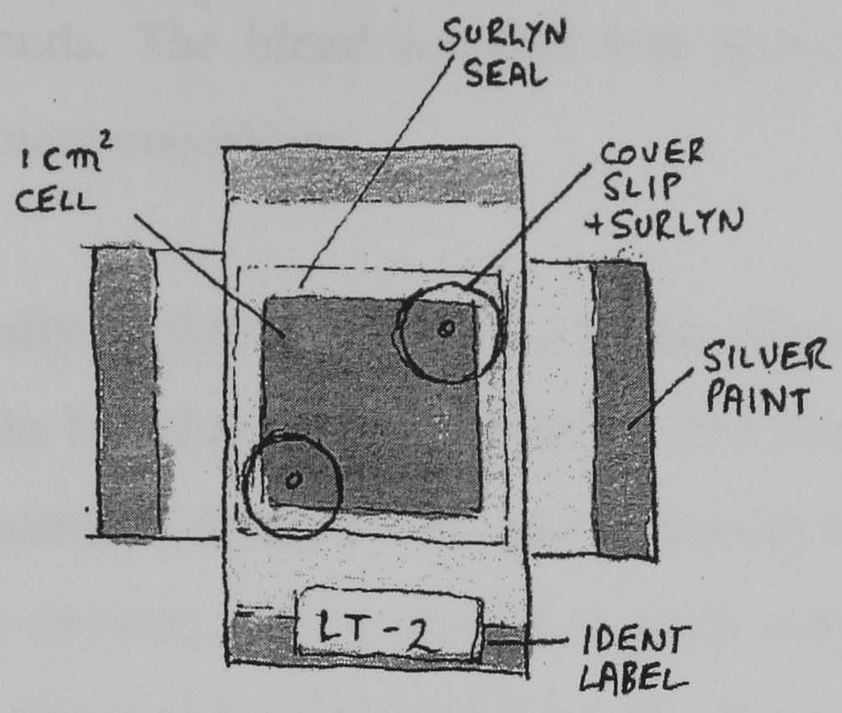

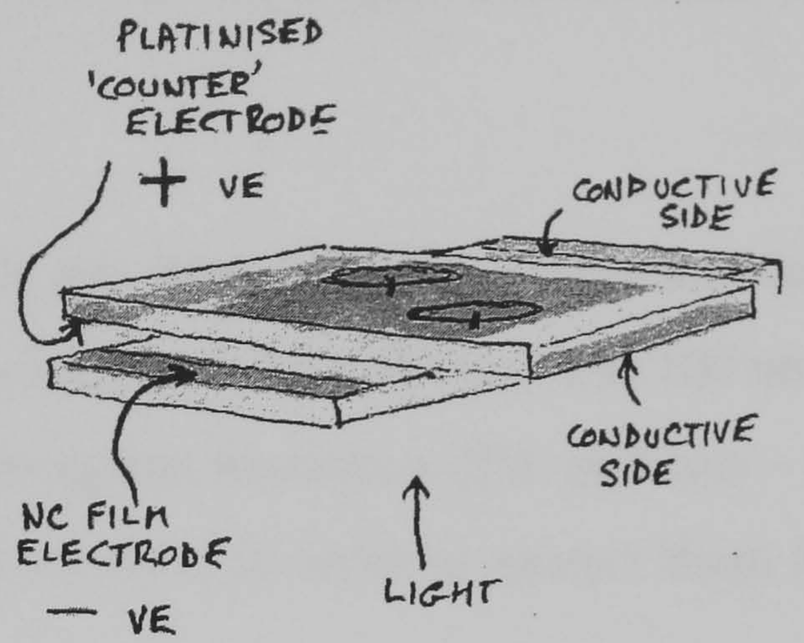

Figure 2.5: *Schematic of a DSSC assembled at Imperial College (courtesy of Richard Monkhouse). The active area is approximately 1 cm^2. The working and counter electrodes are sealed with a Surlyn® square gasket. The electrolyte is introduced in the air pocket through holes sand-blasted in the counter electrode and sealed with Surlyn®.*

2.5 Plastic solar cells and reference samples

The following samples were kindly provided by Dr. Christoph Brabec (now at Siemens Forschung, Erlangen, Deutschland) and co-workers at the Johannes Kepler University, in Linz, Austria:

- complete solar cells sealed with an epoxy resin in order to prevent oxygen- and moisture-induced degradation. The device structure was equal to the one described in figure 2.6. Devices employing an active layer (MDMO-PPV : PCBM 1:4 w/w) deposited from chlorobenzene were provided.
- reference samples consisting of spin-cast blends (MDMO-PPV : PCBM 1:4 or 1:2 w/w) on ITO glass or microscope slides from either toluene or chlorobenzene.

A schematic illustration of a solar cell is shown in figure 2.6.

2.5.1 Devices

Here is a brief summary of how solar cells were prepared:

1) The ITO glass surface was etched with HCN:HNO_3 (1:3) for 30 minutes and then left twice in an ultrasonic bath in pure acetone for 15 minutes each time, followed by another 15 minutes in iso-propanol.

2) 32 mg of PCBM were added to 2 ml of solvent and stirred at 55° C for an hour. 8 mg of MDMO-PPV where then added to the solution that was stirred overnight at 44° C.

PEDOT:PSS from Bayer® was diluted with distilled water and, after filtering, spin-

coated on the etched ITO substrate at 1500 rpm for 40 seconds or 2000 rpm for 30 seconds. The blend solution was spin-coated with the same rpm and duration under ambient conditions.

Finally an 0.6 nm LiF and a 80 nm aluminium layers were thermally evaporated on top of the blend in a single chamber. The thickness of the active blend layer was 100 nm for all samples studied. The optical density at the absorption maximum (500 nm) was ~ 0.3. The devices were enclosed in glass with an epoxy resin in order to protect them from the effect of humidity and mainly oxygen.

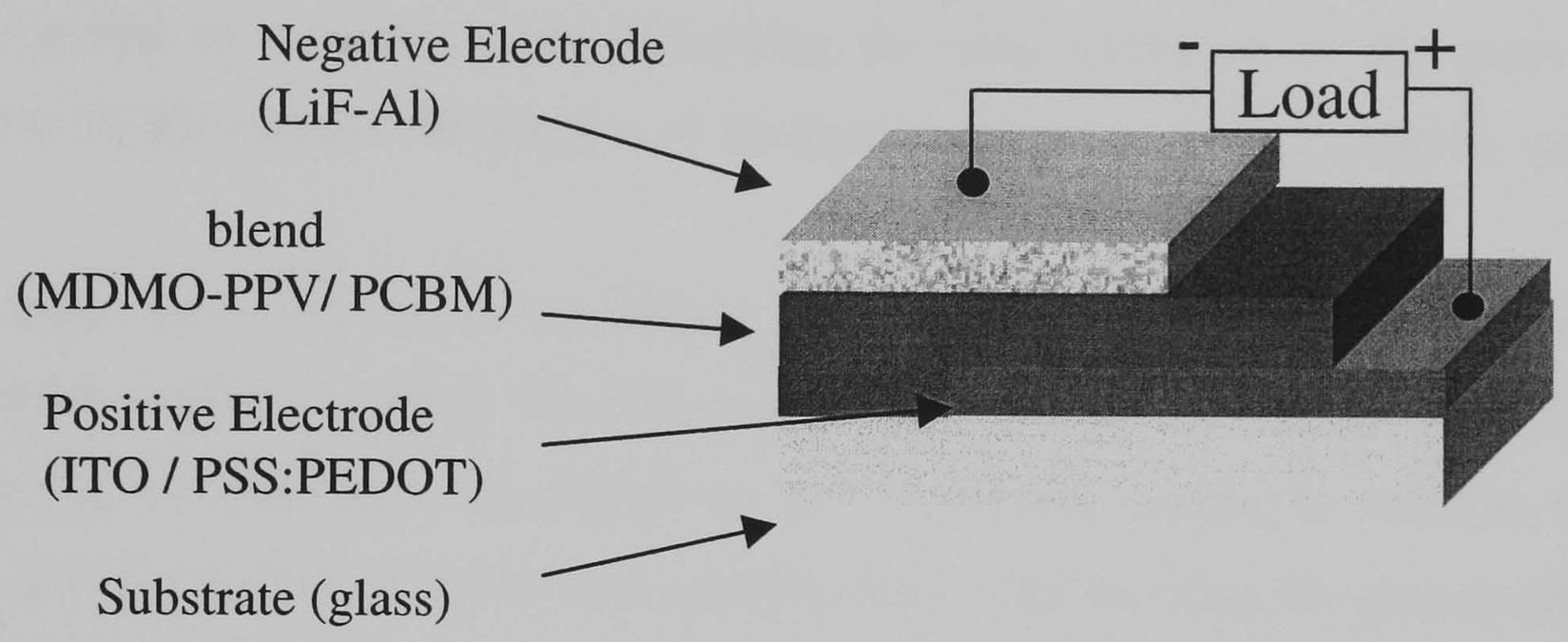

***Figure 2.6**: Schematic of a conducting polymer solar cell. The active layer is a 100 nm thick blend of MDMO-PPV and PCBM (a soluble derivative of fullerene). It is sandwiched between the negative (20 nm thick aluminium with a 0.6 nm LiF layer in contact with the blend) and positive (ITO glass covered with PSS:PEDOT) electrodes.*

2.5.2 Reference samples

Reference samples were also produced following the procedure outlined above but omitting the aluminium electrode thermal evaporation step in order to produce optically transparent reference samples. Blends were deposited from either toluene or chlorobenzene both in a MDMO-PPV: PCBM 1:4 or 1:2 ratio in weight.

2.6 Transient absorption spectroscopy

The main experimental tool employed in the experiments reported in this thesis is transient absorption spectroscopy. The theory behind this technique is briefly reviewed followed by an explanation of the origin of the signals and an explanation of how to extract quantitative information from the experiments. A description of the apparatus, a replica of a system originally set-up by Durrant during his Ph.D. (Durrant 1992) is provided in the next section.

2.6.1 Theory

The technique was invented as early as the beginning of the 50s by Norrish and Porter (Norrish and Porter 1949) for which they received the Nobel Prize in Chemistry in 1967. Porter had worked with radars in the British Navy during the war and applied similar concepts to the study of chemical reactions. The original idea consisted of preparing a gaseous reaction mixture in a transparent glass vessel and flash it with a burst of white light (flash photolysis or optical pumping). As the light triggered the reaction the composition of the mixture would change chemically and so would its absorption spectrum in time. A steady state light beam was let through the reaction mixture acting as a probe beam. Recording the time evolution of the probe beam absorption by the mixture the kinetics of the light induced reaction(s) could be obtained.

In the early days only processes taking place with time constants of the order of milliseconds could be studied. The time resolution of the method improved in time and the next big breakthrough was the advent of commercial lasers. In order to study a process of a given lifetime the optical pumping has to last less than the process object of the study. Lasers provided nano and picosecond pulses of coherent light at a single wavelength, ideal for such experiments. In the simplest form of transient absorption spectroscopy a tungsten lamp powered by a stabilised DC source provides the probe beam. The signal is normally measured by a biased photodiode and some clever electronics is employed to amplify a small time-dependent optical change superimposed onto the DC output of the probe beam. This type of set-ups have a time resolution of micro to nanoseconds that is limited by the response time of the electronic circuitry. Another approach is needed to achieve sub-nanosecond time resolutions and despite this technique has not been employed in any of the experiments discussed in this thesis, it is briefly reviewed here for the sake of completeness. This is the so called "pump-probe" approach. Two laser pulses one of a wavelength absorbed by the sample and one normally generating a pulsed white light continuum in the visible region of the spectrum are superimposed on the sample with an optical delay line determining the time delay between the pulses. Since a 1 μm step in the delay line corresponds to 3.3 fs, successive snapshots of the absorption of the sample can be taken scanning the delay line and their evolution in time reconstructed by points. Time resolutions of about 100 femtoseconds have been comfortably achieved (see for example, Tachibana et al. 1996) and the study

of the primary events in photosynthesis (energy and electron transfer reactions) and in dye sensitised electrodes (ultrafast electron injection) are based on such technique.

Flash photolysis studies in the nanosecond-millisecond timescale reported in the literature vary considerably in the experimental set-up detail. It is therefore worthwhile to summarise here the criteria that should be fulfilled by a suitable set-up:

1) Low excitation power pulsed laser excitation source (<100 μJ/pulse cm^2) in order to excite only a few percent of the dye molecules, corresponding to approximately one injected electron per particle per pulse on average (Haque et al. 1998).
2) Low optical density samples to avoid non-linearities in the excitation profile of the samples.
3) High-gain photodiode detector as opposed to a photomultiplier.
4) Sophisticated amplifier electronics in order to observe transient changes in optical density of the order of 10^{-4} ΔOD and lower. The excitation power mentioned in point 1 above produces initial signals (t=0) of the order of 10^{-3} ΔOD.

2.6.2 Origin of the transient signals

One limitation of transient absorption spectroscopy is that it can only be applied to transparent samples. There are three main reasons why the absorption of a sample illuminated with a short pulse of light should change. These are summarised below:
1) As the ground state absorbs a photon and an excited state is formed the population of the ground state species is depleted and its absorption therefore decreases appearing as a "bleach" in the absorption spectrum of the sample in the spectral region of its ground state absorption region.
2) Newly formed species, namely excited states or the products of their quenching through energy or electron transfer reactions, are formed. These will appear as positive contributions to the absorbance of the sample. The ideal situation is where these transient species absorb at wavelengths were the absorption of the ground state is negligible facilitating the assignment of the kinetics observed.
3) Some or all of the excited states produced by the pump pulse can decay radiatively either within nanoseconds (fluorescence) or after intersystem crossing on slower timescales. Either of these phenomena leads to a positive signal due to the photons emitted by the sample at a wavelength higher than that of the excitation. This latest

contribution to the signal can clearly interfere with the observation of the process being studied and experiments are designed to minimise its contribution to the total signal.

2.6.3 Calculating changes in optical density

Transient absorption spectroscopy consists in detecting changes triggered by a pump pulse in the intensity of the light transmitted by a sample. The Beer-Lambert law relates the optical density (OD) of the sample to the intensity of the probe light beam (eq. 2.1):

$$OD(\lambda) = \varepsilon(\lambda)cl = Log\left[\frac{I_i(\lambda)}{I(\lambda,t)}\right] \qquad (2.1)$$

where $I_i(\lambda)$ is the intensity of the incident light, $I(\lambda,t)$ is the intensity of the transmitted light at time t, λ is the probe wavelength, $\varepsilon(\lambda)$ is the molar extinction coefficient of the absorbing species at the probe wavelength λ, c is the molar concentration of the absorbing species and l is the optical path of the sample. For time-resolved measurements the change in optical density (ΔOD) can be written as (2.2):

$$\Delta OD(\lambda) = OD(\lambda,t_1) - OD(\lambda,0) \qquad (2.2)$$

$OD(\lambda,t_1)$ and $I(\lambda,t_1)$ represent the optical density and transmitted light intensity at a time t_1 after excitation while $OD(\lambda,0)$ and $I(\lambda,0)$ are the corresponding quantities prior to sample excitation. The intensity of the transmitted light at t_1 is $I(\lambda,t_1) = I(\lambda,0) + \Delta I$

Using equation 2.1, ΔOD can be rewritten as:

$$\Delta OD(\lambda) = Log\left[\frac{I_i(\lambda)}{I(\lambda,t_1)}\right] - Log\left[\frac{I_i(\lambda)}{I(\lambda,0)}\right] \qquad (2.3)$$

Rearranging:

$$\Delta OD(\lambda) = Log\left[\frac{I(\lambda,0)}{I(\lambda,t_1)}\right] = Log\left[\frac{I(\lambda,0)}{I(\lambda,0)+\Delta I}\right] \qquad (2.4)$$

$$\Delta OD(\lambda,t) = -\frac{1}{2.303}\ln\left[1+\frac{\Delta I}{I(\lambda,0)}\right] \qquad (2.5)$$

For $x \to 0$, ln (1 + x) ~ x, therefore:

$$\Delta OD(\lambda) \cong -\frac{1}{2.303}\frac{\Delta I}{I(\lambda,0)} \qquad (2.6)$$

The photodiode detector circuit converts these intensity values into voltages, where V_0 is the DC output voltage. Since ΔI is small an amplifier with known gain α outputs a voltage V(t) to a digital storage oscilloscope. ΔOD is given by the equation:

$$\Delta OD(t) = -\frac{1}{2.303\alpha}\frac{V(t)}{V_0} \qquad (2.7)$$

Most of the experimental results presented in the following chapter will therefore be plots of ΔOD as a function of time.

2.7 Transient absorption apparatus

This section briefly describes the transient absorption apparatus. Two different set-ups are employed in order to monitor events happening in the microsecond-millisecond and nanosecond timescales.

2.7.1 Pump light source

The pump light source is shared by the two set-ups. It consists of a PTI Ltd. nitrogen laser pumping a dye laser. The nitrogen laser has a repetition rate that can be externally controlled with a pulse generator and can range from single shots to about 10 Hz. Sub-nanosecond pulses at 337 nm are generated with an energy of approximately 1 mJ. The dye laser has a wavelength dependent efficiency and most of the visible range between about 400 and 700 nm can be covered by choosing a suitable dye. Output power varies with the wavelength and dye used and ranges between 20 and 120 μJ per pulse. The output of the dye laser is collected by a liquid optical guide and can therefore be delivered to different experiments on the optical table. The beam leaving the light pipe is highly divergent. Excitation powers employed were varied between 20 nJ and 100 μJ per cm^2 per pulse thanks to a neutral density wheel mounted between the dye laser and the light pipe and additional neutral density filters. A small fraction of the dye laser output is picked up by a photodiode to trigger a Tektronix TDS 220 100 MHz oscilloscope employed to collect the amplified signal from the probe beam photodiode.

2.7.2 The microsecond transient absorption (MTA) spectrometer

The microsecond transient absorption (MTA) spectrometer employs a Bentham 150 W tungsten lamp with a commercial stabilised DC power supply to generate a steady white light probe beam. A first monochromator (Photon Technology International) allows the selection of the probe wavelength. High pass optical filters can be employed to prevent the UV component of the light reaching the sample. A couple of lenses are then used to collimate the output of the monochromator and to focus the beam on the sample

mounted on the optical table, respectively. The sample is normally mounted at the focus of the latter lens and here is where the light pipe from the dye laser excites the sample. Two more lenses collimate and focus the probe beam on the slit of a second monochromator, respectively. The second monochromator (Photon Technology International) allows minimising the amount of scattered light from the sample and, when present, its emission that would reach the photodetector. A last couple of lenses collimate the beam and focus it onto the photodiode used for detection. The nitrogen laser is typically run at between 1 and 3 Hz and hundreds of shots are averaged to obtain a satisfying signal to noise ratio. The time resolution of the set-up is approximately 300 ns. The two monochromators allow any wavelength between about 400 to 1100 nm to be probed. Figure 2.7 shows a simplified schematic of the set-up.

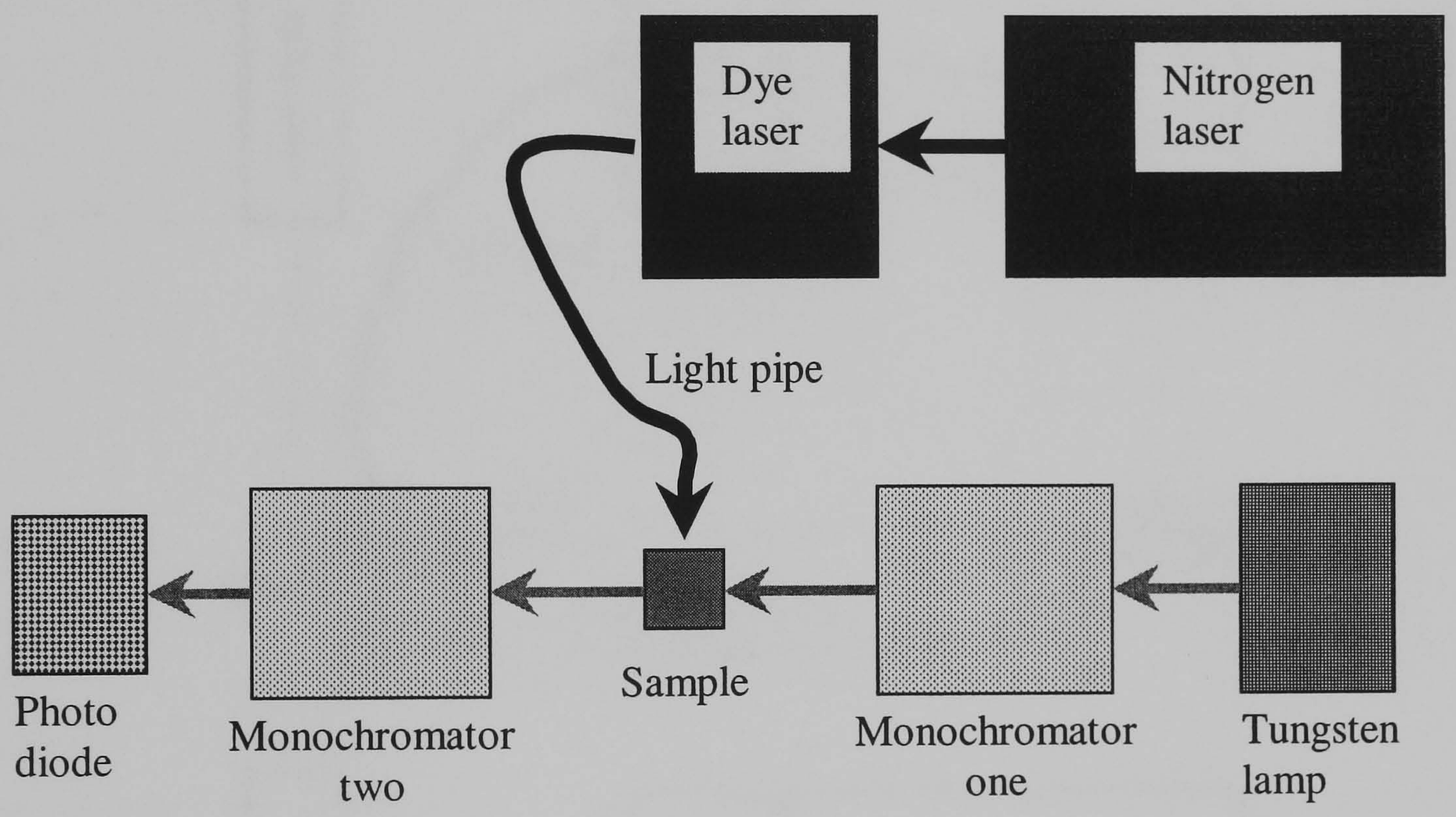

Figure 2.7: *Schematics of the Microsecond Transient Absorption spectrometer. The nitrogen laser pumped dye laser provides the excitation source. A stabilised tungsten lamp provides the probe beam. The first monochromator is used to choose the probe wavelength while the second monochromator helps to reduce the amount of scattered light and sample emission reaching the detector photodiode.*

2.7.3 The nanosecond transient absorption (NTA) spectrometer

The nanosecond transient absorption (NTA) spectrometer has a better time resolution of the order of 10-15 ns. This is achieved using an IR laser diode (Hitachi HL 8325G, 40 mW CW) at 830 nm as the probe beam. The apparatus can be operated either in transmission mode where the laser diode beam is reflected on a mirror and then reaches the detection photodiode going through the sample or in reflection mode where the

sample is held with some BlueTak® on a mirror mount and acts as a mirror for the beam whose reflection is then aligned with the photodetector. The small (a few mm across) beam of the laser diode is well collimated, allowing the use of irises before and after the samples to minimise stray and scattered light. The main disadvantage of the NTA spectrometer is the fact that the only wavelength at which it operates is 830 nm though this is the most suitable for our purposes. Other probe wavelengths are possible using a series of laser diodes emitting in different regions of the electromagnetic spectrum but changing the probe wavelength remains an expensive and cumbersome business. Figure 2.8 shows a schematic description of the nanosecond in both transmission and reflection geometries.

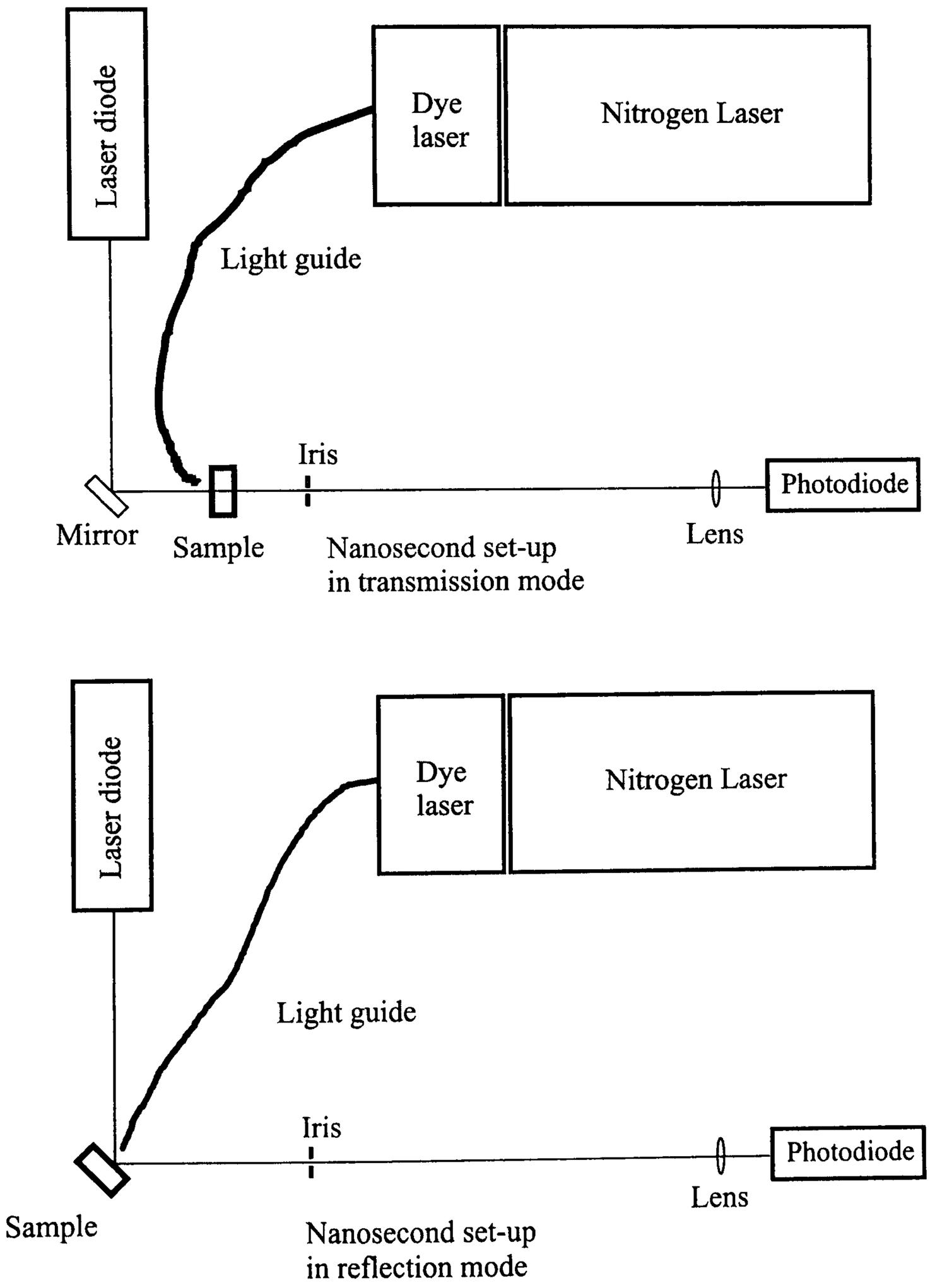

Figure 2.8: *Nanosecond transient absorption (NTA) spectrophotometer shown in both transmission and reflection mode. The excitation source is a nitrogen laser pumped dye laser while the probe beam is provided by a laser diode (830 nm).*

2.8 Transient absorption experiments

This section summarises the most common type of experiments carried out with either of the two apparatuses described in the previous section.

2.8.1 Basic transient absorption experiments

The simplest experiment consists of mounting a sample on an optical mount either at the focus of the MTA spectrometer or about 20 cm after the mirror in the beam path of the laser diode in the NTA spectrometer in transmission mode. A suitable probe wavelength is chosen in the MTA and the time evolution of ΔOD is recorded on a Tektronix TDS 220 oscilloscope. The output of the light pipe coming from the dye laser is then directed on the sample taking care that the whole of the probed area is optically pumped. The intensity and signal to noise ratio of the signal determines the number of traces averaged for each measurement. The slowest timescale process studied provides an upper limit for the repetition rate of the nitrogen laser. In the case of MTA transient absorption, spectra at certain delays after excitation can be obtained recording the ΔOD traces at several wavelengths and reconstructing the transient spectrum at a given delay by points.

2.8.2 Experiments as a function of electrical bias

Experiments as a function of bias are conceptually similar to the ones just described apart from the fact that in this case the electrical contacts of the sample, either a complete solar cell or a dye sensitised electrode in a three-electrode electrochemical cell are connected to a potentiostat. This allows carrying out experiments as a function of bias applied to the semiconductor. Dark currents can be measured prior, during and after the experiments.

2.8.3 Experiments under white light

This type of experiments was only carried out with the MTA set-up. The first monochromator has a setting where the whole spectrum of white light can be allowed through. This allows the illumination of samples with the whole emission spectrum of the tungsten lamp including the probe wavelength, which is then selected through the second monochromator. White light experiments represent a spectrally crude but simple simulation of solar illumination (see section 2.9.2). Coupled with the use of a potentiostat as mentioned in the previous section it allows performing experiments on

solar cells in short circuit and open circuit conditions while monitoring the currents flowing through the system. Despite the discrepancy between the spectrum of an AM 1.5 light source (see 2.9.3 and figure 2.10) and that of a tungsten lamp, this configuration induces in the solar cells photocurrents equivalent to the ones generated under approximately ¼ of a sun light levels.

2.9 Other experimental techniques

2.9.1 Steady state UV/visible absorption spectroscopy

Steady state UV/visible absorption spectroscopy was employed to quantify dye coverage in the case of dye sensitised samples and optical densities in the case of conjugated polymer samples. It was performed before and after most time-resolved experiments in order to assess the integrity of the samples investigated. A Shimadzu UV1601 spectrophotometer was employed for this purpose.

2.9.2 Photocurrent measurements of solar cells.

Last but not least, i-V characteristics of the solar cells were investigated with a home built solar simulator. The apparatus was set-up and calibrated by Dr. Haque. The light source is a Xenon lamp and an AM 1.5 filter is employed to simulate the solar spectrum. The apparatus was calibrated with silicon photodiodes and an NREL GaAs solar cell. A computer-controlled interface developed by Mr. Richard Monkhouse was employed to record i-V curves for the solar cells both under illumination and in the dark. Neutral density filters were employed to carry out such measurements at 1, 1/10 and 1/100 of a Sun. Figure 2.9 provides a scheme of the apparatus.

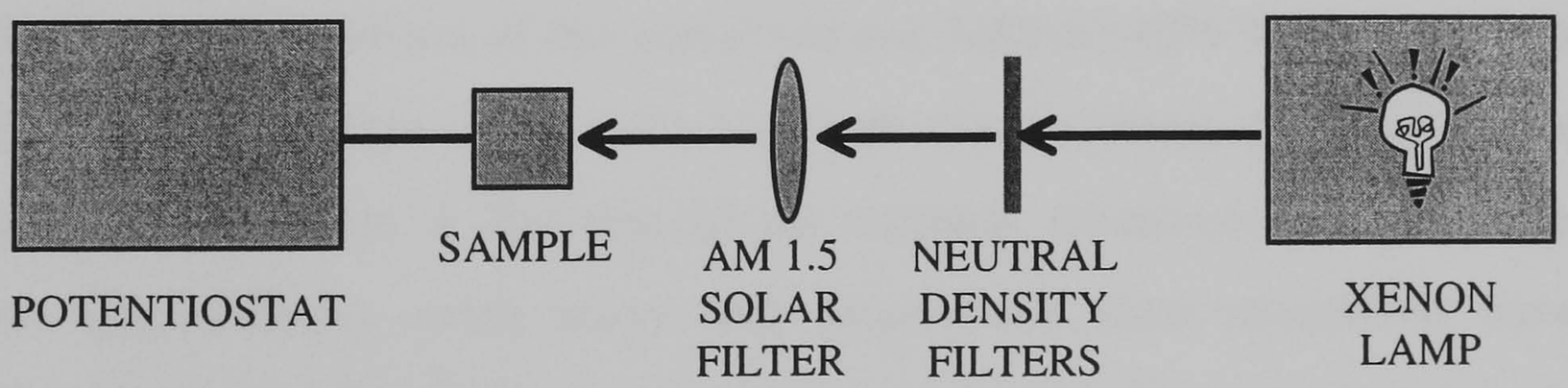

Figure 2.9: *Simplified schematics of the apparatus employed to measure the i-V characteristics of solar cells. A xenon lamp provides the light source and its spectral composition is adjusted with an AM 1.5 solar filter. The potentiostat is controlled by a PC and the i-V curves are recorded with software developed by Richard Monkhouse.*

Alternatively the i-V characteristics of devices were measured *in situ* before or after transient absorption experiments employing the white light tungsten lamp as excitation

source. In this case the incident power was approximately 25 mW/ cm^2 and the spectral distribution was that of the tungsten lamp. Despite the difference in spectral distribution this approach allowed to determine exactly the open circuit voltage at which the kinetics were investigated. The differences in spectral composition between AM 1.5 and a tungsten lamp output are presented in figure 2.10

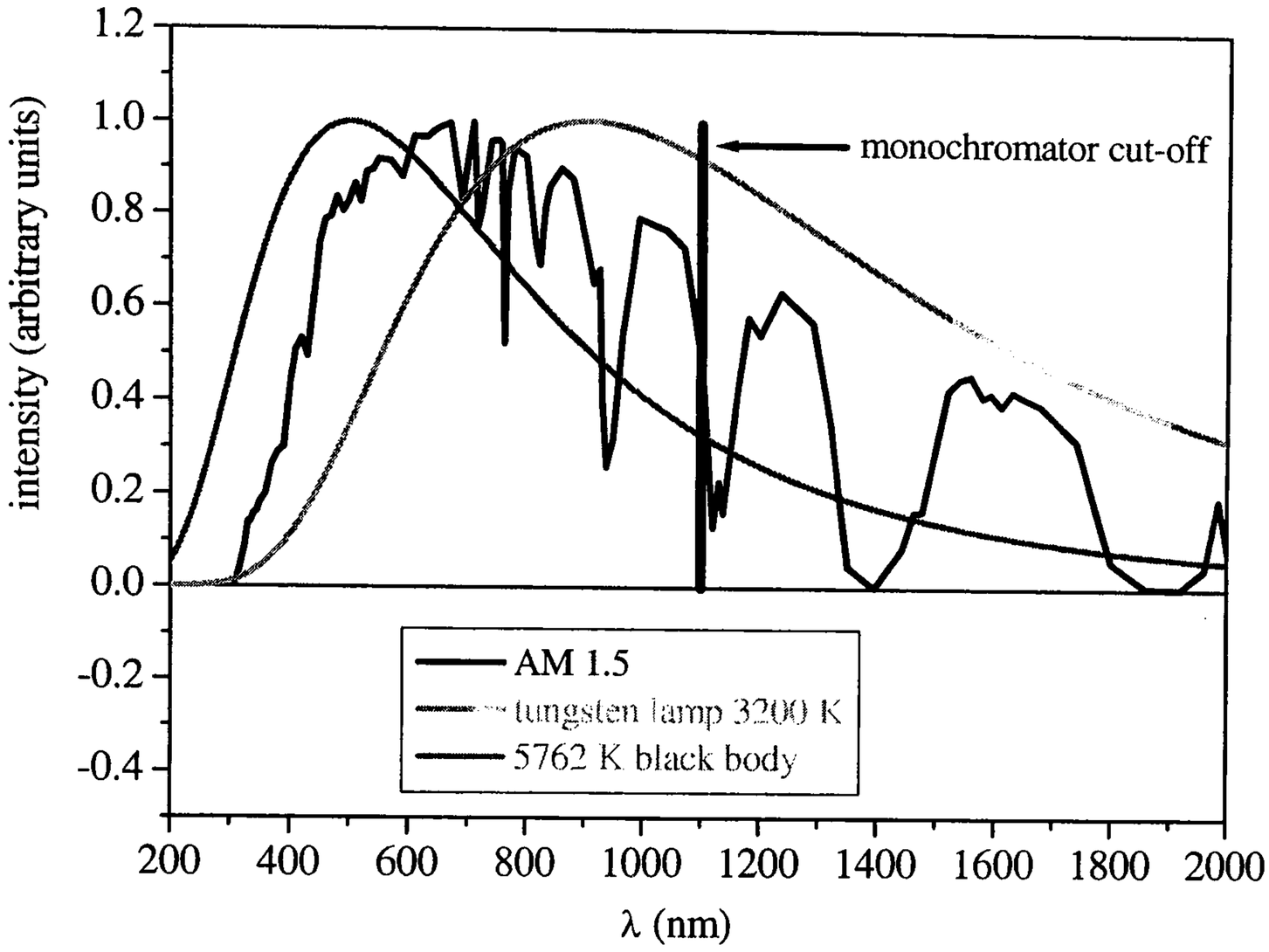

Figure 2.10: *Comparison between the spectral composition of AM 1.5 and a tungsten lamp (black body @ 3200K) and the sun black body radiation.*

2.10 Conclusions

In this chapter the preparation of dye sensitised and MDMO-PPV:PCBM electrodes and solar cells has been explained. A three-electrode electrochemical cell is employed to carry out experiments as a function of an external electrical bias. Two transient absorption spectrometers (with micro and nanosecond time resolution) have been described along with other techniques such as a solar simulator employed in order to characterise devices.

CHAPTER 3

KINETIC COMPETITION IN DYE SENSITISED ELECTRODES

3. KINETIC COMPETITION IN DYE SENSITISED ELECTRODES

This chapter addresses the competition between charge recombination (k_{CR1}) and dye regeneration (k_{RG}) in dye-sensitised TiO_2 electrodes. A systematic study as a function of iodide concentration, externally applied bias, nature of the dye employed and presence of iodine in solution is presented. Implications for solar cells function are discussed.

3.1 Introduction

3.1.1 Competing reactions in dye sensitised electrodes

When a dye sensitised electrode is immersed in a redox inactive electrolyte, the only reaction pathway that can follow photoinduced electron injection is the recapture of the electrons by the dye cations formed on the semiconductor electrode surface. This is the charge recombination (k_{CR1}, eq. 3.1) whose suppression has been identified as a crucial factor in maximising the net charge transfer efficiency (Nazeeruddin et al. 1993).

$$Dye^+ + e_{TiO_2} \rightarrow Dye \qquad k_{CR1} \qquad (3.1)$$

The main findings of previous research focused on the charge recombination reaction k_{CR1} will be summarised in Section 3.1.2.

In a dye-sensitised solar cell (DSSC) this charge recombination reaction is in competition with the dye cation re-reduction (dye ground state regeneration) reaction (k_{RG}, eq. 3.2) by iodide ions in the electrolyte.

$$Dye^+ + I^- \rightarrow Dye + products \qquad k_{RG} \qquad (3.2)$$

As indicated in figure 3.1, the ΔG driving this regeneration reaction is estimated as ~ 0.6 V. This reaction corresponds to the biggest free energy loss in the cell. Optimisation of this reaction is therefore critical to further improvement in device performance.

The detailed mechanism of the regeneration reaction remains unclear. The peculiarities of the iodide / triiodide redox couple and the nature of the products shown in equation 3.2 will be addressed in Section 3.1.3 where the experimental evidence and the interpretations of studies directed at elucidating the mechanism of the dye regeneration reaction (k_{RG}) will also be summarised. The charge recombination (k_{CR1}) and dye regeneration reactions (k_{RG}) are illustrated in Figure 3.1 where they are highlighted. The aims of this chapter are presented in section 3.1.4.

Materials and methods specific to this chapter are briefly reviewed in section 3.2. The experiments presented in section 3.3 address systems where both reaction pathways are present and the competition between the two has been studied in a variety of experimental conditions such as the iodide concentration in solution and the presence of an externally applied electrical bias.

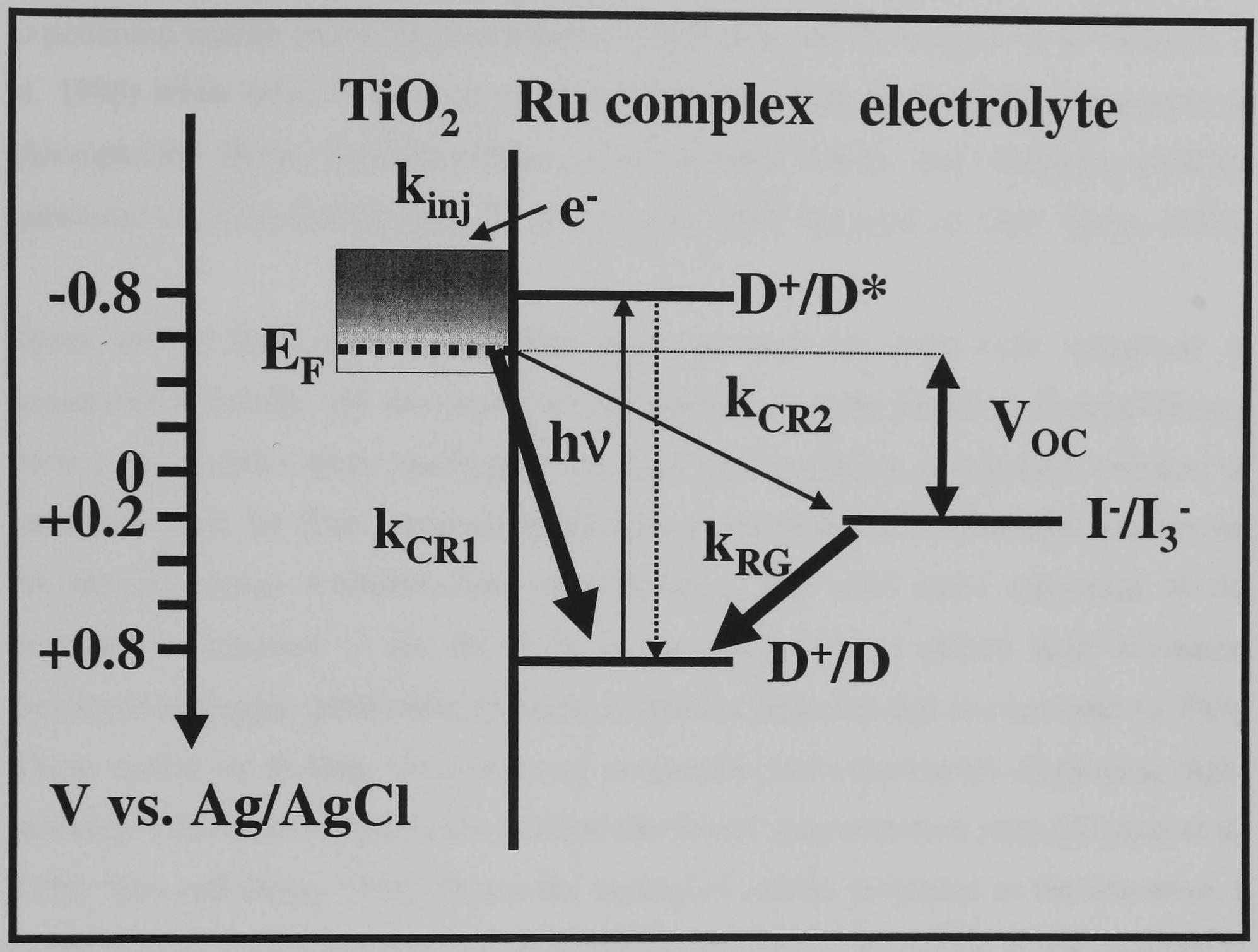

Figure 3.1: *Schematic diagram showing the main interfacial electron transfer steps involved in a dye-sensitised cell. D is the $Ru(dcbpy)_2(NCS)_2$ dye. Highlighted are the recombination of electrons with dye cations k_{CR1} and the dye cations regeneration by iodide k_{RG}. The competition between these two reaction pathways is the subject of the experiments presented in this chapter.*

3.1.2 Charge recombination k_{CR1}

Early reports of optical studies of charge recombination dynamics in nanocrystalline TiO_2 varied widely in the time scale of the reaction and in the temporal shape of the transient absorption data. Time constants ranging from hundreds of nanoseconds to tens of milliseconds were reported (Nazeeruddin et al. 1990; O' Regan et al. 1990; Moser and Grätzel 1993; Kay, Humphry-Baker, and Grätzel 1994; Argazzi et al. 1995; Heimer et al. 1996; Kamat et al. 1996; Tachibana et al. 1996; Meyer 1997). However, it must be stressed that these findings were obtained with a variety of titanium dioxide substrates ranging from colloidal solutions to nanocrystalline films obtained through different

routes, hampering attempts to rationalise them theoretically. A wide variety of dyes were employed as sensitisers ranging from organic molecules (merocyanines and coumarins (Moser and Grätzel 1993), and chlorophyll derivatives (Kay, Humphry-Baker, and Grätzel 1994) among others to various transition metal complexes of ruthenium (II) (O' Regan et al. 1990; Argazzi et al. 1995; Meyer 1997). Single or bi-exponential charge recombination kinetics where reported by Argazzi et al. (Argazzi et al. 1995) while other authors reported multiphasic charge recombination dynamics in chlorophillin (Kay, Humphry-Baker, and Grätzel 1994) and $Ru(dcbpy)_2(NCS)_2$ sensitised titanium dioxide films (O' Regan et al. 1990; Meyer et al. 1995; Meyer 1997).

There are at least two factors that could account for such wide variations in experimental results. As mentioned above titanium dioxide particles obtained from a variety of sources were employed. The fact that preparing a colloidal solution of semiconductors for film preparations remains an art to this day could also account for the diverse charge recombination characteristics. The other main difference in the experiments reported in the literature is the power of the pulsed laser excitation employed to trigger photoinduced electron transfer from the dye excited state to TiO_2. These varied by at least two orders of magnitude and experiments employing high-intensity YAG lasers in particular yielded the fastest recombination rates (Argazzi et al. 1995; Yan and Hupp 1996). Given the variety of results presented in the literature, a useful way of comparing data is $t_{50\%}$ defined as the time at which the signal assigned in transient absorption experiments to the dye cation decay reaches half its initial value.

It has indeed been shown recently by our group that charge recombination dynamics are highly sensitive to excitation power levels, the $t_{50\%}$ of the reaction ranging from ~ 1 ms to ~ 4 μs for excitation pulses ranging from 120 μJ cm^{-2} per pulse to 6 mJ cm^{-2} per pulse, respectively (Haque et al. 2000). As previously mentioned in section 2.6, low excitation powers (≤ 100 μJ/pulse cm^2) and low sample optical densities (ODs) (≤ 0.2-0.3) are required in order to avoid injection of more than one electron per particle on average or double photon absorption processes and other non-linearities in the observed kinetics. The characteristics of the low excitation power experimental set-up employed in this thesis work were described in section 2.7.

Recent results obtained within our research group with an experimental set-up meeting such requirements have revealed dispersive (multi-phasic) charge recombination kinetics in $Ru(dcbpy)_2(NCS)_2$ sensitised TiO_2 (Haque et al. 1998). The kinetics are not easily explained with standard first or second order kinetic models and show a strong dependence on an externally applied electrical bias of approximately one order of magnitude increase of the reaction rate per 100 mV of negative applied bias.

The dependence of the recombination kinetics (k_{CR1}) on an externally applied bias for a $Ru(dcbpy)_2(NCS)_2$ sensitised TiO_2 film is shown in figure 3.2 (from Haque et al. 2000).

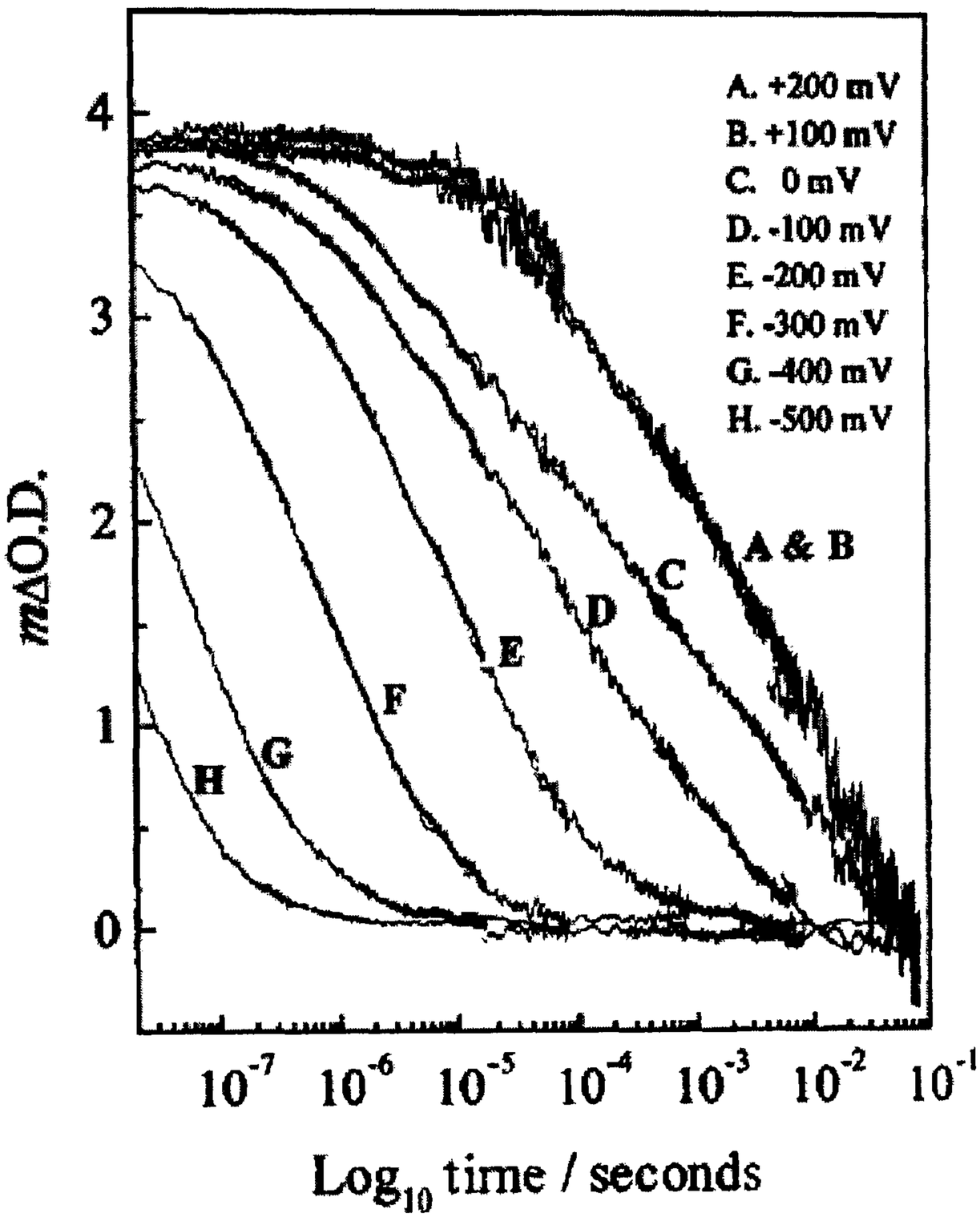

***Figure 3.2**: Dependence of the charge recombination reaction dynamics as a function of the electrical potential applied to a $Ru(dcbpy)_2(NCS)_2$ sensitised titanium dioxide electrode. All potentials vs. Ag/AgCl (From Haque et al. 2000).*

The stretched exponential shape of the decays (eq. 3.3) has been modelled by Nelson in collaboration with our group (Nelson 1999):

$$\Delta OD(t) = \Delta OD(0) * e^{-(t/\tau)^{\alpha}} \qquad (3.3)$$

The model is an adaptation of the so-called Continuous Time Random Walk (CTRW) model first introduced by Scher and Montroll (Scher and Montroll 1975) in order to describe charge transport in materials valuable to laser printer technology. It assumes

that photoinjected electrons undergo a series of trapping-detrapping steps in the presence of a exponential density of states and each detrapping step is delayed, on average, by the time for thermal activation from the site currently occupied. A visual representation of the CTRW model is shown in figure 3.3. Charge recombination occurs when the electron meets a dye cation and is therefore limited by electron diffusion through a distribution of traps. No long range electron-cation forces are included.

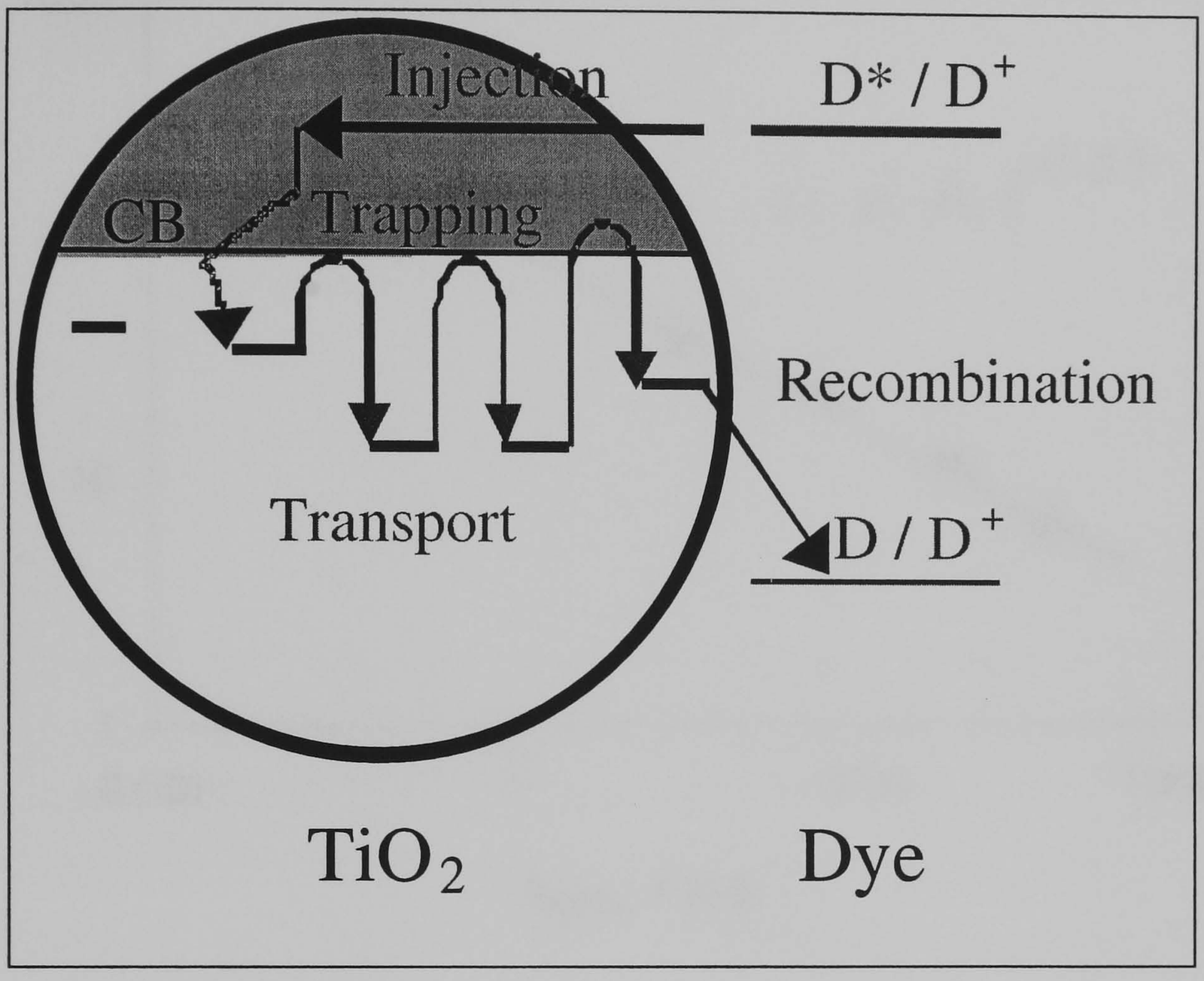

Figure 3.3: *Schematic illustration of the Continuous Time Random Walk (CTRW) performed by the electrons in the TiO_2 film. Electron transport is diffusion-limited with the trapped electrons de-trapping after, on average, the time required for thermal activation from the trap currently occupied. The shape of the density of trap states is chosen to be exponential. The model predicts stretched exponential dye cation kinetics (Nelson 1999).*

The best achievements of this model are that it predicts the stretched exponential shape of the decays and accounts for the dependence on electron density, which is in turn controlled by the applied bias.

According to the model equation 3.4 holds:

$$t_{50\%} \propto n^{-\frac{1}{\alpha}} \qquad (3.4)$$

where $t_{50\%}$ represents the time at which the optical density of the dye cation reaches half the value measured at the fastest time experimentally observable (~100 nanoseconds) as defined above, and n is the number of electrons per nanoparticle. α is an indication of the disorder (α=1 representing the situation of "normal diffusion" without traps).

Figure 3.4, from Nelson et al., 2001 shows a fit of equation 3.4 to experimental data. The details of the CTRW model will be reviewed in section 3.7 where an attempt by Dr. Nelson to apply it to the dye cation regeneration reaction by iodide employing experimental data presented in this thesis will be discussed.

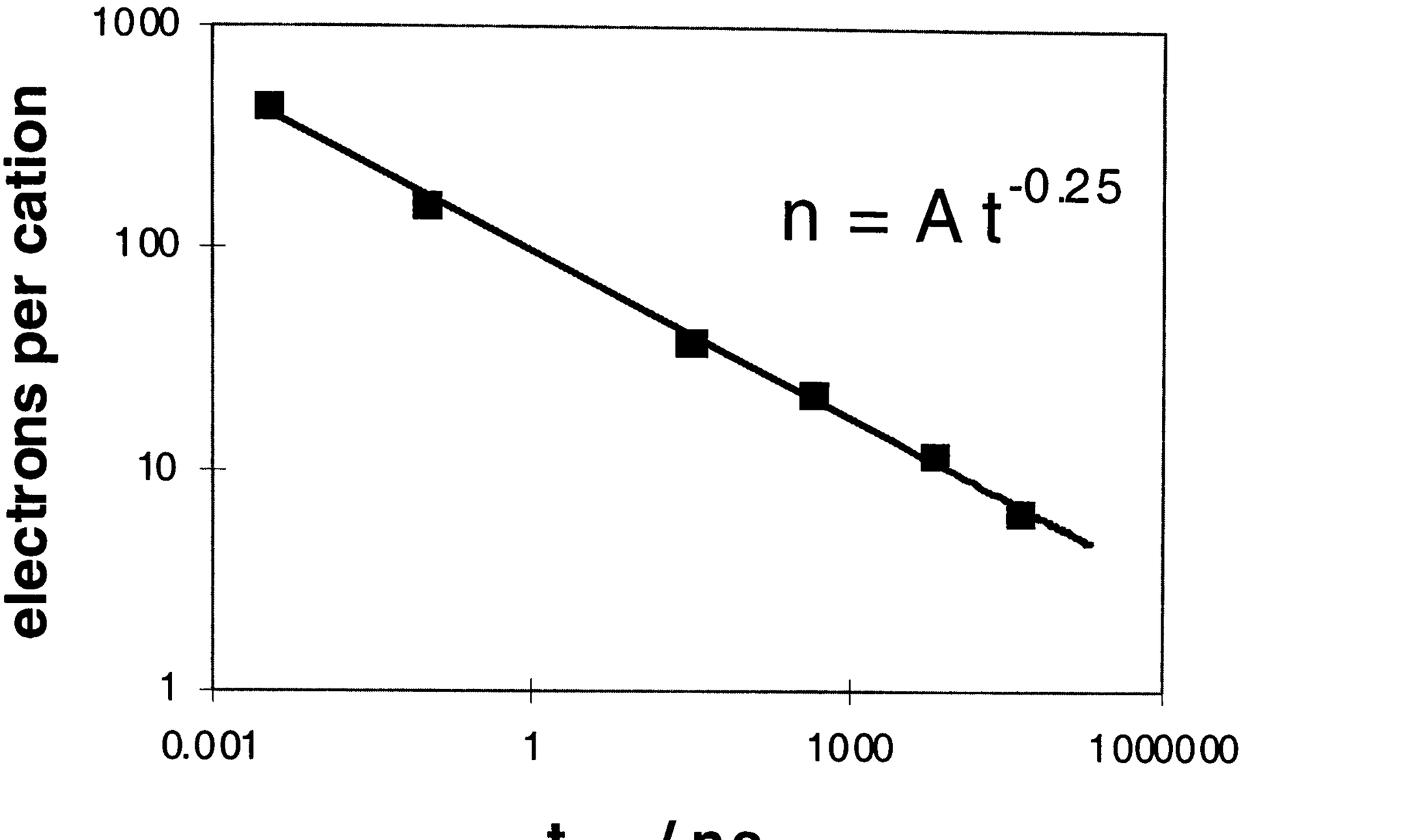

Figure 3.4: *Double logarithmic plot of the initial number of electrons per nanoparticle after excitation by laser pulse against the $t_{50\%}$ of the charge recombination kinetics for a $Ru(dcbpy)_2(NCS)_2$ sensitised TiO_2 electrode in 0.1 M tetra-butyl ammonium triflate in ethanol. The straight line is the best fit to the data. n was determined by spectroelectrochemical measurements (Nelson et al. 2001).*

In summary, the charge recombination reaction (k_{CR1}) as studied with transient absorption spectroscopy has yielded a variety of rates mainly attributed to different methods employed to prepare the semiconductor films and the wide range of excitation powers employed. However, it has become increasing clear that kinetic processes in dye sensitised electrodes are not amenable to conventional descriptions in term of homogeneous reaction kinetics. Modelling in terms of a CTRW performed by the electrons in the semiconductor (Nelson 1999; Nelson et al. 2001) has proved quite successful and a relationship between the kinetics and the number of electrons per particle has been established. Recent charge recombination experiments by other groups also report dispersive kinetics (S. Katoh, personal communication, 2001).

3.1.3 The I^-/I_3^- redox couple and the mechanism of the regeneration reaction k_{RG}

References for the iodide/iodine redox couple date back to at least the beginning of the century (Haber and Russ 1904; Maitland 1906). An equilibrium exists in solution between I^- and I_2, i.e.,

$$I_3^- \rightleftharpoons I_2 + I^- \qquad (3.5)$$

with the equilibrium constant $K = \frac{[I^-][I_2]}{[I_3^-]} = 1.5 \cdot 10^{-3}$ mole dm^{-3} in water (Vetter 1967). The constant of the above equilibrium is $K=10^{-6.6}$ mol dm^{-3} in acetonitrile, $10^{-6.7}$ mol dm^{-3} in nitromethane and $10^{-8.3}$ mol dm^{-3} in acetone (Nelson and Iwamoto 1964). Because of the equilibrium established between I_2 and I_3^- anions, the overall reaction on a platinum electrode is:

$$2\,I^- \rightleftharpoons I_2 + 2\,e^- \qquad (3.6)$$

or at higher I^- concentrations:

$$3\,I^- \rightleftharpoons I_3^- + 2\,e^- \qquad (3.7)$$

The standard electrode potential for these two reactions in aqueous solutions was reported as early as 1906 (Maitland 1906) and found to be $E_0 = +0.41$ V and $E_0 = +0.32$ V vs. Ag/AgCl, respectively.

Studies of re-reduction of the dye cation by iodide are complicated by the fact that the I^- / I_3^- system is a two electron redox couple, requiring the reaction to proceed through one or more intermediate states. Uncertainties remain on the detailed mechanism of the reduction and oxidation reactions of this redox couple.

From electrode kinetics studies, Vetter concluded that atomic iodine is the primary product of electron transfer from I^- to a Pt electrode, followed by the reaction of two iodine atoms to form I_2 (Vetter 1952). A slightly different mechanism of the reaction on dye sensitised colloids and films is generally assumed (Nasr, Hotchandani, and Kamat 1998, L.M. Peter, personal communication, 2001) to involve electron transfer from an iodide ion to the oxidised sensitiser molecule to yield an iodine atom radical that quickly reacts with another iodide ion to form an I_2^- transient species (Schemes 3.1-2):

$$Dye^+ + I^- \rightarrow Dye + I \qquad \text{(Scheme 3.1)}$$

$$I + I^- \rightarrow I_2^- \qquad \text{(Scheme 3.2)}$$

The I_2^- radical would then dismutate to yield iodide and tri-iodide as in Scheme 3.3:

$$2I_2^- \rightarrow I^- + I_3^-$$ (Scheme 3.3)

As early as 1957 a dismutation rate of 7.7 x 10^9 dm^3 mol^{-1} s^{-1} was obtained from flash photolysis of aqueous alkali halides solutions (Grossweiner and Matheson 1957).
Moser and Grätzel have reported I_2^- decay in water according to a second order rate law with a rate k = 7 x 10^9 dm^3 mol^{-1} s^{-1} following 347 nm laser excitation of Fe_2O_3 and TiO_2 colloids in the presence of I^- and attributed it to the reaction (Moser and Grätzel 1982):

$$2I_2^- \rightarrow I_2 + 2I^-$$ (Scheme 3.4)

A second order rate constant of k = 3.1 x 10^{10} dm^3 mol^{-1} s^{-1} has also been reported for TiO_2 powders in aqueous iodide (Draper and Fox 1990). Recently, a much slower dismutation rate ~ 10^5 dm^3 mol^{-1} s^{-1} was reported in TiO_2 films in aqueous iodide, attributed to slow I_2^- diffusion within the pores of the film (Behar and Rabani 2001).

The succession of steps in scheme 3.1-3.3 is certainly an attractive way of summarising the process but their validity is not well established. For instance, the standard redox potential of the atomic iodine/iodide couple (I/I^-) calculated in water (Berdnikov and Bazhin 1970) is + 1.18 V (vs. Ag/AgCl) rendering the formation of atomic iodine thermodynamically prohibited in TiO_2 films sensitised with a typical Ru complex such as $Ru(dcbpy)_2(NCS)_2$ whose Ru^{III}/Ru^{II} potential is + 0.8 V vs. Ag/AgCl. On the other hand the standard redox potential for the I_2^-/I^- couple is + 0.81 V vs. Ag/AgCl (Henglein 1980) predicting practically no driving force for the I_2^- formation. To complicate matters further, it is difficult to observe unambiguously the reaction intermediates spectroscopically.
The I_2^- radical absorption spectrum has been characterised by UV flash photolysis in aqueous solution by Devonshire and Weiss in 1968. The spectrum reported a maximum slightly to the blue of 400 nm as shown previously (Grossweiner and Matheson 1957; Matheson, Mulac, and Rabani 1963) and an additional broad absorption band with a maximum at 750 nm (Devonshire and Weiss 1968).

Fitzmaurice and Frei have postulated the formation of surface-adsorbed atomic iodine (adsorption of iodine atoms has been documented in the chemistry of the couple on Pt electrodes) in ethanolic and aqueous phenylfluorone (PF) and tris(2,2'-biphenyl-4,4'-dicarboxylate) ruthenium (RuL_3) - sensitised TiO_2 sols (Fitzmaurice and Frei 1991).

The same paper reports unconvincing evidence of the formation of I_2^- intermediates and also suggest that a complex formation between ruthenium bipyridyl complexes and iodide ions ($RuL_3I_2^-$ ion pair) may enhance the rate of iodide re - reduction of the dye cation according to the following schemes:

$Ru^{III}L_3 + 2I^- \rightarrow Ru^{II}L_3I_2^-$ (Scheme 3.5)

$Ru^{II}L_3I_2^- \rightarrow Ru^{II}L_3 + I_2^-$ (Scheme 3.6)

Another instance where I_2^- radical formation was reported to have been observed is a study of $Ru(bpy)_2(dcbpy\text{-}COOH)$ - sensitised SnO_2 immersed in 0.2 M LiI acetonitrile. The transient spectrum presented - despite still showing the fingerprint typical of the dye cation as a bleach at approximately 500 nm - could be consistent with the early stages of I_2^- formation. However, the yield of I_2^- appears to saturate at extremely low values of iodide concentration in solution, i.e. 10^{-4} M LiI (Nasr, Hotchandani, and Kamat 1998).

Considering alternative mechanisms that would not involve a iodine atom intermediate Pelet et al. (Pelet, Moser, and Grätzel 2000) have investigated the possibility that the overall reaction may actually be:

$Dye^+ + 2\,I^- \rightarrow Dye + I_2^-$ (Scheme 3.7)

Instead of an unlikely tri-molecular encounter it was suggested that depending on the surface charge of the semiconductor (which was found to depend strongly on the nature and concentrations of ions in the electrolyte) two types of ion pairs can be formed as intermediates of the reaction. The authors concluded suggesting that when the nanoparticles are negatively charged the reaction involves the formation of a dye / iodide ion pair on the surface:

$Dye^+ + 2I^- \rightarrow (Dye^+, I^-) + I^- \rightarrow Dye + I_2^-$ (Scheme 3.8)

while when the semiconductor is positively charged an iodide/iodide ion pair is involved:

$Dye^+ + 2I^- \rightarrow Dye^+ + TiO_2|\,(I^-, I^-) \rightarrow Dye + I_2^-$ (Scheme 3.9)

These hypothesises are based on a progressive reduction of the positive surface charge of the TiO_2 nanoparticles when immersed in a constant concentration of cations such as Li^+ and Mg^{++} and increasing amount of iodide. This observation is taken as evidence for the iodide ions being absorbed on the surface.

The kinetics of dye regeneration at the semiconductor/dye/electrolyte interface and in particular the parameters affecting it had received only limited attention before this thesis work. The following table summarises such work carried out on different systems ranging from colloidal particles to sintered colloidal particle films and complete cells. Most of the early work concentrated on dye sensitised colloidal solutions and their reaction with iodide in both aqueous and non-aqueous solvents was investigated. Table 3.1 summarised the systems investigated in terms of substrate, dye(s), techniques employed and a brief summary of the results obtained.

Author	Substrate	Dye	Technique	Results
Henglein 1982	aqueous TiO_2 sols	-	UV flash photolysis	I_2^- quantum yield 16%
Fitzmaurice et al. 1991	aqueous TiO_2 colloids	PF (phenylfluorone) RuL_3, L = dcbpy	Nd - YAG - flash photolysis	$RuL_3I_2^-$ formation claimed (decaying with $k=3\cdot10^{-3}$ s^{-1})
Fitzmaurice et al. 1993	aqueous TiO_2 colloids	-	Nd - YAG - flash photolysis	I_2^- rise claimed
Kay et al. 1994	TiO_2 nano-crystalline films	chlorin e_6 copper chlorophyllin	Nd - YAG flash photolysis	long lived signal assigned to electrons
Nasr et al. 1998	SiO_2 and SnO_2 nano-crystalline films	$Ru(bpy)_2bpy(COOH)_2$	Steady state emission Nd - YAG - flash photolysis	Ru^*/SiO_2 interactions I^- kinetics on SnO_2 I_2^- formation whose yield saturates at 10^{-4} M $[I^-]$
Alebbi et al. 1998	Solar cells employing Degussa P25 TiO_2 0.5 NaI, 0.05 I_2 in PC / MeCN	$M(dcbpy)_2(CN)_2$ M = Ru, Os	diffuse reflectance spectroscopy	"Sluggishness" of I^- reaction with Os leads to poor cell performance
Heimer et al. 2000	TiO_2 films and solar cells	$Ru(x,x'\text{-dcbpy})_2(CN)_2$ x= 4,5	Nd-YAG flash photolysis	$k_{RG} \sim 7\ 10^7\ s^{-1}$
Kuciauskas et al. 2001	Solar cells	$M(dcbpy)_2(CN)_2$ M = Ru, Os $M(dcbpy)_2(NCS)_2$ M = Ru, Os	Nd-Yag - OPO flash photolysis	Pseudo first order rate $k[I^-]$ 1-8 10^5 s^{-1} for all dyes except $Os(dcbpy)_2(NCS)_2$

Table 3.1: *Summary of the most relevant literature results on the iodide reaction at dye sensitised colloids, films and solar cells as of early 2002.*

From the above it is clear that much remains to be done in order to characterise the dye regeneration reaction by iodide in dye-sensitised TiO_2 electrodes. Similarly to the case of the charge recombination reaction k_{CR1} the wide variety of substrates and experimental conditions employed hampers the rationalisation of observations. Moreover, the complexity of the I^-/I_3^- redox couple and the uncertainties about the mechanistic details of its two-electrons reduction and oxidation steps further complicate matters.

There is no general agreement on why the iodide/tri-iodide couple has resisted all attempts to be replaced as the most efficient redox couple for this kind of devices. An original explanation has been proposed by Prof. Laurie Peter of Bath University and co-workers. Employing frequency-domain electrochemical techniques such as Intensity Modulated Photocurrent Spectroscopy (IMPS) and Intensity Modulated Voltage Spectroscopy (IMVS) they reported measurements of the lifetime of injected electrons and their diffusion constant under various illumination levels. These data provide indirectly information on the reaction k_{CR2} responsible for the dark current (see figure 3.1 and chapter 4). The original finding consists of the conclusion that the solar cells work only because the 2 electron overall reaction of the iodide/tri-iodide couple makes the reaction between I_3^- and electrons in the semiconductor so slow that, however slow the electron transport, electrons can reach the SnO_2 electrode without significant losses. In this context, a recent report that an electrolyte based on a single electron Co^{III}/ Co^{II} redox couple rivals the iodide - triiodide couple in complete solar cells (Nusbaumer and Moser 2001) has been rationalised in terms of a transition from high to slow spin the cobalt (II/III) redox centre undergoes, also yielding slower redox kinetics.

Ever since the first report of a viable dye-sensitised solar cell, increasing the open-circuit voltage obtainable has been high in the agenda of research groups world-wide. In this context it would be very useful to know the redox potentials of dyes on semiconductors , i.e. whether being anchored to the semiconductor surface affects their energetics. The issue has been addressed (Yan and Hupp 1997; Zaban, Meier, and Gregg 1997; Zaban, Ferrere, and Gregg 1998) but success has been limited. Attempts to determine the redox potential of bound dyes through cyclic voltammetry of sensitised films have been unsuccessful (Heimer et al. 2000). In practice cyclic voltammetry of the dyes in solution is employed to determine these potentials but the uncertainty remains

on whether the values so obtained hold true for the dyes anchored on the film. The potential for the couple (Ru^{III}/Ru^{II}) in solution is approximately + 0.8 V vs. Ag/AgCl while that of the iodide couple is generally assumed to be + 0.15 V vs. Ag/AgCl (Myung and Licht 1995; Hagfeldt and Grätzel 1995). In other words the driving force for the reaction amounts to approximately 0.6 V. As already mentioned in chapter 1, the open circuit voltage of a cell is thought to be given by the difference between the Fermi level of the electrons in the semiconductor and the electrochemical potential of the redox couple in the electrolyte.

This 0.6 V is therefore considered a major loss of photovoltage (and therefore overall efficiency) in devices. Efforts have focused on finding alternative redox couples and fine-tuning the redox potential of the dyes' ground state (see for example Oskam et al. 2001). Success has however been limited and it seems that the apparently high driving force is the minimum required for the regeneration reaction step. Results obtained by John N. Clifford in our group with dyes having redox potentials such that the driving force of the regeneration is reduced show a reduction in the regeneration reaction yield and will be touched upon in the discussion.

3.1.4 Aims of the chapter

This chapter consists of a systematic study of the competition between the charge recombination (k_{CR1}) and the dye cation regeneration (k_{RG}) in dye sensitised nanocrystalline electrodes in controlled conditions. The effect of applying an electrical bias to the semiconductor film - i.e. raising the Fermi level in the semiconductor - will be investigated in the absence of iodide in the electrolyte and in the presence of different iodide concentrations. The importance of the nature of the dye employed will be assessed and the addition of iodine to the solution will also be considered.

3.2 Materials and methods

The common features of the samples investigated are described in this section. The electrolytes employed are presented before each set of results. Nanocrystalline titanium dioxide films (8 μm thickness) were prepared as described in section 2.2.1. The films were cut into samples with a semiconductor active area of approx. 1 cm x 1 cm and sensitised with $Ru(dcbpy)_2(NCS)_2$, $Os(dcbpy)_2(NCS)_2$ and ZnTCPP as detailed in section 2.2.2. In the case of $Ru(dcbpy)_2(NCS)_2$ the optical density of the films was approximately 2 at their absorption maximum (~540 nm), resulting in dye coverages readily comparable with films employed in complete solar cells. While the dye load of the films was close to the maximum achievable, the samples were excited at single wavelengths in the range of 620 to 650 nm where the sample optical density was of the order of 0.2 - 0.3 to avoid non-linearities in the excitation profile of the samples. The kinetics were probed at 800 nm.

Transient absorption experiments on the microsecond transient absorption (MTA) spectrometer, as described in chapter 2, were carried out on all samples.

Transient absorption data for $Ru(dcbpy)_2(NCS)_2$ sensitised electrodes in 0.1 M $LiClO_4$ were recorded in a three electrode cell described in section 2.3. Either an home made or a Ministat MK IV potentiostat were used to apply an electrical bias to the working electrode in 3 electrode experiments and all currents were recorded. A series of voltages were applied to the dye-sensitised electrode (working electrode) in steps of 100 mV from 0 to –0.5 V vs. Ag/AgCl and transient absorption data were collected at each bias.

In the experiments as a function of iodide concentration 8 μm $Ru(dcbpy)_2(NCS)_2$ sensitised films were clipped on the inner side of a Sterna 1 x 2 x 3 cm quartz cuvette. Propylene carbonate (Aldrich) solutions containing LiI (Aldrich 99.7%) in the following concentrations were prepared:

A) 0 M; B) 0.001 M; C) 0.005 M; D) 0.01 M; E) 0.03 M; F) 0.1 M

Apart from solution F that already contains 0.1 M [Li^+], $LiClO_4$ (Aldrich 99.99%) was also added in appropriate amounts so as to obtain a constant Li^+ concentration of 0.1 M throughout the series of experiments. This was done in order to maintain the poorly understood (Redmond and Fitzmaurice 1993; Haque et al. 2000; Pelet, Moser, and Grätzel 2000) effect of lithium ions on the energy levels of the semiconductor and their occupancy constant throughout the experiment series. Glass pasteur pipettes were used

to fill and empty the quartz cuvette with the different electrolytes in turn, taking care not to alter the film position with respect to the probe beam. Electrolytes containing increasing amounts of iodide were added to the cuvette in succession alternated with thorough rinsing of the electrode with fresh 0.1 M $LiClO_4$ in propylene carbonate. Control experiments carried out comparing the decay obtained after thorough rinsing with 0.1 M $LiClO_4$ propylene carbonate (solution A) proved the changes in the transient signals to be reversible. The iodide is therefore readily washed off the nanocrystalline film between measurements despite its high porosity. Transient spectra for dye sensitised electrodes immersed in 0.1 M LiI (solution F above) were obtained monitoring the kinetics in the 400-950 nm wavelength range and plotting the intensity of the signal at several wavelengths at delays of 10 μs and 1 ms after excitation, respectively. Nanosecond data was obtained with a sensitised film immersed in electrolytes A and F. Iodide kinetics in TiO_2 films sensitised with $Os(dcbpy)_2(CN)_2$ and ZnTCPP were performed either clipping the films inside the above mentioned Starna quartz cuvette filled with 0.1 m LiI in propylene carbonate or simply covering the films with a drop of electrolyte and a glass slide. Control experiments with $Os(dcbpy)_2(CN)_2$ were carried out covering the film with ethylene carbonate : propylene carbonate 1:1. (EC:PC 1:1) and a microscope glass slide. Experiments with different dyes used different pump and probe wavelengths to excite the dye ground state and monitor the dye cation decay (dye ground state bleach in the case of $Os(dcbpy)_2(CN)_2$), respectively. The excitation and probe wavelengths employed for these three dyes are compared in table 3.2. Transient spectra 10 μs and 1 ms after excitation were reconstructed by points as outlined above.

Dye employed	Excitation wavelength (nm)	Probe wavelength (nm)
$Ru(dcbpy)_2(NCS)_2$	620-650	800
$Os(dcbpy)_2(CN)_2$	530	430
ZnTCPP	560	740

Table 3.2: *Excitation and probe wavelength for transient absorption measurements with TiO_2 films sensitised with $Ru(dcbpy)_2(NCS)_2$, $Os(dcbpy)_2(CN)_2$ and ZnTCPP dyes.*

3.3 Results

3.3.1 Charge recombination in propylene carbonate

The charge recombination k_{CR1} in propylene carbonate was studied as a function of externally applied bias in order to provide a "blank" for the experiments addressing the dye regeneration reaction in the same solvent presented in the next section. Pulsed optical excitation of $Ru(dcbpy)_2(NCS)_2$ sensitised nanocrystalline TiO_2 films results in a broad absorption increase peaking at ~ 800 nm assigned to an absorption band of the $Ru(dcbpy)_2(NCS)_2$ cation (Tachibana et al. 1996). In the absence of redox active species in the electrolyte the experiments monitor the decay of the dye cations reacting with electrons in the semiconductor. The electrons are bound to contribute to the transient absorption signal but uncertainties remain on how sizeable their contribution is. At least some of the photoinjected electrons (e_{TiO2}) are thought to lead to localised Ti^{3+} states, believed to give rise to a broad absorption band in the red / near-infrared. The transient absorption spectrum of a $Ru(dcbpy)_2(NCS)_2$ sensitised film 4 μs after excitation (fig 3.5) in a redox inactive electrolyte reveals a "tail" in the red, consistent with electron absorption. The extent of the electron absorption contribution at 800 nm does not however influence the kinetics since the dye cation and electron populations are depleted simultaneously by the charge recombination k_{CR1}.

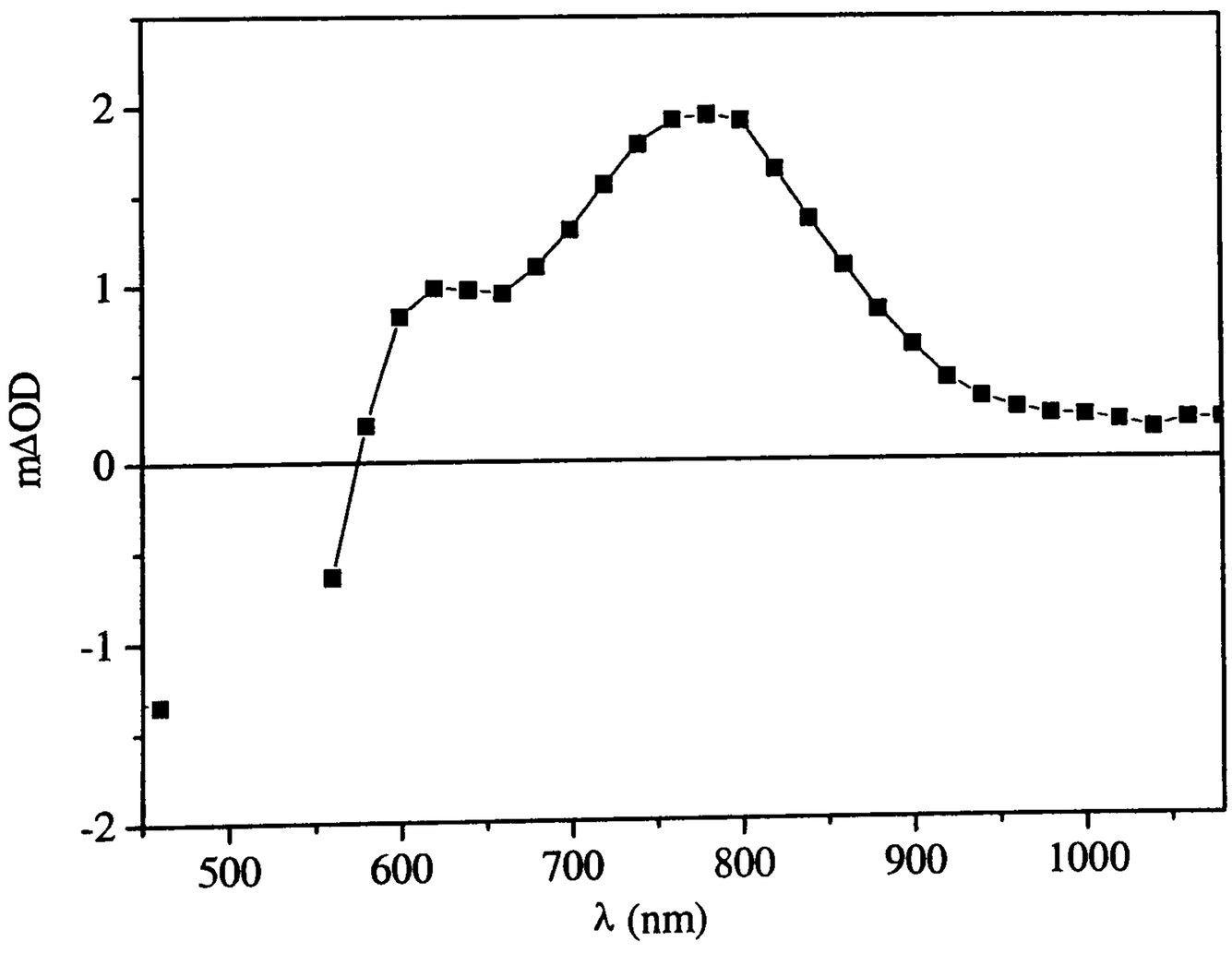

Figure 3.5: *Transient absorption spectra measured 4 μs after excitation for a $Ru(dcbpy)_2(NCS)_2$ sensitised film covered in 0.1M $LiClO_4$ in propylene carbonate.*

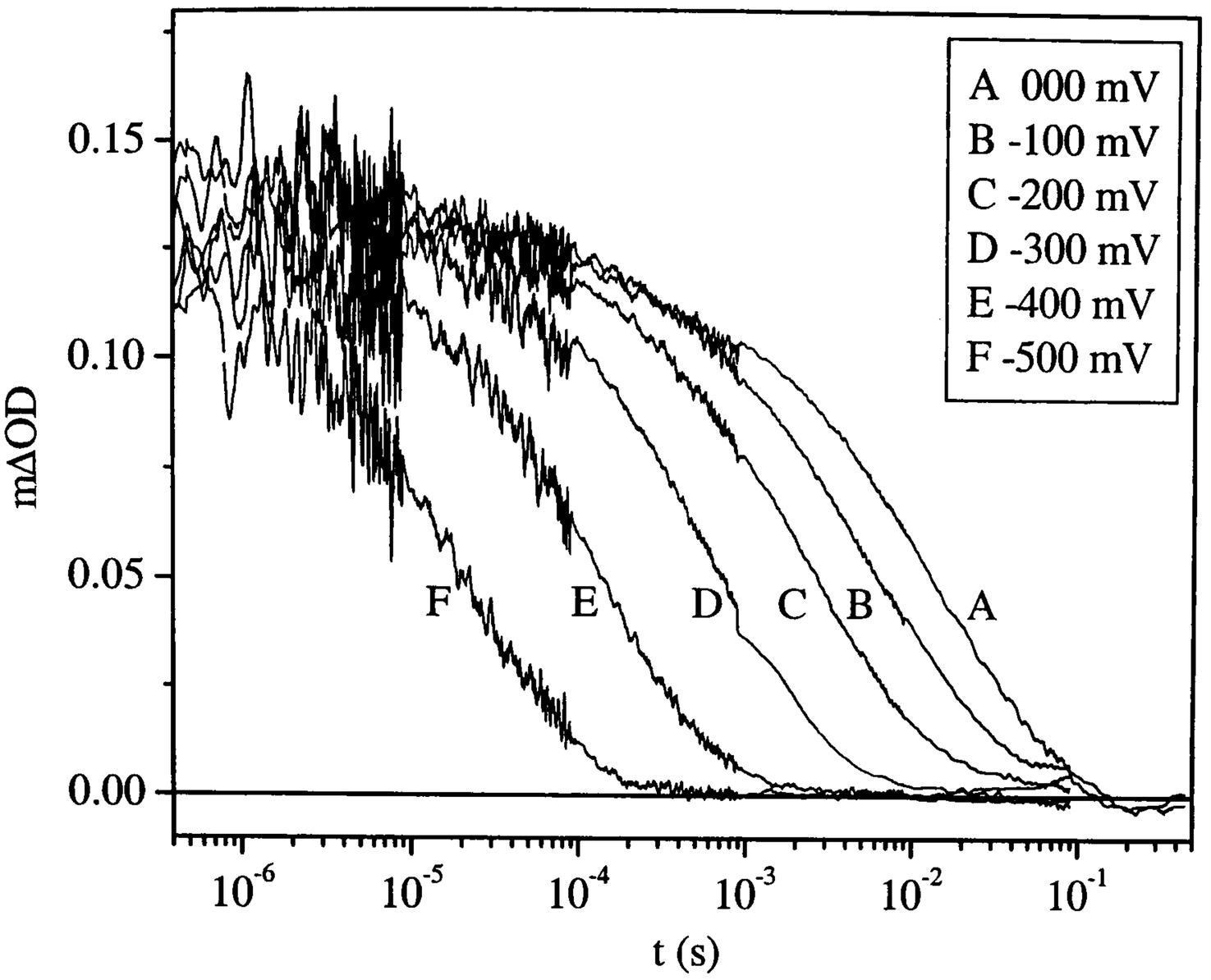

Figure 3.6: *Kinetic decays for a $Ru(dcbpy)_2(NCS)_2$ sensitised TiO_2 film in a three electrode cell measured as a function of externally applied bias. The electrolyte was 0.1 M $LiClO_4$ in propylene carbonate. All voltages vs. Ag/AgCl. The excitation wavelength was 620 nm and the signal was probed at 800 nm where the dye cation absorbs.*

The kinetics span several orders of magnitude and have a stretched exponential shape consistent with that observed by Haque et al (Haque et al. 2000) in ethanol and acetonitrile. As a negative bias is applied to the electrode a strong bias dependence is observed as it can be seen in figure 3.6. The dispersion exponent α of the stretched exponential is 0.4 ± 0.05. The $t_{50\%}$ of the charge recombination kinetics becomes faster by approximately an order of magnitude for each 100 mV. The reproducibility of the onset of the bias dependence varied by $\pm$ 50 mV between samples.

3.3.2 Dye cation regeneration kinetics

The experiments presented in this section studied the reaction of dye cations photogenerated on the semiconductor surface with different concentrations of iodide in the electrolyte in order to assess the dependence of the reaction rate on the concentration of iodide in solution.

3.3.2.1 Results

The addition of increasing amounts of iodide to the electrolyte results in the decay kinetics at 800 nm becoming increasingly biphasic. The faster phase accelerates as a function of iodide concentration. The amplitude of the slower phase increases as the iodide concentration is increased, and exhibits a half-life of approximately 0.2-0.5 s independent of iodide concentration. The insert shows an expansion of data collected with the nanosecond set-up at early times, indicating that the initial amplitude of the signal, assigned to dye cation formation due to electron injection, is independent of iodide concentration, consistent with ultrafast electron injection (Tachibana 2000).

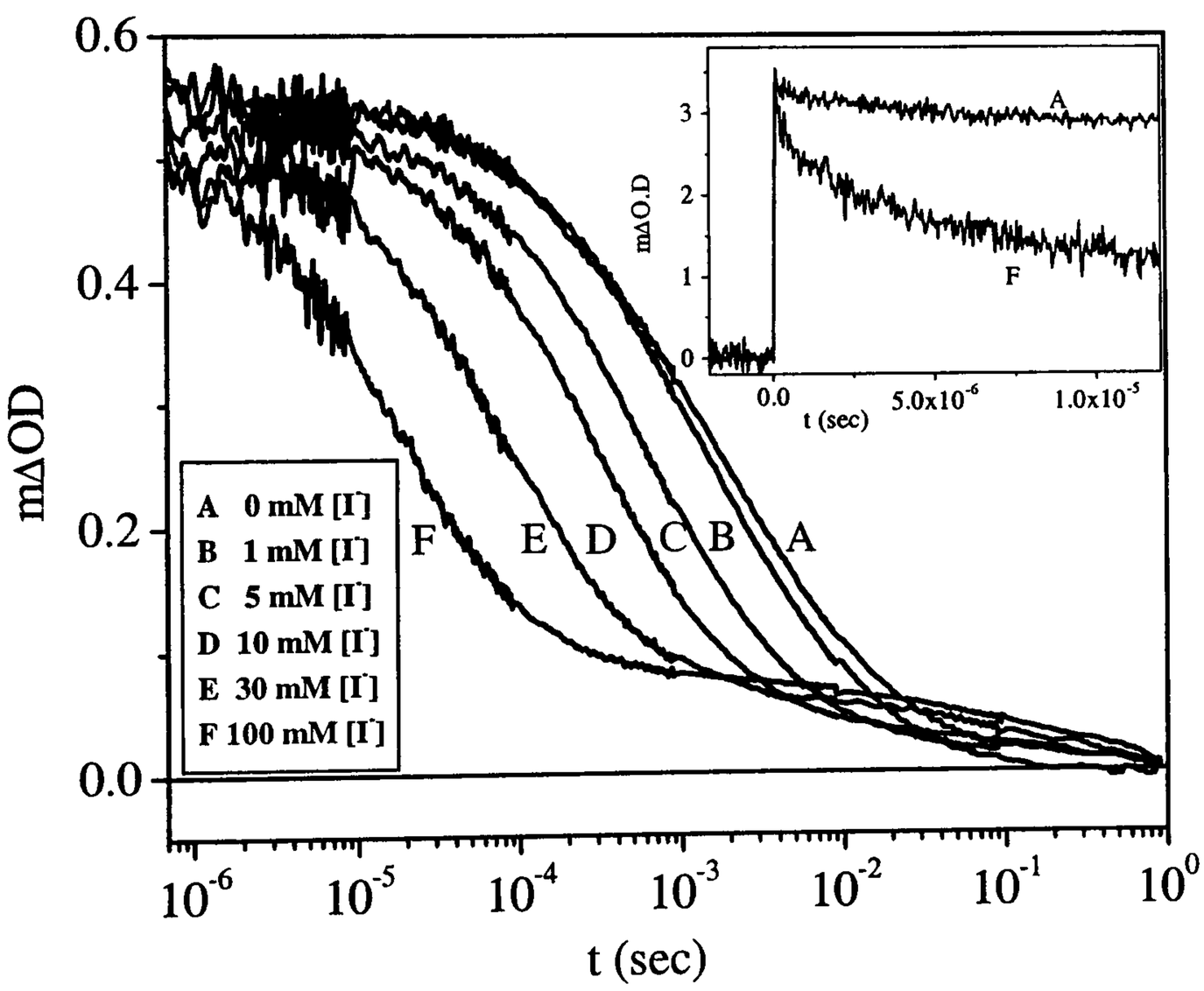

Figure 3.7: *Kinetic decays for a $Ru(dcbpy)_2(NCS)_2$ sensitised film measured as a function of iodide concentration. The electrolytes consisted of $LiClO_4$ and LiI in propylene carbonate, with the lithium perclorate concentration adjusted to maintain a constant Li^+ concentration (0.1 M) and iodide concentrations as indicated in the figure. Also shown in the inset is data collected with the nanosecond set-up at early times for the 0 and 100 mM I^- concentrations, respectively.*

In order to assign the biphasic behaviour shown in figure 3.7 the transient absorption spectra of the species involved at early and later stages of the reaction were recorded as shown in figure 3.8. This figure shows transient spectra collected at 10 μs and 1 ms after excitation of the $Ru(dcbpy)_2(NCS)_2$ / TiO_2 films in the presence of 0.1 M I^- ions. The spectrum at 10 μs (A in figure 3.8) exhibits the characteristic features of the dye cation state, namely an absorption bleach centred at ~ 540 nm - the ground state absorption maximum of the dye (though the size of the bleach is somewhat smaller than it would be expected) - and a broad absorption increasing towards ~ 800 nm assigned to the dye cation (Tachibana et al. 1996; Moser et al. 1998). In contrast, the spectrum at 1 ms (B in Figure 3.7) remains positive throughout the spectral range studied, with increases in the near infrared and towards the blue, and a minimum at 575 nm. The absence of a negative signal around 500 nm clearly indicates this spectrum cannot be assigned to dye cation states.

The increase in the amplitude of the slow component associated with increasing iodide concentration and with decreasing dye cation lifetime indicates that the spectrum at 1 ms corresponds to long lived product states generated by the regeneration of the dye cation by iodide ions (k_{RG}). Comparison with literature spectra indicates that this product state spectrum is in good agreement with the spectrum previously assigned in UV flash photolysis experiments to the radical anion state I_2^- (Devonshire and Weiss 1968; Hug 1981), as illustrated in figure 3.8 (smooth line). These data therefore provide direct support for previous suggestions that iodide reduction of the dye cation results in generation of this species (Nasr, Hotchandani, and Kamat 1998; Pelet, Moser, and Grätzel 2000) (see Scheme 3.7).

The regeneration of the dye ground state by iodide implies the survival of photoinjected electrons in the TiO_2 film:

$e_{TiO2}|Dye^+ + 2I^- \rightarrow e_{TiO2}|Dye + I_2^-$ (Scheme 3.10)

Electron absorption contributing to the long lived product species presented in figure 3.8 can be seen in the 800-950 nm region and this slow phase is therefore assigned to the state I_2^- / e_{TiO2}.

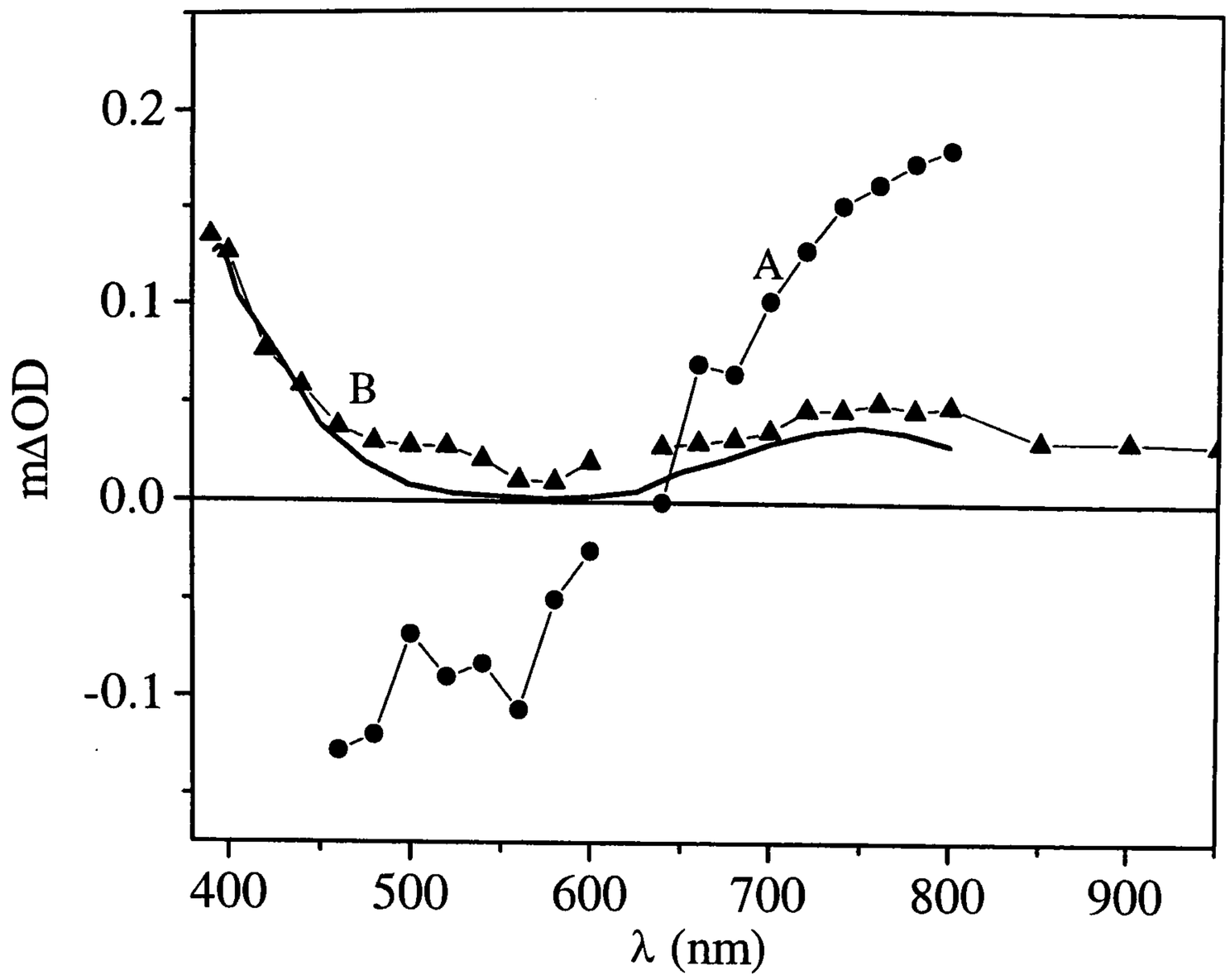

Figure 3.8: *Comparison of the transient absorption spectra measured for a $Ru(dcbpy)_2(NCS)_2$ sensitised film immersed in 0.1 M LiI in propylene carbonate. Spectra are shown at A) 10 μs and B) 1 ms after excitation at 620 nm. Also shown (smooth line) is the spectrum of I_2^- determined previously by UV flash photolysis (Devonshire and Weiss 1968; Hug 1981).*

As mentioned in section 3.3.1 photoinjected electrons (e_{TiO2}) can lead to localised Ti^{3+} states, with a broad absorption increase in the red / near infrared, and contribute to the positive absorption increase observed for both 10 μs and 1 ms spectra at 800 nm. The extinction coefficient for such Ti^{3+} states is however controversial at present (Rothenberger, Fitzmaurice, and Grätzel 1992; Redmond and Fitzmaurice 1993). Studies carried out by Carol Olson in the Physics Department at Imperial College indicate that under the experimental conditions considered here the best estimate for their extinction coefficient is approximately 800 $M^{-1}cm^{-1}$ (in good agreement with results previously reported by Grätzel and co-workers. in 1985 (Kölle, Moser, and Grätzel 1985)) and it is therefore expected to be small relative to those of the dye cation and I_2^- radicals (about 6000 and 2200 $M^{-1}cm^{-1}$ respectively (Tachibana 2000; Hug 1981)). In any case, independent of any uncertainty on the extent of Ti^{3+} absorption contributing to the transient data, the long lived component observed in figure 3.7 must be assigned to a long lived charge separated state generated by the re-reduction of dye cations by iodide ions.

From the above analysis, the biphasic nature of the decay kinetics observed in the presence of iodide ions is assigned to the regeneration reaction k_{RG} (equation 3.2), resulting in the generation of long-lived I_2^- radicals, with a contribution by electron absorption. The nature of the regeneration reaction products will be further adressed in the discussion. At moderate iodide concentrations, kinetic competition occurs between k_{RG} and k_{CR1}, resulting in a lower yield of I_2^-/ e_{TiO2}. As shown in figure 3.7, at iodide concentrations > 30 mM only a small increase in product state yield is observed, indicating that for concentrations ≥ 30 mM k_{RG} largely dominates over k_{CR1} and the products yield is close to maximal. In this respect it can be noted that this result is in contrast with the I_2^- yield saturation observed by Kamat and co-workers (Nasr, Hotchandani, and Kamat 1998) at very low iodide concentration values (i.e. 0.1 mM) although it should be noted that excessive excitation power density were employed in these experiments.

Kay et al. reported very similar kinetics to the ones shown in figure 3.7 when studying chlorin derivatives - sensitised TiO_2 in the presence of lithium iodide. Three probe wavelength (633, 720 and 1000 nm) were monitored and the respective decays were assigned to ground state Q_y band bleach, dye cations and electrons in the TiO_2, respectively. It was suggested that the long lived (>100 ms) signal at 1000 nm assigned to electrons decayed by reaction with iodine or traces of oxygen (Kay, Humphry-Baker, and Grätzel 1994). Unfortunately, this study did not include a transient spectrum of the species observed to be compared with figure 3.8.

3.3.3 Sensitiser dye dependence

$Ru(dcbpy)_2(NCS)_2$ has yielded the most efficient sensitised-TiO_2 photoelectrochemical cells to date. However, hundreds of alternative dyes have been tested either in order to improve the stability of the devices or to extend their absorption to the infra-red region in a quest for a better match with the solar spectrum. Among these, probably due to their ubiquity in natural photosynthesis and their extensive photophysical characterisation, porphyrins and chlorophylls have received a notable amount of attention (Kay and Grätzel 1993; Kay, Humphry-Baker, and Grätzel 1994). In a recent study (Tachibana et al. 2000), our research group has compared the electron injection (k_{inj}) and recombination kinetics (k_{CR1}) of $Ru(dcbpy)_2(NCS)_2$ and Zn-tetra-carboxy-phenyl porphyrin (ZnTCPP) sensitised films. Remarkably, both processes appear to be

essentially indistinguishable for these two dyes lending evidence to the fact that the nature of the semiconductor and its energy / traps levels play a more important role in determining interfacial kinetics than the nature of the sensitiser dye employed (Nelson et al. 2001). Tachibana has suggested that the lower overall efficiency obtained with ZnTCPP sensitised cells could be due to a less efficient reaction of its cation with iodide in the electrolyte (Tachibana 2000). In a study comparing nanocrystalline electrodes sensitised with $Ru(dcbpy)_2(CN)_2$ dyes and its osmium analogue, the poor cell performance obtained with the osmium dye was attributed to the "sluggishness" of the iodide re-reduction reaction, resulting in significant losses through recombination pathway k_{CR1} (Alebbi et al. 1998). These results have however been questioned by Lewis and co-workers (Sauvé et al. 2000; Kuciauskas et al. 2001) who have obtained comparable efficiencies for both Ru and Os centred complexes. In order to investigate the role of the nature of the dye on the regeneration reaction k_{RG}, iodide kinetics were studied in TiO_2 films sensitised with $Os(dcbpy)_2(CN)_2$ an ZnTCPP dyes.

3.3.3.1 Results

Figure 3.9 shows a comparison of transient absorption data obtained with TiO_2 films sensitised with both $Ru(dcbpy)_2(NCS)_2$ and ZnTCPP. It is apparent that both dye cation decay kinetics and the magnitude of the long lived signal are similar between these two dyes. A comparison between spectra at 10 μs and 1 ms for the ZnTCPP sample is shown in figure 3.10. As in the case of $Ru(dcbpy)_2(NCS)_2$ sensitised films the spectrum recorded at 10 μs is consistent with that of the dye cation observed in ultra-fast measurements (Tachibana 2000) while the spectrum recorded at 1 ms is similar to that obtained with $Ru(dcbpy)_2(NCS)_2$ and consistent with the formation of the I_2^- / e_{TiO2} pair. Similar considerations on the contribution of injected electrons to the absorption signal apply. It can therefore be concluded that the kinetics of dye regeneration by iodide ions are similar for these two dyes.

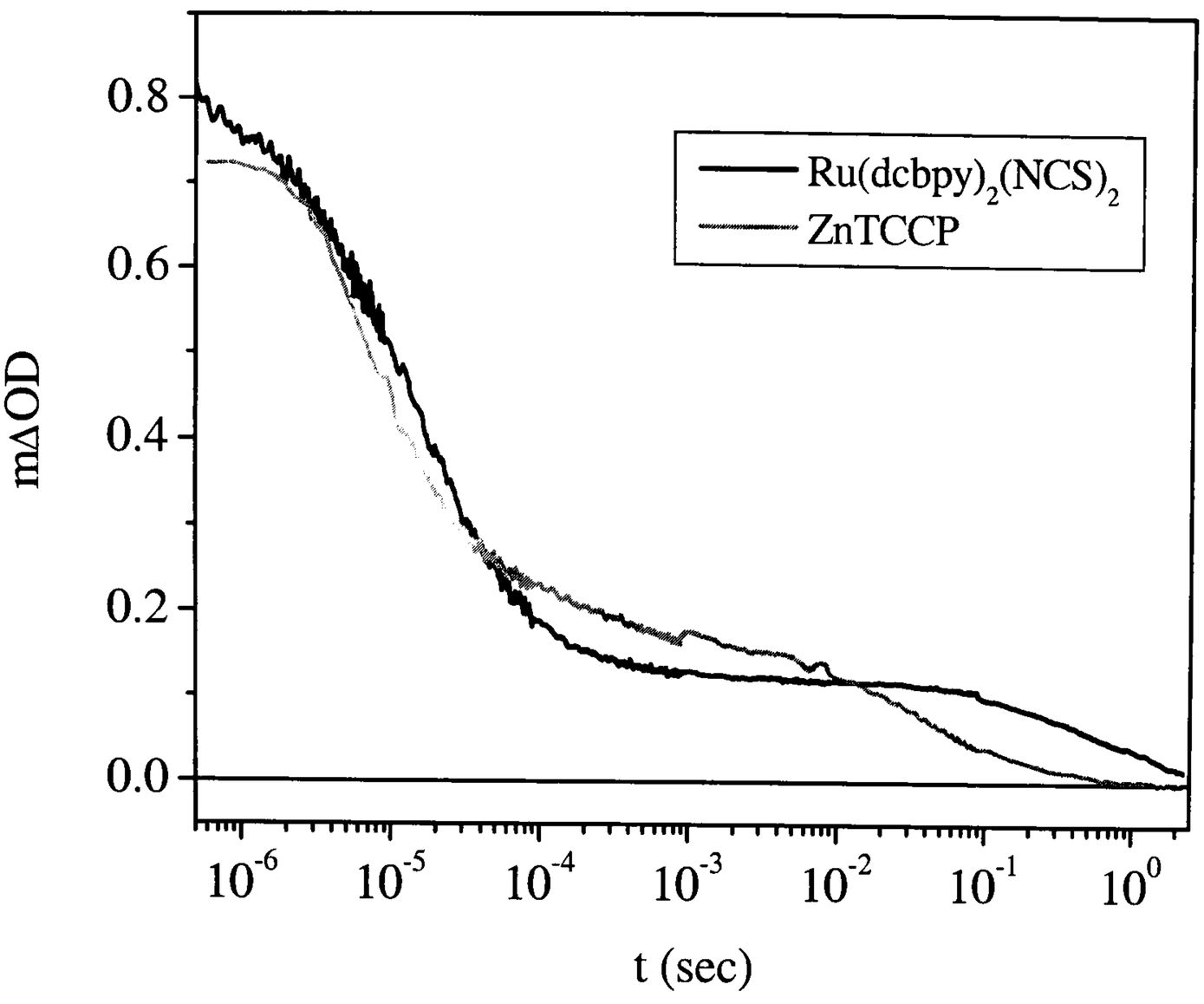

Figure 3.9: *Transient absorption decays observed for $Ru(dcbpy)_2(NCS)_2$ (black) and ZnTCPP (grey) sensitised TiO_2 films immersed in 0.1 M LiI in propylene carbonate. In the former case the excitation and probe wavelengths were 620 and 800 nm respectively while in the latter these were 560 and 740 nm.*

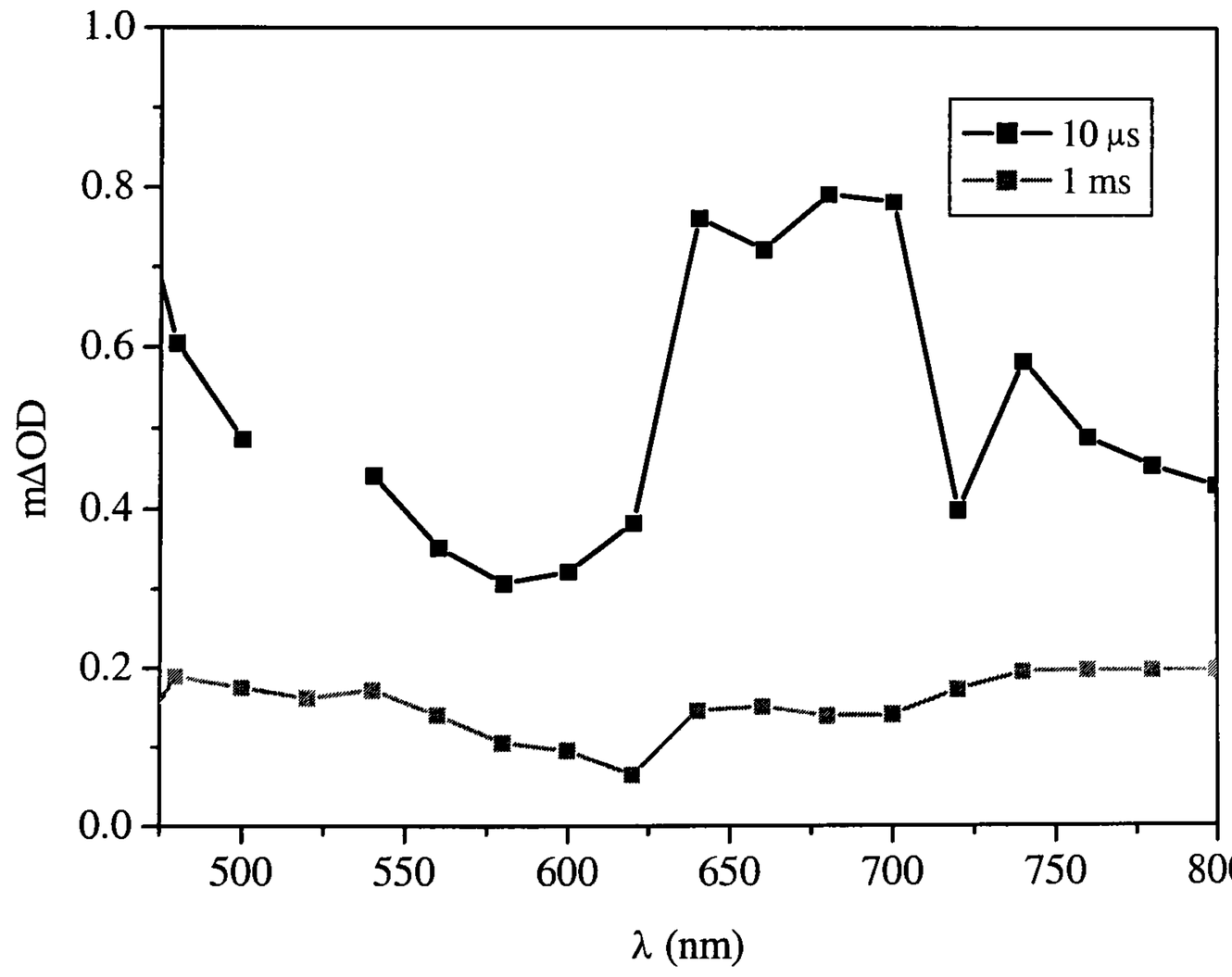

Figure 3.10*: Comparison of the transient absorption spectra measured for a ZnTCPP sensitised film immersed in 0.1 M LiI in propylene carbonate. Spectra are shown at 10 μs (black) and 1 ms (grey) after excitation at 560 nm. The long lived product has a spectra similar to the products at 1 ms observed with $Ru(dcbpy)_2(NCS)_2$ sensitised films.*

Transient kinetics for the $Os(dcbpy)_2(CN)_2$ are presented in figure 3.11. In this case the experiments monitored the decay of the bleach of the dye ground state instead of the decay of the dye cation as in the case of $Ru(dcbpy)_2(NCS)_2$. Results in a redox inactive electrolyte (EC:PC 1:1) and in the presence of 0.1 M lithium iodide are compared. In contrast to earlier reports (Alebbi et al. 1998) and in agreement with subsequent ones (Kuciauskas et al. 2001) the kinetics in the presence of iodide lead to a faster decay of the dye cation indicating efficient dye regeneration by iodide. Furthermore, the formation of products of the dye regeneration reaction is clear from their positive absorption in this region that leads to the signal changing sign at approximately 800 μs.

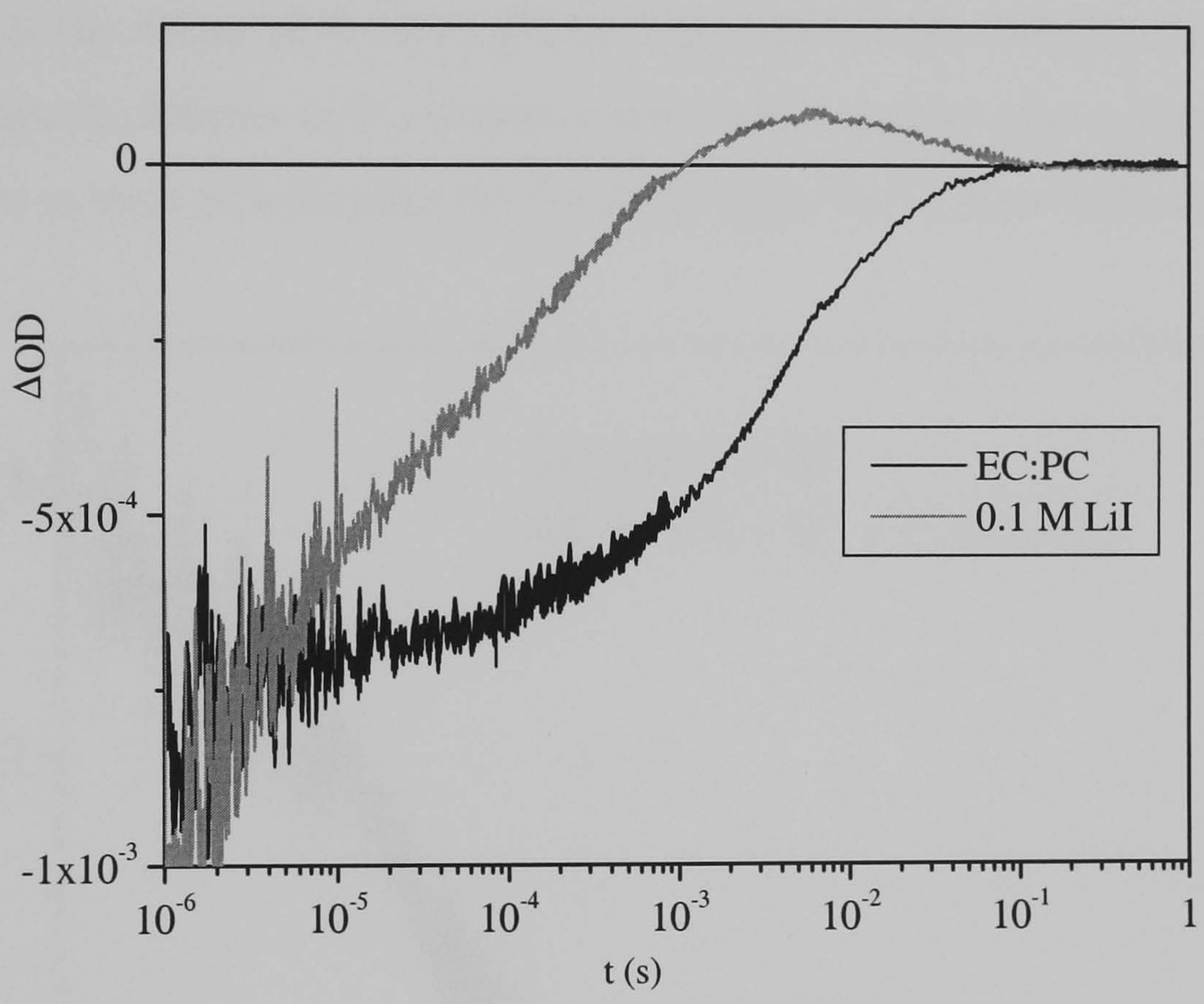

Figure 3.11: *Kinetic decays for a $Os(dcbpy)_2(CN)_2$ sensitised film measured in a redox inactive electrolyte (EC:PC 1:1, black) and in the presence of 0.1 M lithium iodide in propylene carbonate (grey). The excitation and probe wavelengths were 530 and 430 nm respectively. The experiment monitors the recovery of the dye ground state bleach. In the presence of iodide the signal becomes positive at approximately 800 μs as products of the dye regeneration reaction are formed.*

3.3.4 Kinetics in presence of iodine

Heimer et al. (Heimer et al. 2000) have reported a dramatic effect on the kinetics of the iodide reaction when iodine is added to the electrolyte. The result was attributed to I_3^- adsorption on the semiconductor surface. In order to test this hypothesis, experiments conducted on $Ru(dcbpy)_2(NCS)_2$ sensitised films in the presence of 0.1 M iodide were further extended by the addition of 0.01 M iodine to the electrolyte - as the ratio of iodide to iodine employed in devices is usually 10:1.

3.3.4.1 Results

Data collected in the presence and absence of iodine is presented in figure 3.12. The addition of iodine resulted in no change in the transient data apart from a small acceleration of the decay of the slow phase. This observation indicates that, contrary to what was found by Heimer et al., neither iodine nor I_3^- species play a significant role in the dye cation re-reduction kinetics for the $Ru(dcbpy)_2(NCS)_2$ sensitiser dye.

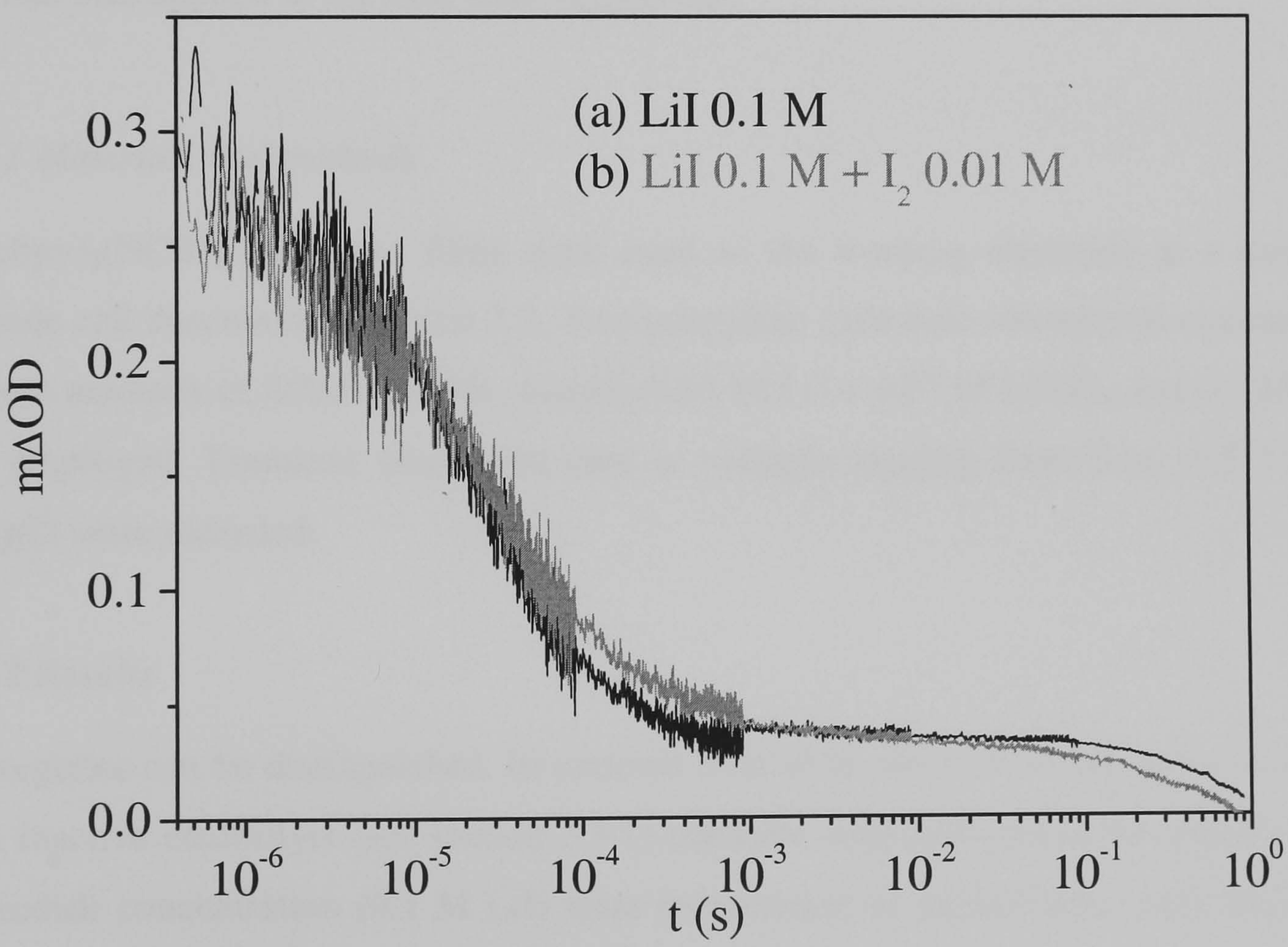

Figure 3.12: *Transient kinetic decays recorded for a $Ru(dcbpy)_2(NCS)_2$ sensitised film in 0.1 M LiI in propylene carbonate (black) and with the addition of 0.01 M I_2 to the electrolyte (grey). The dye regeneration kinetics is unaffected while the decay of the products accelerates slightly.*

3.3.5 Kinetic competition in presence of an externally applied bias

It has been seen above that the charge recombination reaction is strongly dependent on an electrical bias applied to the dye-sensitised electrode and in turn the Fermi level of the electrons in the semiconductor. In devices under illumination the electrodes of the cell are at a difference in potential corresponding to the open circuit voltage. As explained in chapter 1 the open circuit voltage is, as a first approximation, determined by the difference between the Fermi level in the semiconductor and the redox potential of the I^-/I_3^- redox couple. The ratio of iodide to tri-iodide concentrations can be assumed to be constant at least on the timescale of the experiment. Therefore, an increase of open circuit voltage in a device corresponds mainly to a shift of the Fermi level for the electrons in the semiconductor. It is therefore important to characterise how the different reactions at play in dye sensitised electrodes are affected by a shift in the Fermi level in the TiO_2. To this end experiments where the kinetics of dye cation regeneration in the presence of two different iodide concentrations as a function of electrical bias applied to the film were carried out.

3.3.5.1 Materials and methods

$Ru(dcbpy)_2(NCS)_2$ sensitised films were used as the working electrode in a three - electrode cell described in section 2.3. Two propylene carbonate electrolytes containing different amounts of lithium iodide, namely 0.03 M LiI + 0.07 M $LiClO_4$ and 0.1 M LiI were employed. Transient absorption data at voltages ranging from 0 to -0.5 V vs. Ag/AgCl were recorded.

3.3.5.2 Results

Two regimes can be distinguished. In contrast with what observed in the presence of a redox inactive electrolyte (see section 3.3.1) transient data collected in the presence of high iodide concentration (0.1 M LiI) were independent of applied bias, with the data being similar to that collected at this iodide concentration in the absence of any applied bias (figure 3.7). Typical data are shown in figure 3.13. At this iodide concentration, the dye cation decay kinetics are expected to be dominated by the regeneration reaction k_{RG}. The bias independence of the transient data at this iodide concentration indicates that k_{RG} is independent of applied electrical bias within the range employed in the

experiments. In fact, a small change in the kinetics becomes apparent when the maximum negative bias (-0.5 V) is applied and the yield of the product states is somewhat reduced. Such effect may be related to instability of the sensitiser dye as suggested previously (Haque et al. 2000).

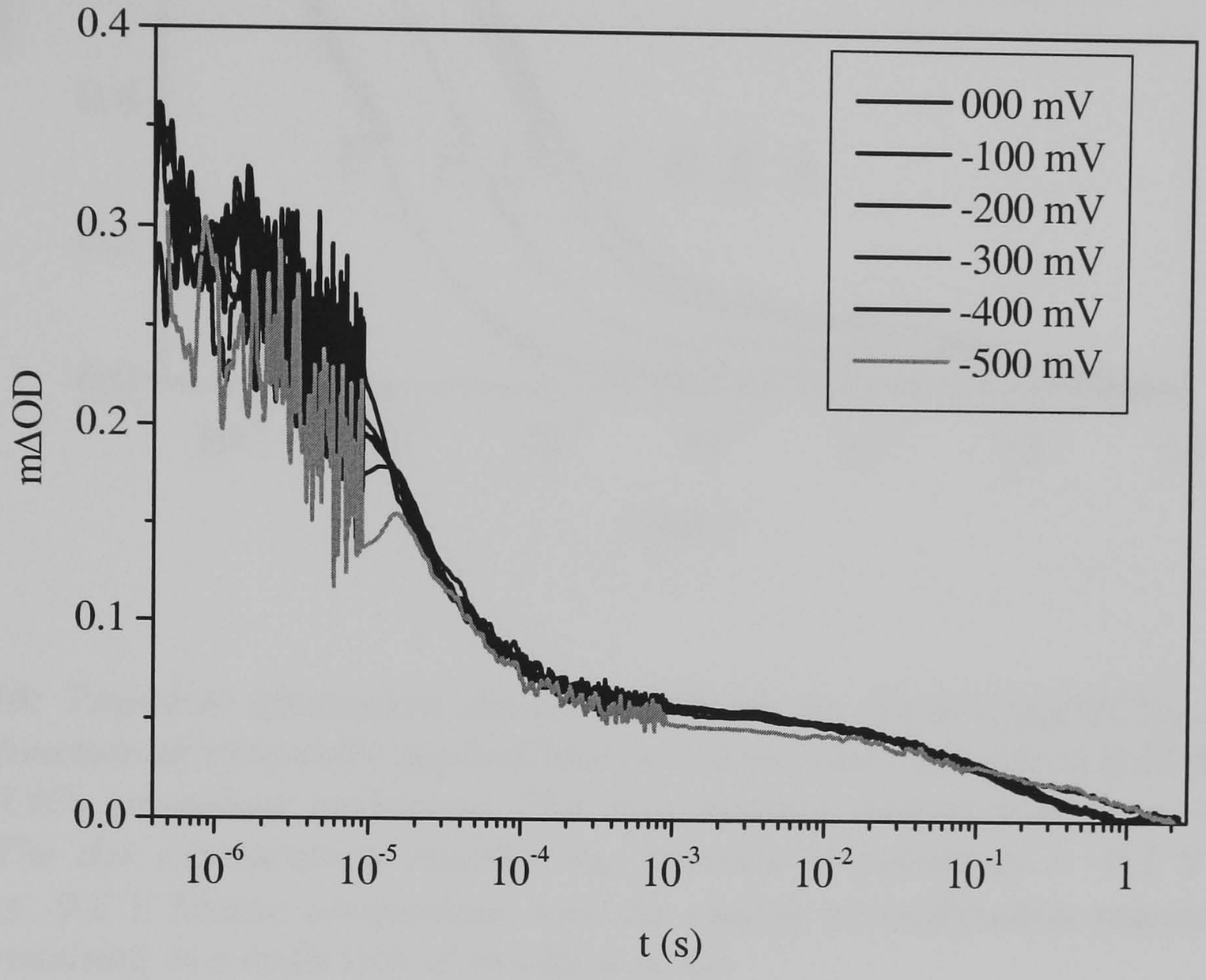

Figure 3.13: *Transient absorption decays observed at 800 nm for $Ru(dcbpy)_2(NCS)_2$ sensitised films as a function of externally applied bias in a three electrode cell in 0.1 M LiI propylene carbonate. The kinetics are not effected by the applied bias up to -0.5 V vs. Ag/AgCl where a small decrease in I_2^-/e_{TIO2} yield is just noticeable (grey line).*

Kinetic competition between k_{RG} and k_{CR1} is expected at more moderate iodide concentrations. Such data is shown in figure 3.14, where data collected as a function of applied bias for a 0.03 M iodide concentration is presented. For potentials > -0.2 V vs. Ag/AgCl, the kinetics are independent of applied bias, consistent with the dye cation decay being dominated by the regeneration reaction k_{RG}. However, for potentials ≤ -0.2 V vs. Ag/AgCl, an acceleration of the dye cation decay kinetics is observed, and the yield of I_2^-/e_{TiO2} products is reduced. This observation is consistent with the expected acceleration of k_{CR1} at negative biases resulting in the recombination reaction dominating the decay kinetics at negative applied biases in these conditions.

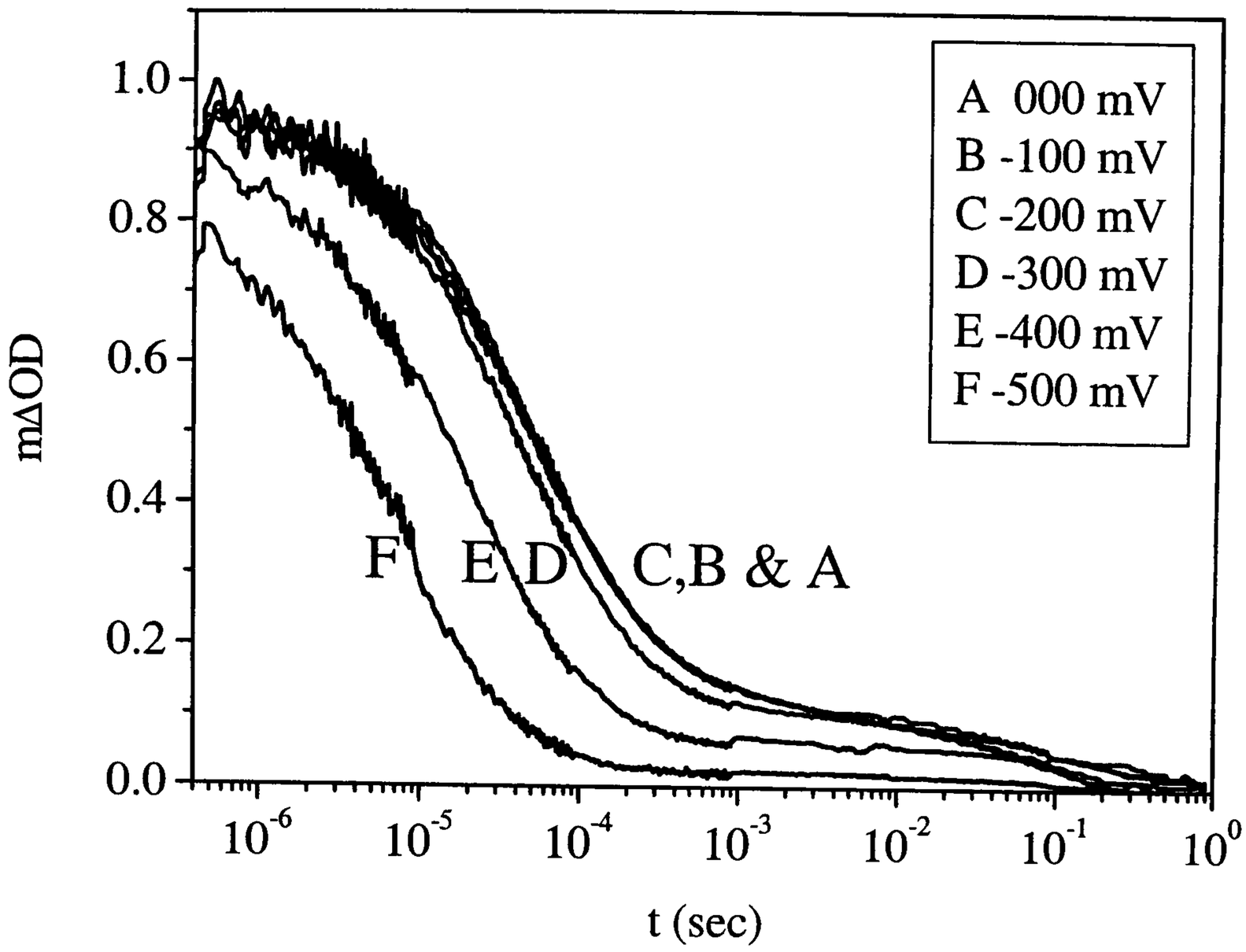

Figure 3.14: *Transient absorption decays at 800 nm for $Ru(dcbpy)_2(NCS)_2$ sensitised films as a function of externally applied bias in a three electrode cell in 0.03 M LiI and 0.07 M $LiClO_4$ propylene carbonate. The bias applied ranged from 0 to -0.5 V vs. Ag/AgCl. The dye regeneration reaction k_{RG} prevails at potentials > -0.2 V while at potentials ≤ -0.2 V kinetic competition with the charge recombination reaction k_{CR1} is observed, resulting in a reduction of products yield.*

3.3.6 Summary of results

Transient absorption spectroscopy has been employed to characterise the decay kinetics of the dye cation in $Ru(dcbpy)_2(NCS)_2$ sensitised TiO_2 films immersed in lithium iodide in propylene carbonate. The addition of increasing amount of iodide to the electrolyte leads to the dye cation decays becoming biphasic and the formation of long-lived products of the dye regeneration reaction by iodide is apparent. The transient absorption spectrum of the products is consistent with both the formation of I_2^- radicals and electron absorption in the TiO_2 nanocrystals.

A comparison between nanocrystalline TiO_2 films sensitised with three different dyes, i.e. $Ru(dcbpy)_2(NCS)_2$, $Os(dcbpy)_2(CN)_2$ and ZnTCPP reveals qualitatively similar kinetics in the absence and presence of iodide.

The kinetics were also studied as a function of applied bias to the semiconductor electrode. When a high iodide concentration (0.1 M) is employed the decays are independent of applied bias within the range employed.

The dye regeneration reaction k_{RG} clearly dominates in this case and is independent of the applied bias. When an intermediate iodide concentration (0.03 M) is employed the kinetics are unaffected up to -0.2 V vs. Ag/AgCl. At more negative biases the $t_{50\%}$ of the dye cations is reduced and in turn the yield of the reaction products is reduced. In this regime the charge recombination k_{CR1}, which is strongly bias dependent as shown earlier in section 3.3.1, becomes the dominant mechanism for the dye cation disappearance, reducing the amount of the iodide reaction products formation. Numerical modelling of the charge recombination reaction in terms of a Continuous Time Random Walk of the electrons in the semiconductor as done by Nelson (Nelson 1999; Nelson et al. 2001) introduced in section 3.1.2 will now be described in more details and an attempt to extend the model to the iodide kinetics will be discussed (Montanari, Nelson, and Durrant 2002).

3.3.7 Numerical modelling

3.3.7.1 CTRW modelling of the charge recombination reaction

As introduced in Section 3.1.2 a model of electron transport in nano-particulate TiO_2, based on the CTRW of Scher and Montroll (Scher and Montroll 1975) has been remarkably successful in explaining bias dependent charge recombination kinetics in dye-sensitised film (Haque et al. 1998; Nelson 1999; Haque et al. 2000; Nelson et al. 2001). The CTRW model as applied to nanocrystalline TiO_2 particles by Dr. Nelson was schematically shown in figure 3.3. It will now be described in more detail.

The photoinduced electron injection step is followed by trapping and the electrons perform a CTRW to recombine with dye cations, i.e. an injected electron will have to find its way back to a dye cation going through a series of trapping and de-trapping steps. The trap energies distribution is assumed to be exponential. Each de-trapping step is delayed by a waiting time determined by the time for thermal activation out of the site currently occupied. The set of waiting times for a distribution of trap energies form a waiting time distribution (WTD, $\chi(t)$). This distribution is chosen to correspond to an exponential trap density distribution in the semiconductor particles. The waiting times distribution for the de-trapping steps $\chi(t)$ mimics the disorder in the system and could correspond to both a distribution of activation energies (energetic disorder) or of the physical distribution of electrons (spatial disorder). The former is related to transport via thermally activated trapping and de-trapping while the latter is associated with transport through tunnelling. In the case of energetic disorder $\chi(t)$ is related to the density of trap states g(E):

$$g(E) = \frac{\alpha N_t}{kT} e^{-\alpha(E_c - E)/kT} \tag{3.8}$$

where E_c is the conduction-band edge energy, N_t is the density of traps per unit volume, k is Boltzmann's constant, T is the temperature, and α is the dispersion parameter such that $0 < \alpha < 1$. For this g(E) distribution $\chi(t)$ has a power law form:

$$\chi(t) = At^{-1-\alpha} \tag{3.9}$$

where $\alpha = \frac{T}{T_0}$ and T_0 is the characteristic temperature of the exponential distribution.

For a waiting time distribution (WTD) with a sufficiently long tail the average number of steps taken in time t, H(t), increases more slowly than t.

In the case of the power law $\chi(t)$,

$$H(t) \propto t^{\alpha} \tag{3.10}$$

In the limit where the lattice is sparsely populated and the number of electrons outnumbers the dye cations the survival probability of the dye cation D^+ varies as equation 3.11:

$$[D^+](t) = [D^+]_0 e^{-B[e^-]H(t)} \tag{3.11}$$

where $[e^-]$ is the electron density and B is a constant.

The half-life $t_{50\%}$ of the dye cations, defined as $S(t_{50\%}) = \frac{1}{2}S(0)$ is:

$$t_{50\%} = H^{-1}\left(\frac{\ln 2}{[e^-]}\right) \tag{3.12}$$

where H^{-1} is the inverse function of H.

For the power law $\chi(t)$, $[D^+](t)$ is a stretched exponential function:

$$[D^+](t) \propto e^{-(t/\tau)^{\alpha}} \tag{3.13}$$

and $t_{50\%} \propto [e^-]^{-1/\alpha}$. (3.14)

as introduced in section 3.1.2 (equation 3.4, $n=[e^-]$).

The behaviour expected from equation 3.14 is indeed observed as can be seen in figure 3.15 where a plot of $t_{50\%}$ vs. the number of electrons in the particle for previous studies (Nelson et al. 2001) is presented. The predicted behaviour of electron diffusion, tunnelling and CTRW models are compared. The CTRW is the one in best agreement with experiments.

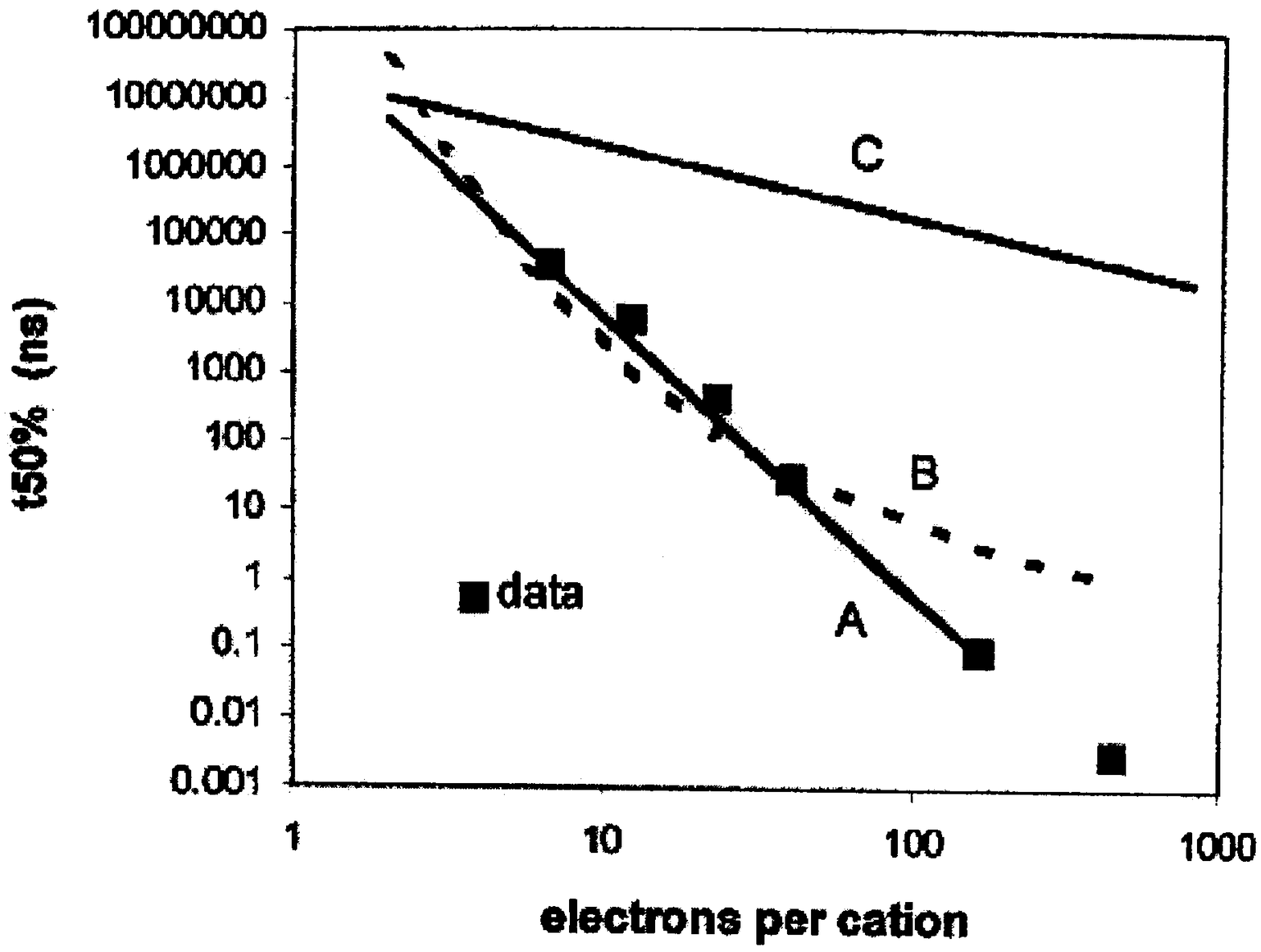

FIG. 3. Comparison of experimental results for n vs. $t50\%$ for the ethanol electrolyte (filled squares), with results of the CTRW model with $\alpha = 0.25$ (curve A) and the hopping model in the limit where $k_S \gg k_0$ (curve B). Notice that over narrow ranges of $t_{50\%}$ the hopping model appears to resemble the data and can only be ruled out by the subnanosecond data, which is capable of distinguishing between the models. Curve C shows the variation expected for normal diffusion when $n \propto t_{50\%}^{-1}$. The recombination times predicted in that case are clearly incompatible with the data.

Figure 3.15: *Comparison of the theoretical prediction of the charge recombination rate k_{CRI} as a function of the number of electrons per particle (in turn, the applied electrical bias) for: A) CTRW, B) hopping C) diffusion of the electrons through the semiconductor (from Nelson et al. 2001).*

This is clearly also an appealing physical description for the charge transport by the electrons within the particles and to the back contact (the ITO/TiO_2 interface) though the model has not been tested in this respect as yet. The application of the CTRW model to the charge recombination reaction data shown in figure 3.6 is presented in figure 3.16. The simulations were performed by Dr. Jenny Nelson in the Physics Department at Imperial College. The original data from figure 3.6 is superimposed to the simulation results. The agreement is good but seems to worsen at longer times, a discrepancy attributed to the lack of information on the real density of states which might deviate from the exponential form assumed here (Nelson et al. 2001). The value of α obtained from the modelling is approximately 0.4.

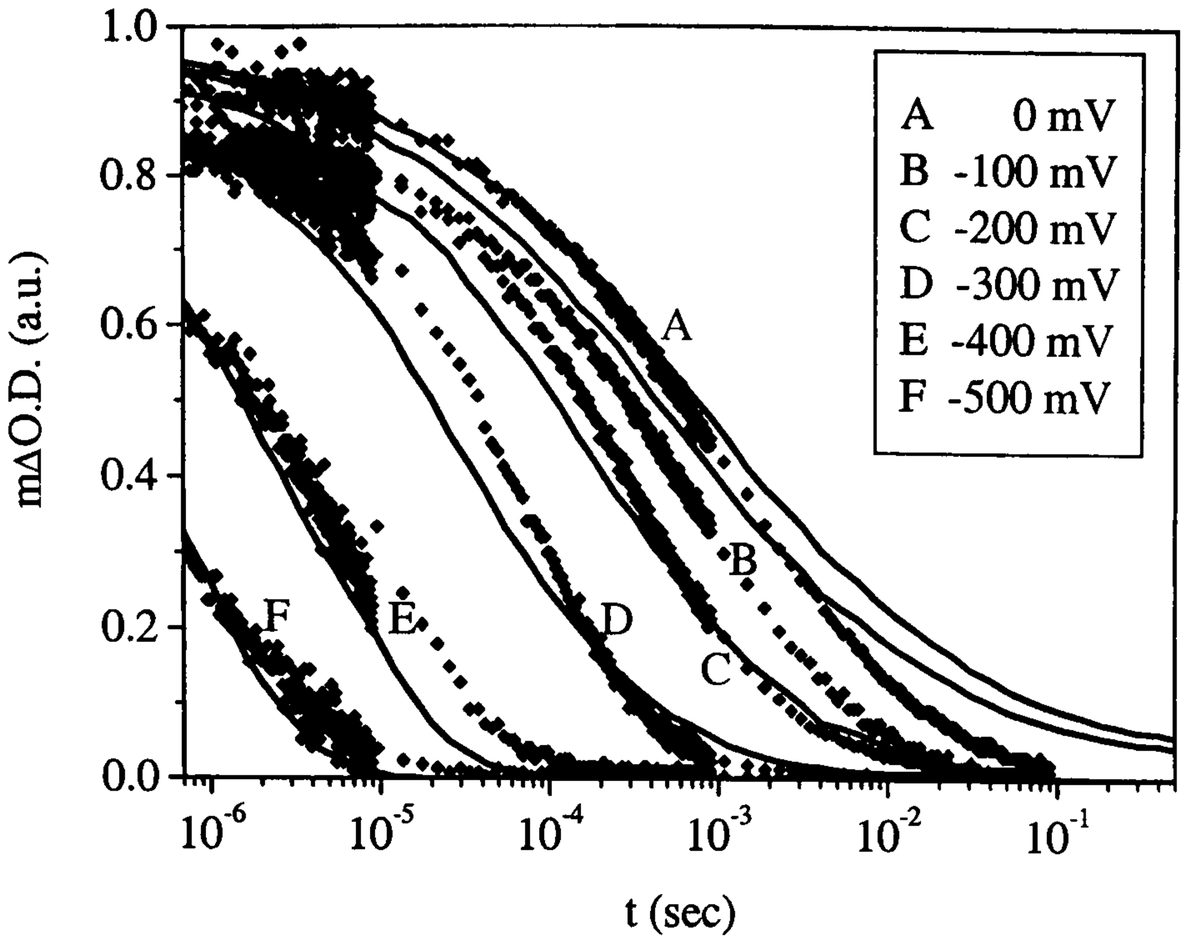

Figure 3.16: *Bias dependent charge recombination kinetics for a* $Ru(dcbpy)_2(NCS)_2$ *sensitised* TiO_2 *film in 0.1 M* $LiClO_4$ *in propylene carbonate (data from figure 3.6) All voltages vs. Ag/AgCl. Superimposed are fittings of the data (continuous line) in terms of a Continuous Time Random Walk performed by the electrons through an exponential distribution of trap states (modelling by Dr. Jenny Nelson in the Physics Department).*

3.3.7.2 Extending the CTRW model to the kinetic competition

The following is a summary of the extension of the CTRW model to the regeneration reaction as carried out solely by Dr. Jenny Nelson in Physics. It is reported here as it is the most advanced modelling to date of my experimental data. I will discuss the achievements and limitations of the model later in the chapter.

In order to extend the CTRW model to the competition between the charge recombination k_{CR1} and dye cation regeneration k_{RG} it needed to be modified in two respects:

(i) the re-reduction of D^+ by I^- must be allowed, and

(ii) the optical absorbance of the products of this alternative reaction at the probe wavelength must be included.

The regeneration of the dye ground state by iodide was assumed to be first order in $[D^+]$, and characterised by a rate constant $k(I^-)$ which is some function of $[I^-]$. This assumption requires that $[I^-] >> [D^+]$, (a condition which is valid in the systems studied here - with the possible exception of 0.001 M iodide - where approximately one dye is excited per nanoparticle and iodide concentrations exceed 1 mM), but does not involve any assumption about the order of reaction with respect to $[I^-]$.

During each simulation, one dye cation and *n* electrons were implanted at random on a lattice inside a spherical shell which represents the nanoparticle, as previously (Nelson et al. 2001). Each dye cation was assigned a lifetime with respect to I^- according to

$$\tau_I = -\frac{\ln X}{k(I^-)} \tag{3.15}$$

where X is a random number between 0 and 1. The electrons performed the random walk, and the simulation stopped when either an electron walked on to the cation site (reduction according to eq. 3.1), or the regeneration lifetime τ_I was reached (eq. 3.2), whichever happened first.

The cation lifetime and type of event was recorded. Simulations were repeated for 5000 realisations of the lattice for each value of n and $k(I^-)$. The relative dye cation density was compiled from the set of reduction times.

The evolution of the absorbing products is due to regeneration by iodide (scheme 3.7) only. It was assumed that each regeneration event produced exactly one product species P, assigned above to the charge separated state e_{TiO2} / I_2^-. The disappearance of the product was assumed to be second order, as discussed below. Then the product concentration obeyed:

$$\frac{dP}{dt} = -\frac{d[I^-]}{dt} - kP^2 \tag{3.16}$$

where k is a constant and the initial condition P(0) = 0 applies. P was calculated from the simulation results for $[I^-]$ by numerical integration of equation 3.16 with k as a fitting parameter. Finally, the relative absorbance of the system was calculated from $[D^+(t)]$ and P(t) by

$$\Delta OD(t) = \Delta OD(0) \times \frac{[D^+(t)] + \left(\varepsilon_P / \varepsilon_{D^+}\right) P}{[D^+(0)]} \tag{3.17}$$

where $(\varepsilon_P / \varepsilon_{D^+})$ is the ratio of extinction coefficients of products and dye cation.

ΔOD(t) was compared with the experimental optical density relative to its initial value. To generate ΔOD(t) the following parameters were required: α; the relationship between n and applied bias; the absolute time scale; the functional form of $k(I^-)$; k and the ratio $(\varepsilon_P / \varepsilon_{D^+})$. First, the value of α was determined by fitting the data in the absence of iodide (fig. 3.16) to a stretched exponential. This yielded $\alpha = 0.4 \pm 0.05$.

α also yielded the relationship between n and applied bias: Using equation 3.14 and observed $t_{50\%}$ values it was estimated that n increased by a factor of approximately 3 per 100 mV. Note that the bias at which n = 1 may vary by up to +/- 50 mV between samples. Using these values for n (V) and α the kinetics in the iodide free case were reproduced, as shown in figure 3.16.

To determine the product decay constant k and the ratio ($\varepsilon_P / \varepsilon_{D^+}$) the shape of the kinetic curve in the case of a high iodide concentration (figure 3.13) was analysed. Evolution of the reaction products added a slow tail on to the roughly exponential form of the cation absorbance, much as observed. A best fit was obtained with k = 5.10^4 dm^3 mol^{-1} sec^{-1} and ($\varepsilon_P / \varepsilon_{D^+}$) = 0.15. These values were used throughout the simulations.

Finally, first and second order forms for $k(I^-)$ were evaluated by comparing model predictions with experimental kinetics at different iodide concentrations.

Comparisons of the results of the numerical model with experimental decays are shown in figure 3.17. The top half of figure 3.17 shows the comparison as a function of iodide concentration while the bottom half as a function of applied bias at low (0.03 M) iodide concentration. It is apparent that the simulations as a function of applied bias are in good agreement with experimental observations. Comparisons as a function of iodide concentration are in reasonable agreement with a first order dependence $k(I^-) = k_{RG}[I^-]$ with k_{RG} = 1.6 x 10^5 dm^3 mol^{-1} s^{-1}, although it is apparent that this model predicts a somewhat weaker dependence upon iodide concentration than is observed. This deviation will be addressed in the discussion.

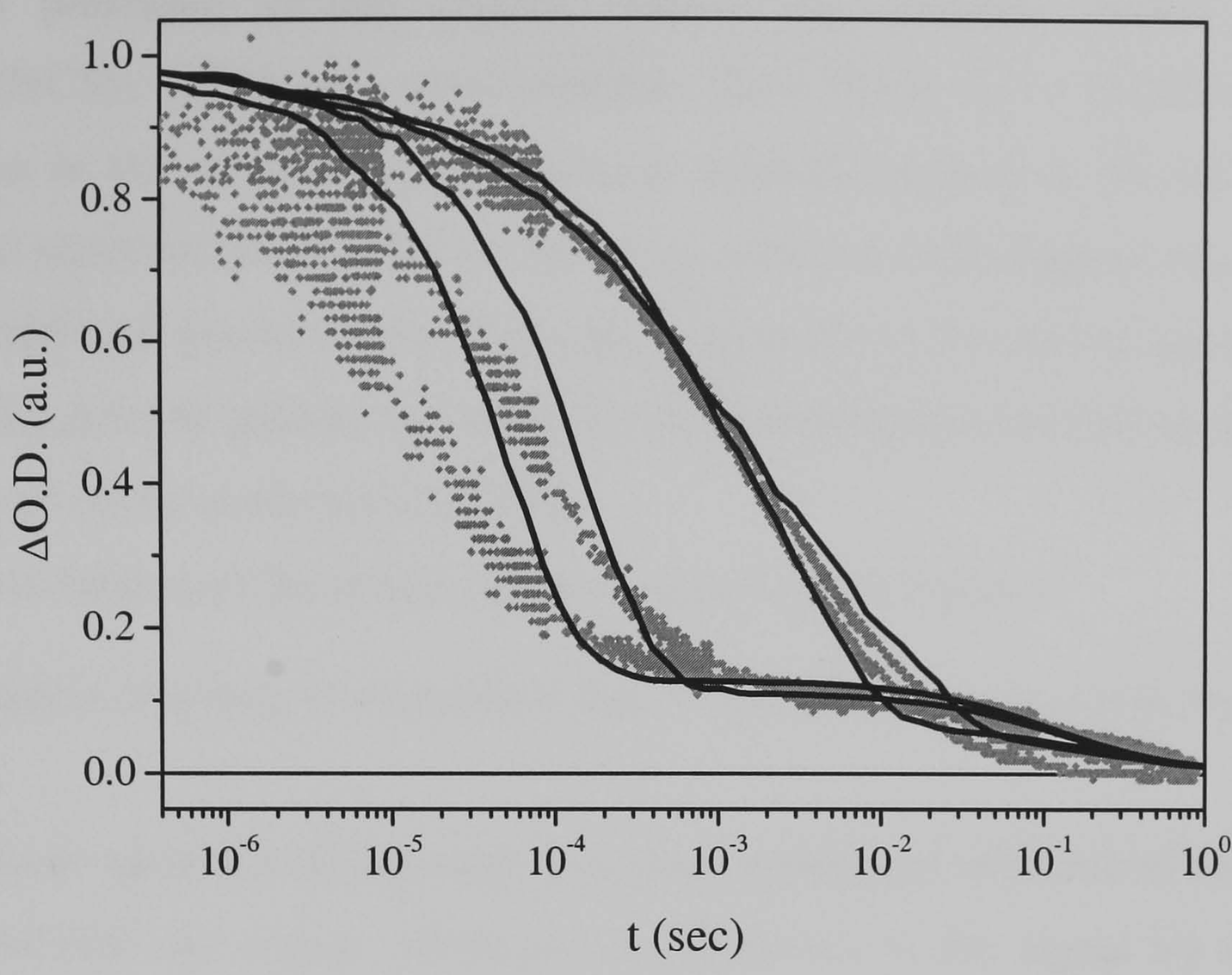

Figure 3.17: *Comparison of experimental transient absorption data at 800 nm (+) with CTRW model calculations (smooth lines) (a) as a function of iodide concentration in the absence of applied bias and (b) as function of applied bias with a iodide concentration of 0.03 M. Data for (a) and (b) taken from figures 3.6 and 3.14 respectively. (a) data and model calculations for iodide concentrations of 0, 1, 30 and 100 mM, (b) data and model calculations for applied bias of -0.3, -0.4 and -0.5 V vs. Ag/AgCl in 0.03 M LiI.*

3.4 Discussion

The results presented in this chapter address the electron transfer kinetics of $Ru(dcbpy)_2(NCS)_2$ sensitised nanocrystalline TiO_2 films as a function of iodide concentration in the electrolyte and electrical potential applied to the TiO_2 film. The experimental observations focused on the decay kinetics of photogenerated dye cations and the formation of product states of the dye regeneration reaction by iodide ions in the electrolyte (k_{RG}) in the presence of different iodide concentrations and while controlling the Fermi level in the semiconductor film.

The main conclusions of the results can be summarised as follows:

1) The formation of a long-lived product state of the iodide reaction with the dye cations is observed.

2) The transient spectrum of this state is in good agreement with that of the radical ion I_2^- in the 400-800 nm region. However, contributions to the signal by electrons are evident at higher wavelengths and therefore this state is assigned to e_{TiO2}/I_2^-. Similar kinetics observed with chlorophyllin sensitised TiO_2 electrodes were assigned solely to photoinjected electrons but a transient spectrum of the long-lived species was not provided (Kay, Humphry-Baker, and Grätzel 1994).

3) The rate of iodide regeneration of the dye (k_{RG}) is independent of applied bias and iodine presence in the electrolyte

4) Similar regeneration kinetics k_{RG} are observed for three different sensitiser dyes $Ru(dcbpy)_2(NCS)_2$, $Os(dcbpy)_2(CN)_2$ and ZnTCPP.

5) A numerical model of the dye cation decay developed by Dr. Jenny Nelson at the Physics Department of Imperial College in which the charge recombination reaction k_{CR1} is limited by electron diffusion through an exponential distribution of trap states in the metal oxide film and k_{RG} is modelled as a first order reaction in iodide concentration is in reasonable agreement with experimental observations.

The model however neglects contributions by electrons to the absorption of products and could be improved in this respect.

3.4.1 Charge recombination (k_{CR1})

The charge recombination reaction k_{CR1} in propylene carbonate shows dispersive kinetics in accordance with what was reported by Haque et al. in alternative electrolyte systems (Haque et al. 2000). Recent reports (S. Katoh, personal communication, 2001) of the kinetics of this reaction confirm that it is difficult to describe the process in terms of a simple homogeneous kinetic model. This finding is after all not surprising given the extreme complexity of the three-dimensional interface on which the reaction takes place. It is reasonable that at the microscopic level dye molecules will be attached differently to the various TiO_2 surface planes resulting on distributions for parameters such as the strength of the chemical bonding, energy levels of single dye molecules as they occupy differing microenvironments and Ru-Ti distances leading in turn to a spread in energetic coupling. One should therefore be cautious when attaching a time constant to this and other processes in dye-sensitised electrodes and the underlying complexity of the kinetics should be kept in mind. The charge recombination reaction can be quantified using $t_{50\%}$ that is found to be of the order of 1 ms in propylene carbonate in agreement with what is observed in other solvents.

3.4.2 Dye regeneration reaction (k_{RG})

The rate of dye regeneration (k_{RG}) by iodide is independent of applied bias and iodine presence in the electrolyte. The bias independence of k_{RG} is in marked contrast to the strong bias dependence of the recombination reaction k_{CR1}. If the current understanding of the physical chemistry of dye sensitised electrodes is correct the majority of the potential drop (i.e. the main electric field) in solar cells is at the semiconductor / electrolyte interface (Gregg, Zaban, and Ferrere 1999) rather than at the SnO_2 / TiO_2 interface (Schwarzburg and Willig 1999). It should also vary as a function of applied bias, in which case it should affect the reaction of dye cations at the interface with I^- in solution. The bias independence of this reaction is consistent with the screening of the surface charge of nanoporous electrode by lithium ions in the electrolyte. Such screening, studied in the absence of applied electrical biases, has been addressed by Gregg and co-workers (Zaban, Ferrere, and Gregg 1998) that suggested the potential drop at the interface occurs mainly between the surface and the dye when small positive cations such lithium are present in solution. In fact, in this case the redox potential of the dye is independent of electrical bias applied to the TiO_2 leading to bias independent reaction of the dye cations with iodide in solution.

3.4.3 Iodide concentration dependence of k_{RG}

The rate of the regeneration reaction is expected to be of the form:

$$\text{rate} = k_{RG}[D^+][I^-]^x \qquad (3.18)$$

The order x of this reaction with respect to iodide concentration is currently the subject of some controversy (Nasr, Hotchandani, and Kamat 1998; Pelet, Moser, and Grätzel 2000; Kuciauskas et al. 2001). From scheme 3.7 it is apparent that a second order behaviour might be expected, although it was mentioned in the introduction that formation of an I radical intermediate has also been suggested and would yield first order kinetics in iodide concentration (Nasr, Hotchandani, and Kamat 1998). Alternatively the reaction is thought to proceed through the formation of (dye^+ / I^-) and / or (I^- / I^-) ion pairs on the semiconductor surface (Pelet, Moser, and Grätzel 2000) although the experiments presented here are incapable of verifying whether this is the case. The order of the reaction with respect to iodide concentration has been shown to be first order, though only over a very limited range of iodide concentrations (0 - 10^{-4} M) (Nasr, Hotchandani, and Kamat 1998). It is apparent from figure 3.7 that an increase in the iodide concentration from 1 mM to 100 mM results in an approximately 100 fold increase in the rate of dye cation decay, consistent with first order behaviour over this range of iodide concentrations. More quantitatively, the numerical model illustrated in section 3.7 assuming first order behaviour in iodide concentration, provides a reasonable fit to these data although it somewhat underestimates the iodide concentration dependence of the dynamics. However, a significantly worse fit is obtained if second order behaviour is assumed and it can therefore be concluded that the reaction is close to first order with respect to iodide concentration for the 0 to 0.1 M [I^-] range.

The rate constant for the regeneration reaction estimated from the data is $k_{RG} = 1.6 \times 10^5$ $dm^3\ mol^{-1}\ s^{-1}$. This rate constant is of similar magnitude to values recently reported by Pelet et al. (Pelet, Moser, and Grätzel 2000) and Kuciauskas et al. (Kuciauskas et al. 2001) although significantly smaller than those reported by Heimer et al. ($> 2 \times 10^7$ $dm^3\ mol^{-1}\ s^{-1}$) (Heimer et al. 2000) and Kamat et al. (1.2×10^{10} $dm^3\ mol^{-1}\ s^{-1}$) (Nasr, Hotchandani, and Kamat 1998).

3.4.4 The dye cation kinetics are not monoexponential when k_{RG} dominates

At high iodide concentrations the transient absorption experiments are conducted in the limit $[D^+] << [I^-]$. Under these conditions the iodide concentration is constant, and pseudofirst order kinetics are expected, independent of the reaction order with respect to iodide ($k_{eff} = k_{RG} [I^-]^x$). If the regeneration dynamics were homogeneous throughout the film, as assumed in the numerical modelling, a monoexponential decay of the dye cation would be expected. It is however apparent from figures 3.7 and 3.17 that this is not the case.

In order to address the origin of this behaviour, the regeneration dynamics were studied as a function of dye coverage. Fillinger and Parkinson (Fillinger and Parkinson 1999) have suggested the onset of a cation-hopping mechanism in $Ru(dcbpy)_2(NCS)_2$ sensitised TiO_2 films at dye coverages exceeding 30%, resulting in the dye cation produced by electron injection migrating among adjacent sensitiser molecules, potentially complicating the observed regeneration dynamics. However, indistinguishable dynamics were observed at high and low (~10 and ~100%) dye coverages (data not shown), indicating that such hopping dynamics are not important for consideration of the dye regeneration dynamics reported here. Alternatively this non-exponential behaviour may derive from inhomogeneity in the energetics of the regeneration reaction, consistent with our recent modelling (Tachibana et al. 2001) of non-exponential injection kinetics for this experimental system in terms of an energetic distribution of injection driving force.

3.4.5 Comparison with other studies

Previous studies on dye sensitised colloids (Fitzmaurice and Frei 1991) have suggested that a complex formed between $Ru(dcbpy)_3$ and iodide ions may enhance the rate of iodide re-reduction of the dye cation. The present experiments provide no evidence for such a complex formation, in agreement with those reported in subsequent work (Nasr, Hotchandani, and Kamat 1998; Heimer et al. 2000; Pelet, Moser, and Grätzel 2000). The observation of similar regeneration kinetics for three different dyes - $Ru(dcbpy)_2(NCS)_2$, $Os(dcbpy)_2(CN)_2$ and ZnTCPP - is also not readily reconciled with specific dye/ iodide complex formation. Furthermore it rules out Hagfeldt and Grätzel's recent suggestion that the substantial amount of S3p-character from the -NCS groups (that point towards the solution) in the HOMO of $Ru(dcbpy)_2(NCS)_2$ might contribute to explaining the high efficiency of cells employing this sensitiser by facilitating reduction by iodide in solution (Hagfeldt and Grätzel 2000).

It should be noted that the three dyes employed here exhibit similar oxidation potential in solution. Studies with alternative dyes with less positive oxidation potentials result in significantly lower I_2^- product yields (J. Clifford, J. R. Durrant, unpublished), consistent with recent comparisons of the function of osmium and ruthenium sensitiser dyes (Kuciauskas et al. 2001).

3.4.6 Nature and decay of regeneration reaction products

Optical absorption by electrons in TiO_2 remains one of the least understood and most controversial aspects of research in dye-sensitised electrodes. Nonetheless, it is probably the single most important unresolved issue in the field.

As mentioned earlier, the extinction coefficient of electrons in titanium dioxide is controversial and has been reported ranging between $\varepsilon_{800} = 700 \pm 50\ M^{-1}\ cm^{-1}$ (Safrany, Gao, and Rabani 2000) and $\varepsilon_{780} = 3400\ M^{-1}\ cm^{-1}$ (Rothenberger, Fitzmaurice, and Grätzel 1992). Our best estimate is of the order of $800\ M^{-1}\ cm^{-1}$ at 800 nm, approximately a third of that of I_2^- that is reported as $2200\ M^{-1}\ cm^{-1}$(Hug 1981). Note that the simplified model presented in section 3.7.2 only accounts for one generic product species P assumed to decay according to a second order rate. Considering the best estimate available for the $Ru(dcbpy)_2(NCS)_2$ cation at 800 nm, i.e. $6000\ M^{-1}\ cm^{-1}$

(Tachibana 2000) one would expect the value of ($\varepsilon_P / \varepsilon_{D^+}$) to be approximately 0.5. The model presented earlier yields a value of 0.15.

Possible reasons (or combinations thereof) for this discrepancy include:

1) The efficiency of the regeneration reaction is less than unity in the present conditions.

2) The literature value of the I_2^- extinction coefficient might be overestimated. Literature transient spectra are often reproducible in term of spectral shape but much less reliable in terms of absolute signal sizes. Furthermore, the value reported by Hug (Hug 1981) was determined in water.

3) There is some evidence that the size of the signal attributed to dye cations at 800 nm appears to be smaller in the presence of lithium in the solution. The origin of this phenomenon is not clear at present and is being investigated by John Clifford. The estimate for the dye cation extinction coefficient reported above refers to films covered in EC:PC 1:1.

The signal is therefore assigned primarily to I_2^- absorption of the charge separated state e_{TiO2} / I_2^-. It is puzzling that the decay of this signal is independent of electrically applied bias (see figure 3.13), suggesting that the rate limiting step does not involve electrons as it would be the case of the charge recombination between electrons in the semiconductor (e_{TiO2}) and I_2^-:

$$e_{TiO2} + I_2^- \rightarrow 2I^- \qquad (3.19)$$

In that case, the kinetics should accelerate with the increased electron occupancy in the semiconductor brought about by the electrical bias.

The slow timescale decay is tentatively mainly assigned to the I_2^- dismutation reaction:

$$2\, I_2^- \rightarrow I^- + I_3^- \qquad (3.20)$$

From the model presented in section 3.7.2 the rate constant k for this dismutation reaction is determined using equation 3.16 to be 5 x 10^4 dm^3 mol^{-1} s^{-1}. The I_3^- will presumably subsequently decay by charge recombination with e_{TiO2} (k_{CR2}) although neither species can be unambiguously distinguished in the experiments reported here. The slow rate of the dismutation reaction ($t_{1/2}$ ~ 0.2 - 0.5 s) is remarkable and attributed in part to the low concentration of I_2^- generated by the low energy laser excitation. Consideration of the literature diffusion constants for analogous species such as I_3^- would yield a significantly higher dismutation rate constant than that observed here,

assuming the reaction is diffusion controlled, and suggesting that diffusion of I_2^- radicals within the film pores may be impeded by interactions with the film surface. This conclusion is consistent with a recent study which suggested that the diffusion constant for the analogous species I_3^- is approximately 10 fold smaller within the film pores relative to bulk solution (Kebede and Lindquist 1998). As mentioned in the introduction, most measurements of this reaction rate report values approximately five orders of magnitude higher. However, the value reported here is in good agreement with a recent report (Behar and Rabani 2001) that interpreted the result in terms of strongly impeded diffusion of I_2^- species within the pores of titanium dioxide films. The rate constant k for this dismutation reaction is of similar magnitude to that of the regeneration reaction k_{RG}, which may be indicative of both reactions being rate limited by the diffusion of iodide species within the film pores. Furthermore, in analogous experiments employing a iodide / iodine based polymer electrolyte, the decay of this signal was observed to accelerate rapidly under continuous white light illumination (Nogueira et al. 2001). This acceleration is consistent with assignment of this signal to the dismutation reaction, with the white light illumination resulting in the steady state accumulation of I_2^- species in the polymer electrolyte and faster decay kinetics as a result.

3.4.7 Implications for solar cell function

The voltage output of dye sensitised solar cells is primarily limited by the acceleration of interfacial recombination reactions (k_{CR1} and k_{CR2}) as the Fermi level, and therefore electron density, of the nanocrystalline TiO_2 film is raised. Two recombination reactions are possible; injected electrons may recombine either with oxidised dyes (k_{CR1} in figure 3.1) or with the oxidised form of the redox couple (i.e. I_3^-, k_{CR2} in figure 3.1). This chapter addressed directly for the first time the kinetic competition between k_{CR1} and the desired regeneration reaction k_{RG} as a function of the voltage applied to the TiO_2 film. It is found that, in contrast to the recombination reaction k_{CR1}, the regeneration reaction is independent of applied voltage. Kinetic competition between k_{CR1} and k_{RG} is observed to be important for moderate iodide concentrations (30 mM), resulting in a significant loss in the yield of k_{RG} as the TiO_2 Fermi level is raised to levels comparable to V_{oc}, the cell open circuit voltage. However, for higher iodide concentrations, $k_{RG} > k_{CR1}$ for all applied voltages, suggesting that in liquid electrolyte devices employing such iodide concentrations, charge recombination between injected electrons and oxidised dye species will not be a significant loss mechanism limiting device performance. This conclusion is consistent with previous frequency domain analyses of device performance, which have assumed that the primary recombination loss mechanism in liquid electrolyte devices is between injected electrons and oxidised species in the electrolyte (I_3^- ions) (Huang et al. 1997; Duffy et al. 2000) and in contrast with what was found by Franco et al. (Franco et al. 1999). These issues will be addressed in more detail in the next chapter. However, extensive studies are currently under way to develop alternative electrolytes, including polymer electrolytes and molten salts. In such alternative electrolytes, the slower iodide diffusion dynamics may result in kinetic competition between k_{CR1} and k_{RG} being a more significant loss mechanism limiting device performance. Furthermore, the remarkably slow dismutation rate for I_2^- species reported here may result in charge recombination with this species (equation 3.19 above) being a significant loss mechanism in functioning devices.

CHAPTER 4

KINETIC COMPETITION IN DYE SENSITISED SOLAR CELLS

4. KINETIC COMPETITION IN DYE SENSITISED SOLAR CELLS

This chapter addresses the role played by charge recombination of electrons in the TiO_2 with dye cations (k_{CR1}) and triiodide (k_{CR2}) in dye-sensitised solar cells. Cells where k_{CR2} dominates the recombination losses or where both k_{CR1} and k_{CR2} play a role are distinguished with transient absorption spectroscopy. An attempt is made to relate the findings to the i-V characteristics of devices.

4.1 Introduction

In the previous chapter the kinetic competition between charge recombination of the photoinjected electrons with dye cations (k_{CR1}) and their regeneration by iodide in solution (k_{RG}) was addressed in a three-electrode set-up. In this chapter these studies are extended to complete dye sensitised solar cells.

The key issue addressed by the experiments in this chapter is whether the charge recombination reaction between electrons and dye cations (k_{CR1}) is functionally important in complete cells. It is a commonly held assumption (see Huang et al. 1997; Schlichthörl, Park, and Frank 1999) that the recombination losses in dye-sensitised cells are dominated by the reaction of the electrons in the semiconductor with tri-iodide in solution (k_{CR2}). The same assumptions have been made in a proposed electrical model for devices (Ferber, Stangl, and Luther 1998).

The assumption stems from the fact that the dye regeneration by iodide is usually considered to be sufficiently fast for k_{CR1} not to contribute significantly to the recombination losses in devices. However, reports of direct experimental evidence of the validity of this assumption have been limited to date.

4.1.1 Recombination losses in dye sensitised cells

As it was seen in chapter 1, a peculiarity of dye-sensitised solar cells is that two possible recombination pathways are present, in contrast with conventional silicon solar cells where the recombination losses can be entirely attributed to electron - hole recombination in the bulk of the device. The first mechanism, only active under illumination, consists of the recapture of an injected electron by a dye cation on the surface of the semiconductor. This process (eq. 4.1) is in competition with dye regeneration (eq. 4.2) as discussed in the previous chapter.

$$Dye^+ + e_{TiO2} \rightarrow Dye \qquad k_{CR1} \qquad (4.1)$$

$$Dye^+ + I^- \rightarrow Dye + products \qquad k_{RG} \qquad (4.2)$$

The second recombination pathway, present both in the dark when an electrical bias is applied to the device and under illumination, is the recombination of (photo-injected under illumination) electrons with the oxidised form of the redox shuttle I_3^-, by-passing the dye. As usual when dealing with the redox chemistry of iodide in solution, the detailed mechanism is not fully established but the overall reaction can be summarised as in equation 4.3:

$$2e^- + I_3^- \rightarrow 3I^- \qquad k_{CR2} \qquad (4.3)$$

Figure 4.1 illustrates these points schematically.

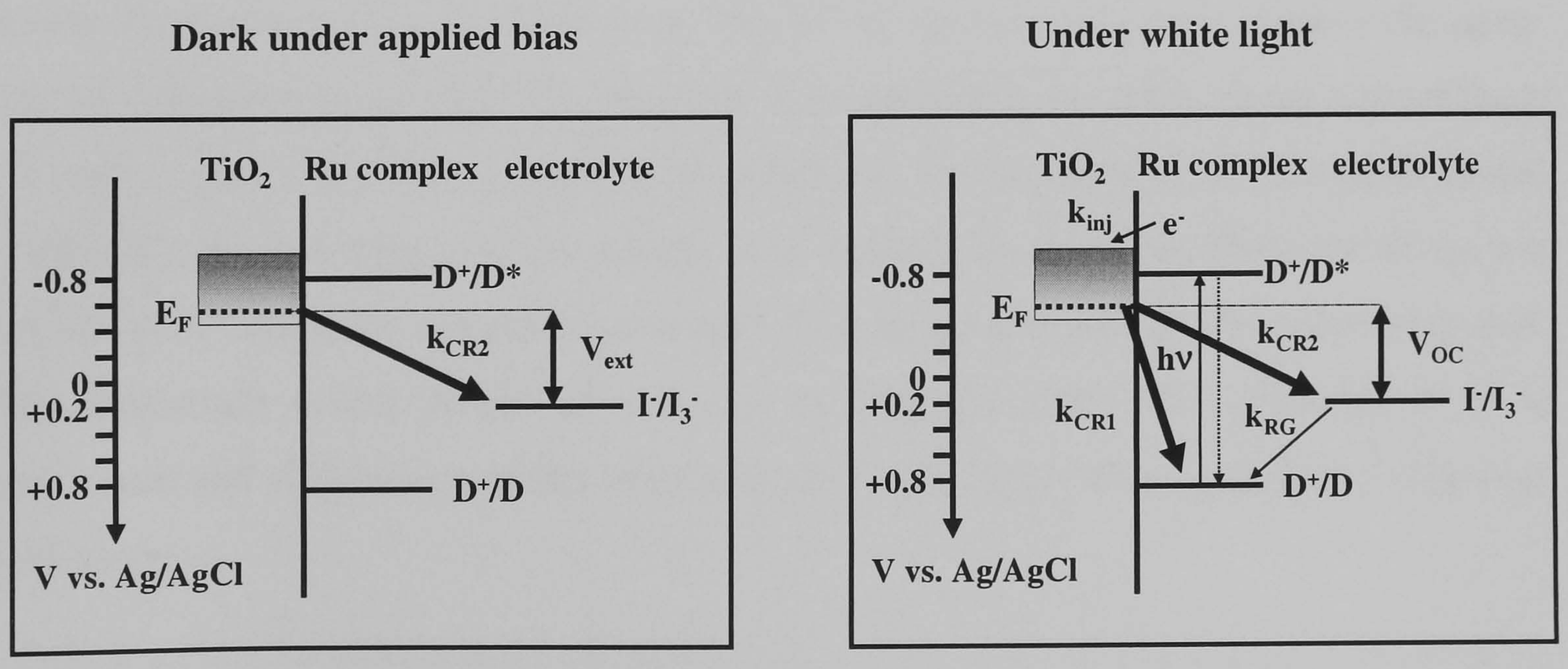

Figure 4.1: *Recombination loss mechanisms in dye sensitised solar cells in the dark under applied bias (V_{ext}, left) and under illumination (right). In the dark, electrons reduce I_3^- to I^- in the solution. Under illumination they can also react with dye cations in competition with I^-. The latter recombination route is often neglected, but may be significant at voltages approaching open circuit conditions.*

4.1.2 General i-V characteristics of solar cells

The characteristics of photovoltaic devices are usually described in terms of their i-V curve in the dark and under illumination. Typical i-V plots are shown in figure 4.2.

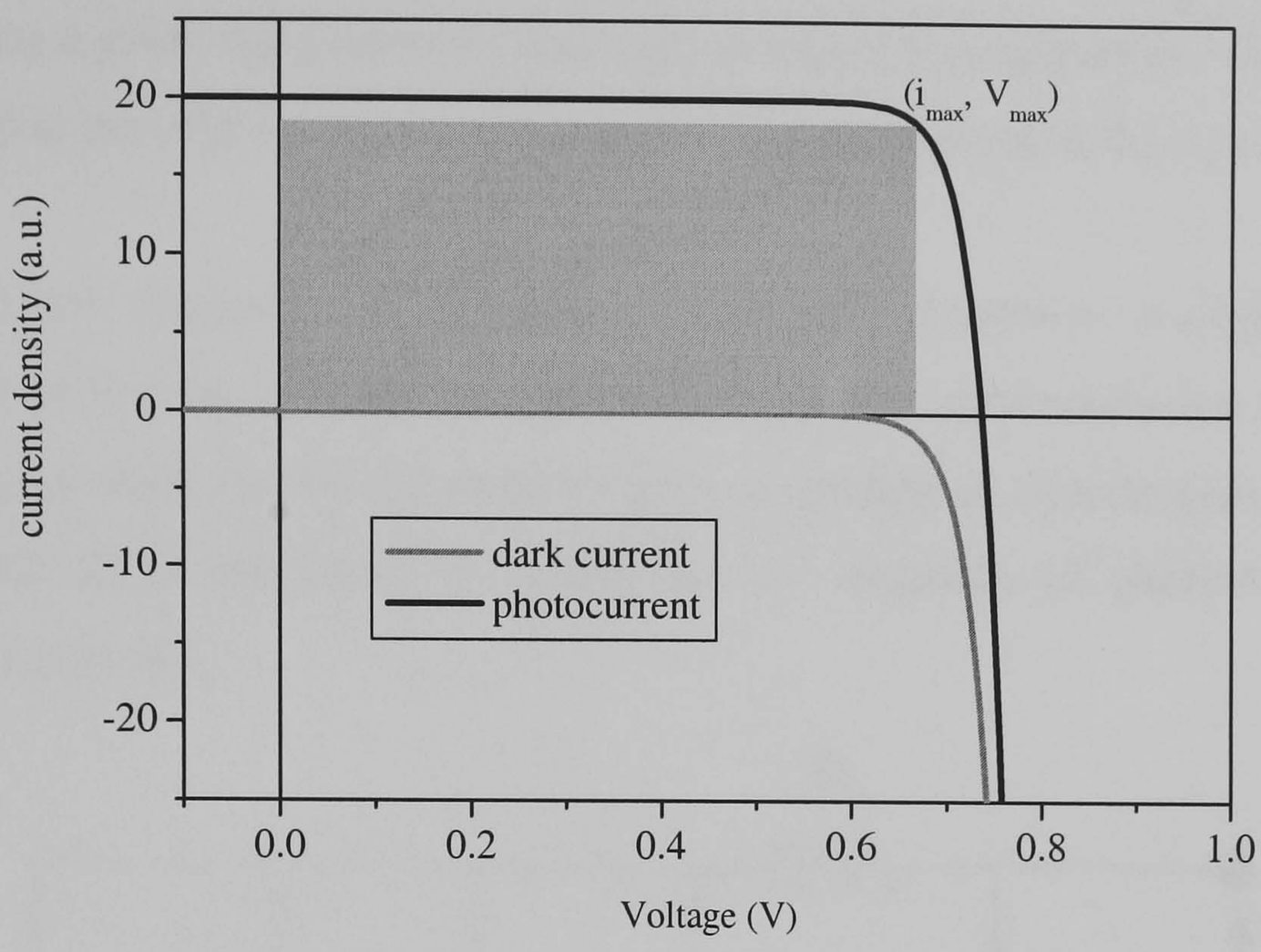

Figure 4.2: *Generic i-V curves of a solar cell in the dark (grey) and under illumination (black). The open circuit voltage V_{OC} and short-circuit current i_{SC} correspond to the intersection with the x (V) and y (A) axis respectively. The inner rectangle corresponds to the maximum power point (i_{max}, V_{max}) and defines the fill-factor FF.*

Under illumination, the intersection of the i-V curve with the x-axis defines the open-circuit voltage of the device (V_{OC}) and that with the y-axis the short circuit current (i_{SC}). At open circuit (V_{OC}) the charge carrier generation and recombination processes cancel each other out and there's no net current flow through the contacts. Short circuit (i_{SC}) is the situation where the maximum amount of carriers is collected in the external circuit. The maximum output power of a device is obtained where the product i x V is maximum and will be higher the more the i-V curve resembles a rectangle of sides i_{SC} and V_{OC}.

The ratio of the rectangles $(iV)_{max}$ and $i_{SC}V_{OC}$ define the fill factor (FF) of the device,

$$FF = \frac{(iV)_{max}}{i_{SC}V_{OC}} \qquad (4.4)$$

The voltage / current combination that gives the largest power rectangle is known as the maximum power point.

The power conversion efficiency η (λ) is therefore defined as:

$$\eta(\lambda) \equiv \frac{i_{SC}(\lambda) \cdot V_{OC}(\lambda) \cdot FF(\lambda)}{P_{light}} \qquad (4.5)$$

where P_{light} is the incident light power. Power conversion efficiencies are only meaningful for a given light intensity and a given spectral distribution. The most widely used standard is the AM 1.5 spectrum described in more details in the Appendix.

Equivalent circuit diagrams (ECDs) are employed to represent in a simplified manner the electrical behaviour of complex electrical circuits or semiconductor devices. They are a network of ideal circuit components such as voltage or current generators, diodes etc. The basic ECD employed to model the i-V response of photovoltaic cells is presented in figure 4.3.

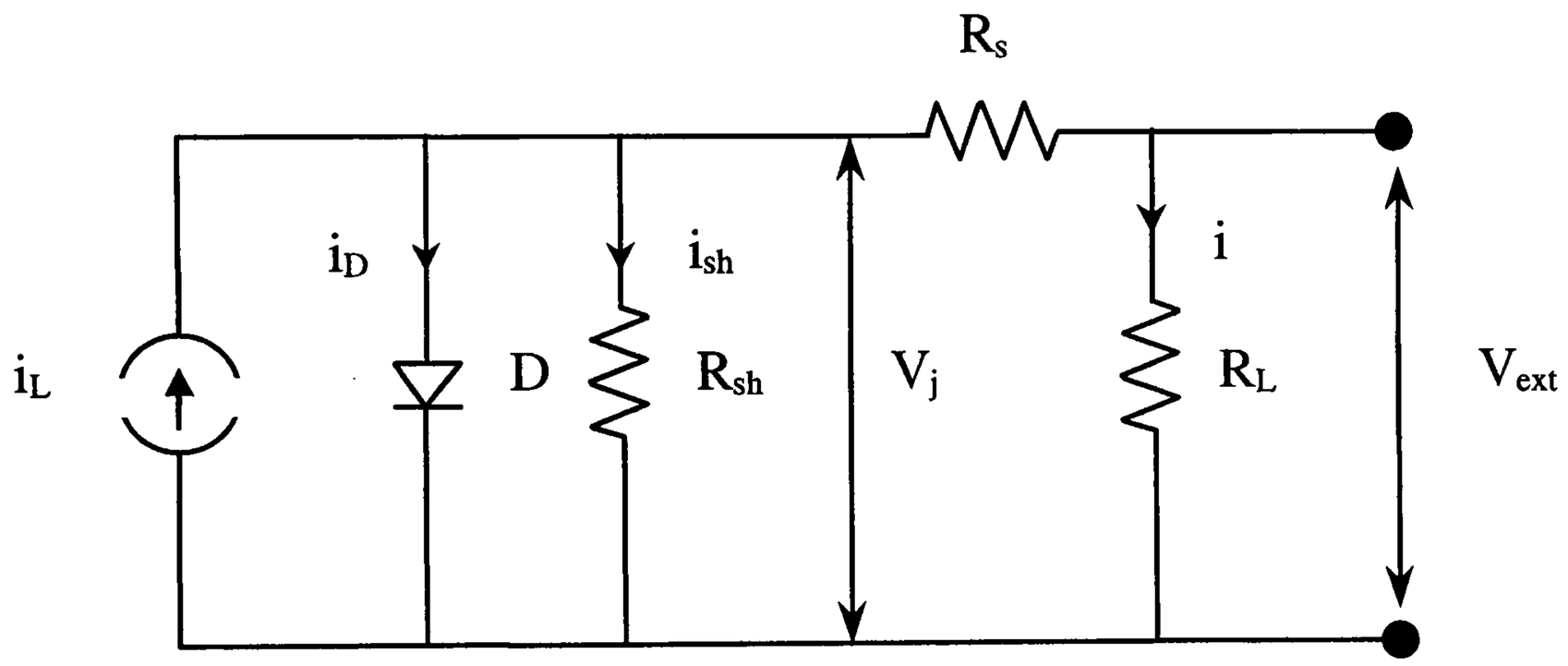

***Figure 4.3**: Equivalent circuit diagram employed to simulate a solar cell. All components are ideal. A current source i_L represents the light-generated current and the diode D account for the non-linear voltage dependence. R_s and R_{sh} are the series and shunt resistance of the device. R_L represents an external load. The cell output voltage is V_{ext} while the junction voltage is $V_j = V_{ext} + iR_s$.*

The following components constitute the basic ECD shown above.

A *current source* I_L: an ideal current generator whose current is constant at a given illumination level. The current output depends on the illumination level but is independent of applied bias.

An *ideal diode* D, i.e. a voltage-dependent resistor used to describe the non-linear shape of the i-V curve. It reproduces exactly the behaviour of an ideal p-n junction when $R_s = 0\ \Omega$ and $R_{sh} = \infty$

A *series resistance* R_s linked to the conductivity i.e. mobilities of the charge carriers in the device. The series resistance can be estimated from the slope of the dark current at biases $V > V_{OC}$ where the i-V curve becomes linear:

$$R_s \approx \left(\frac{i}{V}\right)_{V>V_{OC}} \tag{4.6}$$

A *shunt resistance* R_{sh} associated with short circuits across the device (leak current). Its value can be estimated from the i-V curve from the slope in the vicinity of 0 V.

$$R_{sh} \approx \left(\frac{i}{V}\right)_{V=0} \tag{4.7}$$

This approximation holds when (as it is typically the case in inorganic cells) R_{sh} is much larger than R_s. The diode D is not conducting for voltages ~ 0 V and therefore the current driven by the external voltage is only determined by $R_{sh} + R_s \sim R_{sh}$.

These are the basic components that will qualitatively describe a photovoltaic device. Extra electrical components can be added to the basic design to form more complex ECDs that can be employed to model the i-V characteristics of strongly non-linear devices. These can include a counter diode (in the opposite direction to D), a capacitor to account for charging / discharging effects and a shunt between the contacts among others. However, it is clear that the more components are used the less well-defined physical processes they describe.

An ideal solar cell has no series resistance and an infinite shunt resistance and behaves like the ideal diode D of figure 4.3. The i-V curve in the dark follow the Shockley equation for p-n junctions (Shockley 1949):

$$I_d = I_0\left(e^{qV_j/nkT} - 1\right) \tag{4.8}$$

where V_j is the voltage drop across the p-n junction (otherwise referred to as the in-built bias) and n=1.

Upon illumination the light generates a constant photocurrent I_L from which the dark current equation 4.8 is subtracted:

$$I = I_L - I_0\left(e^{qV_j/nkT} - 1\right) \tag{4.9}$$

In a dye-sensitised solar cell R_s is not negligible and V_j is replaced by: $V_j = V_{ext} + iR_s$.

$$I = I_L - I_0\left(e^{q(V_{ext}+iR_s)/nkT} - 1\right) \tag{4.10}$$

When considering real devices, it is often found that their i-V characteristics fit the diode equation only for n ≠ 1, where n is the *ideality factor* n. Typical values for the non-ideality factor range between 1 and 2 for c-Si depending on the level of impurities in the crystal, and tend to be approximately 2 for Ga-As cells, respectively. In the case of dye sensitised solar cells values of 1.05 (Dittrich et al. 1998), 1.08 (Liu et al. 1998) and close to 2 (Södergren et al. 1994; Huang et al. 1997) have been reported. The physical origin of the ideality factor remains not fully established at present.

4.1.3 Relationship between i-V characteristics and recombination losses

At a given illumination, the current source I_L employed in the equivalent circuit diagram shown above has a constant output independent of voltage. In other words, a constant current source corresponds to assuming that the charge separation yield is voltage independent. This might be an oversimplification in dye sensitised solar cells, expecially since it is established that the reverse step (k_{CR1}) of the initial photoinduced charge separation (k_{inj}) is strongly dependent on electrical bias (O' Regan et al. 1990; Haque et al. 1998). This recombination path is only present in the light and could result in recombination losses in the proximity of open circuit conditions. Therefore in the equivalent circuit illustrated in fig. 4.3, k_{CR1} losses will appear as a voltage dependent I_L, I_L (V).

In a dye sensitised solar cell the i-V curve in the dark is linked to the recombination reaction between electrons in the titanium dioxide film and the triiodide in the electrolyte (k_{CR2}). If this recombination pathway was the prevailing one under illumination it would be reasonable to expect the i-V curve under illumination to be modelled well by the equivalent circuit shown in figure 4.3.

On the other hand, under illumination the other recombination pathway between electrons and dye cations (k_{CR1}) is present and, under illumination, the i-V curve of a cell where k_{CR1} contributes to the recombination losses is expected to show lower current values in the proximity of the open circuit voltage. In this case the i/V curve will not be well modelled by the equivalent circuit shown in figure 4.3.

4.1.4 Frequency domain studies

A series of frequency domain measurements have addressed the lifetime of the electrons in devices as an indirect probe of the recombination losses. In these studies the response of the system to small, periodic modulations of the driving force is studied as a function of the disturbance. The driving force, that might be optical or electrical, and the phase and amplitude of the response, that may be a current, voltage, or optical density, is measured as a function of modulation frequency. The results are often presented in the complex plane as the locus of the complex response as frequency is swept. For a simple system with a single time constant, τ, the response is a semicircle in the complex plane, and it can be shown that the frequency at the point where the imaginary component of the response is a minimum, ω_{min}, is equal to $1/\tau$. Distorted semicircles imply multiphasic responses, which would be modelled with several time constants in the time domain. The techniques provide lifetimes for processes without much information as to the nature of these processes. In the context of DSSCs the observables are interpreted in terms of electron lifetimes in the semiconductor.

The two most significant techniques are intensity modulated photocurrent spectroscopy (IMPS) that is used to probe electron lifetimes at short circuit and intensity modulated photovoltage spectroscopy (IMVS) that probes the competition between charge transport and recombination in open circuit conditions. The time constant $1/\omega_{min}$ obtained from IMVS corresponds to the recombination lifetime τ_{rec} while in the case of IMPS the derived lifetime is determined by both charge recombination and collection.

$$\tau_{IMPS} = \left(\frac{1}{\tau_{rec}} + \frac{1}{\tau_{coll}} \right)^{-1} \tag{4.11}$$

The results of IMPS and IMVS are only meaningful when associated with a model. IMVS studies of dye-sensitised solar cells have assumed that the only recombination mechanism at work in devices is k_{CR2} (eq. 4.4) while k_{CR1} has been generally neglected.

From these experiments it has been suggested that reaction between electrons and triiodide (k_{CR2}) is second order in I_3^- concentration with a time constant of about 10 ms at 1 sun (Schlichthörl et al. 1997). On the other hand, Fisher et al. have inferred from the illumination power dependence of τ_{IMVS} and τ_{IMPS} the reaction to be second order in electron density (Fischer 2000).

Franco et al. assessed electron accumulation in illuminated DSSCs by using intensity-modulated 514 nm laser light and measuring the photoinduced change in transmission at 940 nm, assigned to absorption by electrons in the film. Steady state measurements of the cell impedance were also part of this study. From a comparison of these two techniques, it was concluded that the net electron injection efficiency was 1 at short circuit but only 0.3 at open circuit (Franco et al. 1999). It was therefore suggested that in the proximity of the V_{OC}, referred to as accumulation conditions, the reaction of electrons from the TiO_2 with the oxidized dye (k_{CR1}) competes with dye regeneration by iodide ions (k_{RG}).

Interpretation of IMVS, IMPS and electrical impedance data for dye sensitised solar cells is far from straightforward, not least because of the complexity of the systems investigated and remains therefore open to speculation. Interestingly, it has also been suggested that the very reason the iodide/iodine couple has not been surpassed by any other to date is its 2-electron couple nature. The slow electron diffusion through the TiO_2 network result in good collection yields at the ITO substrate mainly because the reaction of I_3^- with electrons k_{CR2} is a slow 2-electron process (Salafsky et al. 1998; Gregg et al. 2001).

Transient absorption spectroscopy studies of complete cells have been limited to date. Among the few studies of complete cells published so far, some have focused only on the nanosecond to microsecond timescales (Alebbi et al. 1998; Kuciauskas et al. 2001) while others have erroneously assigned dye regeneration (k_{RG}) kinetics observed in complete dye-sensitised ZnO cells to the charge recombination reaction k_{CR1} (Bauer et al. 2001). Recently experiments distinguishing between electron absorption in the TiO_2 and in the ITO back contact have been reported (van 't Spijker, O' Regan, and Goosens 2001; van 't Spijker and Goosens 2002).

4.1.5 Aims and methodology

The goal of this chapter is to assess the importance of the two recombination pathways CR1 and CR2 in DSSCs by monitoring the effect of the regeneration reaction in DSSC under illumination with transient absorption spectroscopy. To this end transient kinetics in the dark and under illumination (both at open and short-circuit conditions) have been recorded. All cells employ $Ru(dcbpy)_2(NCS)_2$ as a sensitiser and differ in the electrolyte. Electrolytes prepared in both acetonitrile and propylene carbonate have been employed. The consistency of the results with the i-V characteristics of devices is assessed.

4-t-butyl-pyridine is a commonly employed additive to the electrolyte of a DSSC. The influence of white light illumination and the effect of 4-t-butyl-pyridine on the charge recombination reaction k_{CR1} has been assessed in control experiments with dye-sensitised films.

4.2 Materials and methods

The assembling of complete solar cells was detailed in section 2.4. Here only the composition of the electrolytes employed will be detailed.

The two solvents employed were acetonitrile (A) and propylene carbonate (B).
The electrolyte composition employed in cells A_1 and B_1 is referred to as standard here since it represents a widely utilised composition. A_1 and B_1 therefore differ only because of the solvent (propylene carbonate being more viscous than acetonitrile). B_2 differ from B_1 for its lower iodide concentration. Table 4.1 outlines the composition of the electrolytes:

Electrolyte	Solvent	Composition
A1 (Standard)	Acetonitrile	0.1 M LiI, 0.6 M Tetra-butyl-ammonium iodide, 0.01 M I_2 and 0.5 M 4-t-butyl-pyridine
B1 (Standard)	Propylene carbonate	0.1 M LiI, 0.6 M Tetra-butyl-ammonium iodide, 0.01 M I_2 and 0.5 M 4-t-buytl-pyridine
B2	Propylene carbonate	0.1 M LiI, 0.01 I_2, 0.5 M 4-t-buytl-pyridine

Table 4.1: *Electrolytes employed in dye sensitised solar cells studied in this chapter.*

All electrolytes were stored in dark air-tight glass bottles.
Care was taken to minimise the amount of water in the solvents. To this end propylene carbonate was syringed from a capped bottle. Karl Fischer titrations were used in some cases to assess the water content of solvents. A freshly opened bottle of propylene carbonate (Aldrich) yielded readings between 50 and 100 ppm of water while carefully prepared electrolytes would contain between 100 and 200 ppm of water. However, cells sealed in an inert atmosphere with electrolytes prepared in a dry box have yielded identical performance to the ones prepared on an open bench (Willis 2002).
The cell were connected to a potentiostat operating in a two electrode configuration and the kinetics were measured in the dark and under white light illumination both at short circuit and at open circuit conditions.

The i-V characteristics of the cells were recorded either *in situ* before the transient absorption experiments employing the white light probe beam in the laser set-up or with the i-V rig described in chapter 2. The difference in spectral composition and light intensity between the AM 1.5 standard and the tungsten lamp used as the probe beam in

the microsecond transient absorption set-up have been discussed in section 2.9.2. For simplicity, ¼ Sun will be used to refer to such excitation conditions.

Transient absorption spectroscopy experiments were performed with the MTA spectrometer detailed in section 2.7.2. The excitation wavelength was set to 620 or 640 nm and the transient signal was recorded at 800 nm. i-V curves were fitted to the non-ideal diode equation using PVIV, a software program developed by Mr. Richard Monkhouse.

The majority of transient absorption measurements on cells are performed under white light illumination. In order to establish the dependence of the kinetics of the charge recombination k_{CR1} on background illumination, control experiments were performed on $Ru(dcbpy)_2(NCS)_2$ sensitised TiO_2 electrodes prepared as described in section 2.2.2.

The effect of 4-t-butyl-pyridine on the charge recombination reaction k_{CR1} was assessed on $Ru(dcbpy)_2(NCS)_2$ sensitised TiO_2 films in a 3-electrode set-up. The kinetics were measured as a function of externally applied bias in the 0 to -0.8 V vs. Ag/AgCl range in the following propylene carbonate electrolytes: 0.1 M $LiClO_4$, 0.1 M $NaClO_4$ and 0.1 M $NaClO_4$ + 0.5 M 4-t-butyl-pyridine.

4.3. Results and discussion

4.3.1 Transient kinetics in the dark

Transient absorption kinetics in the dark for all three types of solar cells are compared in figure 4.4. A common characteristic of the three decays presented is that they all have a long lived tail with the signal returning to zero only after approximately 1 second. This observation is only made in the dark.

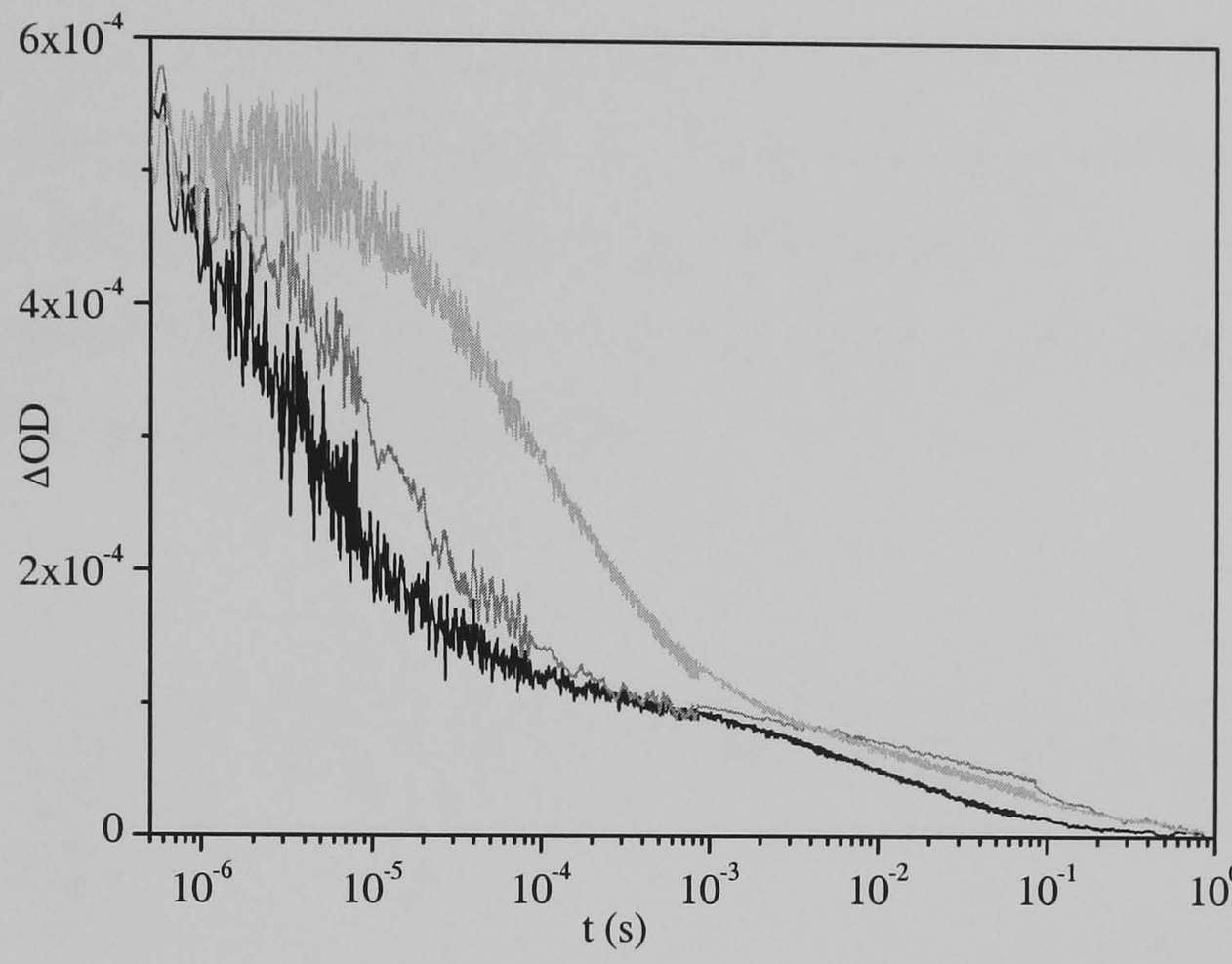

Figure 4.4: *Transient absorption kinetics in the dark for a standard acetonitrile cell (A1, black) and two cells employing propylene carbonate electrolytes (standard B_1, grey and 0.1 M iodide B_2, light grey)*

When acetonitrile and propylene carbonate standard cells are compared (A_1 and B_1 respectively, in figure 4.4) it is apparent that on the tens of microsecond timescale the kinetics, assigned in the previous chapter to the decay of the dye cation absorption due to reaction with iodide, are slower in propylene carbonate. Furthermore, the long-lived products of the regeneration reaction assigned in the previous chapter to I_2^-/e_{TiO2} are also longer lived in propylene carbonate These are in qualitative agreement with the higher viscosity of propylene carbonate (Barthel, Neueder, and Roch 2000) when compared with acetonitrile (Nikam, Shirsat, and Hasan 1998) (η = 2.512 mPa s and η = 0.342 mPa s at 25°C, respectively). However the acceleration of the kinetics is somewhat less than it would be expected if an inverse proportionality of the rate of the regeneration reaction on the viscosity $k \propto \frac{T}{\eta(T)}$ (Steinfeld, Francisco, and Hase 1998) is assumed.

When the two cells employing propylene carbonate are compared (B_1 and B_2, 0.7 M and 0.1 M iodide, respectively) it is apparent how the lower iodide concentration results in almost one order of magnitude slower dye regeneration reaction, consistent with results shown in chapter 3. Similar product yields are observed indicating that the dye regeneration reaction (k_{RG}) successfully competes with recombination (k_{CR1}) already at the lower iodide concentration.

Comparison of the kinetics in cells with those in dye-sensitised electrodes in chapter 3 shows how the $t_{50\%}$ of the regeneration reaction in cell B2 is remarkably higher and corresponds to the reaction being slower by an order of magnitude when compared with figure 3.7. The electrolytes only differ by the addition of 0.5 M 4 - tert-butyl-pyridine. Pyridine and other similar bases are regularly added to the electrolyte in order to improve the open circuit potential of devices.

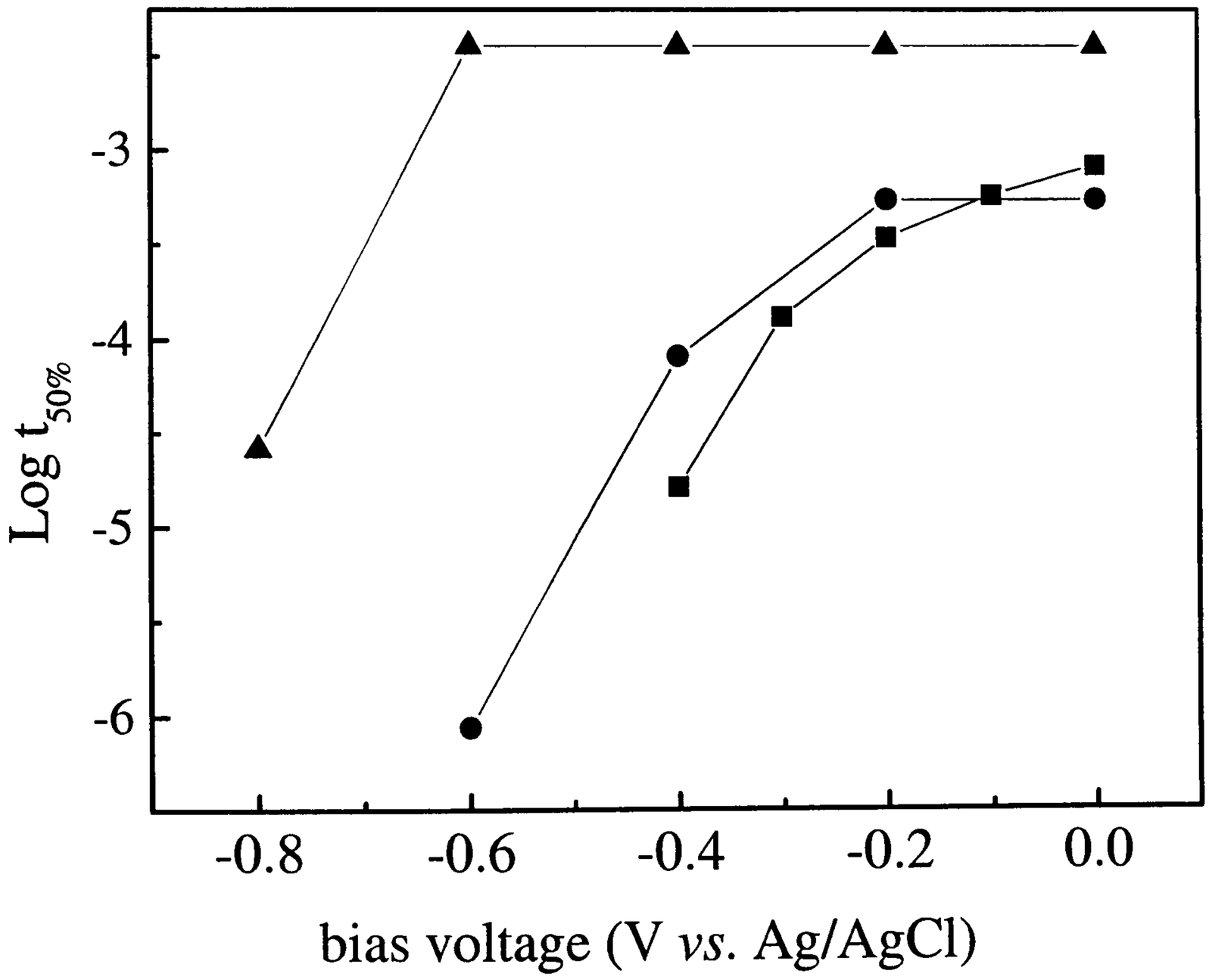

Figure 4.5: *Plot of log $t_{50\%}$ vs applied potential to the dye sensitized TiO_2 electrode in a three electrode electrochemical cell, employing different electrolytes in propylene carbonate: 0.1 M $LiClO_4$ (squares); 0.1 M $NaClO_4$ (circles); 0.1 M $NaClO_4$ with additional 0.5 M tert-butyl-pyridine (triangles).*

The influence of 4-t-butyl-pyridine was further investigated by experiments probing the charge recombination reaction k_{CR1} in the absence of redox active electrolyte. Data shown in figure 4.5 are the $t_{50\%}$ of the dye cation decay in propylene carbonate as a function of applied bias in 0.1 M $LiClO_4$, 0.1 M $NaClO_4$ and 0.1 M $NaClO_4$ with added 0.5 M 4-t-butyl-pyridine, respectively. Two effects are clear. Firstly the rate of the recombination reaction is slowed remarkably when 4-t-butyl-pyridine is added to the electrolyte and secondly, the onset of the charge recombination bias dependence is retarded to more negative voltages.

The high yield of products observed in cell B2 (light gray in figure 4.4) despite the slower $t_{50\%}$ of the decay is compatible with a slower k_{CR1} induced by the presence of 4-tert-butyl-pyridine. It appears to slow down the iodide reaction as well (k_{RG}) but further experiments are needed to prove this hypothesis unambigously.

4.3.2 Transient kinetics under illumination: k_{CR1} in propylene carbonate

As a prerequisite for transient absorption studies of solar cells under illumination, studies of charge recombination between photoinjected electrons and dye cations (k_{CR1}) in the dark were extended to white light conditions, as explained in section 2.8.3. Comparison of k_{CR1} dynamics in a redox inactive ($LiClO_4$ 0.1 M) propylene carbonate electrolyte in the dark and under white light illumination (¼ sun tungsten lamp white light superimposed on the 800 nm probe beam) is shown in figure 4.6. The extra electrons injected by the steady white light illumination cause an acceleration of the CR1 reaction. The charge recombination reaction (k_{CR1}) accelerates by approximately an order of magnitude - i.e. its $t_{50\%}$ is reduced from ~ 1 ms to just less than 100 μs under approximately ¼ of a sun. It is reasonable to extrapolate that under 1 sun illumination levels the charge recombination reaction k_{CR1} will therefore have a $t_{50\%}$ in the region of 20 to 50 μs.

The electron injection yield, as assessed from the initial size of the transient absorption signal, also appears to be reduced in this time window, though it is reasonable to assume that the signals will converge at approximately 50-100 ns. Data subsequently acquired by Mr. Niroj Abeyasinghe confirms that the injection yield is largely unaffected.

Previous kinetics studies (Haque et al. 1998; Haque et al. 2000) have investigated the charge recombination reaction k_{CR1} in the dark in ideal conditions and also shown an acceleration of k_{CR1} by applying an electrical bias in the dark. The issue of whether and how the dependence of k_{CR1} on either electrical bias or white light illumination can be related to observations in complete cells is still being debated within our research group.

The stretched exponential nature of the dynamics of the traces shown in figure 4.6 is maintained with the α exponent increasing from ~ 0.35 to ~ 0.6.

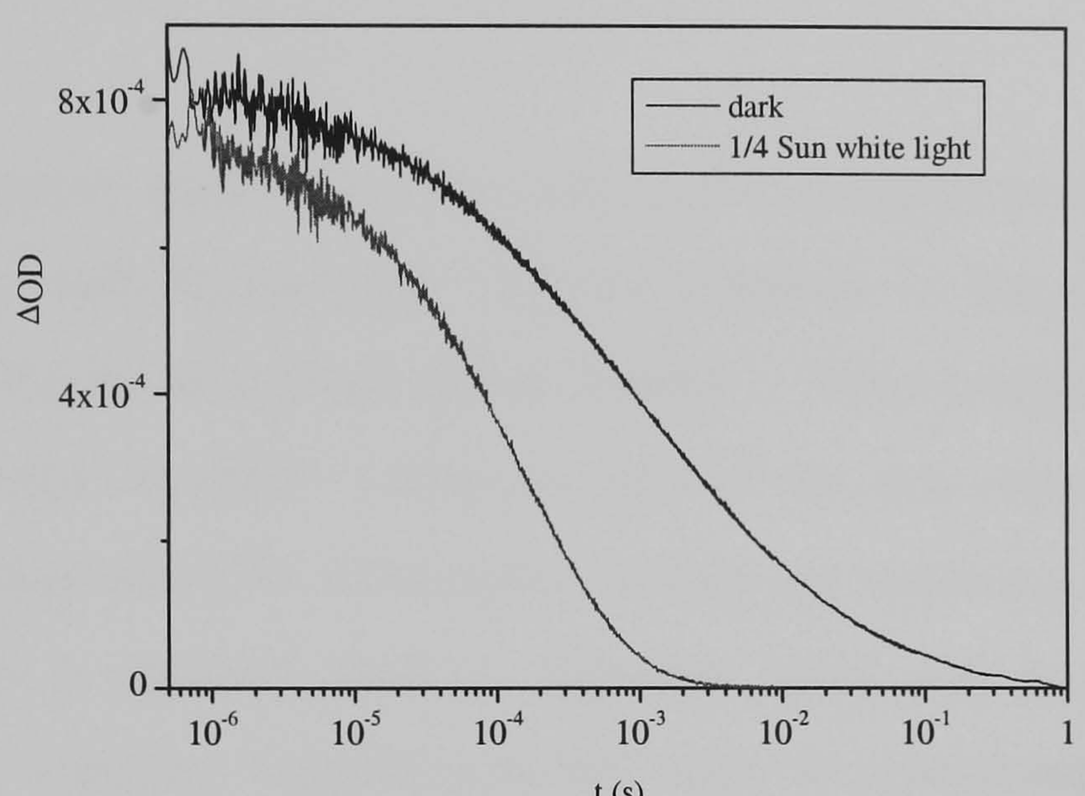

***Figure 4.6**: Charge recombination kinetics in a N719-sensitised TiO_2 electrode probed at 800 nm in the dark (black) and under white light illumination from the tungsten lamp (grey). The incident power in the latter case is approximately ¼ of a Sun.*

A qualitative interpretation of these results can be attempted within the framework of the CTRW model described in the previous chapter. Under white light illumination the electron occupancy of the tail of the exponential density of states g(E) (eq. 3.8; chapter 3) assumed in the CTRW model should increase and the apparent dispersion parameter of the charge recombination kinetics (α) should increase approaching one at longer times. The observed α in the experiment presented in figure 4.6 increases from ~ 0.35 to ~ 0.6 in qualitative agreement with the expected behaviour. The only partial filling of the tail of density of states could also contribute to explaining the observed behaviour.

4.3.3 Transient absorption studies under white light: acetonitrile cells

Results of transient absorption experiments on the acetonitrile cell are presented in figure 4.7. The early (~ 500 ns to ~100 μs) part of the decays are superimposable for the three conditions considered (dark plus short and open circuit under illumination). The formation of products of the regeneration reaction appears to plateau, though not as clearly as in some of the data discussed in chapter 3. As seen earlier, the kinetics in the dark extend up to ~ 1 sec. In contrast, under white light the signal decays back to zero within 10 ms. Open circuit conditions lead to only marginally slower kinetics on slow timescales.

The nature of the species probed by the experiment is assigned to dye cation absorption in the early phases and regeneration reaction products in the slower timescales in analogy with the interpretation presented in chapter 3. What is apparent from the earlier (500 ns - 100 μs time window) is that the size of the dye cation transient signal is independent of voltage and CW illumination within the operating range of the device. This result implies a constant electron injection yield and is in accordance with observations by Dr. Yasuhiro Tachibana in the femto- to picosecond scale for analogous solar cells. On an ultrafast time-scale it was in fact found that the rate of electron injection and its yield, as assessed by the rise and the maximum size of the cation transient absorption signal at 800 nm (Tachibana et al. 1996), is independent of bias in a comparable range (Tachibana 2000). The yield of products of the regeneration reaction k_{RG} as assessed by the transient absorption signal size at approximately 200 μs (see also chapter 3) is constant and therefore independent of both applied electrical bias and background illumination. The independence of the injection and regeneration products yields on the applied electrical bias point to k_{CR1} not being a significant loss mechanism in these cells even at open circuit voltage. Recombination losses can therefore be exclusively attributed to k_{CR2} in this type of cells in accordance with widespread literature assumptions (Huang et al. 1997; Ferber, Stangl, and Luther 1998; Schlichthörl, Park, and Frank 1999) but in contrast to the results reported by Franco et al. (Franco et al. 1999) on cells with a similar composition.

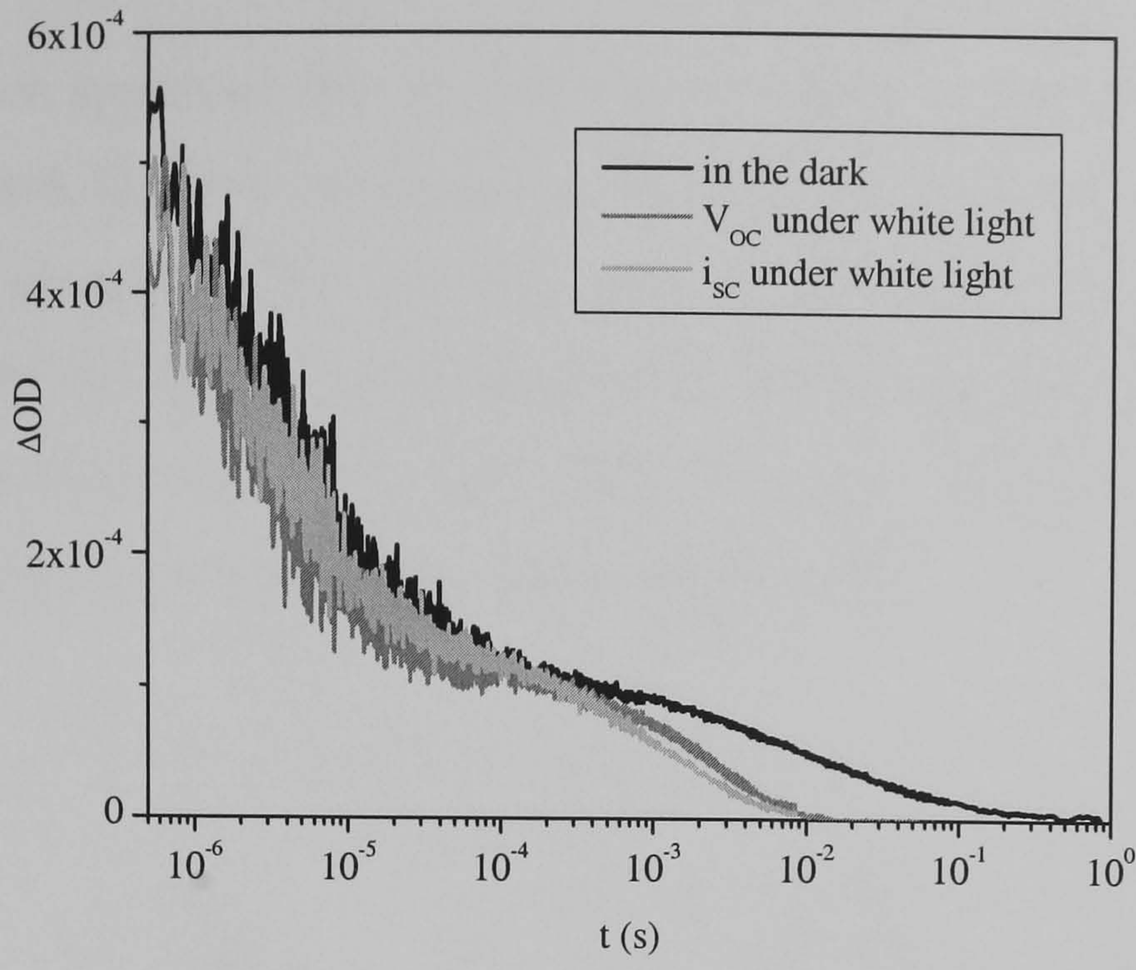

Figure 4.7: *Transient absorption spectroscopy of a standard acetonitrile solar cell in the dark (black) and under white light (¼ Sun) at open circuit (grey, 675 mV) and in short circuit conditions (light grey, i= 2.67 mA).*

The lifetime of the regeneration products is strongly affected by the white light with the $t_{50\%}$ of the products tail accelerating to ~ 2 ms as compared to ~ 20 ms in the dark. The signal is slightly longer lived when the cell is at open circuit conditions compared to short circuit.

Under white light illumination a steady state of photons is absorbed by the sensitiser molecules, and a steady state of iodide anions regenerate the ground state of the dye resulting in I_2^- formation and electron build-up in the semiconductor. The shorter lifetime for the I_2^- / e_{TiO2} products under white light illumination has previously been interpreted in terms of the higher concentration of I_2^- radicals and subsequent faster dismutation under white light (Nogueira et al. 2001). Also, the faster recombination kinetics between photoinjected electrons and dye cations observed under white light illumination (as shown in figure 4.6) could be partly responsible for the acceleration of the slow phase decay observed here. It must be noted that this effect of white light is observed in all cells irrespective of solvent electrolyte employed. The difference in regeneration reaction products' lifetime at open circuit compared to short circuit is small and of the same order of magnitude if not smaller than the reproducibility limits of the experiment so a quantitative analysis will not be attempted.

4.3.4 Transient absorption studies under white light: propylene carbonate cells

Transient absorption spectroscopy experiments performed on propylene carbonate cells (electrolytes B_1 and B_2) are presented in figures 4.8 and 4.9. In contrast to the acetonitrile based electrolyte the kinetics, even the fast decay dynamics (assigned to k_{RG}) are affected by the background illumination. At short circuit conditions, the early part of the decay is faster than in the dark while at slower timescales ($t > 10^{-4}$ seconds) the signal rapidly decays to zero within a few milliseconds.

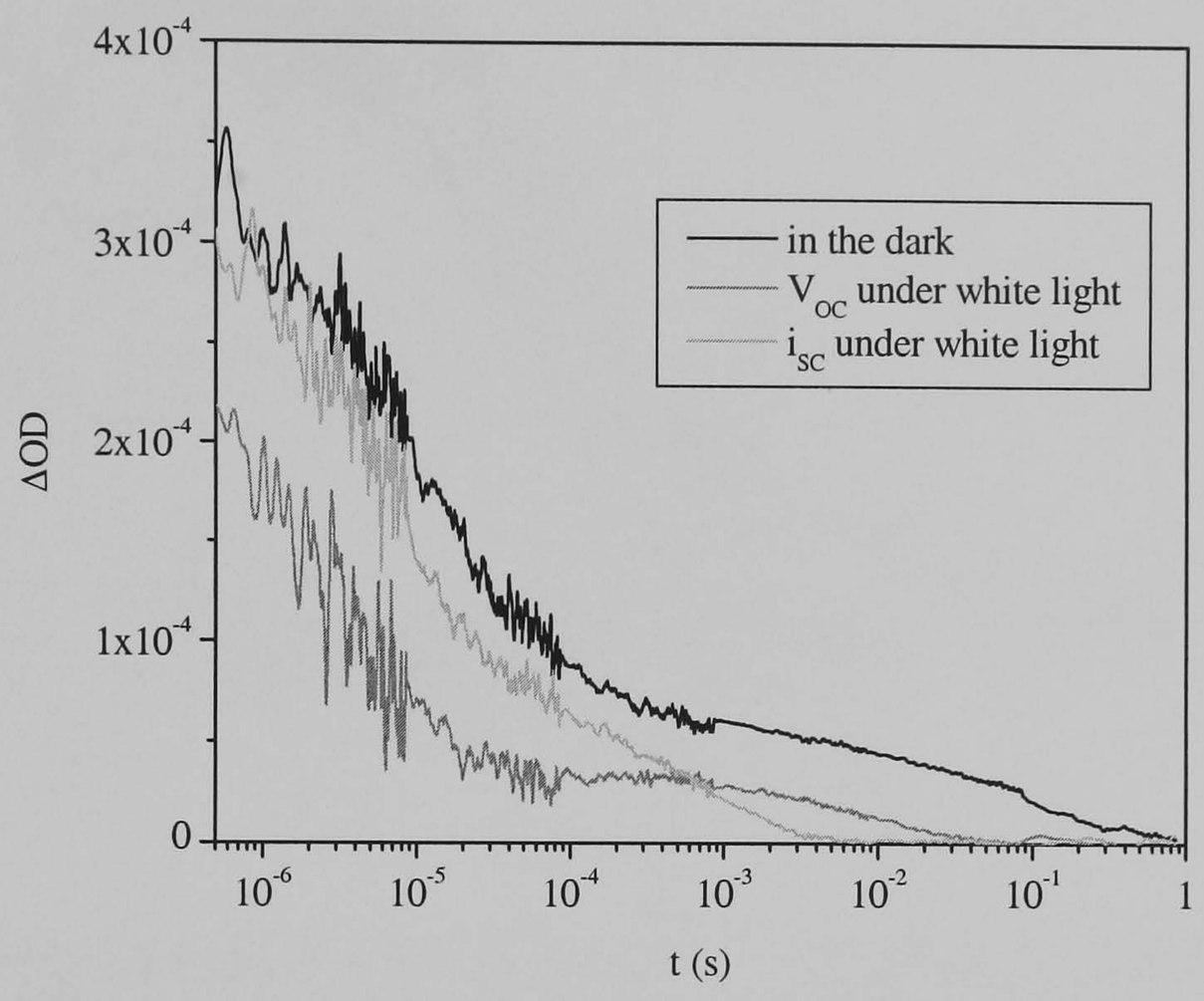

Figure 4.8: *Transient absorption spectroscopy of a propylene carbonate solar cell (electrolyte B_1) in the dark (black) and under white light (¼ Sun) both at open circuit (dark grey, 676 mV) and at short circuit (light grey, i=2.3 mA). The cation decay kinetics are faster under white light and become even faster at open circuit voltage conditions. The product yield is affected by both the white light and the voltage. The products' lifetime is strongly reduced by the background illumination and increases at open circuit voltage.*

At open circuit voltage conditions the fast phase of the decay accelerates by one order of magnitude indicating kinetic competition between dye regeneration by iodide (k_{RG}) and recombination between photoinjected electrons and dye cations (k_{CR1}). The lifetime of the long lived transient is strongly dependent on illumination and voltage, more than in acetonitrile. The time resolution of the apparatus prevents direct comparison of electron injection yields as assessed from the initial size of the transient absorption signal. However, changing solvent viscosity is not expected to affect the injection yield. It is therefore reasonable to assume the injection yield to be unchanged in the three conditions shown.

In favour of this assumption is the data presented in figure 4.9 for a propylene carbonate cell containing less iodide. The lower iodide concentration results in slower dye regeneration kinetics and displays the initial amplitude of the dye cation signal. In this case the values are comparable under open and short circuit conditions indicating voltage independent injection yield.

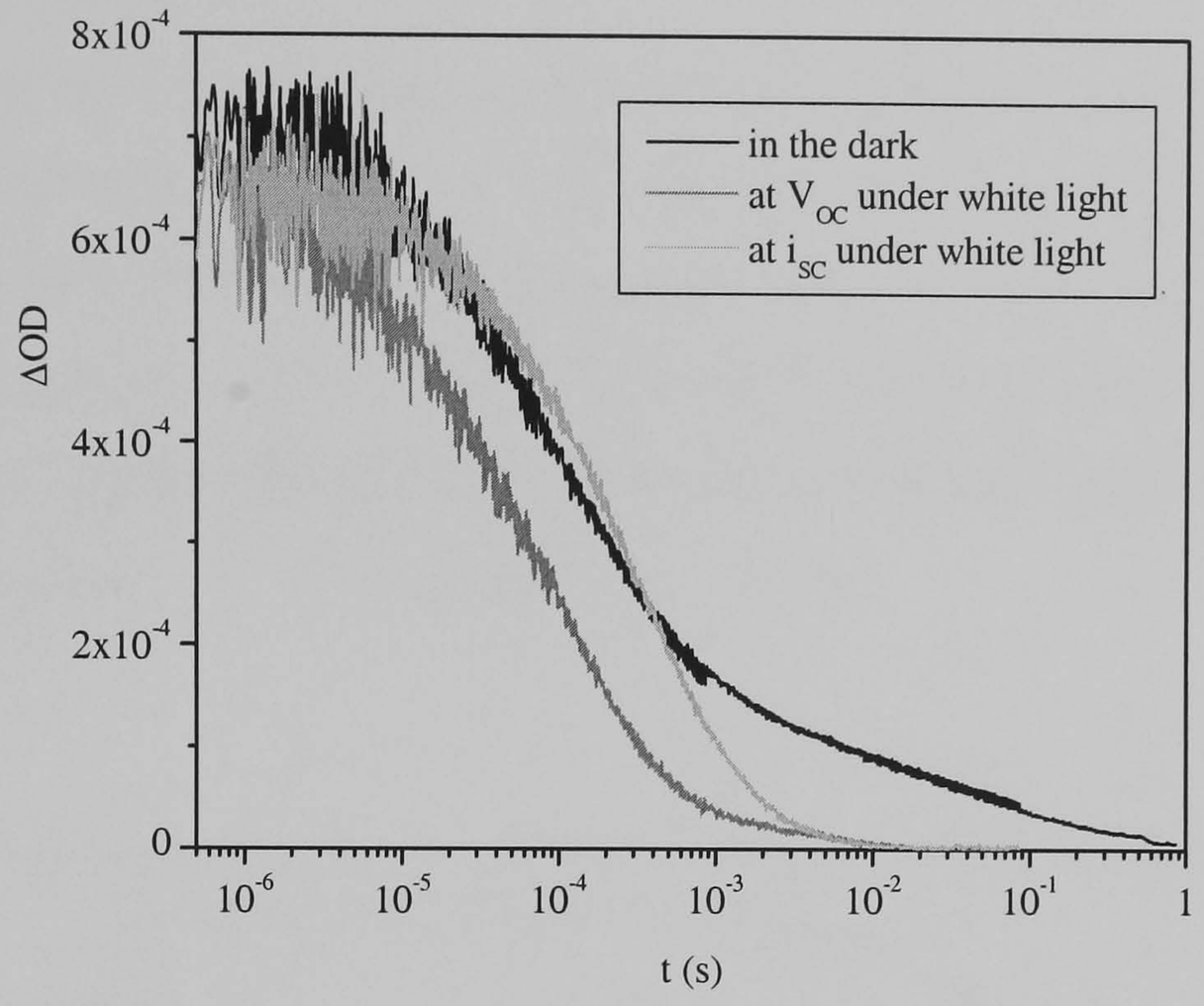

Figure 4.9: *Transient absorption spectroscopy of a propylene carbonate solar cell (electrolyte B2) in the dark (black) and under white light (¼ Sun) both at open circuit (dark grey, 635 mV) and at short circuit (light grey, 1.8 mA). The cation decay kinetics are faster at open circuit. The I_2^- / e_{TiO2} formation yield is affected by both the white light and the voltage. The lifetime is strongly reduced by the background illumination and increases at open circuit voltage.*

At open circuit voltage, the lifetime of the decay decreases, and the product yield is reduced. Both observations indicate that k_{CR1} competes with k_{RG} at V_{OC}. The yield of the regeneration reaction products is reduced in the case of electrolyte B1 by the background illumination and the applied bias while the case of electrolyte B2 is less clear cut. This result, combined with the faster decay of the dye cation strongly support the fact that in these cells employing a viscous solvent the regeneration reaction k_{RG} is slower and the recombination pathway k_{CR1} can effectively compete with it at open circuit voltage in a similar fashion to what observed and discussed at low iodide concentrations in chapter 3. In viscous solvents and/or in presence of low iodide concentrations both k_{CR1} and k_{CR2} recombination losses mechanisms determine the i-V characteristics of devices.

The effect of white light illumination on the lifetime of I_2^-/e_{TiO2} products is analogous to what is observed in acetonitrile cells and interpreted likewise. The longer lived products observed at open circuit voltage in figure 4.9 are consistent with lower concentration of I_2^- radicals leading to a slower dismutation rate.

4.3.5 i-V characteristics

The i-V characteristics of a standard acetonitrile solar cell both in the dark and under ¼ Sun conditions are presented in figure 4.10. The open circuit voltage obtained is 0.67 V and the short circuit current reaches 2.64 mA/cm^2. The i-V curve can be fitted using the non-ideal diode equation (eqs. 4.8 and 4.9) shown as the dotted line in figure 4.10. The fitting results in a series resistance R_s of 22 Ω and a shunt resistance of $R_{sh} > 10$ kΩ and a non-ideality factor of 1.96. The value of I_0 is ~ 2 nA.

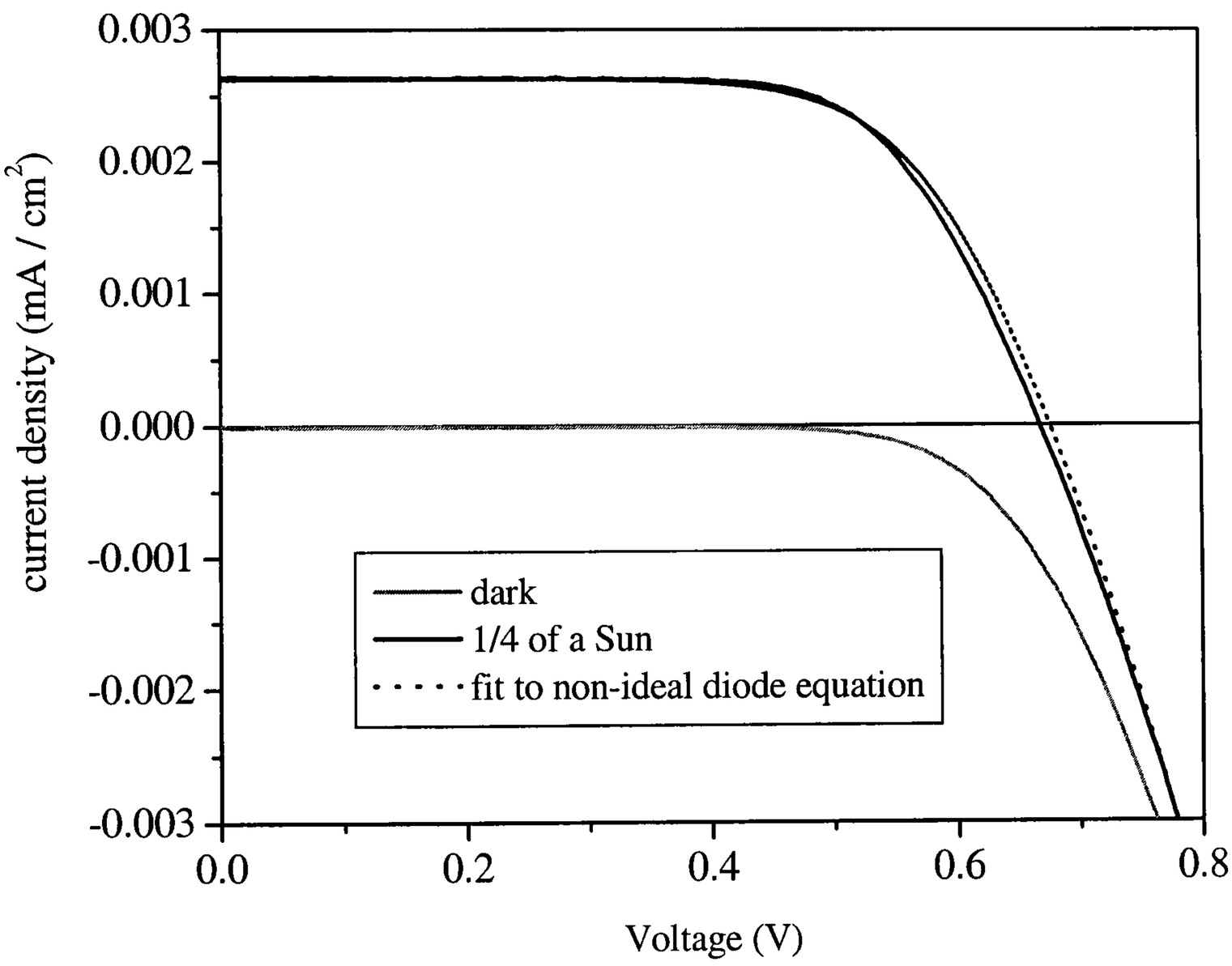

Figure 4.10: *i-V characteristics of a standard acetonitrile (electrolyte A1) DSSC in the dark (black) and under white light (grey) from the probe beam of the MTA. The incident white light was approximately ¼ of a Sun in intensity.*

The good fit to the diode equation, coupled with the identical kinetics observed at short and open circuit (see figure 4.6 above) indicates that in standard acetonitrile cells k_{CR2} is the only recombination loss in agreeement with the transient absorption data shown in

figure 4.7. This result confirms the validity of the assumption generally made in the literature that the majority of photocurrent losses can be attributed to the reaction between electrons and tri-iodide (Huang et al. 1997; Schlichthörl, Park, and Frank 1999) and is in contrast with the suggestion that k_{CR1} competes effectively with k_{RG} at voltages approaching open circuit voltage conditions for a similar electrolyte (Franco et al. 1999).

Unfortunately, reproducible i-V data for the propylene carbonate cells (that show recombination k_{CR1} losses in the proximity of open circuit conditions in transient absorption experiments, see figure 4.8 & 4.9) could not be acquired so a quantitative comparison with the i-V characteristics of acetonitrile cells is prevented.

Since the end of my experimental work, another study employing polyethylene glycol to increase the viscosity of an acetonitrile solar cell's electrolyte has been carried out by Mr. Niroj Abeyasinghe. Transient absorption data indicating competition between k_{CR1} and k_{RG} at open circuit voltage analogous to those presented in figure 4.8 & 4.9 were observed. A quantitative comparison of the i-V characteristics in the dark and under illumination was prevented by the lower series resistance observed in the latter case and attributed to heating and subsequent decrease in viscosity of the electrolyte in the cells exposed to the solar simulator.

4.4 Conclusions

The key conclusion that can be drawn from the results presented in this chapter is that in a standard cell employing acetonitrile and large concentrations of iodide the charge recombination reaction with dye cations k_{CR1} is functionally unimportant and the majority of the recombination losses can be attributed to the reaction of electrons with I_3^- (k_{CR2}). It only becomes an issue in cells with low regeneration rate k_{RG}, whether because of the viscosity of the solvent and/or low iodide concentration. In such cases the charge recombination reaction k_{CR1}, known to be strongly dependent on the applied bias, is capable of successfully competing with the regeneration reaction at voltages approaching open circuit conditions and is responsible for a non-negligible amount of the recombination losses. Furthermore:

1) The injection yield is independent of applied bias in a range from 0 V (short- circuit conditions) to the open circuit voltage for all cells studied here. This result is consistent with ultrafast measurements performed by Dr. Yasuhiro Tachibana that found the injection yield in N719-sensitised films in a three electrode cell and complete cells to be independent of applied voltage in a range equivalent with the one studied here (Tachibana 2000).

2) In a DSSC employing a nitrile solvent such as employed in the best liquid electrolyte cells produced to date, the yield of regeneration reaction products is independent both of white light illumination and of an applied bias up to and including open circuit conditions. These results point to the fact that the open circuit voltage obtainable with these cells is limited exclusively by the reaction of electrons in the semiconductor with I_3^- (k_{CR2}) in accordance with what is generally assumed in the literature.

3) In a DSSC employing a viscous solvent such as propylene carbonate, and when low iodide concentrations are employed, the regeneration of the dye cation by iodide (k_{RG}) is slower and therefore charge recombination between electrons in the semiconductor and dye cations (k_{CR1}) becomes significant at voltages approaching open circuit voltage. In such cells therefore photoinjected electrons are lost both through recombination with dye cations (k_{CR1}) and I_3^- (k_{CR2}) limiting the efficiency of devices.

4) The lifetime of the regeneration reaction products is dependent upon white light illumination in all DSSC considered here. This observation can be rationalised in terms of a large amount of these radical species being produced in working conditions leading to a faster dismutation rate (see also Nogueira et al. 2001). In cells employing viscous solvents such as propylene carbonate or low iodide concentrations the yield of I_2^- is reduced at open circuit voltage as the recombination pathway k_{CR1} becomes significant. The reduced concentration of I_2^- radicals leads to a slower dismutation rate as observed.

CHAPTER 5

CHARGE RECOMBINATION IN PPV/C_{60} BLENDS

5. CHARGE RECOMBINATION IN PPV / C_{60} BLENDS

This chapter addresses room-temperature charge recombination dynamics in PPV-C_{60} derivatives blends employing time-resolved transient absorption spectroscopy. From the influence of the excitation power on the dynamics a mobility edge is found at polaron concentrations of approx. 10^{17} cm^{-3}. Implications for device function are discussed.

5.1 Introduction

5.1.1 Conducting polymers / fullerene solar cells

The discovery of photoinduced electron transfer from a PPV derivative (MEH-PPV or poly(2-methoxy-5-(2'-ethylhexoxy)-p-phenylene-vinylene)) to buckminsterfullerene (C_{60}) (Sariciftci et al. 1992) was a breakthrough in semiconducting polymer based photovoltaic devices research. Addition of C_{60} substantially improved the photocurrent quantum efficiency obtainable compared with devices based solely on conjugated polymers.

The PPV acts as a chromophore and its excited state as electron donor (D) when illuminated (D*). The fullerene is an extremely good electron acceptor (A), known to accept up to 6 electrons in vacuum and charge separation takes place leading to D^+/A^-.

$$D/A \xrightarrow{h\nu} D^*/A \xrightarrow{k_{et}} D^+/A^- \qquad (5.1)$$

One way of describing the driving force of this process is to think in terms of HOMOs of the donor and LUMOs of the acceptor. In this context the driving force of the charge separation step is 0.9 eV (Winder 2001).

Early devices, fabricated from conjugated polymer/C_{60} bilayers (Sariciftci et al. 1993; Halls et al. 1996), were limited in their power conversion efficiencies (<0.1%) by the low solubility of fullerene in organic solvents, which lead to poor interfacial contact area between the donor and acceptor domains. In other words, the fraction of acceptor molecule within the diffusion length of the PPV exciton was small.

The problem was overcome by Hummelen and co-workers (Hummelen et al. 1995) at Groningen University who synthesised soluble fullerene derivatives such as PCBM (1-(3-(Methoxycarbonyl)propyl)-1-phenyl[6.6]C_{61}). By blending this soluble methanofullerene directly into the conjugated polymer film (Yu et al. 1995) a

monochromatic (430 nm) carrier collection efficiency (η_c) of 29% of electrons per absorbed photon was achieved under 20 mW/cm^2 illumination.

As it was pointed out in Chapter 1 morphology plays a key role in determining charge separation, recombination and transport dynamics. The quantum efficiency of charge separation has steadily increased with improvements in the morphology of donor-acceptor systems. State of the art devices use as photo-active layer a blend of MDMO-PPV (poly(2-methoxy-5-(3,7-dimethyloctyloxy)-1,4-phenylene vinylene)) and PCBM, spin coated in controlled conditions. Further improvements have addressed the design of the electrodes contacts (Brabec, Cravino, Meissner et al. 2001; Brabec et al. 2002). They have recently obtained quantum efficiencies per absorbed photon approaching unity (Brabec, Sariciftci, and Hummelen 2001) and an encouraging 2.5 - 3 % efficiency under 80 mW/cm^2 (AM 1.5 spectral mismatch factor 0.753) (Shaheen et al. 2001; Brabec et al. 2002). The chemical structure of the above mentioned PPV and fullerene derivatives is shown in Figure 5.1. Note the extended aliphatic chain of MDMO-PPV and the derivatisation of fullerene that lead to improved solubility.

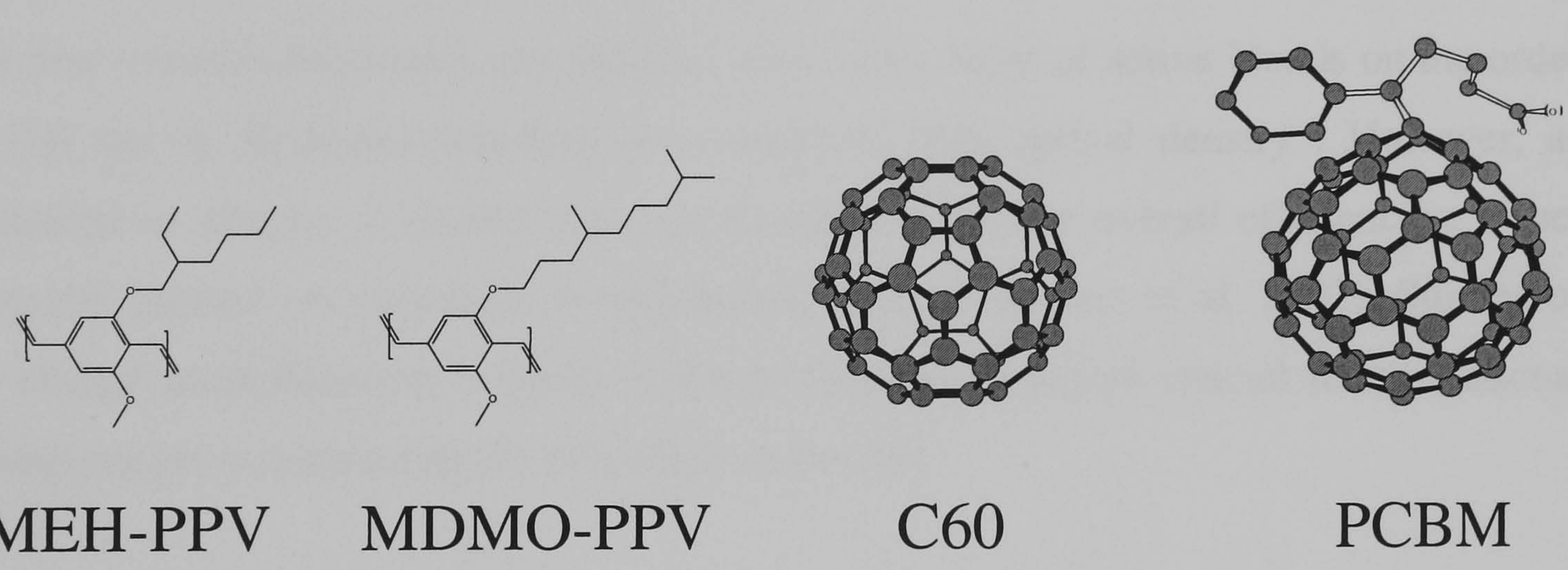

Figure 5.1: *Chemical structure of MEH-PPV, MDMO-PPV, C_{60} and PCBM.*

The donor / acceptor blend is deposited between an ITO-glass substrate that acts as the cathode and an aluminium layer acting as anode. An 80 nm layer of PSS – doped PEDOT [poly(3,4-ethylenedioxythiophene)-poly(styrene-sulfonate)] commercially available from Bayer is usually spin-coated from solution between the ITO and the blend. The PSS-PEDOT is thought to allow a better match of the work function of ITO with MDMO-PPV, improving hole collection. A subnanometer (~0.6 nm) layer of LiF deposited between the blend and the Al contact has been shown to improve the fill factor, and in turn, the efficiency of devices. Shaheen and Brabec have recently

investigated this effect (Brabec et al. 2002). Several other metals have been tested as alternatives to Al though the voltage obtained from devices was found to be rather independent of the work function of the metal employed in the anode (Brabec, Cravino, Meissner et al. 2001). Under photovoltaic function, the electrons are collected at the Al anode and injected from the ITO cathode (often referred to as the hole collection at the ITO). A schematic of a state-of-the-art device (Brabec, Sariciftci, and Hummelen 2001) is shown in figure 5.2.

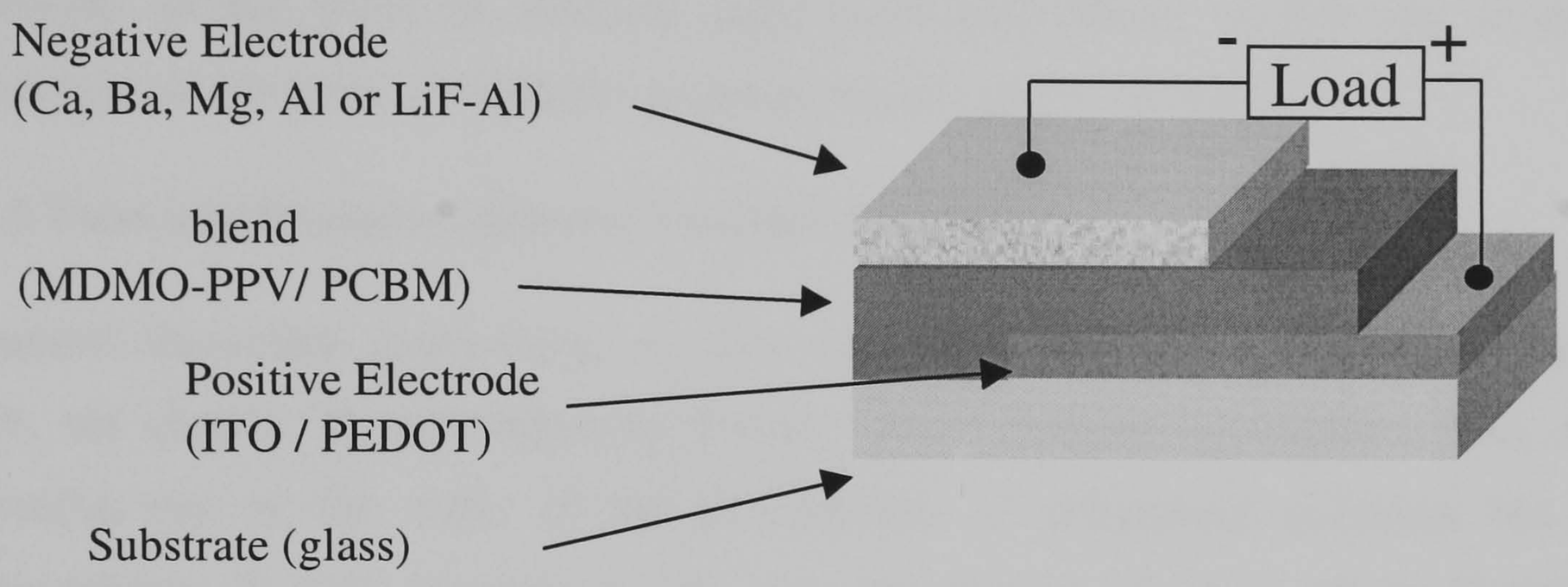

Figure 5.2: *Schematic illustration of a MDMO-PPV: PCBM solar cell (courtesy of Dr. Christoph Brabec).*

The best overall efficiencies are obtained with a thin layer of active blends on the order of 100 nm in thickness resulting in a relatively low optical density . However, as explained in chapter 1, thicker films do not lead to higher overall efficiencies, a fact normally blamed on increased recombination losses (Munters et al. 2002). Studies of the charge recombination reaction in these films are therefore crucial to any rational attempt aimed at improving the efficiency of devices.

Despite these results much remains to be done for plastic solar cells to become an established branch of photovoltaics. One of the main problems common to all applications of conducting polymers is the issue of chemical stability. The combination of light and oxygen is known to be lethal for the devices. There is Fourier-Transform infrared spectroscopy evidence of irreversible photo-oxidation of the conducting polymer chains in devices exposed to oxygen (Neugebauer et al. 2000; Neugebauer et al. 1999). Moisture is another issue, although oxygen remains the main cause of sample degradation. Recently, a detailed study of the stability of these devices has highlighted how thermal stress induces morphological changes in the photoactive layer and prolonged irradiation induces photochemical degradation with detrimental effects on the

stability of the cells (Kroon et al. 2002). Devices need to have a shelf lifetime of several years and operational lifetimes of tens of thousand of hours in order to make an impact as alternatives to inorganic semiconductor analogues in durable applications. Conjugated polymers therefore need to be protected from air and humidity in order to achieve such lifetimes. These issues are also relevant to organic LEDs made of similar compounds which are being developed at present. Sealing methods are being developed for polymer LEDs, and there are encouraging signs that the stability problem has been overcome to the point of entering large-scale applications. A fall out of these technological advances onto plastic photovoltaics is eagerly awaited.

5.1.2 Time and frequency domain transient absorption

Transient absorption spectroscopy in both time (Transient Absorption Spectroscopy, TAS, see chapter 3) and frequency domain (Photo Induced Absorption, PIA), is a powerful tool in the study of the photophysics of conjugated polymers but the interpretation of such experiments has been the subject of much debate (Sariciftci 1997).

Photo-Induced Absorption (PIA) employs a chopped CW laser source to excite the sample and create a quasi-steady state of products. A lock-in amplifier is used in conjunction with the chopper on the excitation beam and a range of probe wavelengths from a white light tungsten halogen lamp is scanned. The technique provides a relatively simple way of screening new polymer blends for photoinduced charge transfer and has a better sensitivity compared with time resolved methods. The major drawback is that it does not provide much information on the temporal shape of the decay kinetics with monomolecular and bimolecular processes hardly distinguishable (Botta et al. 1993). Most previous studies of charge recombination dynamics in polymer / C_{60} blends have largely been PIA experiments with chopping frequencies up to ~ 10 kHz, corresponding to a time resolution for the transient species observed of up to approximately 100 μs. These studies were normally carried out at low temperature in order to increase the signal to noise ratio of the experiments. However, they are bound to be more relevant at room temperature, the condition at which devices operate. Time resolved measurements allow to follow the kinetics of processes but their lower sensitivity complicates unambiguous spectral characterisation. It must be noted that some scientists refer to time-resolved methods, especially femto- and picosecond studies, also as PIA.

The transient absorption features observed on fast timescales in PPV and its derivatives have been variously attributed to triplet excitons (Sinclair et al. 1992), polarons (Blatchford et al. 1996), singlet intrachain excitons (Harrison et al. 1996) (also referred to as "singlet polaron excitons") (Denton et al. 1997; Klimov et al. 1997) and spatially indirect excitons (also referred to as polaron pairs) (Hsu et al. 1994; Yan et al. 1994; Yan et al. 1995; Rothberg et al. 1996; Klimov et al. 1997). Furthermore, the species originally referred to as polaron pairs have been lately renamed as excimers (Samuel et al. 1998; Jakubiak et al. 1999; Nguyen, Doan, and Schwartz 1999). Figure 5.3 summarises visually most of these radical species thought to be produced by illumination of conducting polymers alone or donor / acceptor mixtures.

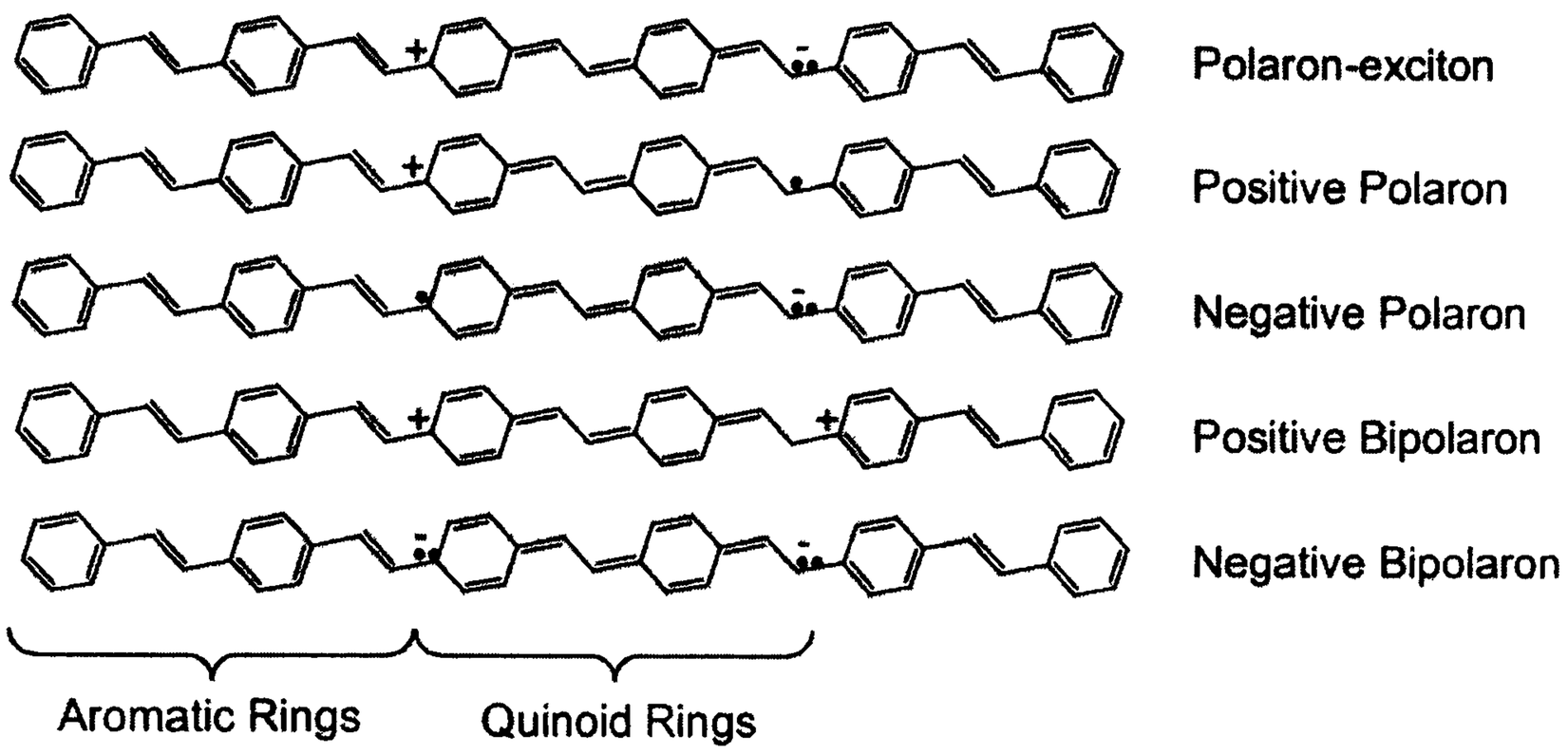

Figure 5.3: *Polaron-exciton, positive polaron, negative polaron, positive bipolaron, negative bipolaron (from J. J. Dittmer Ph.D. thesis adapted from N. C. Greenham and R. H. Friend in Solid State Physics – Advances in Research and Applications, edited by H. Ehrenreich and F. Spaepen (Academic Press, New York, 1995) vol. 49 p.1*

Several factors contribute to the variety of experimental results that have been reported in the literature, including widely varying experimental conditions for each measurement (excitation energy and wavelength of the excitation light among others), and the physical state of the samples investigated (solutions, films cast from various solvents, or thermally converted, insoluble films), or the degree of photochemical degradation. Also, the purity of the samples investigated varied widely.

Given the confusion reigning in the literature it is appropriate to summarise the spectral features of the transient species likely to be formed in PPV-C_{60} derivatives blends and in pristine MDMO-PPV films. In the latter case, low-temperature PIA spectra (approximately millisecond lived species) have been assigned to triplet excitons (triplet

PPV excited states in molecular terms). These are responsible for a single absorption peak in the region of 1.4 eV (885 nm) (Kraabel et al. 1993; Kraabel et al. 1996; Zerza et al. 2000). In the case of blends the high quantum efficiency of the charge separation step (the PPV emission is quenched by 3 orders of magnitude (Sariciftci et al. 1992)) leads to the observation of PPV cations (polarons) in PIA experiments. Their spectrum is characterised by a broad absorption having two maxima, the first at an energy similar to the one of the triplets and a second maximum in the 2 eV region (620 nm) separated from the first by a minimum in the positive absorption signal. McBranch and co-workers have recently tried to establish a general description of the ultrafast photophysics of phenylene-based conjugated polymers and identified the spectral features of singlet intrachain excitons and photoinduced polarons in this class of materials (Kraabel et al. 2000).

5.1.3 The bulk heterojunction picture

Lately, the concept of a bulk hetero-junction (Yu et al. 1995) has been introduced in order to describe intimate donor / acceptor blends. If any point in the composite is within a few nanometers of a D / A interface, such a composite is a "bulk D / A heterojunction" material. Brabec et al. have depicted pictorially a simplified energy diagram for such bulk heterojunctions as illustrated in figure 5.4

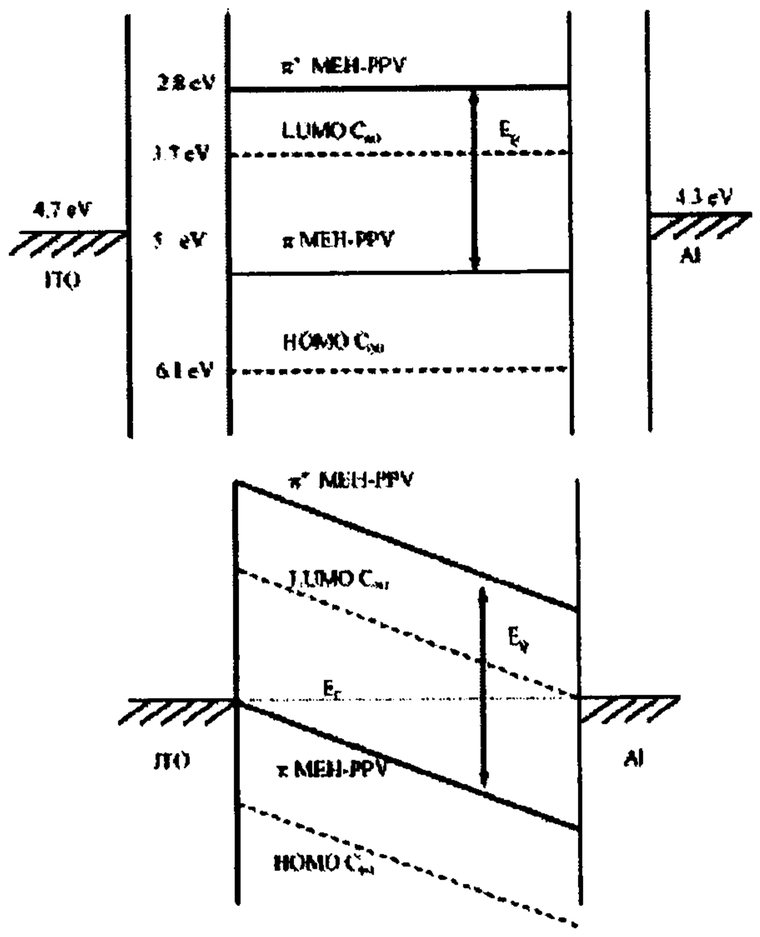

Figure 5.4: *The Bulk Heterojunction concept. The simplified diagram shows the energy levels of a MEH-PPV/C_{60} bulk heterojunction system taken as example under flat band conditions (higher half) and under short circuit conditions (lower half) and does not take into account possible interfacial barriers at the metal/semiconductor interface (from Brabec et al. 2001).*

By admission of the same authors the idealised schematic description in figure 5.4 is by far not realistic in any actual composite sample. As shown by AFM pictures (Shaheen et al. 2001), it is rather a disordered ensemble of islands of phases with differing polymer / C_{60} ratios.

The solvent used to prepare blend solutions for spin-coating influences the morphology of the films and the efficiency of the resulting devices. AFM images (Figure 5.5, taken from Shaheen et al. 2001) and cross-sections of blends deposited from toluene and chlorobenzene exhibit different morphologies. The blends cast from chlorobenzene result in a much smoother surface and even mixture of the components while in the toluene case bigger "lumps" assigned to phase-segregated regions containing different concentrations of fullerene are observed. Devices employing blends cast from chlorobenzene result in a 3-fold increase in the overall efficiency of solar cells relative to blends deposited from toluene (Shaheen et al. 2001).

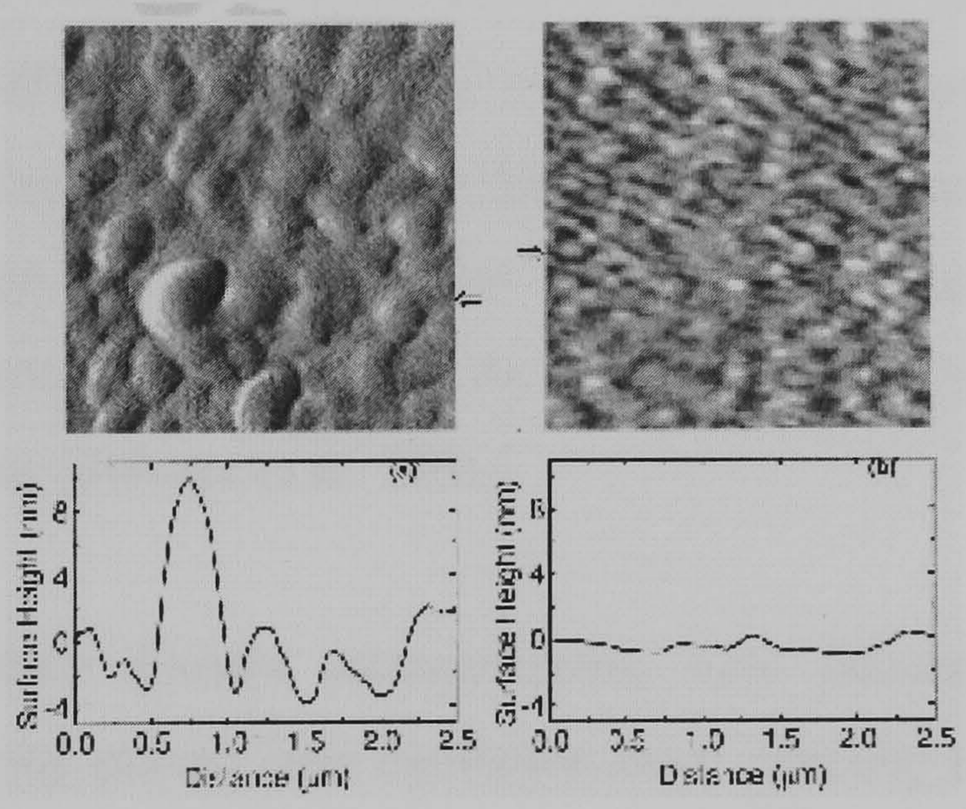

Figure 5.5: *AFM images showing the morphology of MDMO-PPV:PCBM (1:4 in weight) spin cast from toluene (left) and chlorobenzene (right); (from Shaheen et al. 2001).*

The increase in efficiency in blends spin-cast from chlorobenzene as opposed to toluene has been linked to an increase of charge carrier mobility as observed by field-effect mobility measurements of single components as well as of the mixtures processed from the different solvents (Geens et al. 2000). Poor charge transport is expected in toluene deposited films since they are rich in phase segregated C_{60} zones. However, much remains to be done to characterise this parameter and the overall process of charge migration to the electrodes.

5.1.4 Charge recombination vs. charge transport

The photoinduced charge separation can in principle be followed by either charge recombination of the photogenerated positive polarons (delocalised on the polymer backbone) and electrons (localised on the fullerene to form a negative anion) or charge migration to the electrodes. The competition between these two processes is critical in determining the overall conversion efficiency of devices. However little is known about the parameters affecting them. As it was introduced in chapter 1, the interpenetrating network of MDMO-PPV and PCBM at the heart of the bulk heterojunction concept leads to a closer proximity in space of the positive polarons and the PCBM anions and might also favour charge recombination.

The charge recombination reaction has been the object of PIA experiments at low temperatures (Smilowitz et al. 1993). Using this technique, the lifetime of the charge separated state was estimated to be of the order of milliseconds at 80 K (Smilowitz et al. 1993). In the case of MDMO-PPV / PCBM blends extremely long-lived (hours!) charge carriers were detected using Light-induced Electron Spin Resonance (LESR) in the 10-40 K temperature range (the signal is absent at room temperature). These observations were modelled in terms of tunnelling of the charged carriers species to increasingly distant opposite charges (Schultz et al. 2001).

In contrast to frequency domain measurements, time domain transient absorption studies (TAS) employing pulsed laser excitation have typically reported recombination dynamics in polymer / C_{60} films on the picosecond and nanosecond timescales (Kraabel et al. 1996; Kraabel et al. 1993; Mizrahi et al. 1999; Meskers et al. 2000). It has been suggested that these different charge recombination timescales may result from different processes and the slower process observed in PIA studies to recombination dynamics of trapped polarons. Sub-nanosecond TAS and 10 kHz PIA experiments on poly(thiophene) derivatives and C_{60} composites have been interpreted in terms of fast geminate recombination leading to up to 80% of the charge carriers formed to recombine within 30 ns while thermalised carriers trapped in the lowest states of the inhomogeneously broadened density of states followed millisecond timescale recombination dynamics (Meskers et al. 2000).

Perhaps surprisingly, far less is known about charge recombination processes at operating conditions due to the scarcity of PIA studies at room temperature.

5.1.5 Aims of this chapter

The aim of the work reported in this chapter is a preliminary investigation of the charge recombination dynamics in blends employed in plastic solar cells at room temperature, the condition most relevant to device function. The time scale of recombination dynamics at room temperature has not previously been established although it is a key parameter for device function. The essence of this work has been recently accepted for publication by Applied Physics Letters (Montanari et al. 2002).

Time-resolved pulsed transient absorption spectroscopy techniques analogous to those applied to dye-sensitised electrodes and solar cells in previous chapters were employed. A variety of experimental conditions were investigated such as dependence on the excitation power density, the casting solvent and white light CW illumination. The medium term goal is that of being able to discriminate between the decay of the polaron population due to charge recombination vs. charge transport to the electrodes. A comparison of possible theoretical models for the charge recombination step along with the limitations of the experiments and possible ways forward will be discussed later in the chapter.

5.2 Materials and methods

5.2.1 Samples studied

The following samples were kindly provided by Dr. Christoph Brabec (now at Siemens Forschung, Erlangen, Deutschland) and co-workers at the Johannes Kepler University, in Linz, Austria. Their preparation was covered in section 2.5.

- complete solar cells sealed with an epoxy resin in order to prevent oxygen- and moisture-induced degradation. The device structure was equal to the one described in figure 5.2. Devices employing an active layer (MDMO-PPV : PCBM 1:4 w/w) deposited from either toluene or chlorobenzene were provided.
- reference samples consisting of spin-cast blends (MDMO-PPV : PCBM 1:4 or 1:2 w/w) on ITO glass or microscope slides from either toluene or chlorobenzene.

The thickness of the active blend layer was approximately 100 nm for all samples studied. The optical density at the absorption maximum (500 nm) was ~ 0.3. The absorption spectrum of a blend deposited from chlorobenzene is shown in figure 5.6:

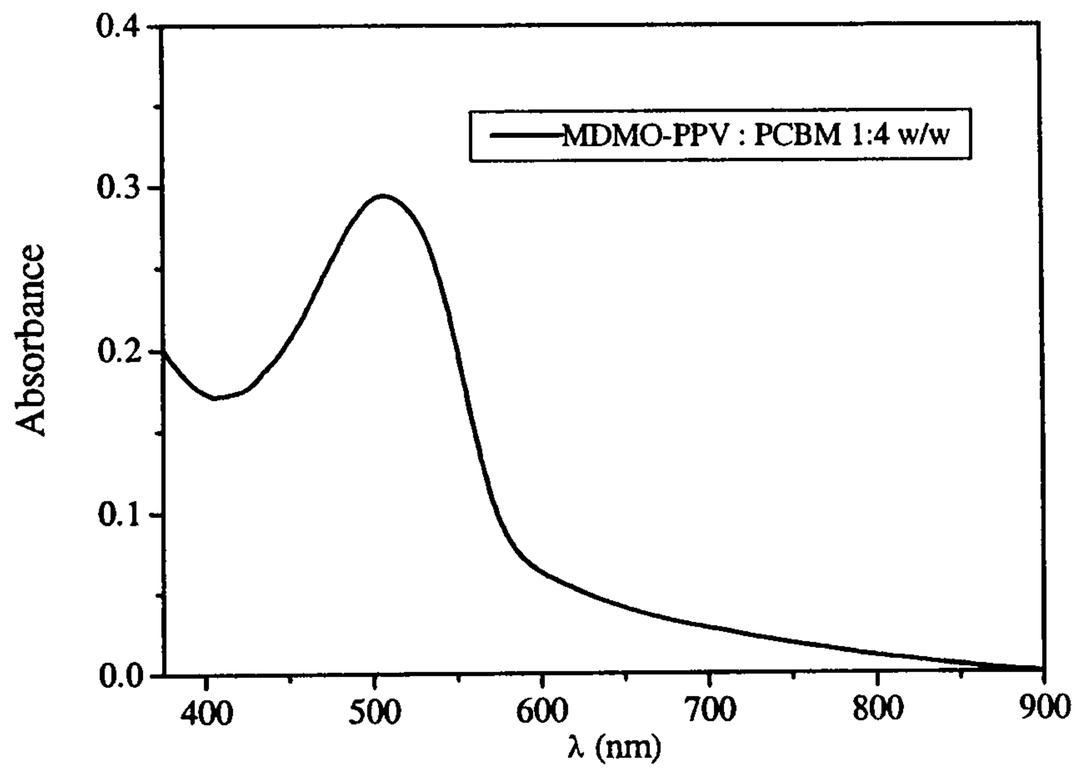

***Figure 5.6**: Absorption spectrum of a MDMO-PPV: PCBM 1:4 w/w blend deposited from chlorobenzene.*

All experiments with the reference samples were performed under Ar or N_2. In practice, the samples were stored under inert gas and experiments were carried out inside a quartz cuvette filled with argon or nitrogen and capped with a stopper. The i-V characteristics of the devices were measured on a home-made i-V curve rig originally set-up for dye-sensitised solar cells as described in section 2.9.2.

5.2.2 Transient absorption measurements

Both microsecond and nanosecond transient absorption experiments were performed on the samples with an excitation source repetition rate of 4 Hz. The excitation wavelength was 500 nm (2.48 eV, corresponding to the absorption maximum of MDMO-PPV) and the probe wavelength for the μs kinetics was 940 nm (1.32 eV). The time resolution of the microsecond set-up is of the order of 0.5 μs. Transient absorption spectra were obtained by pumping as described above and probing different wavelengths with the two monochromators on the probe beam. Transient spectra were measured at a 125 μs delay after excitation. Typical traces are the result of ~ 300 averaged shots.

A series of measurements were performed crudely simulating white light illumination as described in section 2.9.2. Suffice to recall here that the incident white light power was of the order of 25 mW cm^{-2} (~¼ of 1 sun)

Nanosecond spectroscopy was carried out both in transmission and reflection modes, as described in section 2.7.3. The excitation wavelength was 500 nm (2.48 eV) and the probe wavelength the 830 nm output (1.49 eV) of the laser diode.

Experiments as a function of the excitation power on both microsecond and nanosecond timescales employed a neutral density (ND) filter wheel in combination with ND filters as described in chapter 2. This allowed attenuation of the energy of the excitation laser pulse by over three orders of magnitude from approximately 80 μJ/pulse x cm^2 to approximately 30 nJ/pulse x cm^2. Accurate power densities were measured with a Molectron EPM-1000 power-meter employing a J-5 pyroelectric head.

5.3 Results

5.3.1 i-V characteristics of the complete cells

The complete solar cells received from Linz were tested in the i-V rig in order to assess their stability. A typical i-V curve for a chlorobenzene deposited device (7 mm^2 active area) is shown in figure 5.7:

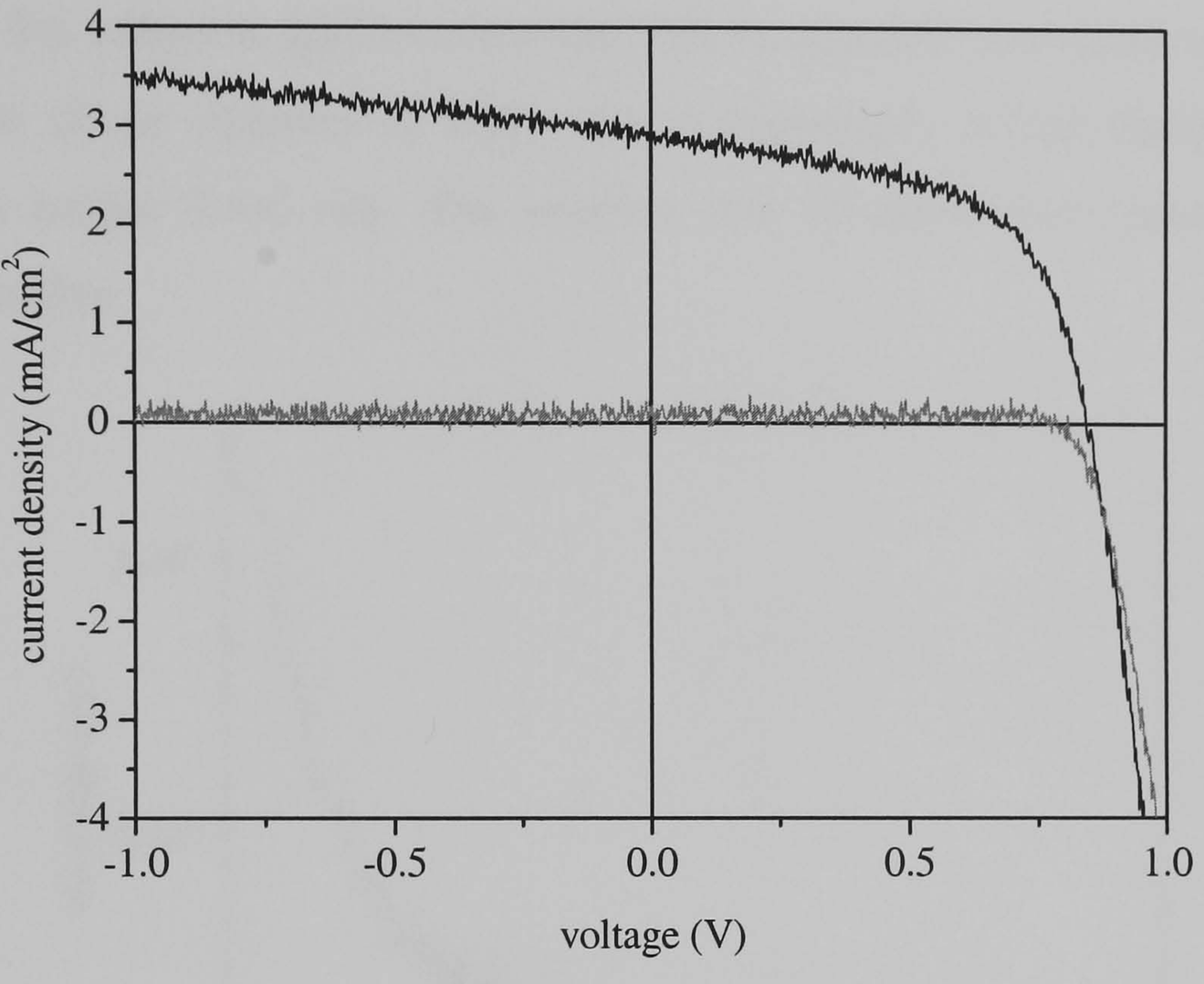

***Figure 5.7**: i-V characteristics of a 7 mm^2 MDMO-PPV : PCBM 1:4 w/w solar cell under 1sun illumination (black) and in the dark (grey). The open circuit voltage is approximately 0.84 V and the short circuit current density of the order of 3 mA / cm^2.*

The open circuit voltage is approximately 0.84 V while the short circuit current density is of the order of 3 mA / cm^2 and an overall efficiency of ~ 1.4%. The slope of the current density in the voltage range between -1 V and +0.5 V is indicative of a small shunt resistance (~ 1 KΩ) indicating short circuits across the device present only under illumination. The origin of this behaviour will be briefly addressed in the discussion once a model for hole dynamics in these systems has been introduced.

5.3.2 Transient absorption kinetics

Preliminary decay kinetics for a complete cell deposited from chlorobenzene obtained by Dr. Sven Södergren prior to this thesis work are shown in Fig. 5.8. The excitation wavelength was 500 nm and the signal was probed at 950 nm. The data illustrate the main issues raised by the study of transient kinetics in plastic solar cells that will be addressed in this chapter.
The nature of the transient species observed will be assessed determining their transient spectrum. The decay appears to have two components: a fast instrument-response limited and a longer lived one. The relative role of these two components will be addressed hereafter.

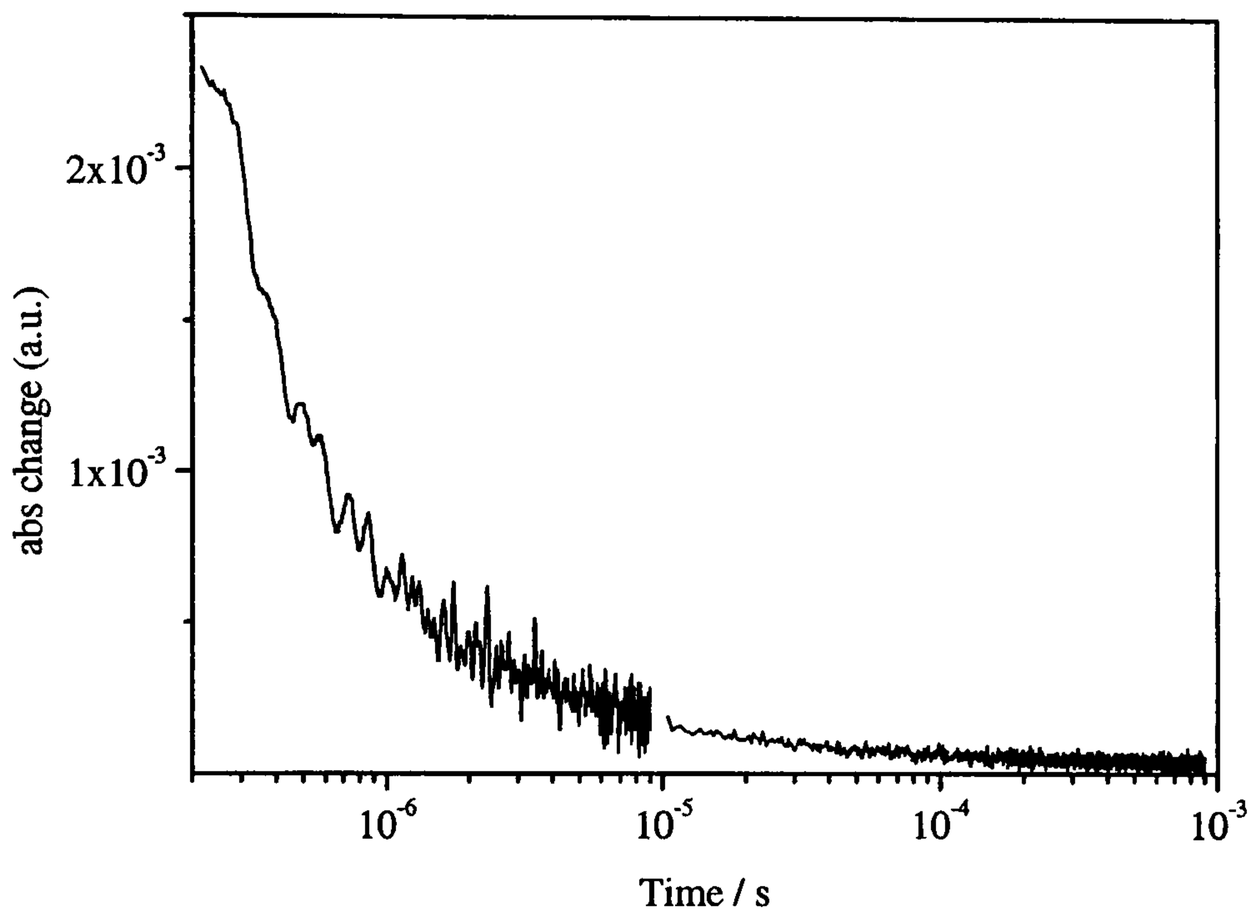

***Figure 5.8**: Microsecond decay kinetics from a MDMO-PPV : PCBM 1:4 w/w device. (transmission mode - complete cell) The excitation wavelength was 500 nm and the signal was probed at 950 nm. The decay is long-lived and extends from the instrument response (several hundreds of nanoseconds) to the millisecond time-domain (data by Dr. Sven Södergren).*

In order to characterise the dynamics of the fast component experiments were performed on the nanosecond set-up. Results of such experiments on a MDMO-PPV : PCBM 1:4 w/w blend are reported in Fig. 5.9. The oscillations in the signal after the initial spike are due to ringing of the amplifiers but the main features are clear. The trace consists of a fast instrument response limited (~20 ns) component and a long-lived absorption that appears almost constant on this time-scale. This is the same component observed in Fig.5.8 and it extends up to approximately 1 ms.

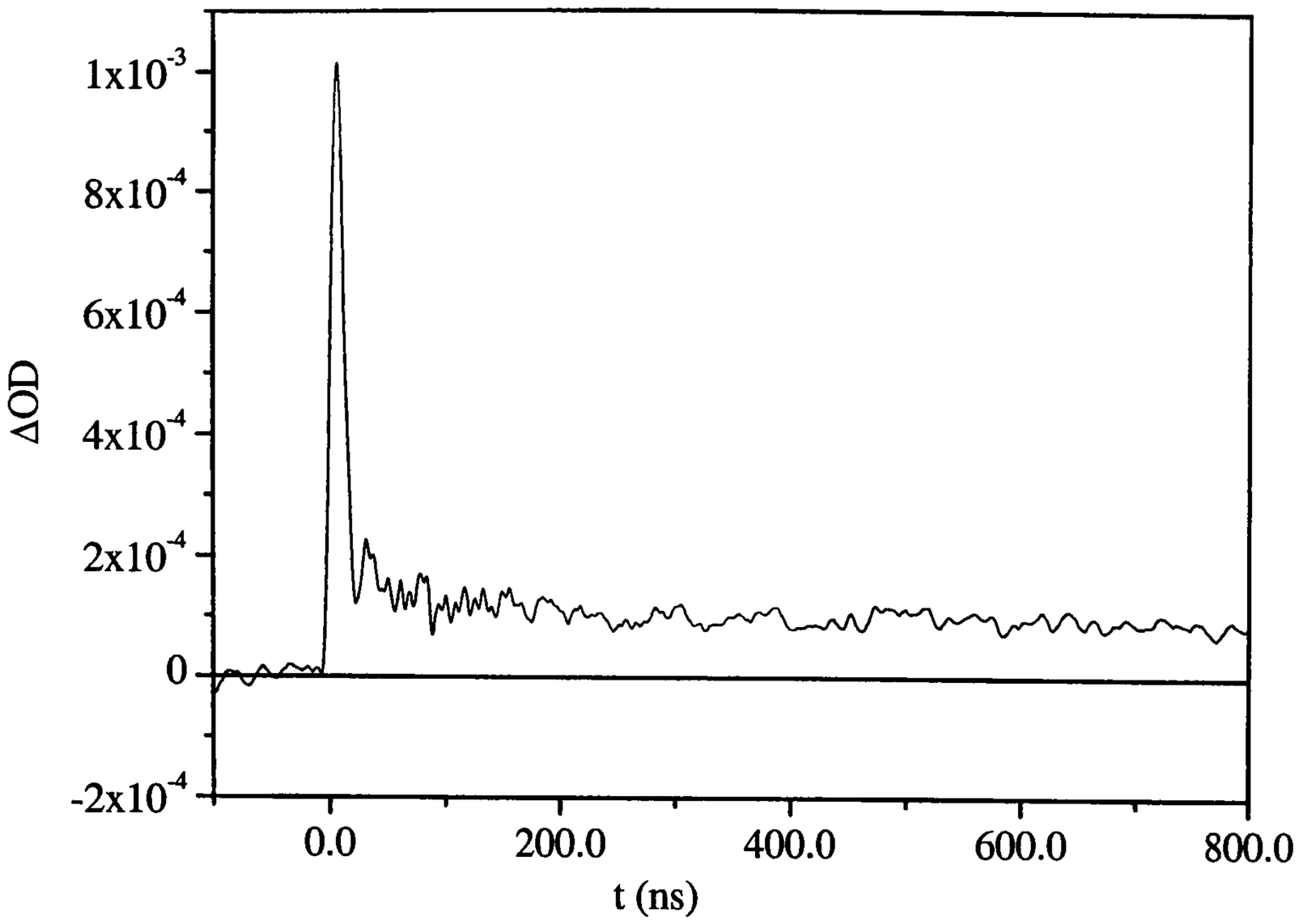

***Figure 5.9**: Nanosecond transient absorption measured on a MDMO-PPV : PCBM 1:4 w/w blend. A fast (instrument response limited) and a longer lived component (almost constant on this timescale) can clearly be distinguished. The excitation intensity was 80 μJ cm^{-2} per pulse.*

5.3.3 Absorption spectrum of the observed transient species

In order to assign spectroscopically the transient species observed in the blends the spectrum of the decaying species was measured. Despite the fact that the emission by MDMO-PPV is quenched by approximately 3 orders of magnitude in blends (Brabec, Sariciftci, and Hummelen 2001) the residual emission is still sizeable compared with the small transient absorption signal. Indeed, satisfactory results were obtained only when the residual emission was carefully subtracted and the data processed with averaging software. These results are shown in the figure 5.10a. As a comparison, figures 5.10b and 5.10c show the frequency domain photoinduced absorption (PIA) spectra of a pristine MDMO-PPV film and the MDMO-PPV/PCBM blend measured in Linz by Dr. Gerald Zerza using 132 Hz modulation at 100 K.

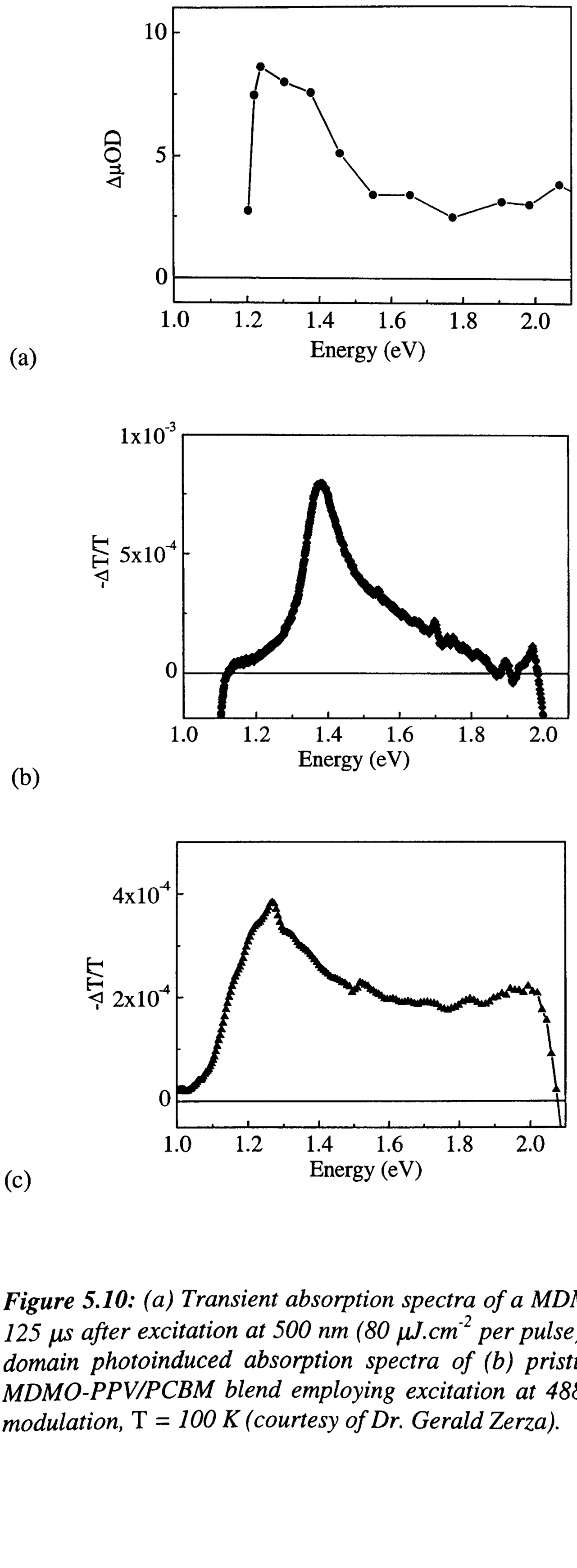

Figure 5.10: *(a) Transient absorption spectra of a MDMO-PPV/PCBM blend obtained 125 μs after excitation at 500 nm (80 μJ.cm^{-2} per pulse),* T = *300 K; (b&c) Frequency domain photoinduced absorption spectra of (b) pristine MDMO-PPV and (c) of a MDMO-PPV/PCBM blend employing excitation at 488 nm with 40 mW and 132 Hz modulation,* T = *100 K (courtesy of Dr. Gerald Zerza).*

In the case of the pristine MDMO-PPV film (figure 5.10 b), the PIA spectrum exhibits a single maximum at 1.38 eV. This photoinduced absorption feature has been previously assigned to absorption of the MDMO-PPV triplet state (Kraabel et al. 1993; Kraabel et al. 1996; Zerza et al. 2000). In contrast, the PIA spectrum for the MDMO-PPV / PCBM blend (figure 5.10c) exhibits a broad absorption increase with two maxima at 1.2 and 2.2 eV previously assigned to MDMO-PPV cations (polarons) (Brabec et al. 1998; Brabec, Cravino, Zerza et al. 2001). Comparison of figure 5.10a with the two PIA spectra in figures 5.10b and 5.10c clearly shows that the transient spectrum observed in time-resolved TAS reported here closely matches that observed in the frequency domain PIA studies of the blend, and is therefore also assigned to positive MDMO-PPV polarons generated by photoinduced electron transfer from MDMO-PPV to PCBM. The data presented in this chapter will therefore be interpreted in terms of MDMO-PPV^+ polaron dynamics.

5.3.4 Excitation power dependence

The excitation power employed in charge recombination studies of dye-sensitised electrodes has been shown to strongly affect the kinetics observed (Haque et al. 2000). Likewise, the excitation pulse power dependence of the fast and the slower components described in section 5.3.2 was investigated with a series of measurements as a function of the laser excitation power, attenuating the pump pulses as described in section 5.2.2.

The results of these experiments on the nanosecond timescale are presented in figure 5.10 for excitation energy pulses ranging between 2 and 80 $\mu J/pulse \bullet cm^2$ (corresponding to 5 to 200 x 10^{12} photons cm^{-2} per pulse). The amplitude of the fast phase is strongly excitation density dependent, reducing in amplitude by at least 20 fold over the range of excitation densities employed, in contrast with the longer timescale data which is relatively insensitive to laser power. At the lowest excitation power employed, (2 $\mu J\ cm^{-2}$ per pulse), the amplitude of the instrument response limited (<20 ns) decay is negligible, and the decay is dominated by the slower timescale dynamics.

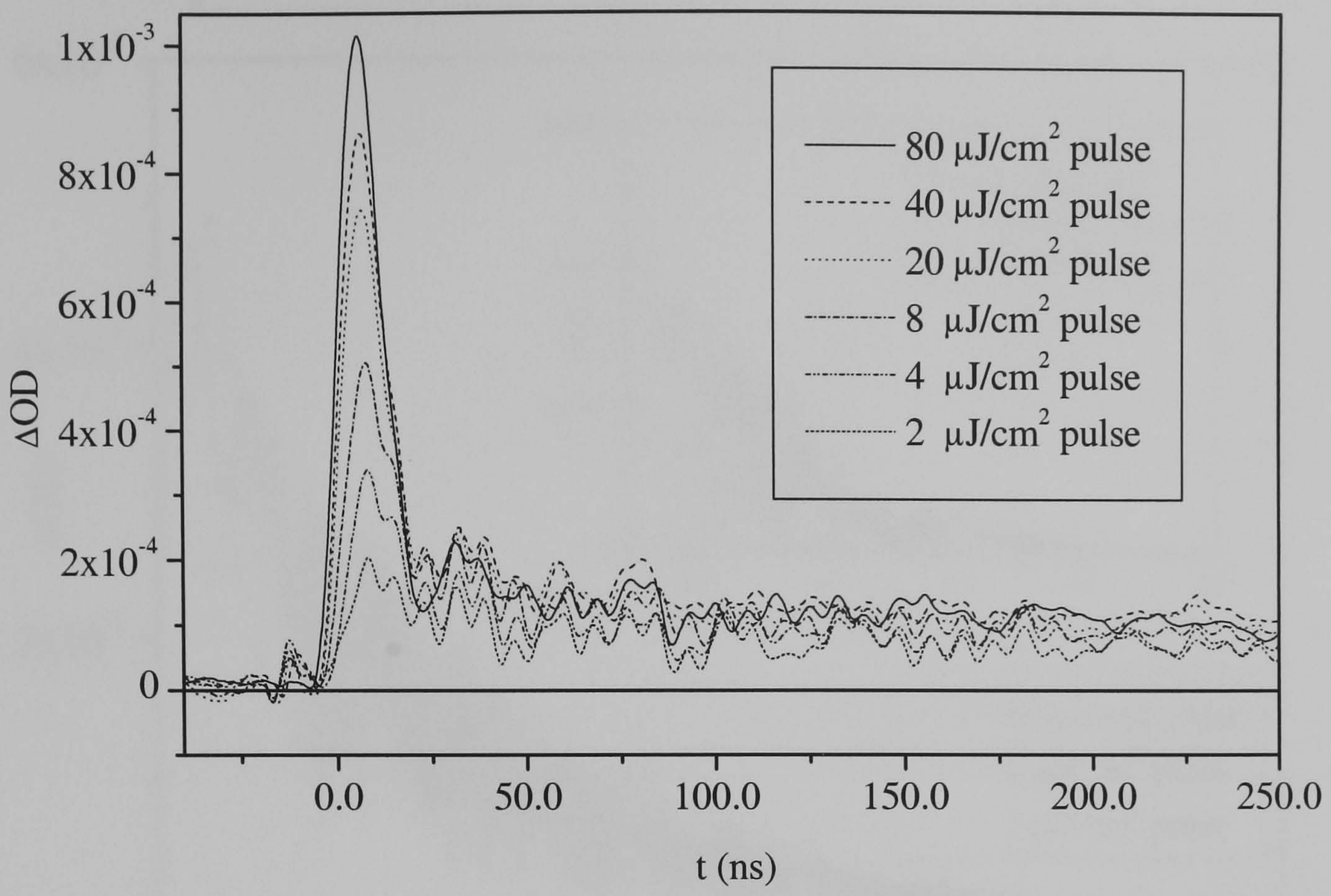

***Figure 5.11**: Nanosecond flash photolysis excitation power dependence. The signal is affected by electronic noise from the amplifiers. It is nevertheless obvious that the fast spike has a strong power dependence while the amplitude of the slower phase is hardly affected by the excitation power.*

The independence of the slow component on the excitation power density is clearer when observed on a microsecond timescale. The amplitude of the transient signal is unchanged within error for an excitation energy range between 80 and 2 μJ cm^{-2} per pulse (figure 5.12). Only when the power is further reduced to 0.22 μJ x cm^{-2} per pulse (0.55 x 10^{12} photons cm^{-2} per pulse) the intensity of the signal is reduced (see inset - figure 5.12) to almost disappear when an excitation power of 30 nJ x cm^{-2} per pulse (0.08 x 10^{12} photons cm^{-2} per pulse) is employed.

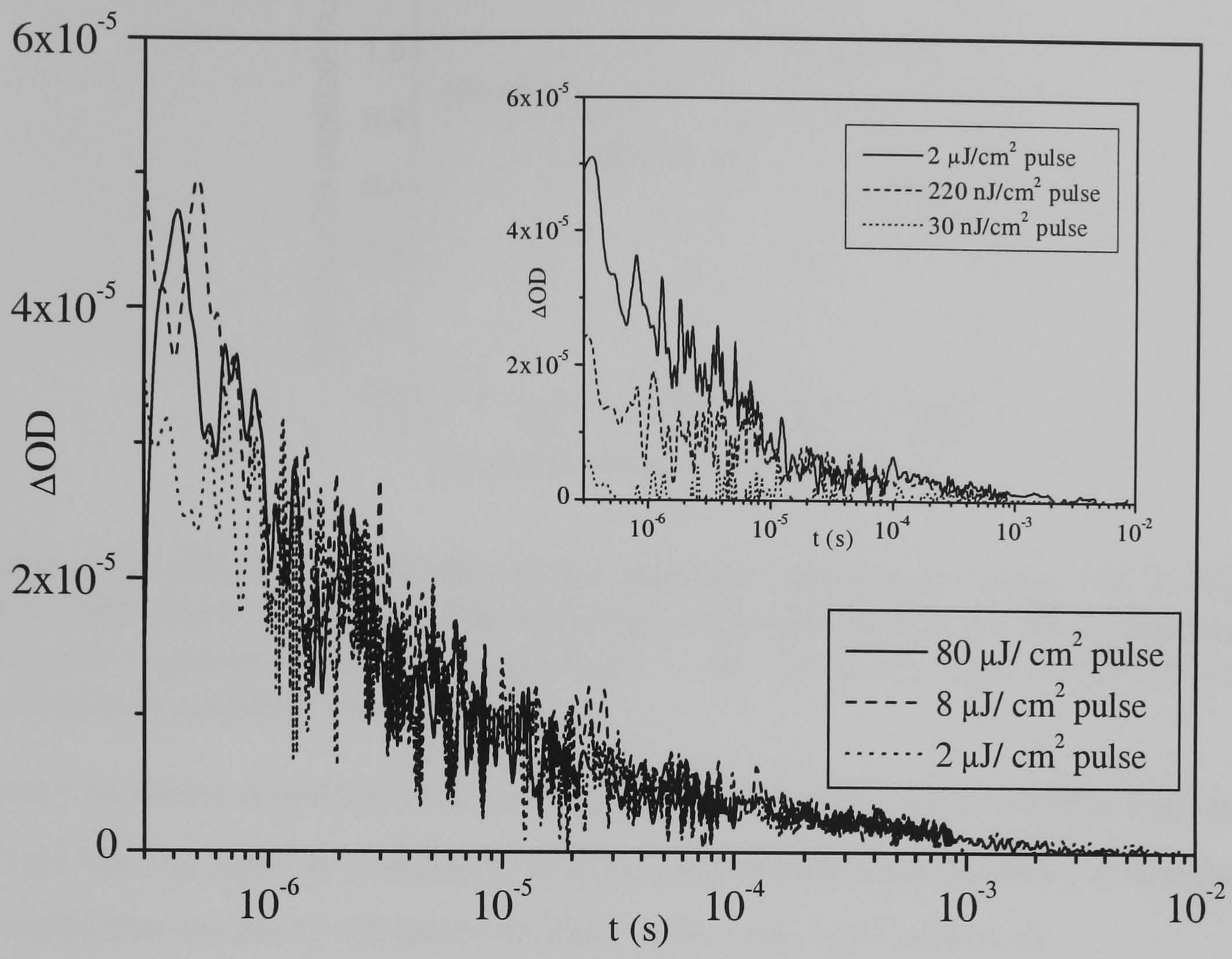

Figure 5.12: *Laser excitation power dependence of kinetics observed pumping MDMO-PPV : PCBM 1:4 w/w from chlorobenzene at 500 nm and probing at 940 nm. The microsecond timescale is reported here. The excitation power ranged between about 80 and 2 μJ/pulse x cm^2. The range is further extended in the inset where 2, 0.22 and 0.03 μJ/pulse x cm^2 are compared.*

A quantitative comparison of the excitation power dependence of the signal at different delays after the excitation pulse is shown in figure 5.13 where the relative amplitude of the two components over three orders of magnitude in excitation power is presented. As shown in the previous figures, at longer time delays the transient signal becomes increasingly less sensitive to the excitation density employed. Indeed, at time delays in the 100-400 μs window, the transient signal is independent of excitation density for values down to < 2 μJ cm^{-2} per pulse (for excitation densities < 1 μJ cm^{-2} per pulse, the amplitude of the signal starts to decrease, as can be seen in figure 5.13. (--■--)).

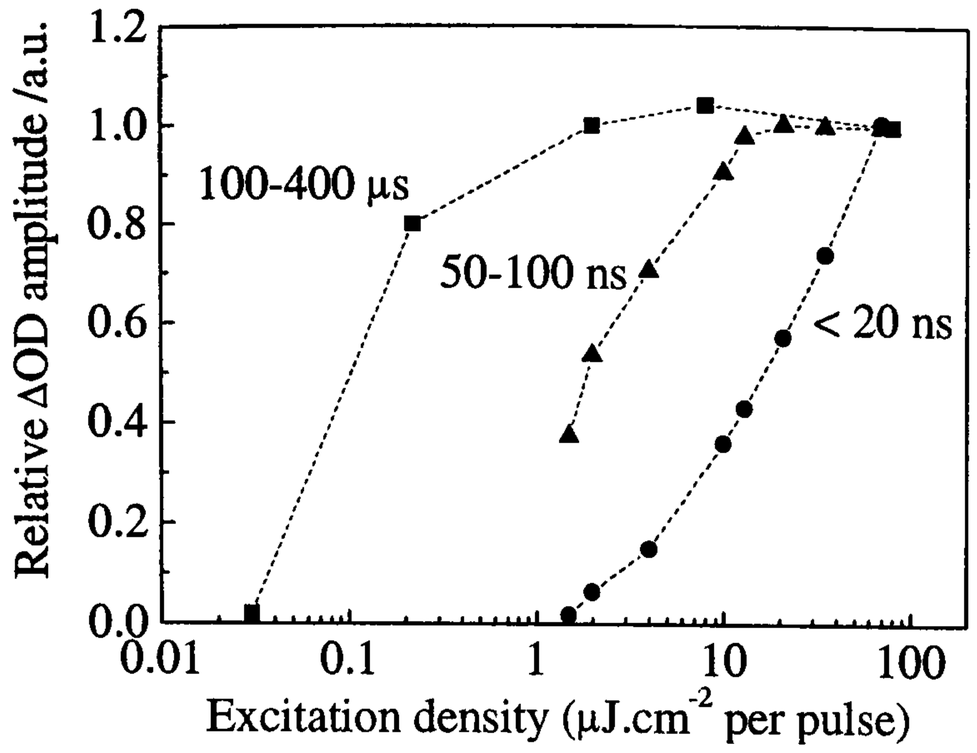

Figure 5.13: *Relative amplitude of the transient absorption signal for a MDMO-PPV/PCBM blend as a function of laser excitation power: (--●--) amplitude of instrument response (~ 20 ns) limited decay; (--▲--) transient signal at 50-100 ns; (--■--) transient signal at 100-400 μs.*

Figure 5.14 shows a combined plot of nano- to millisecond data (excitation 2 μJ/ pulse x cm^2) on log-log axes. It is apparent that the data follow approximately a straight line, indicating that the decay dynamics exhibit a power law type behaviour:

$$\Delta O.D. \propto t^{-\alpha} \qquad (5.2)$$

From the gradient of the decays, $\alpha = 0.4 \pm 0.02$ is obtained. The trace deviates from a power law after 1 ms.

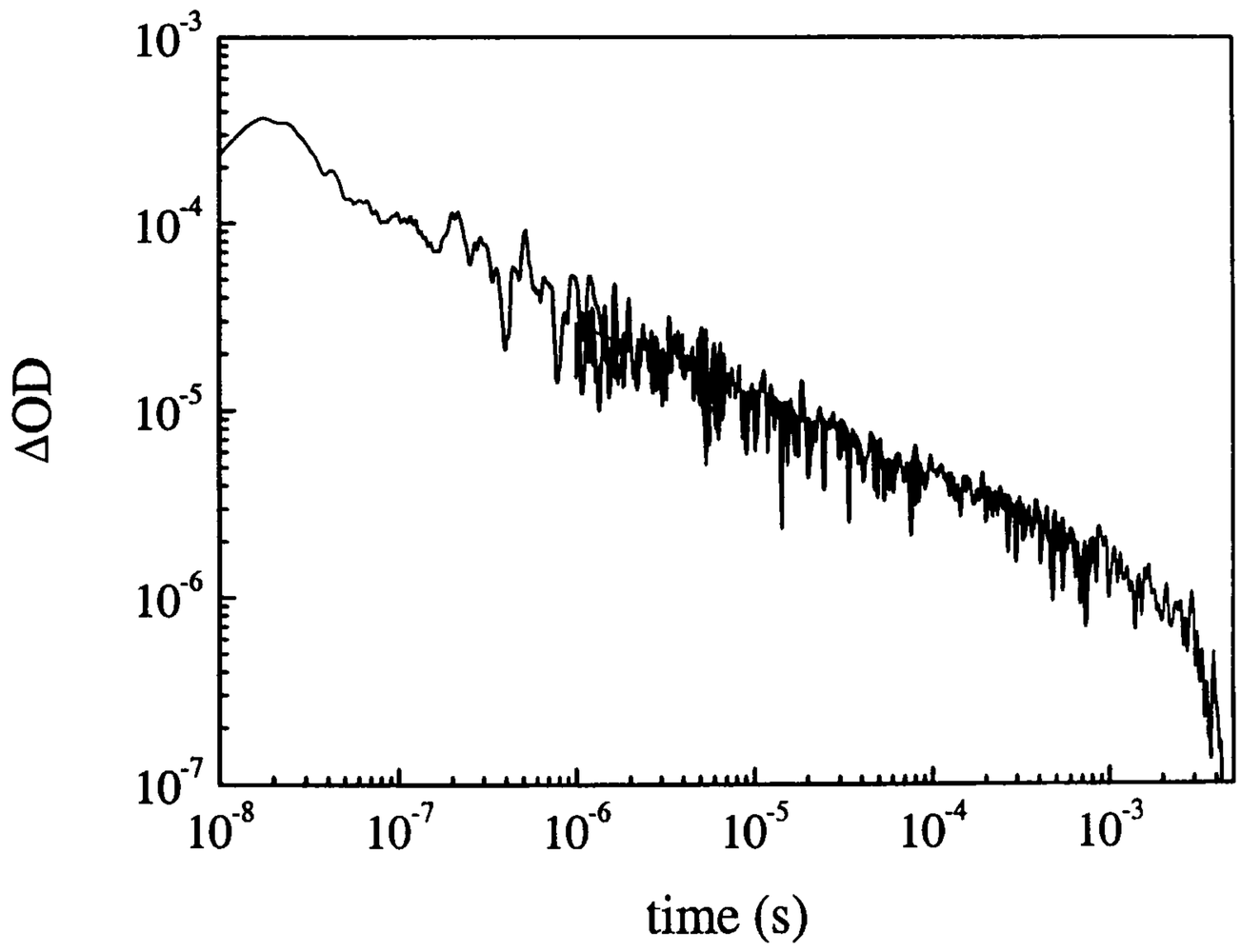

Figure 5.14: *Micro-millisecond decay kinetics at the threshold excitation energy E_{th}.(2 μJ cm^{-2} per pulse) The decay follows a power law with $\alpha = 0.4 \pm 0.02$.*

Possible origins of this feature are being investigated at present by Dr. Ana Flavia Nogueira and are currently attributed to electrons (PCBM anions) dynamically recombining with deeply trapped polarons. It can therefore be concluded from the data shown in figures 5.12 to 5.14 that the decay dynamics of MDMO-PPV positive polarons in photoexcited MDMO-PPV / PCBM heterojunctions can be approximated by two decay phases – a fast (instrument response limited, < 20 ns) phase whose amplitude is dependent upon excitation density and a slow phase that exhibits a power law decay and whose amplitude is independent of excitation density in the range 2 to 80 μJ cm^{-2} per pulse.

5.3.5 Spin casting solvent dependence

As noted in section 5.1.4, blend films deposited from chlorobenzene result in improved morphology and a trebling of the photocurrent of devices and of their overall efficiency. In order to investigate the charge recombination dynamics dependence on sample morphology, microsecond transient absorption measurements were performed on samples cast from either toluene or chlorobenzene. Indistinguishable dynamics are obtained in the two cases as shown in figure 5.15.

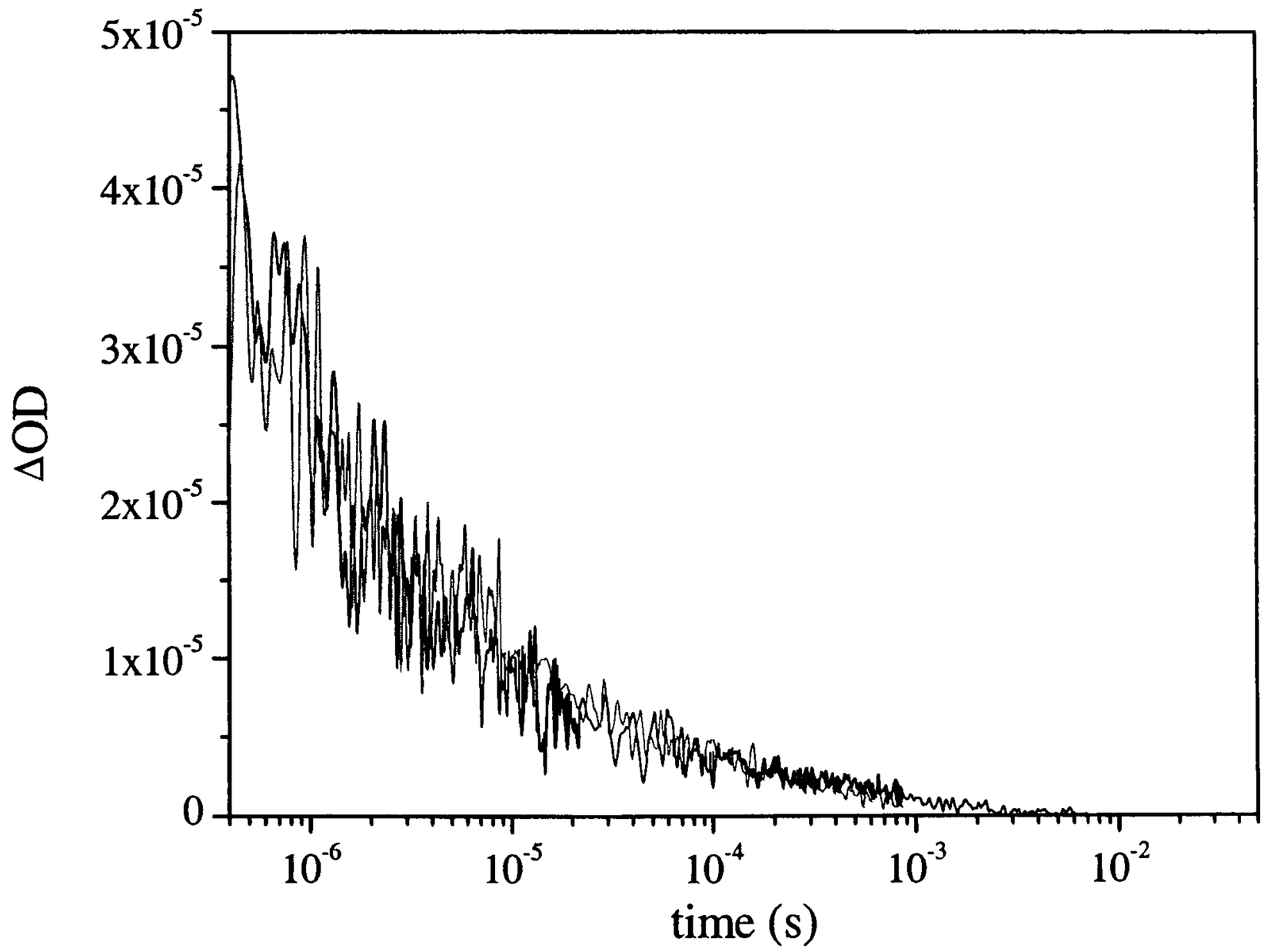

Figure 5.15: *MDMO-PPV polaron dynamics of MDMO-PPV / PCBM heterojunctions cast from chlorobenzene (black) and toluene (grey) solutions. The charge recombination dynamics is indistinguishable in the two samples.*

5.3.6 Experiments under white light illumination

In order to investigate the charge recombination dynamics under conditions more relevant to solar cells operation, experiments were performed on films under CW white light illumination. In figure 5.16 a comparison between polaron recombination kinetics in the dark and under steady-state white light illumination is presented. The latter situation simulates, although crudely (see section 2.9), the open circuit conditions of solar cells. The initial amplitudes of both signals are similar while the decay kinetics observed under background light illumination diverge at approximately 1 μs as the polaron population is depleted under white light illumination The lifetime of the polarons under white light illumination (trace B) is approximately 1-10 μs.

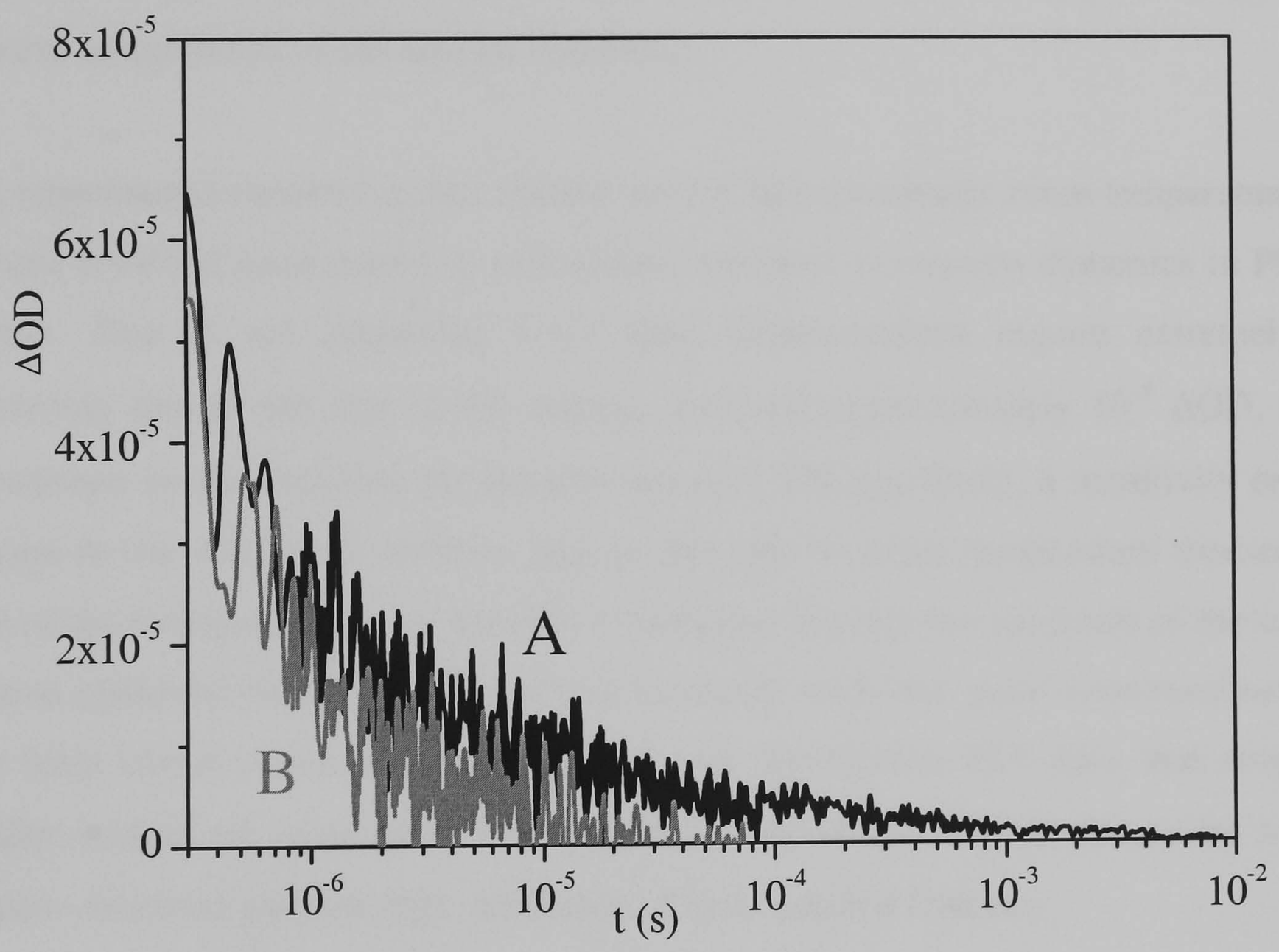

***Figure 5.16**: Comparison between kinetics observed exciting a MDMO-PPV: PCBM 1:4 blend cast from chlorobenzene in the dark (A) and under approximately ¼ of a sun ($I \sim 25\ mW\ cm^{-2}$) power (B, tungsten lamp spectral composition, see chapter 2).*

5.4 Discussion

5.4.1 Assignment of spectrum: polarons

The nature of photoexcitations in conjugated polymers and their blends with electron acceptors have been subject of extensive debate as mentioned earlier. The time resolution of experimental methods that can establish directly the electrical charge of the transient species formed in these materials, such as Light induced Electron Spin Resonance (LESR), is limited to milliseconds. It is hence experimentally impossible to monitor simultaneously the time evolution and electrical charge of species produced on the timescale of the photoinduced charge separation. Therefore, optical spectroscopic methods are the best available tools in characterising charge transfer dynamics of these materials in the femtosecond to millisecond time domain but require unambiguous spectral assignments of the species observed.

The experiments reported in this chapter are the first systematic room temperature study of time-resolved nanosecond to millisecond transient absorption dynamics in PPV-C_{60} blends. This is not surprising since these measurements require extremely high sensitivity due to the size of the signals involved (approximately 10^{-5} ΔOD, in turn determined by the fact that the samples are only 100 nm thick), a sensitivity only few set-ups in the world can achieve. Due to the lack of room temperature time-resolved data in the literature, it is not possible to compare directly the spectrum of the transient species observed here on a millisecond timescale with any prior time-resolved work. The most useful comparison is done with low temperature PIA data, that despite the smaller amount of information they provide on the temporal evolution of the transient species observed, provide high resolution of their spectral features.

As it was shown in Figure 5.10 the spectrum of the transient species observed here is consistent with the spectrum of MDMO-PPV polarons observed in PIA experiments (Kraabel et al. 2000). The dynamics are therefore assigned to photoinduced MDMO-PPV positive polarons recombining with PCBM anions after charge separation. However, only the former absorb at the probe wavelength and their decay following photoinduced charge separation is monitored in the experiments. It is worth stressing that though these materials are essentially two nanometer-scale intertwined networks of

donor and acceptor materials only the MDMO-PPV "network" and its dynamics is visible in the experiments reported here. Although the transient spectrum of the fast (ns) component was not measured due to technical limitations of the experimental setup, assignment to singlet excitons can be ruled out given the ultrafast timescale and close to unity yield of the charge separation step (Brabec, Zerza et al. 2001). It is therefore reasonable to attribute the fast phase observed above to an excess of polarons formed when higher excitation intensities are employed.

5.4.2 Power law kinetics and excitation power dependence

The MDMO-PPV polarons decay kinetics can be approximated by two decay components: – a fast (instrument response limited, < 20 ns) one, whose amplitude depends on the excitation density, and a slow component exhibiting a power law decay and whose amplitude is independent of excitation density in the range 2 to 80 μJ cm^{-2} per pulse (5 to 200 x 10^{12} photons cm^{-2} per pulse). The lower end of the range clearly represents a threshold in excitation energy density E_{th}. For excitation energy densities smaller than E_{th} the amplitude of the micro- to milli-second time scale dynamics is excitation power dependent as shown in the inset of figure 5.12. The power law type recombination dynamics observed for time delays > 300 ns are indicative of localised carriers, as previously suggested by Meskers et al. (Meskers et al. 2000). These dynamics are consistent with pico- and nanosecond relaxation of the charge carriers to the lowest energy states of the inhomogeneously broadened density of states typical of these materials, below the mobility edge of the holes (polarons).

A perhaps simplistic but useful description of the energy levels available to MDMO-PPV $^{+}$ radicals is proposed in figure 5.17. The absence of a regular lattice in these samples, that can be thought of as solid solutions of donor and acceptor molecules, gives rise to a certain amount of localised states at lower energies. At higher energies the density of the energy levels increases and their energy spacing is reduced to the point of presenting the characteristics of the valence band. These "localised states" could in a sense be seen as traps.

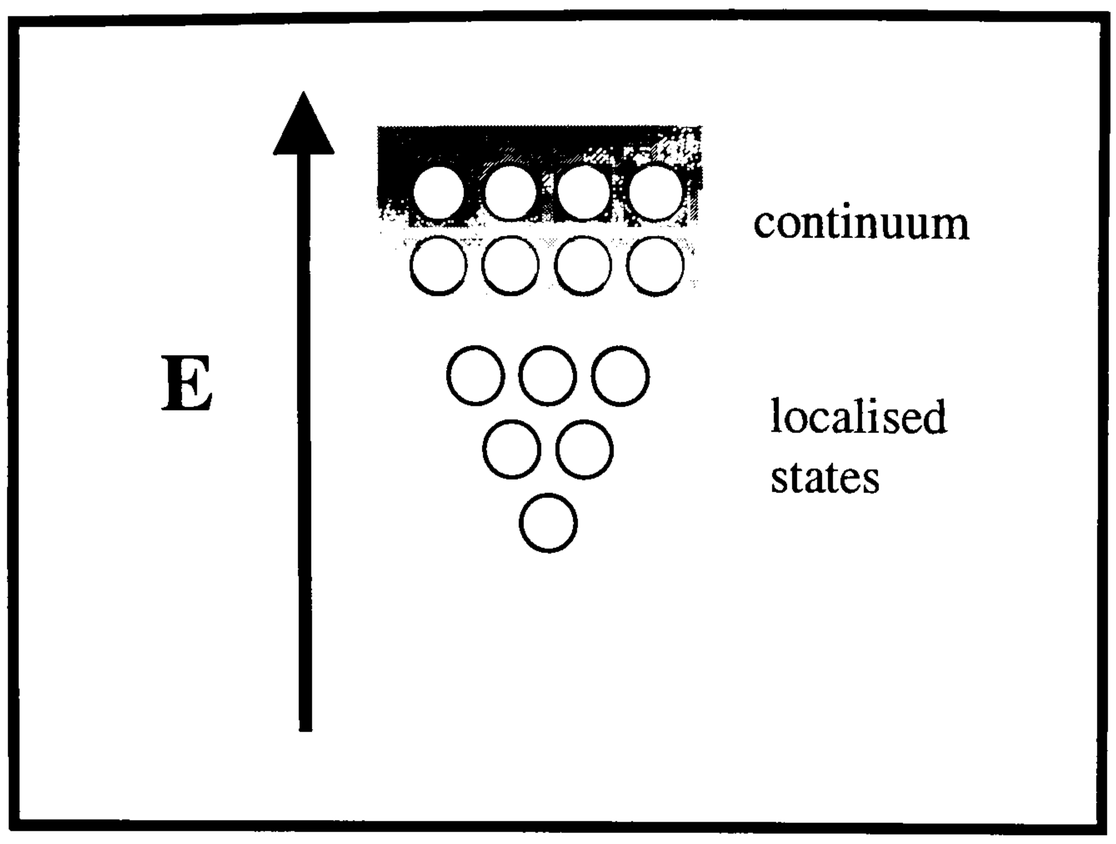

Figure 5.17: *Schematic representation of the energy levels available to photogenerated polarons in MDMO-PPV / PCBM blends. A certain amount of localised states (inhomogeneous broadening) lie at the lowest energy extending into the bandgap of MDMO-PPV, while at higher energy a thicker manifold of states are present.*

Figure 5.17 has no pretence of being accurate in terms of absolute and relative energy levels or density of states, it only serves to illustrate the point that a tail of localised states are available to MDMO-PPV positive polarons. In a conventional band diagram this tail of localised states would extend above the valence band, into the bandgap.

Three regimes can therefore be distinguished in figure 5.18.

I) For excitation energies below 2 μJ cm^{-2} per pulse only some of the localised lower energy states are filled giving rise to the long-lived transient absorption signal (a, see inset of figure 5.12).

II) When the excitation density reaches the 2 μJ cm^{-2} per pulse threshold (~ 5 10^{12} photons cm^{-2} per pulse) the localised states are full (b, see also figure 5.12) and their recombination dynamics with $PCBM^-$ anions follows the power law shown in figure 5.14.

III) When the photon density threshold is exceeded the additional polarons formed occupy the band-like upper part of the diagram where they are relatively more mobile due to the manifold of closely spaced energy levels available to them (c). The instrument response limited (<20 ns) excitation power dependent component observed for excitation densities exceeding 2 μJ cm^{-2} per pulse arises from the faster recombination dynamics of these more mobile radicals. In the sense outlined above, E_{th} corresponds to a "mobility edge" for the photogenerated positive charge carriers (polarons).

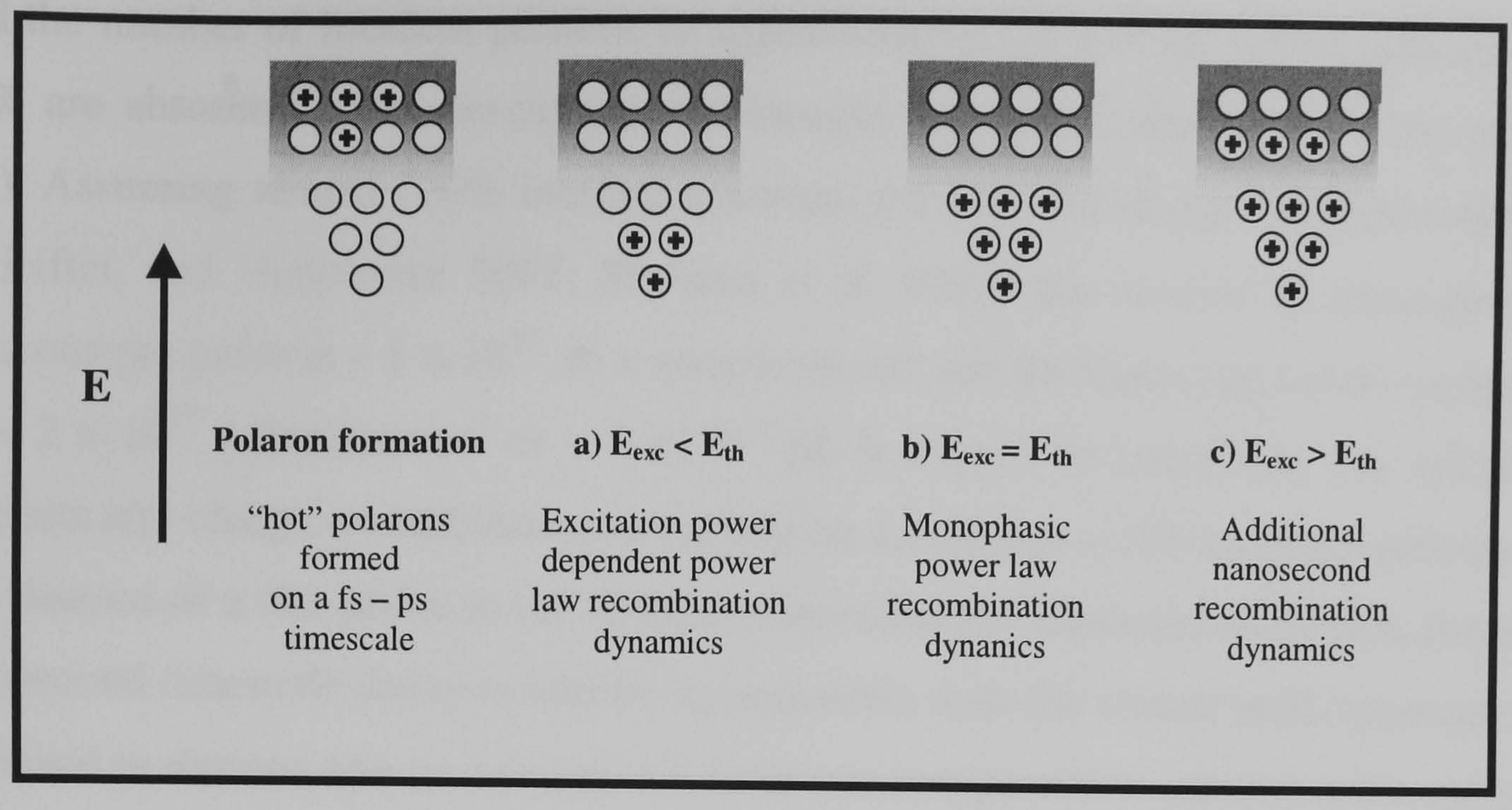

Figure 5.18: *Photoinduced population of the energy level available to MDMO-PPV polarons (as of figure 5.17) under different excitation density levels. Excitation density levels smaller (a), comparable (b) and exceeding (c) an excitation energy threshold E_{th} characteristic of the material.*

Within this framework the picosecond to nanosecond recombination rate reported in the literature from TAS measurements can perhaps be rationalised in terms of fast recombination induced by the high photon density employed in such experiments - well in excess of photon densities typical of solar illumination levels relevant to device functioning. An example of such measurements is reported by Meskers et al. who proposed a model for biphasic recombination dynamics observed in poly(3-hexylthiophene) (P3HT) / PCBM at 80 K. A fast (~ 30 ns) decay phase was assigned to geminate recombination of the photogenerated charge carriers, and a slow phase to localised charge carriers which had escaped the initially formed geminate pairs (Meskers et al. 2000). This work does not however report the excitation intensity of the nanosecond measurements (the millisecond PIA employed ~ 0.8 W/cm^2 (!)). The excitation density dependence of the room temperature data reported here is not consistent with this model, as the proportion of geminate recombination (i.e. the relative amplitude of the fast and slow phases) would be expected to be independent of laser power, contrary to the results presented here.

The threshold excitation density (E_{th}) of 2 μJ cm^{-2} per pulse of 500 nm (2.48 eV) photons correspond to ~ 5 10^{12} photons. The size of the pump beam is about 1 cm^2, and considering that only about a quarter of that surface is being probed, the area of the sample studied (assuming a thickness of 100 nm) is 0.25 cm^2, its volume 2.5 10^{-6} cm^3

and the number of incident photons is approximately 1.2 10^{12} of which approximately 50% are absorbed (at the excitation wavelength the optical density is of the order of 0.3). Assuming almost 100% internal quantum yield for the charge separation (Brabec, Sariciftci, and Hummelen 2001; Shaheen et al. 2001) the amount of photogenerated polarons per pulse is ~ 1 x 10^{12}. In a sample of 100 nm thickness this value corresponds to ~ 2 x 10^{17} polarons cm^{-3} or ~ 3 x 10^{-4} M. It should be noted that this calculation neglects any charge recombination occurring on timescales <<20 ns, in accordance with the absence of a fast phase in the decays observed at the threshold excitation density. A picosecond timescale decay would be incompatible with the almost unity quantum yield achieved in devices and no nanosecond timescale component is present at the excitation energy levels considered here. The concentration of MDMO-PPV monomer units in a 1:4 w/w blend can be estimated to be ≈ 0.7 M (assuming d = 1 g/l as a first approximation for the density of the blend). The threshold energy E_{th} therefore corresponds to approximately one photogenerated polaron generated per two thousand MDMO-PPV monomer units.

It is perhaps remarkable that no literature data exist for the extinction coefficient (optical cross section in physicists' terms) of positively charged MDMO-PPV polarons. From the size of the transient absorption signal an estimate for its value at the absorption maximum can be calculated subject to some assumptions. At the threshold excitation energy E_{th} the fast decay phase is absent and the ΔOD at 25 ns (2 x 10^{-4}) can be used to obtain an estimate for the MDMO-PPV$^+$ cations extinction coefficient using Lambert-Beer law as follows:

$$\varepsilon = \Delta OD / lc = \sim 40000\ M^{-1}\ cm^{-1} \qquad (5.3)$$

This value represents a lower limit for the extinction coefficient of the MDMO-PPV polarons at 940 nm (1.32 eV).

Following from this analysis, the fast, <20 ns decay phase observed for laser intensities > 2 μJ cm^{-2} per pulse is assigned to relatively mobile polarons present when the density of photogenerated polarons exceeds the density of localised states below the PPV's mobility edge. The use of the term "mobility edge" might be improper in this context. It is used solely to indicate the energy level that separates the two regimes for carrier mobility in the sense outline below. Below the "mobility edge" the polarons have at their disposal discrete states and can move from one to the other through thermally

activated excitation to the higher manifold whereas above the mobility edge there is a continuum of closely spaced energy levels favouring high carrier mobilities.

5.4.3 Model: Shklovskii vs. CTRW

The data presented in this chapter is insufficient in order to develop a refined model for the charge recombination dynamics of PPV polarons in these blends. For example, experiments as a function of temperature would be advisable in order to test the compatibility of any such model with experimental observations. Dr. Ana Flavia Nogueira is indeed carrying out these experiments at present in order to gain a better insight into the mechanism of the charge recombination step. Given these limitations, an approach to theoretical modelling of the charge recombination dynamics can at least be outlined. Schultz et al. (Schultz et al. 2001) employed a model originally devised by Shklovskii and co-workers for disordered semiconductors (Shklovskii, Fritzsche, and Baranovskii 1989) in order to explain long lived charged states they observed in MDMO-PPV / PCBM blends in the 10 to 40 K temperature range employing LESR (Light Induced Electron Resonance Spectroscopy). The Skhlovskii model was however originally devised for low temperatures and neglects thermal excitation (T = 0 K). It is essentially a geometrical model considering a distribution of distances between charged particles in a disordered matrix.

The basic assumption of the model is that spatially close carriers have a much higher recombination rate than distant carriers. The recombination rate can be written as

$$\nu(R) = \nu_0 \exp\left(-\frac{2R}{a}\right) \tag{5.4}$$

where $\nu(R)$ describes the recombination rate of any electron and hole that are separated by a distance R, ν_0 is a recombination constant that may be interpreted as an attempt to recombine frequency and a is an effective localisation radius.

After some time t, spatially close carriers will have recombined and the nearest neighbour distance R(t) increases as:

$$R(t) = \frac{a}{2}\ln\left(\frac{t}{\tau_0}\right) \tag{5.5}$$

where τ_0 is ν_0^{-1}.

When the photoexcitation is turned off at some time t_0=0 (corresponding to a charge carrier concentration n_0), following geminate recombination at the earliest times, the

remaining concentration of charge carriers n(t) can be written as:

$$n(R) = \frac{n_1}{1 + \frac{4\pi}{3} n_1 (R^3 - R_1^3)} \qquad (5.6)$$

where the time dependence is contained in R=R(t) given by the previous equation with $t>t_1$. The time dependence of the residual carrier concentration does not follow a simple exponential decay, but shows a more logarithmic time behaviour. At long times, i.e. large Rs, the amount of residual carriers is independent of the initial carrier density n_0. It must however be stressed that this model is only valid at zero Kelvin and unless it is modified to allow for a temperature dependence it is unlikely to be useful in explaining the data presented here.

On the other hand, a continuous time random walk (CTRW) model along the lines of the one employed by Nelson to describe charge recombination dynamics in dye sensitised electrodes (see chapter 3) could also help in understanding the PPV polaron dynamics. Within an exponential distribution of localised state energies, CTRW modelling of charged pairs predicts a stretched exponential decay when the concentration of one of the recombining species largely exceeds the other (as it was seen in chapter 3). However, it results in a power law decay when the initial concentrations are equal, a condition satisfied in the present case where photoinduced electron transfer results in formation of MDMO-PPV^+ / $PCBM^-$ pairs.

In the implementation of the model to this system, charge pairs are generated at random with immobile PCBM anions and MDMO-PPV polarons which are allowed to hop to a nearest neighbour site by thermal activation over a barrier. Direct tunnelling without activation to a "band" (schematically represented by the upper part in figure 5.17) is forbidden. An exponential density of states (DOS) is available to the positive polarons a fraction ϕ of which represents the localized states schematically shown in the lower part of figure 5.17. If we define the initial concentration of positive and negative charges as $[p_0]$ and $[n_0]$, such an exponential DOS generates a waiting time distribution for carrier hopping of the form $\chi(t) \sim t^{-1-\alpha}$ and leads to $[p_0] \propto e^{-Bnt^{\alpha}}$ when $[n_0] >> [p_0]$ but $[p_0] \propto t^{-\alpha}$ if $[n_0] = [p_0]$, i.e. the initial concentrations of opposite charges are equal (J. Nelson, 2002 personal communication).

The lower energy tail in the density of states described by an exponential differs from the density of polaron states frequently used when considering charge transport in these materials that has often been assumed to have a gaussian shape, with a typical width of approximately 100 meV (Gailberger and Bässler 1991).

Preliminary results of CTRW simulations carried out by Dr. Jenny Nelson on a set of data including some of those presented in this chapter integrated by measurements as a function of temperature (carried out by Dr. Ana Flavia Nogueira) are quite encouraging (Nelson 2002) and are being written up for publication.

5.4.4 Blend morphology and localised polaron density

MDMO-PPV polaron dynamics in blends deposited from both toluene and chlorobenzene appear indistinguishable. Since PCBM and its anion do not absorb at the wavelength investigated, all the experiments reported in this chapter effectively only monitor the dynamics of the MDMO-PPV component of the heterojunction. The different degree of phase segregation shown by AFM measurements is not important for the dynamics observed here as the presence of larger fullerene clusters in the blend cast from toluene results in poorer charge collection at the electrodes affecting the device performance but not the MDMO-PPV polaron dynamics. Furthermore, the hole mobility in pristine MDMO-PPV is approximately one order-of-magnitude greater in films spin-coated from chlorobenzene as compared to toluene cast ones (Geens et al. 2000). It can therefore be concluded that what differentiates films deposited from either chlorobenzene or toluene is the charge transport dynamics and not the charge recombination dynamics determined by the PPV rich regions.

5.4.5 Implications for cell function

It was suggested above that the density of localised states below the mobility edge of the composites is of the order of 10^{17} cm^{-3}. The recombination dynamics are faster under white light illumination. This observation can be rationalised as follows:
A steady population of polarons is present under white light illumination occupying the lower energy states below the mobility edge of the holes in the composite. In other words, the bottom of the tail of states lying under the "mobility edge" is continuosly occupied by polarons generated by the background illumination. Additional polarons

generated by the pulsed excitation occupy shallower localised states and their charge recombination rate is therefore faster. The slow tail of the recombination dynamics, corresponding to detrapping from the lowest energy localised states is not observed. The concept is schematically represented in Fig. 5.19. The figure is quantitatively misleading in the sense that the steady state of polarons created by white light (indicated by the gray positive charges) has been estimated as not exceeding 10 % of the available states (~ 2 x 10^{16} cm^{-3}) as outlined below.

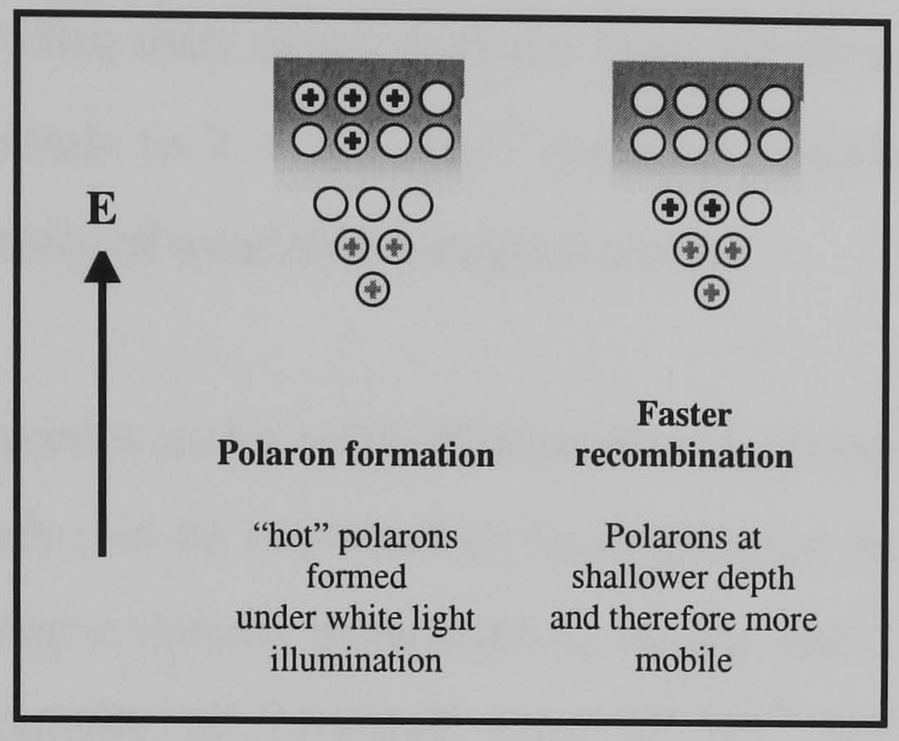

Figure 5.19: *Pictorial representation of photoinduced polaron dynamics in a blend under steady-state white light background illumination picoseconds and milliseconds after pulsed excitation. A steady state of polarons occupying the lower localised states is present at all times and the tail of states available to polarons produced by the laser pulse is effectively cut off resulting in faster recombination of the polarons whose energy is closer to the continuum of states.*

The current density obtained in a cell is ~ 3 mA/ cm^2 as shown in figure 5.7. Given the close to unity external quantum yield in these devices this corresponds to 2 x 10^{16} s^{-1} carriers reaching the external circuit under 1 sun. In a 100 nm thick device this corresponds to a carrier generation rate of 2 x 10^{21} cm^{-3} s^{-1}. Under ¼ of a Sun illumination their number is approximately a quarter (5 x 10^{20} s^{-1}). The lifetime of polarons under white light was estimated earlier at 1-10 μs.

In the simplest possible case the number of charges leaving the device is given by:

$$\frac{dp}{dt} = G - \frac{p}{\tau} \qquad (5.7)$$

where G is the charge photogeneration rate, p is the polaron concentration and τ is their lifetime. In the absence of external contacts, as in the experiments reported here, no charges leave the active film and a steady state population of polarons is generated under white light.

$\frac{dp}{dt} = 0 = G - \frac{p_{ss}}{\tau}$ where p_{ss} is the steady-state concentration of polarons.

Therefore $p_{ss} = G * \tau$. (5.8)

G was calculated above as ~ 5 x 10^{20} cm^{-3} s^{-1} and the polaron lifetime under white light illumination was estimated in figure 5.16 as ~ 1-10 μs resulting in a steady-state polaron concentration of 0.5-5 x 10^{15} cm^{-3}.

Alternatively, the concentration of polarons under white light can be estimated from figure 5.16 at the time when their decay deviates from the dynamics in the dark. ΔOD (1 μs) ~ 2 x 10^{-5} corresponds to 2 x 10^{16} cm^{-3} polarons. Neither of these two numbers exceeds 10% of the density of available localised states.

The recombination dynamics under solar illumination in photovoltaic devices fabricated from polymer/C_{60} blends can be expected to be dominated by the slower decay phase reported here as the polaron density generated by steady state solar illumination is well below the estimated density of localised state (2 10^{17} cm^{-3}). In particular, carrier collection by electrodes must be faster than thermal relaxation into trap states.

The i-V characteristics of a device was shown in figure 5.7. It was noted there that the shunt resistance appears to decrease considerably under illumination. A qualitative explanation in terms of the model outlined above could rationalise the light-dependent shunt resistance. The partial occupation of the tail of states by the steady state of polarons present under illumination leads to higher mobilities therefore facilitating shorts across the active layer.

To understand the photovoltaic function of these materials the competition between charge collection, trapping and recombination needs to be elucidated. The experiments presented here are a step in this direction. Experiments in complete devices building on the results presented here are currently underway but are beyond the scope of this thesis.

5.5 Conclusions

The results shown and discussed in this chapter can be summarised as follows:

1) The recombination dynamics are primarily controlled by the dynamics of MDMO-PPV$^+$ polarons in the bulk of the MDMO-PPV matrix. The MDMO-PPV$^+$ dynamics are identical whether the blends are deposited from chlorobenzene or toluene. The higher efficiency of devices obtained when spin casting solutions in the former solvent is therefore ascribed to better mobility of the carriers as shown by FET mobility measurements.

2) A threshold E_{th} is found delimiting two different regimes. The threshold energy corresponds to a density of localised states (or shallow traps) of ~ 2 x 10^{17} cm^{-3} associated with a "mobility edge" for positive polarons. Below E_{th} the decay kinetics are dominated by trapping and detrapping of positive polarons and result in a power law type behaviour. Above E_{th} the decay kinetics include a fast (<20 ns) excitation power dependent phase attributed to recombination of polarons exceeding the "mobility edge".

3) Under white light background illumination the charge recombination reaction is faster consistent with a steady state of photogenerated polarons occupying the lower part of the tail distribution of states below the mobility edge of the samples.

CHAPTER 6

CONCLUSIONS AND FURTHER WORK

6. CONCLUSIONS AND FURTHER WORK

This thesis set out to study the regeneration of dye molecules by iodide following photoinduced electron injection. In chapter 3 it was demonstrated in the clearest way yet that the regeneration reaction proceeds via formation of the I_2^- intermediate thereby elucidating the reaction mechanism. I_2^- is found to be a long-lived species decaying by dismutation and negligible reaction with electrons. In contrast to the charge recombination reaction k_{CR1} the regeneration reaction was found to be insensitive to electron density on the semiconductor ruling out direct reaction between electrons and I_2^-. The iodide reaction is found to be first-order in iodide concentration and the formation of Ru-I intermediates is ruled out in the systems studied here.

The kinetic competition between dye regeneration by iodide and photoinjected electrons is observed experimentally and a lower limit for iodide concentration in working cells is determined. The rate of the regeneration reaction by iodide is proven to be independent of the electron density in the titanium dioxide. These results allow further testing of the model developed by Nelson for charge motion within the semiconductor particles.

The k_{CR1} and k_{RG} behaviour determined in three-electrode studies fits well with full device data e.g. RG is independent of electron density but dependent on viscosity while CR1 is dependent on applied bias. The injection yield in a complete cell is found to be independent of the bias level between open circuit and short circuit conditions. Results presented here are consistent with the reaction between injected electrons and tri-iodide being the main loss channel in best cells. The reaction rates are in qualitative agreeement with the viscosity of the solvent employed although somewhat lower than inversely proportional. The addition of a common additive, 4-t-butyl-pyridine is found to considerably slow down k_{CR1}.

The empirical observation that nitrile based cells are the most efficient to date is confirmed experimentally. The output voltage can be limited by kinetic competition in cells employing viscous solvents (e.g. propylene carbonate). A correlation between spectroscopical data and the diode behaviour of acetonitrile cells was found although the inability to prevent warming up of propylene carbonate cells prevented the results from being extended to these cells.

In the case of MDMO-PPV: PCBM blends the first room temperature study of charge recombination dynamics in polymer photovoltaics materials has been achieved. A solid spectral assignment of the observed transient to PPV polarons is made. This indicates that the recombination dynamics observed is dominated by PPV moieties.

Surprisingly, two processes on different time scales are distinguished and assigned to rapid and slow recombination times above and below the equivalent of a "mobility edge" that is quantified. A simple model consistent with these and subsequent observations is suggested. Similar recombination dynamics on morphologically differing materials is proven and the better performance obtained from blends deposited from chlorobenzene is attributed to increased charge mobility. The behaviour under white light illumination is explained in this conceptual framework and a link to CTRW modelling is mentioned. Finally, the recombination dynamics relevant to cell function are identified in the slow dynamics below the "mobility edge".

Suggestions for further work include extension of the iodide kinetics to a series of dyes with differing ΔG for the dye regeneration reaction step. It would be worth repeating the iodide kinetics measurements on recently achieved coated semiconductors. Furthermore, whether I_2^- formation involves a prior intermediate remains an unanswered question.

It would be instructive for the general picture drawn here to establish systematically the effect of t-butyl-pyridine on k_{RG} in three electrode experiments. A direct consequence of the results presented in chapter 4 is that propylene carbonate cells i-V characterisation should be repeated in temperature controlled conditions.

Last but not least the approach employed in chapter 5 to study charge recombination in polymer photovoltaic materials could be extended to complete devices. It should be possible to experimentally observe the competition between charge recombination and charge migration to the electrodes.

APPENDIX : STANDARD SOLAR CELLS EFFICIENCIES

The power convertion efficiency η of solar cells depends on the intensity and the spectral composition of the incident light. In order to compare solar cells efficiencies, solar radiation standards have been defined and the most widely accepted is the AM 1.5 spectrum. The sun emission is that of a black body at 5762 K. Outside the earth's atmosphere the solar power density is 1353 W/m^2 known as the solar constant and its spectral composition is referred to as AM 0. AM 1.5 is the spectral composition of solar light hitting the ground at an angle of 48.2° with the zenith and takes into account light scattering and absorption by atmospheric gases (mainly CO_2 and water) in the form of the Air Mass the sun rays travel through (EU regulations, 1980). In fact under such condition the solar power density reaching the earth's surface is 827 W/m^2 but it has been agreed to take as a standard a light flux with the AM 1.5 spectral composition and a power density of 1000 W/m^2 (100 mW/cm^2) at 25°C. The AM 1.5 spectral composition can be approached by commercial solar simulators. The National Renewable Energy Labs (NREL), in Boulder, Colorado and the Fraunhofer Institute for Solar Energy Systems in Freiburg, Germany among others, provide certified efficiencies.

Quantum efficiencies indicate the percentage of incident photons resulting in electrons collected in an external circuit (external quantum efficiency, EQE also often referred to as IPCE). The internal quantum efficiency (IQE or alternatively APCE) is obtained if only the fraction of photons absorbed is considered:

$$IQE(\lambda) = \frac{EQE(\lambda)}{1 - R(\lambda) - T(\lambda)} \qquad (A.1)$$

where R (λ) and T(λ) are the fraction of reflected and transmitted light, respectively.

LIST OF PUBLICATIONS:

J.P. Collin, J.O. Dalbavie, V. Heitz, J.P. Sauvage, L. Flamigni, N. Armaroli, V. Balzani, F. Barigelletti, I. Montanari; *A transition-metal-assembled dyad containing a porphyrin module and an electro-deficient ruthenium complex*; Bull.Soc.Chim.Fr. (1996) **133**, 749-754

A.M. Biswas, S.A.Haque, T. Lutz, I.Montanari, C.Olson, R.L. Willis, J.R. Durrant and J.Nelson; *"Charge recombination and transport in dye sensitised TiO_2 photovoltaic devices"* paper presented at the 28th IEEE Photovoltaic Specialists' Conference, (2000) Anchorage, Alaska, USA

A. F. Nogueira, M.-A. De Paoli, I. Montanari, R. Monkhouse, J.Nelson and J. R. Durrant; *Electron transfer dynamics in dye sensitized nanocrystalline solar cells using a polymer electrolyte* J.Phys.Chem. B (2001),**105**, 7517-7524

Y. Tachibana, I. V. Rubtsov, I. Montanari, K. Yoshihara, D. R.Klug and J. R. Durrant; *Transient luminescence studies of electron injection in dye sensitised nanocrystalline TiO_2 films;* Journal of Photochemistry and Photobiology: A Chemistry **142** (2001) 215-220

I. Montanari, J. Nelson and J.R. Durrant, *Iodide Electron Transfer Kinetics in Dye-Sensitized Nanocrystalline TiO_2 Films,* Journal of Physical Chemistry B **106**, (2002) 12203-12210.

I. Montanari, A. F. Nogueira, J. Nelson, J. R. Durrant, C. Winder, M. A. Loi, N. S. Sariciftci and C. Brabec, *"Transient optical studies of charge recombination dynamics in a polymer/fullerene composite at room temperature"* Applied Physics Letters, **81** (2002) 3001-3003

A.F. Nogueira, I. Montanari, C. Brabec, N. S. Sariciftci, J. Nelson, J.R. Durrant; *Charge recombination in conjugated polymer / fullerene blended films studied by transient absorption spectroscopy* Journal of Physical Chemistry B **107**, (2003) 1567-1573.

A.F. Nogueira, I. Montanari, J. Nelson, J.R. Durrant, C. Winder, N.S. Sariciftci and C. Brabec, *Charge recombination dynamics in a polymer/fullerene heterojunction studied by transient absorption spectroscopy;* Synthetic Metals, **137** (2003) 1505-1506

C. Winder, C. Lungenschmied, G. Matt, N.S. Sariciftci, A.F. Nogueira, I. Montanari J.R. Durrant, C. Arndt, U. Zhokhaveth and G. Gobsch; *Excited state spectroscopy in polymer fullerene photovoltaic devices under operation conditions;* Synthetic Metals, **139** (2003) 577-580

Bibliography

Alebbi, M., C. A. Bignozzi, T. A. Heimer, G. M. Hasselmann, and G. J. Meyer. 1998. The Limiting Role of Iodide Oxidation in *cis*-$Os(dcb)_2(CN)_2/TiO_2$ Photoelectrochemical Cells. *J. Phys. Chem. B* 102:7577-7581.

Argazzi, Roberto, Carlo A. Bignozzi, Todd A. Heimer, Felix N. Castellano, and Gerald .J. Meyer. 1995. Long-Lived Photoinduced Charge Separation across Nanocrystalline TiO_2. *J. Am. Chem. Soc.* 117 (47):11815-11816.

Bach, U., D. Lupo, P. Comte, J. E. Moser, F. Weissörtel, J. Salbeck, H. Spreitzer, and M. Grätzel. 1998. Solid-State Dye-Sensitized Mesoporous TiO_2 Solar Cells with High Photon-to-Electron Conversion Efficiencies. *Nature* 395:583-585.

Barth, S., and H. Bässler. 1997. Intrinsic photoconduction in PPV-Type conjugated polymers. *Physics Review Letters* 79:4445-4448.

Barthel, J., R. Neueder, and H. Roch. 2000. Density, Relative Permittivity etc.. *J. Chem. Eng. Data* 45:1007-1011.

Bauer, Christophe, Gerrit Boschloo, Emad Mukhtar, and Anders Hagfeldt. 2001. Electron Injection and Recombination in Ru(dcbpy)2(NCS)2 Sensitized Nanostructured ZnO. *Journal of Physical Chemistry A* 105:5585-5588.

Behar, David, and Joseph Rabani. 2001. Laser Photolysis of TiO_2 Layers in the Presence of Aqueous Iodide. *Journal of Physical Chemistry B* 105:6324-6329.

Berdnikov, V. M., and N. M. Bazhin. 1970. Redox Potentials of some inorganic radicals in acqueous solution. *Zh. Fiz. Khim.* 44 (3):712-716.

Blatchford, J., S. W. Jessen, L. B. Lin, J. J. Lih, T. L. Gustavson, A. J. Epstein, D. K. Fu, M. J. Marsella, U. M. Swager, A. G. MacDiarmid, S. Yamaguchi, and H. Hamaguchi. 1996. Exciton Dynamics in Poly(*p*-Pyridyl Vinylene). *Physical Review Letters* 76:1513.

Botta, C., S. Luzzati, R. Tubino, D. D. C. Bradley, and R. H. Friend. 1993. Photoinduced absorption of polymer solutions. *Physical Review B* 48:14809-14817.

Brabec, C. J., A. Cravino, G. Zerza, N. S. Sariciftci, R. Kiebooms, D. Vanderzande, and J. C. Hummelen. 2001. Photoactive Blends of Poly(*para*-phenylenevinylene) (PPV) with Methanofullerenes from a Novel Precursor: Photophysics and Device Performance. *J. Phys. Chem. B* 105:1528-1536.

Brabec, C. J., V. Dyakonov, N. S. Sariciftci, W. Graupner, G. Leising, and J. C. Hummelen. 1998. Investigation of photoexcitations of

conjugated polymer/fullerene composites embedded in conventional polymers. *Journal of Chemical Physics* 109:1185-1195.

Brabec, C. J., N. S. Sariciftci, and J. C. Hummelen. 2001. Plastic Solar Cells. *Adv. Funct. Mater.* 11:15-26.

Brabec, C. J., G. Zerza, N. S. Sariciftci, G. Cerullo, S. De Silvestri, S. Luzzati, and J. C. Hummelen. 2001. Tracing photoinduced electron transfer process in conjugated polymer/fullerene bulk heterojunctions in real time. *Chem. Phys. Lett.* 340:232-236.

Brabec, Christoph J., Antonio Cravino, Dieter Meissner, N. Serdar Sariciftci, Thomas Fromherz, Minze T. Rispens, Luis Sanchez, and Jan C. Hummelen. 2001. Origin of the open circuit voltage of plastic solar cells. *Advanced Functional Materials* 11 (5):374-380.

Brabec, Christoph J., Sean E. Shaheen, Christoph Winder, N. Serdar Sariciftci, and Patrick Denk. 2002. Effect of LiF/metal electrodes on the performance of plastic solar cells. *Applied Physics Letters* 80 (7):1288-1290.

Burroughes, J. H., D. D. C. Bradley, A. R. Brown, R. N. Marks, K. Mackay, R. H. Friend, P. L. Burns, and A. B. Holmes. 1990. Light-emitting diodes based on conjugated polymers. *Nature* 347 (6293):539-541.

Cao, Fei, Gerko Oskam, Gerald J. Meyer, and Peter C. Searson. 1996. Electron Transport in Porous Nanocrystalline TiO_2 Photoelectrochemical Cells. *Journal of Physical Chemistry* 100:17021-17027.

Chandross, M., S. Mazumdar, S. Jeglinski, X. Wei, Z. V. Vardeny, E. W. Kwock, and T. M. Miller. 1994. Excitons in poly(para-phenylenevinylene). *Phys. Rev. B* 50 (19):14702-14705.

d. Costa, P. G., and E. M. Conwell. 1993. Excitons and the band gap in PPV-Type Conducting polymers. *Am. Phys. Soc. Rap. Comm.* 48:1993-1997.

Denton, G., N. Tessler, N. Harrison, and Richard H. Friend. 1997. Factors Influencing Stimulated Emission from Poly(*p*-phenylenevinylene). *Physical Review Letters* 78:733-736.

Devonshire, R., and J. J. Weiss. 1968. Nature of the Transient Species in the Photochemistry of Negative Ions in Aqueous Solution. *J. Phys. Chem.* 72:3815.

Dittrich, Th., P. Beer, F. Koch, J. Weidmann, and I. Lauermann. 1998. Barrier lowering in dye-sensitized porous- TiO_2 solar cells. *Applied Physics Letters* 73 (13):1901-1903.

Draper, R. Barton, and Marye Anne Fox. 1990. Titanium Dioxide Photosensitized Reactions Studied by Diffuse Reflectance Flash Photolysis in Aqueous Suspensions of TiO_2 Powder. *Langmuir* 6:1396-1402.

Duffy, N. W., L. M. Peter, R. M. Rajapakse, and K. G. U. Wijayantha. 2000. Investigation of the Kinetics of the Back Reaction of Electrons with Tri-Iodide in Dye-Sensitized Nanocrystalline Photovoltaic Cells. *Journal of Physical Chemistry B* 104:8916-8919.

Duffy, Noel W., Laurence M. Peter, R. M. G. Rajapakse, and K. G. U. Wijayantha. 2000. A novel charge extraction method for the study of electron transport and interfacial transfer in dye sensitised nanocrystalline solar cells. *Electrochemistry Communications* 2:658-662.

Durrant, J. R. 1992. Transient Absorption Spectroscopy of Photosystem II. Ph.D. Thesis, Department of Biology, Imperial College, London.

Fahrenbruch, A. L., and R. H. Bube. 1983. *Fundamentals of Solar Cells. Photovoltaic Solar Energy Conversion*. New York: Academic Press.

Ferber, Jörg, Rolf Stangl, and Joachim Luther. 1998. An electrical model of the dye-sensitized solar cell. *Solar Energy Materials and Solar Cells* 53:29-54.

Fillinger, A., and B. A. Parkinson. 1999. The Adsorption Behavior of a Ruthenium-Based Sensitizing Dye to Nanocrystalline TiO_2 Coverage Effects on the External and Internal Sensitization Quantum Yields. *J. Electrochem. Soc.* 146:4559-4564.

Fischer, A.C. 2000. Intensity dependence of the back reaction and transport of electrons in dye-sensitised nanocrystalline TiO_2 solar cells. *Journal of Physical Chemistry B* 104 (5):949-958.

Fitzmaurice, D. J., and H. Frei. 1991. Transient Near-Infrared Spectroscopy of Visible-Light Sensitized Oxidation of I^- At Colloidal TiO_2. *Langmuir* 7 (6):1129-1137.

Franco, G., J. Gehring, L. M. Peter, E. A. Ponomarev, and I. Uhlendorf. 1999. Frequency-Resolved Optical Detection of Photoinjected Electrons in Dye-Sensitized Nanocrystalline Photovoltaic Cells. *J. Phys. Chem. B* 103 (4):692-698.

Frenkel, J. 1931. Some remarks on the theory of the photoelectric effect. *Phys. Rev.* 38:309-320.

Gailberger, M., and H. Bässler. 1991. The d.c. and transient photoconductivity of poly(2-phenyl-1,4-phenylenevinylene). *Physical Review B* 44 (16):8643-8651.

Garnier, Francis, Ryad Hajlaoui, Abderrahim Yassar, and Pratima Srivastava. 1994. All-polymer field-effect transistor realized by printing techniques. *Science* 265 (5179):1864-1866.

Geens, Wim, Sean E. Shaheen, Christoph J. Brabec, Jozef Poortmans, and N. Serdar Sariciftci. 2000. Field-Effect Mobility Measurements of Conjugated Polymer / Fullerene Photovoltaic Blends. Paper read at Electronic Properties of Novel Materials -- Molecular Nanostructures, at Leuven, Belgium.

Granström, M., K. Petritsch, A. C. Arias, A. Lux, M. R. Andersson, and R. H. Friend. 1998. Laminated fabrication of polymeric photovoltaic devices. *Nature* 395:257-260.

Grätzel, M. 2001. Photoelectrochemical cells. *Nature* 414 (6861):338-344.

Green, Martin A., K. Emery, David L. King, Sanekazu Igari, and Wilhelm Warta. 2002. Solar Cell Efficiency Tables (Version 19). *Progress in Photovoltaics: Research and Applications* 10:55-61.

Gregg, Brian, A., François Pichot, Suzanne Ferrere, and Clark L. Fields. 2001. Interfacial Recombination Processes in Dye-Sensitized Solar Cells and Methods To Passivate the Interfaces. *Journal of Physical Chemistry B* 105:1422-1429.

Gregg, Brian, A., Arie Zaban, and Suzanne Ferrere. 1999. Dye sensitized solar cells. Energetic considerations and applications. *Zeitschrift für physikalische chemie* 212 (1):11-22.

Grossweiner, L. I., and M. S. Matheson. 1957. The kinetics of the dihalide ions from the flash photolysis of aqueous alkali halide solutions. *Journal of Physical Chemistry* 61:1089-1095.

Haber, F., and R. Russ. 1904. *Zeitschrift für physikalische chemie* 47:257.

Hagfeldt, Anders, and Michael Grätzel. 1995. Light-Induced Redox Reactions in Nanocrystalline Systems. *Chem. Rev.* 95 (1):49-68.

Hagfeldt, Anders, and Michael Grätzel. 2000. Molecular Photovoltaics. *Accounts of Chemical Research* 33:269-277.

Halls, J. J. M., K. Pichler, R. H. Friend, S. C. Moratti, and A. B. Holmes. 1996. Exciton diffusion and dissociation in a poly(*p*-phenylenevinylene)/C_{60} heterojunction photovoltaic cell. *Applied Physics Letters* 68:3120-3122.

Haque, S. A., Y. Tachibana, D. R. Klug, and J. R. Durrant. 1998. Charge Recombination Kinetics in Dye-Sensitized Nanocrystalline Titanium Dioxide Films. *J. Phys. Chem. B* 102 (10):1745-1749.

Haque, S. A., Y. Tachibana, R. L. Willis, J. E. Moser, M. Grätzel, D. R. Klug, and J. R. Durrant. 2000. Parameters influencing Charge Recombination Kinetics in Dye-Sensitized Nanocrystalline Titanium Dioxide Films. *J. Phys. Chem. B* 104:538-547.

Harrison, N., G. Hayes, R. Phillips, and Richard H. Friend. 1996. Singlet Intrachain Exciton Generation and Decay in Poly(*p*-phenylenevinylene). *Physical Review Letters* 77 (9):1881-1884.

Heimer, T. A., E. J. Heilweil, C. A. Bignozzi, and G. J. Meyer. 2000. Electron Injection, Recombination, and Halide Oxidation Dynamics at Dye-Sensitized Metal Oxide Interfaces. *J. Phys. Chem. A* 104:4256-4262.

Heimer, T.A., S.T. D'Arcangelis, F. Farzad, J.M. Stipkala, and G.J. Meyer. 1996. An Acetylacetonate-Based Semiconductor-Sensitizer Linkage. *Inorg. Chem.* 35 (18):5319-5324.

Henglein, Arnim. 1980. Energetics of reactions of O_{aq}^{-} and of O^{--} transfer reactions between radicals. *Radiat. Phys. Chem.* 15 (2-3):151-158.

Hsu, J., M. Yan, T. M. Jedju, L. J. Rothberg, and B. R. Hseih. 1994. Assignment of the picosecond photoinduced absorption in phenylene vinylene polymers. *Physical Review B* 49 (1):712-715.

Huang, S. Y., G. Schlichthörl, A Nozik, J., A. J. Frank, and M. Graetzel. 1997. Charge Recombination in Dye-Sensitized Nanocrystalline TiO_2 Solar Cells. *Journal of Physical Chemistry B* 101 (14):2576-2582.

Hug, G. L. 1981. Optical spectra of nonmetallic inorganic transient species in aqueous solution. *Natl. Stand. Ref. Data Ser. (U.S. Natl. Bur. Stand.)* 69:541-706.

Hummelen, Jan C., Brian W. Knight, F. Lepeq, and Fred Wudl. 1995. Preparation and Characterization of Fulleroid and Methanofullerene Derivatives. *Journal of Organic Chemistry* 60:532-538.

Ito, T., H. Shirakawa, and S. Ikeda. 1974. Simultaneous polymerization and formation of polyacetylene film on the surface of a concentrated soluble Ziegler type catalyst solution. *J. Polym. Sci., Polym. Chem. Ed.* 12 (1):11-20.

Jakubiak, R., Christopher J. Collison, Wai Chou Wan, Lewis J. Rothberg, and Bing R. Hseih. 1999. Aggregation Quenching of Luminescence in Electroluminescent Conjugated Polymers. *Journal of Physical Chemistry A* 103 (14):2394-2398.

Kamat, P.V., I. Bedja, S. Hotchandani, and L.K. Patterson. 1996. Photosensitization of Nanocrystalline Semiconductor Films. Modulation of Electron Transfer between Excited Ruthenium Complex and $Sn0_2$ Nanocrystallites with an Externally Applied Bias. *J. Phys. Chem.* 100:4900-4908.

Kay, Andreas, and Michael Grätzel. 1993. Artificial Photosynthesis. 1. Photosensitization of TiO_2 Solar Cells with Chlorophyll Derivatives and Related Natural Porphyrins. *Journal of Physical Chemistry* 97:6272-6277.

Kay, Andreas, Robin Humphry-Baker, and Michael Grätzel. 1994. Artificial Photosynthesis. 2. Investigations on the Mechanism of Photosensitization of Nanocrystalline TiO_2 Solar Cells by Chlorophyll Derivatives. *J. Phys. Chem.* 98:952-959.

Kebede, Zerihun, and Sten-Eric Lindquist. 1998. The obstructed diffusion of the I_3^- ion in mesoscopic TiO_2 membranes. *Solar Energy Materials and Solar Cells* 51 (3-4):291-303.

Klimov, V., D. McBranch, N. Barashkov, and J. Ferraris. 1997. Femtosecond dynamics of excitons in p-conjugated oligomers: the role of intrachain two-exciton states in the formation of interchain species. *Chemical Physics Letters* 277 (1-3):109-117.

Kölle, Ulrich, Jacques Moser, and Michael Grätzel. 1985. Dynamics of interfacial charge transfer reactions in semiconductor dispersions. Reduction of cobaltoceniumdicarboxylate in colloidal titania. *Inorganic Chemistry* 24 (14):2253-2258.

Kraabel, B., J. C. Hummelen, D. Vacar, D. Moses, N. S. Sariciftci, A. J. Heeger, and F. Wudl. 1996. Subpicosecond photoinduced electron transfer from conjugated polymers to functionalized fullerenes. *J. Chem. Phys.* 104:4267-4273.

Kraabel, B., V. I. Klimov, R. Kohlman, S. Xu, H.-L. Wang, and D. W. McBranch. 2000. Unified picture of the photoexcitations in phenylene-based conjugated polymers: Universal spectral and dynamical features in subpicosecond transient absorption. *Physical Review B* 61:8501-8515.

Kraabel, B., C. H. Lee, D. McBranch, D. Moses, N. Serdar Sariciftci, and A. J. Heeger. 1993. Ultrafast photoinduced electron transfer in conducting polymer-buckmisterfullerene composites. *Chemical Physics Letters* 213:389-394.

Kroon, J. M., M. M. Wienk, W. J. H. Verhees, and J. C. Hummelen. 2002. Accurate efficiency determination and stability studies of conjugated polymer / fullerene solar cells. *Thin Solid Films* 403-404:223-228.

Kuciauskas, D., M. S. Freund, H. B. Gray, J.R. Winkler, and N. S. Lewis. 2001. Electron Transfer Dynamics in Nanocrystalline Titanium Dioxide Solar Cells Sensitized with Ruthenium or Osmium Polypyridyl Complexes. *J. Phys. Chem. B* 105:392-403.

Lee, C. H., G. Yu, D. Moses, and A. J. Heeger. 1994. Picosecond transient photoconductivity in poly(*p*-phenylenevinylene). *Physical Review B* 49:2396-2407.

Lee, K., R. A. J. Janssen, N. S. Sariciftci, and A. J. Heeger. 1994. Direct evidence of photoinduced electron transfer in conducting-polymer-C_{60} composites by infrared photoexcitation spectroscopy. *Phys. Rev. B* 49:5781-5784.

Liu, Yao, Anders Hagfeldt, Xu-Rui Xiao, and Sten-Eric Lindquist. 1998. Investigation of influence of redox species on the interfacial energetics of a dye-sensitized nanoporous TiO_2 solar cell. *Solar Energy Materials and Solar Cells* 55:267-281.

Maitland, A. 1906. *Z. Elektrochem.* 12:268.

Marks, R. N., J. J. M. Halls, D. D. C. Bradley, R. H. Friend, and A. B. Holmes. 1994. The photovoltaic response in PPV thin film devices. *Journal of Physics of Condensed Matter* 6:1379-1394.

Markvart, Tomas. 2000. *Solar Electricity*. London: John Wiley & Sons.

Matheson, M. S., W. A. Mulac, and J. Rabani. 1963. Formation of the hydrated electron in the flash photolysis of aqueous solutions. *J. Phys. Chem.* 67 (12):2613-2617.

Meskers, S. C. J., P. A. van Hal, A. J. H. Spiering, J. C. Hummelen, A. F. G. van der Meer, and R. A. J. Janssen. 2000. Time-resolved infrared-absorption study of photoinduced charge transfer in a polythiophene-methanofullerene composite film. *Physical Review B* 61:9917-9920.

Meyer, G.J. 1997. Efficient light-to-electrical energy conversion: nanocrystalline TiO_2 films modified with inorganic sensitisers. *J. Chem. Educ.* 74 (6):652-656.

Meyer, H., D. Haarer, H. Naarmann, and H. H. Hörhold. 1995. Trap distribution for charge carriers in poly(paraphenylene vinylene) (PPV) and its substituted derivative DPOP-PPV. *Physical Review B* 52:2587-2598.

Mizrahi, U., I. Shtrichman, D. Gershoni, E. Ehrenfreund, and Z. V. Vardeny. 1999. Picosecond time resolved photoinduced absorption by infrared active vibrations as a probe for charge photogeneration in MEH-PPV/C_{60} composites. *Synthetic Metals* 102:1182-1185.

Montanari, Ivan, Jenny Nelson, and James Robert Durrant. 2002. Iodide kinetics in dye-sensitised electrodes.submitted to the Journal of Physical Chemistry B.

Montanari, Ivan, Ana Flavia Nogueira, James R. Durrant, Christoph Winder, Maria Antonietta Loi, N. Serdar Sariciftci, and Christoph J. Brabec. 2002. Transient optical studies of charge recombination dynamics in a polymer / fullerene composite at room temperature. *Applied Physics Letters* in press.

Moser, J. E., and M. Grätzel. 1982. Photoelectrochemistry with Colloidal Semiconductors; Laser Studies of Halide Oxidation in Colloidal Dispersions of TiO_2 and α-Fe_2O_3. *Helv. Chim. Acta* 65:1436-1444.

Moser, J. E., D. Noukakis, U. Bach, Y. Tachibana, D. R. Klug, J. R. Durrant, R. HumphryBaker, and M. Grätzel. 1998. Comment on "measurement of ultrafast photoinduced electron transfer from chemically anchored Ru-dye molecules into empty electronic states in a colloidal anatase TiO_2 film". *Journal of Physical Chemistry B* 102 (18):3649-3650.

Moser, J.E., and M. Grätzel. 1993. Observation of temperature independent heterogeneous electron transfer reactions in the inverted Marcus region. *Chemical Physics* 176 (2-3):493-500.

Moses, D., J. Wang, A. J. Heeger, N. Kirova, and S. Brazovski. 2001. Singlet exciton binding energy in poly(phenylene vinylene). *Proceedings of the National Academy of Sciences* 98:13496-13500.

Munters, T., T. Martens, L. Goris, V. Vrindts, J. Manca, L. Lutsen, W. De Ceuninck, D. Vanderzande, L. De Schepper, J. Gelan, N. S. Sariciftci, and Brabec C.J. 2002. A comparison between state-of-the-art "glitch" and "sulphinyl" synthesised MDMO-PPV/PCBM bulk hetero-junction solar cells. *Thin Solid Films* 403-404:247-251.

Myung, N., and S. Licht. 1995. Potential enhancement of Polyiodide Redox Couples via Solution Modification. *Journal of the Electrochemical Society* 142 (8):L129-L131.

Nasr, C., S. Hotchandani, and P. V. Kamat. 1998. Role of iodide in Photoelectrochemical Solar Cells. Electron Transfer between Iodide Ions and Ruthenium Polypyridyl Complex Anchored on Nanocrystalline SiO_2 and SnO_2 Films. *J. Phys. Chem. B* 102:4944-4951.

Nazeeruddin, M.K., A. Kay, I. Rodicio, R. Humphry-Baker, E. Mueller, P. Liska, N. Vlachopoulos, and M. Grätzel. 1993. Conversion of Light to Electricity by *cis*-X_2Bis(2,2'-bipyridyl-4,4'-dicarboxylate)ruthenium(II) Charge-Transfer Sensitizers (X = Cl^-, Br^-, I^-, CN^-, and SCN^-) on Nanocrystalline TiO_2 Electrodes. *JACS* 115:6382-6390.

Nazeeruddin, M.K., P. Liska, J.E. Moser, N. Vlachopolous, and M. Grätzel. 1990. Conversion of light into electricity with trinuclear ruthenium complexes adsorbed on textured titanium dioxide films. *Helv. Chim. Acta* 73 (6):1788-1803.

Nelson, Ivory V., and Reynold T. Iwamoto. 1964. Voltammetric evalutation of the stability of trichloride, tribromide, and triiodide ions in nitromethane, acetone and acetonitrile. *Journal of Electronanalytical Chemistry* 7:218-221.

Nelson, J. 1999. Continuous-Time Random-Walk Model of electron transport in nanocrystalline TiO_2 electrodes. *Phys. Rev. B* 59 (23):15374-15380.

Nelson, J. 2001. Charge transport in dye sensitised systems. In *Encyclopedia of Electrochemistry*, edited by S. Licht. New York: Wiley.

Nelson, J., S. A. Haque, D. K. Klug, and J. R. Durrant. 2001. Trap-limited recombination in dye-sensitised nanocrystalline metal oxide electrodes. *Phys. Rev. B* 63:205321.

Nelson, Jenny. 2002. Modelling charge recombination in molecular solar cells. Paper read at Electrochemical Society Spring Meeting, at USA.

Neugebauer, H., C. Brabec, J. C. Hummelen, and N. S. Sariciftci. 2000. Stability and photodegradation mechanisms of conjugated polymer / fullerene plastic solar cells. *Solar Energy Materials & Solar Cells* 61:35-42.

Neugebauer, H., C. J. Brabec, J. C. Hummelen, R. A. J. Janssen, and N. S. Sariciftci. 1999. Stability Studies and Degradation Analysis of Plastic Solar Cell Materials by FTIR Spectroscopy. *Synthetic Metals* 102:1002-1003.

Nguyen, Thuc-Quyen, Vinh Doan, and Benjamin J. Schwartz. 1999. Conjugated polymer aggregates in solution: Control of interchain interactions. *Journal of Chemical Physics* 110 (8):4068- 4078.

Nikam, Pandharinath S., Laxman N. Shirsat, and Medhi Hasan. 1998. Density and Viscosity Studies of Binary Mixtures of Acetonitrile with Methanol, Ethanol, Propan-1-ol, Propan-2-ol, Butan-1-ol, 2-. *J. Chem. Eng. Data* 43:732-737.

Nogueira, A.-F., M.-A. De Paoli, and J. R. Durrant. 2001. Dye-Sensitized Nanocrystalline Solar Cells Employing a Polymer Electrolyte. *Adv. Mat.* 13:826-830.

Nogueira, A.-F., M.-A. De Paoli, I. Montanari, R. Monkhouse, J. Nelson, and J. R. Durrant. 2001. Electron Transfer Dynamics in Dye Sensitized Nanocrystalline Solar Cells Using a Polymer Electrolyte. *J. Phys. Chem. B* 105:7517-7524.

Norrish, R. G. W., and George Porter. 1949. Chemical reactions produced by very high light intensities. *Nature* 164:658.

Nusbaumer, Hervé, and Jacques-E. Moser. 2001. $Co^{II}(dbbip)_2^{2+}$ Complex Rivals Tri-iodide/Iodine Redox Mediator in Dye-Sensitized Photovoltaic Cells. *Journal of Physical Chemistry B* 105:10461-10464.

O' Regan, B., and M. Grätzel. 1991. A low-cost, high-efficiency solar cell based on dye sensitized colloidal TiO_2 films. *Nature* 353:737-739.

O' Regan, B., J. E. Moser, M. Anderson, and M. Grätzel. 1990. Vectorial Electron Injection into Transparent Semiconductor Membranes and Electric Field Effects on the Dynamics fo Light-Induced Charge Separation. *J. Phys. Chem.* 94 (24):8720-8726.

Oskam, Gerko, Bryan V. Bergeron, Gerald .J. Meyer, and Peter C. Searson. 2001. Pseudohalogens for Dye-Sensitized TiO_2 Photoelectrochemical Cells. *Journal of Physical Chemistry B* 105:6867-6873.

Peierls, R. 1932. The theory of the absorption spectra of solid bodies. *Ann. Physik* 13:905-952.

Pelet, S., J. E. Moser, and M. Grätzel. 2000. Cooperative Effect of Adsorbed Cations and Iodide on the Interception of Back Electron Transfer in the Dye Sensitization of Nanocrystalline TiO_2. *J. Phys. Chem. B* 104:1791-1795.

Petrisch, K. 2000. Organic Solar Cell Architectures. Ph. D., Cambridge and Graz.

Peumans, P., and S. R. Forrest. 2001. Very-high-efficiency double-heterostructure copper phthalocyanine/C_{60} photovoltaic cells. *Applied Physics Letters* 79 (1):126-128.

Peumans, P., and S. R. Forrest. 2002. Erratum: "Very-high-efficiency double heterostructure copper phthalocyanine/C_{60} photovoltaic cells"

[Appl. Phys. Lett. 79, 126 (2001)]. *Applied Physics Letters* 80 (2):338.

Redmond, G., and D. Fitzmaurice. 1993. Spectroscopic Determination of Flatband Potentials for Polycristalline TiO_2 Electrodes in Nonaqueous Solvents. *J. Phys. Chem.* 97:1426-1430.

Rothberg, L. J., M. Yan, F. Papadimitrakopoulos, M. E. Galvin, E. W. Kwock, and T. M. Miller. 1996. Photophysics of phenylenevinylene polimers. *Synthetic Metals* 80 (1):41-58.

Rothenberger, G., D. Fitzmaurice, and M. Grätzel. 1992. Spectroscopy of Conduction Band Electrons in Transparent Metal Oxide Semiconductor Films: Optical Determination of the Flatband Potential of Colloidal Titanium Dioxide Films. *J. Phys. Chem.* 96 (14):5983-5986.

Safrany, Agnes, Ruomei Gao, and Joseph Rabani. 2000. Optical Properties and Reactions of Radiation Induced TiO_2 Electrons in Aqueous Colloid Solutions. *Journal of Physical Chemistry* 104:5848-5853.

Salafsky, J. S., W. H. Lubberhuizen, E. van Fassen, and R. E. I. Schropp. 1998. Charge Dynamics following Dye Photoinjection into a TiO2 Nanocrystalline Network. *Journal of Physical Chemistry B* 102:766-769.

Samuel, I., G. Rumbles, C. J. Collison, S. C. Moratti, and A. B. Holmes. 1998. Intra- and inter-molecular photoexcitations in a cyano-substituted poly(*p*-phenylenevinylene). *Chemical Physics* 227 (1-2):75-82.

Sariciftci, N. S., ed. 1997. *Primary Photoexcitations in Conjugated Polymers: Molecular Exciton versus Semiconductor Band Model*. Singapore: World Scientific Publishing.

Sariciftci, N. S., D. Braun, C. Zhang, V. I. Srdanov, A. J. Heeger, G. Stucky, and F. Wudl. 1993. Semiconducting polymer - buckmisterfullerene heterojunctions: Diodes, photodiodes, and photovoltaic cells. *Appl. Phys. Lett.* 62:585-587.

Sariciftci, N. S., L. Smilowitz, A. J. Heeger, and F. Wudl. 1992. Photoinduced Electron Transfer from a Conducting Polymer to Buckmisterfullerene. *Science* 258:1474-1476.

Sauvé, G., M. E. Cass, G. Coia, S. J. Doig, I. Lauermann, K. E. Pomykal, and N. S. Lewis. 2000. Dye Sensitization of Nanocrystalline Titanium Dioxide with Osmium and Ruthenium Polypyridyl Complexes. *J. Phys. Chem. B* 104:6821-6836.

Scher, H., and E. W. Montroll. 1975. Anomalous transit-time dispersion in amorphous solids. *Phys. Rev. B* 12:2455-2477.

Schlichthörl, G., S. Y. Huang, J. Sprague, and A. J. Frank. 1997. Band edge movement and recombination kinetics in dye-sensitized nanocrystalline TiO_2 solar cells: A study by intensity modulated

photovoltage spectroscopy. *Journal of Physical Chemistry B* 101:8141-8155.

Schlichthörl, G., N. G. Park, and A. J. Frank. 1999. Evalutation of the Charge-Collection Efficiency of Dye-Sensitized Nanocrystalline TiO_2 Solar Cells. *Journal of Physical Chemistry B* 103 (5):782-791.

Schultz, N. A., M. C. Scharber, C. J. Brabec, and N. S. Sariciftci. 2001. Low-temperature recombination kinetics of photoexcited persistent charge carriers in conjugated polymer/fullerene composite films. *Physical Review B* 64:245210-245216.

Schwarzburg, Klaus, and Frank Willig. 1999. Origin of Photovoltage and Photocurrent in the Nanoporous Dye-Sensitized Electrochemical Solar Cell. *Journal of Physical Chemistry B* 103 (28):5743-5746.

Serpone, N., I. Texier, A. V. Emeline, P. Pichat, H. Hidaka, and J. Zhao. 2000. Post-irradiation effect and reductive dechlorination of chlorophenols at oxygen-free TiO_2 / water interfaces in the presence of prominent hole scavengers. *Journal of Photochemistry and Photobiology: A Chemistry* 136:145-155.

Shaheen, S. E., C. J. Brabec, N. S. Sariciftci, F. Padinger, T. Fromherz, and J. C. Hummelen. 2001. 2.5% efficient organic plastic solar cells. *Applied Physics Letters* 78:841-843.

Shirakawa, H., E. J. Lewis, A. G. MacDiarmid, C. K. Chiang, and A. J. Heeger. 1977. Synthesis of electrically conducting organic polymers: halogen derivatives of polyacetylene, $(CH)_x$. *J. Chem. Soc. Chem. Commun.*:578.

Shklovskii, B. I., H. Fritzsche, and S. D. Baranovskii. 1989. Electronic Transport and Recombination in Amorphous Semiconductors at Low Temperatures. *Phys. Rev. Lett.* 62:2989-2992.

Shockley, W. 1949. *Bell Syst. Tech. J.* 28:435.

Sinclair, M., D. McBranch, T. Hagler, and A. J. Heeger. 1992. Subpicosecond photoinduced absorption in poly[2,5-thienylene vinylene] and poly[3-methoxy-6-(2-ethylhexyloxy) phenylene vinylene]. *Synthetic Metals* 50 (1-3):593-602.

Skotheim, Terje A. 1978. Dye-sensitized Schottky barrier solar cells. USA.

Smilowitz, L., N. S. Sariciftci, R. Wu, C. Gettinger, A. J. Heeger, and F. Wudl. 1993. Photoexcitation spectroscopy of conducting polymer-C_{60} composites: Photoinduced electron transfer. *Physical Review B* 47:13835-13842.

Södergren, Sven, Anders Hagfeldt, Jörgen Olsson, and Sten-Eric Lindquist. 1994. Theoretical Models for the Action Spectrum and the Current-Voltage Characteristics of Microporous Semiconductor Films in Photoelectrochemical Cells. *Journal of Physical Chemistry* 98:5552-5556.

Solbrand, Anita, Henrik Lindström, Håkan Rensmo, Anders Hagfeldt, Sten-Eric Lindquist, and Sven Södergren. 1997. Electron Transport in the Nanostructured TiO_2-Electrolyte System Studied with Time-Resolved Photocurrents. *Journal of Physical Chemistry B* 101:2514-2518.

Steinfeld, Jeffrey I., Joseph S. Francisco, and William L. Hase. 1998. *Chemical Kinetics and Dynamics*. New York: Prentice-Hall, Inc.

Stübinger, Thomas, and Wolfgang Brütting. 2001. Exciton diffusion and optical inteference in organic donor-acceptor photovoltaics cells. *Journal of Applied Physics* 90 (7):3632-3641.

Tachibana, Y., S. A. Haque, I. P. Mercer, J. R. Durrant, and D. R. Klug. 2000. Electron Injection and Recombination in Dye Sensitized Nanocrystalline Titanium Dioxide Films: A Comparison of Ruthenium Bipyridyl and Porphyrin Sensitiser Dyes. *J. Phys. Chem. B* 104:1198-1205.

Tachibana, Y., J. E. Moser, M. Grätzel, D. R. Klug, and J. R. Durrant. 1996. Subpicosecond Interfacial Charge Separation in Dye-Sensitised Nanocrystalline Titanium Dioxide Films. *J. Phys. Chem. B* 100:20056-20062.

Tachibana, Y., I.V. Rubtsov, I. Montanari, K. Yoshihara, D. R. Klug, and J.R. Durrant. 2001. Transient luminescence studies of electron injection in dye-sensitised nanocrystalline TiO_2 electrodes. *Journal of Photochemistry and Photobiology: A Chemistry* 142:215-220.

Tachibana, Yasuhiro. 2000. Charge separation and recombination in dye-sensitised nanocrystalline TiO_2. Ph.D. Thesis, Chemistry, Imperial College, London.

Tang, C. W. 1986. Two-layer organic photovoltaic cell. *Applied Physics Letters* 48:183-185.

Van Overstraeten, R. J., and R. P. Mertens. 1986. *Physics, Technology and Use of Photovoltaics*. Edited by N. H. Lipman, *Modern Energy Studies*: Adam Hilger Ltd.

van 't Spijker, Hans, and Albert Goosens. 2002. Quantitative study of electron transport in nanostructured materials by means of transient absorption spectroscopy. *Thin Solid Films* 403-404:410-414.

van 't Spijker, Hans, Brian O' Regan, and Albert Goosens. 2001. Quantitative Study of Electron Losses in Nanoporous Anatase Using Transient Absorption Spectroscopy. *Journal of Physical Chemistry B* 105:7220-7226.

Vetter, K. J. 1952. *Zeitschrift für physikalische chemie* 199:285.

Vetter, Klaus J. 1967. *Electochemical kinetics: theoretical and experimental aspects*. New York, London: Academic Press. Original edition, Electrochemische Kinetik.

Willis, Richard Lance. 2002. *Nature*:manuscript in preparation.

Winder, Christoph. 2001. Sensitization of Low Bandgap Polymer Bulk Heterojunction Solar Cells. Diplomarbeit, Chemistry, Johannes Kepler Universität, Linz.

Yan, M., L. J. Rothberg, E. Kwock, and T. M. Miller. 1995. Interchain Excitations in Conjugated Polymers. *Physical Review Letters* 75 (10):1992-1995.

Yan, M., L. J. Rothberg, F. Papadimitrakopoulos, M. E. Galvin, and T. M. Miller. 1994. Spatially Indirect Excitons as Primary Photoexcitations in Conjugated Polymers. *Physical Review Letters* 72 (7):1104-1107.

Yan, Susan G., and Joseph T. Hupp. 1996. Semiconductor-Based Interfacial Electron-Transfer Reactivity: Decoupling Kinetics from pH-Dependent Band Energetics in a Dye-Sensitised Titanium Dioxide/Aqueous Solution System. *Journal of Physical Chemistry B* 100 (17):6867-6870.

Yan, Susan G., and Joseph T. Hupp. 1997. Energetics of Electron Transfer at the Nanocrystalline Titanium Dioxide Semiconductor/Aqueous Solution Interface: pH Invariance of the Metal-Based Formal Potential of a Representative Surface-Attached Dye Couple. *Journal of Physical Chemistry B* 101 (9):1493-1495.

Yu, G., J. Gao, J. C. Hummelen, F. Wudl, and A. J. Heeger. 1995. Polymer Photovoltaic Cells: Enhanced Efficiencies via a Network of Internal Donor-Acceptor Heterojunctions. *Science* 270:1789-1791.

Zaban, A., A. Meier, and B.A. Gregg. 1997. Electric Potential Distribution and Short-Range Screening in Nanoporous TiO_2 Electrodes. *J. Phys. Chem. B* 101:7985-7990.

Zaban, Arie, Suzanne Ferrere, and Brian Gregg, A. 1998. Relative Energetics at the Semiconductor/Sensitizing Dye/Electrolyte Interface. *Journal of Physical Chemistry B* 102:452-460.

Zerza, G., M. C. Scharber, C. J. Brabec, N. S. Sariciftci, R. Gómez, J. L. Segura, N. Martin, and V. I. Srdanov. 2000. Photoinduced Charge Transfer between Tetracyano-Antraquino-Dimethane Derivatives and Conjugated Polymers for Photovoltaics. *J. Phys. Chem. A* 104:8315-8322.

PAGES ARE BLANK IN ORIGINAL

NOTES

NOTES

NOTES

NOTES

NOTES